Microbiota regulate short chain fatty acids and influence histone acylations in intestinal epithelial cells.

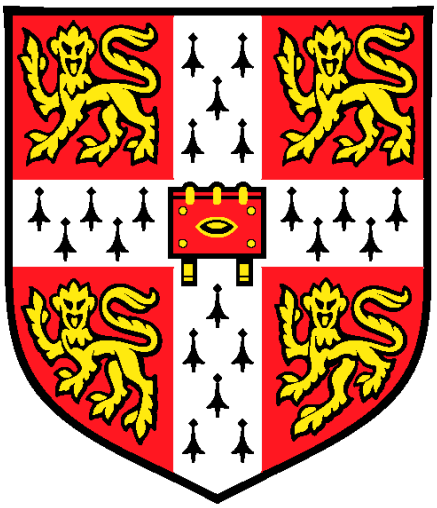

Rachel Claire Fellows

The Babraham Institute

Gonville and Caius College

University of Cambridge

This dissertation is submitted for the degree of

Doctor of Philosophy

May 2019

Declaration

This dissertation is the result of my own work and includes nothing which is the outcome of work done in collaboration except as declared in the Preface and specified in the text.

It is not substantially the same as any that I have submitted, or, is being concurrently submitted for a degree or diploma or other qualification at the University of Cambridge or any other University or similar institution except as declared in the Preface and specified in the text. I further state that no substantial part of my dissertation has already been submitted, or, is being concurrently submitted for any such degree, diploma or other qualification at the University of Cambridge or any other University or similar institution except as declared in the Preface and specified in the text.

This thesis does not exceed 60,000 words, excluding bibliography, figures and appendices.

Cambridge, UK, May 2019

Rachel Claire Fellows

Microbiota regulate short chain fatty acids and influence histone acylations in intestinal epithelial cells.

Rachel Claire Fellows

Summary

The intestinal microbiota have a vital role in aiding digestion by metabolising dietary fibres. In this process, they produce short chain fatty acids (SCFAs) such as butyrate, an important energy source for intestinal epithelial cells. SCFAs are chemically related to histone acylations, a growing number of post-translational modifications that include histone acetylation, butyrylation and crotonylation. Histone post-translational modifications are thought to be involved in the regulation of gene expression as they can specifically recruit transcription factors and chromatin remodellers. Histone acylations are abundant in the intestine and are associated with active chromatin. In this project, I have identified that butyrate can upregulate histone acylations in both colon carcinoma cells and intestinal organoids in a dynamic manner. In addition, I identified that class I histone deacetylases (HDACs) are efficient histone decrotonylases. I have achieved this through a combination of biological analysis of the effects of treatment with HDAC inhibitors and *in vitro* analysis of purified proteins, which enabled determination of kinetic parameters. When investigating how SCFAs could influence histone acylations *in vivo*, I identified that antibiotic induced depletion of the microbiota in mice caused reduction in luminal SCFA concentration and global changes in histone acetylation and crotonylation, particularly those at histone H4. RNA-sequencing of these mice identified changes in the expression of genes which were involved in many important biological processes, such as cell signalling, energy generation and metabolism. Further to this, I studied lysine crotonylation and H4K8 acetylation at dysregulated genes to understand the how the presence of these modifications at the promoter influences gene expression in this context. These intriguing findings suggest that histone acylations could act as a nutrient sensors to couple changes in microbiota composition to that of gene expression and cellular function.

Acknowledgements

I would not have made it this far without the support and encouragement of so many people. Firstly, a huge thank you to Patrick Varga-Weisz who was always willing to discuss ideas, gave me lots of support and supervision with different aspects of my PhD and helped me at every step along the way. Next, to everyone in Patrick's group, especially Juri, Elena, Payal and Claudia who were always happy to help and made the lab a wonderful place to be part of. Thanks also go to Patrick and Marco Vinolo for giving me the opportunity to go to Brazil and to Marco and all his group for their kindness and support that made me feel immediately included, despite my terrible Portuguese! I would like to thank many people at the Babraham Institute, including Anne Segonds-Pichon and Simon Andrews for all their help with statistics and bioinformatics, and to Kristina Tabbada for sequencing my samples and giving me advice. Particular thanks go to my assessor Michelle Linterman who provided me with valuable support and guidance throughout. My experience at Babraham would not be the same without my fellow PhD students, especially Lina, Michiel, Jo, Marco, Carolyn and Stephen. I would like to thank them for their friendship and providing a great environment to work. Thanks also to everyone from the Babraham bus crew for making the commute so much better! I would also like to thank all my friends at Caius, particularly Lucy, Olivia, Marta, Ale, Lindsay and Hugo who have made being at Cambridge so much more fun! Last but not least, I would like to say a big thank you to my parents who have always been super supportive and loving.

Acknowledgement of assistance received during the course of the thesis

1) Initial training in techniques and laboratory practice and subsequent mentoring

- Juri Kazakevych, Claudia Stellato, Payal Jain and Patrick Varga-Weisz for help to learn western blot, ChIP-sequencing, RNA-sequencing, qPCR, library preparation and bioanalyser protocols.
- Claudia Stellato, Payal Jain and Renan Correa for help learning mouse collection techniques.
- Anne Segonds-Pichon for help with statistics.
- Simon Andrews for help with Seqmonk and processing sequencing data.
- Stephen Bevan for help learning how to use ChromHMM.
- Renan Oliviera Corrêa, Anke Liebert, Joana Guedes, Claudia Stellato and Hélène Perée for help using organoids and providing materials.
- Juri Kazakevych and Payal Jain for mentoring.
- Michelle Linterman for feedback on reports and advice.
- Marco Aurélio Ramirez Vinolo for supervision and support whilst in Brazil.
- Patrick Varga-Weisz for help with experiments, scientific advice and supervision.

2) Data obtained from a technical service provider (e.g. DNA sequencing, illustrations, simple bioinformatics information etc.)

- DNA sequencing was performed by Kristina Tabbada and coworkers at the Babraham Sequencing Facility.
- Adaptor trimming and mapping of sequencing data was performed by the Babraham Bioinformatics Facility.
- ChIP-sequencing data on H3K27me3, H3K27ac, H3K4me1, H3K4me3 and H3K36me from adult liver was generated by Bing Ren and obtained from ENCODE.
- ChIP-sequencing data on H3K27me3, H3K27ac and H3K4me1 from adult colon was generated by Qin *et al.* (2018) and Lo *et al.* (2017) and obtained from GEO.

3) Data produced jointly (e.g. where it was necessary or desirable to have two pairs of hands)

- High fibre diet and antibiotic treatment experiments were performed with Marco Aurélio Ramirez Vinolo's group. Renan Oliviera Corrêa, José Luís Fachi, Fabio Takeo

Sato, Lais Pral, Bruna Karadi, Aline Vierira, Erica Sernaglia, Mariana Portovedo and Marina Caxias helped with tissue collection, processing and performed faecal bacterial colony analysis.

- Some western blots on cell culture extracts were performed with Hélène Perée.
- Organoid seeding was performed with Claudia Stellato and Anke Liebert.
- Renan Oliviera Corrêa produced the organoids for one of the western blots.
- Dietary restricted mice were provided by Linda Patridge's group.
- Germ-free butyrate treated mice were collected by José Luís Fachi.
- RNA-sequencing on antibiotics treated colons was performed jointly with Juri Kazakevych.
- Juri Kazakevych performed some of the western blots on mouse extracts.

4) Data/materials provided by someone else (e.g. one-off analysis, bioinformatics analysis, where parallel data or technical provision in a very different area is needed to provide a connected account of the thesis)

- Short chain fatty acid measurements were performed by Caroline Marcantonio Ferreira's group including Willian R. Ribeiro.
- Zoltán Hajnády and Szabina Balázsi helped with some *in vitro* enzymatic experiments.
- RNA-sequencing on HCT116 cells was performed by Claudia Stellato.
- Claudia Stellato and Payal Jain produced the H3K18cr ChIP-sequencing data in colon.
- Jeremy Denizot produced the H3K4me3 ChIP-sequencing data in colon
- Claudia Stellato performed RNA-sequencing on DMSO treated HCT116 cells.
- Payal Jain performed the H3K18cr ChIP-qPCR on small intestines of crotonic acid fed mice

Contents

List of figures and tables

List of abbreviations

β-HBu – β-hydroxybutyrate

ACAD – Short chain acyl-CoA dehydrogenase

ACLY – ATP citrate lyase

ACP – Acyl carrier protein

ACSS1 - Acyl-CoA synthetase short chain family member 1 (Also known as AceCS2)

ACSS2 – Acyl-CoA synthestase short chain family member 2 (Also known as AceCS1)

AMPK – Adenosine monophosphate-responsive protein kinase

BSA – Bovine serum albumin

bp – Base pairs

ChIP – Chromatin immunoprecipitation

ChIP-seq – ChIP sequencing

CDYL – Chromodomain Y-like protein

CoA – Coenzyme A

DPF – Double plant homodomain finger

EGF – Epidermal growth factor

FBS – Foetal bovine serum

H3K27me3 – Histone 3 lysine 27 trimethylation

H3K4me1 – Histone 3 lysine 4 monomethylation

HAT – Histone acetyltransferase

HBSS – Hank's balanced salt solution

HDAC – Histone deacetylase

HDCR – Histone decrotonylase

HIF – Hypoxia inducible factor

HRP – Horseradish peroxidase

hPTM – Histone post-translational modification

IEC – Intestinal epithelial cell

Kac – Lysine acetylation

Kbu – Lysine butyrylation

Kbz – Lysine benzoylation

Kcr – Lysine crotonylation

Kglu – Lysine glutarylation

Khib – Lysine 2-hydroxyisobutyrylation

Kmal – Lysine malonylation

Kpr – Lysine propionylation

Ksucc – Lysine succinylation

Kβ-HBu – Lysine β-hydroxybutyrylation

PBS – Phosphate buffered saline

PCAF – p300/CBP associated factor

PCR – Polymerase chain reaction

PDH – Pyruvate dehydrogenase

PDB – Protein database

PGAM1 – Phosphoglycerate mutase 1

PIC – Protease inhibitor cocktail

PKM1 – Pyruvate kinase isoform M1

PKM2 – Pyruvate kinase isoform M2

qPCR – Quantitative polymerase chain reaction

RNA-seq – RNA sequencing

RT – Room temperature

SAHA – Suberoyl anilide hydroxamic acid

SCFA – Short chain fatty acid

SOPF – Specific or pathogen free

SIRT – Sirtuin

TAF1(2) – Second bromodomain of TAF1

TCA – Tricarboxylic acid

TBS – Tris buffered saline

TSA – Trichostatin A

TSS – Transcription start site

1

1 Introduction

1.1 Epigenetics

1.1.1 The environment influences gene regulation

From its first beginnings identifying euchromatin and heterochromatin by staining cells over 100 years ago through to next generation sequencing today, the epigenetic field has transformed our understanding of the cell (Allis and Jenuwein, 2016). The meaning of the term epigenetics has changed over time, but an up to date definition is "the study of molecules and mechanisms that can perpetuate alternative gene activity states in the context of the same DNA sequence" (Cavalli and Heard, 2019). Epigenetic regulation enables an organism to respond and adapt to its environment. This is apparent in studies of monozygotic twins who diverge in phenotype and epigenotype over time, providing an opportunity to investigate how epigenetic variation influences complex traits (Bell and Spector, 2011). Epigenetic regulation has been implicated in a wide range of diseases, as any gene or set of genes can be affected (Cavalli and Heard, 2019).

1.1.2 Chromatin enables spatial organisation of the genome

Chromatin describes the complex of proteins, DNA and RNA found in the nucleus. If the DNA from all 46 human chromosomes were laid out end to end it would be approximately 2 meters long, but it must be packaged into the nucleus, which is typically 6 μM in diameter (Alberts *et al.*, 2015). Therefore, it is essential that the genetic material is well organised so that it can be contained in the nuclear space. The chromatin structure provides an elegant mechanism for fine control of gene expression. The basic unit is the histone octamer, containing pairs of histones H2A, H2B, H3 and H4. The DNA is coiled around the histone octamer in 147 base pair segments, with extensive DNA-histone contacts, to create the nucleosome as shown in Figure 1.1 (Alberts *et al.*, 2015). There are two types of chromatin. In heterochromatic regions, nucleosomes are densely packed, resulting in resistance to gene expression. Euchromatic regions are much less compact and are sites of actively expressed

genes. This spatial organisation is a key epigenetic regulator as genes can be turned on or off simply by changing the packaging between histones and DNA. Additionally, the chromatin can be remodelled to bring together distal genetic elements, for example, an enhancer and a promoter, to activate gene expression (Alberts *et al.*, 2015). Chromatin state can be influenced by many factors including DNA, RNA and histone modifications, non-coding RNA species, protein chaperones and chromatin remodelling enzymes.

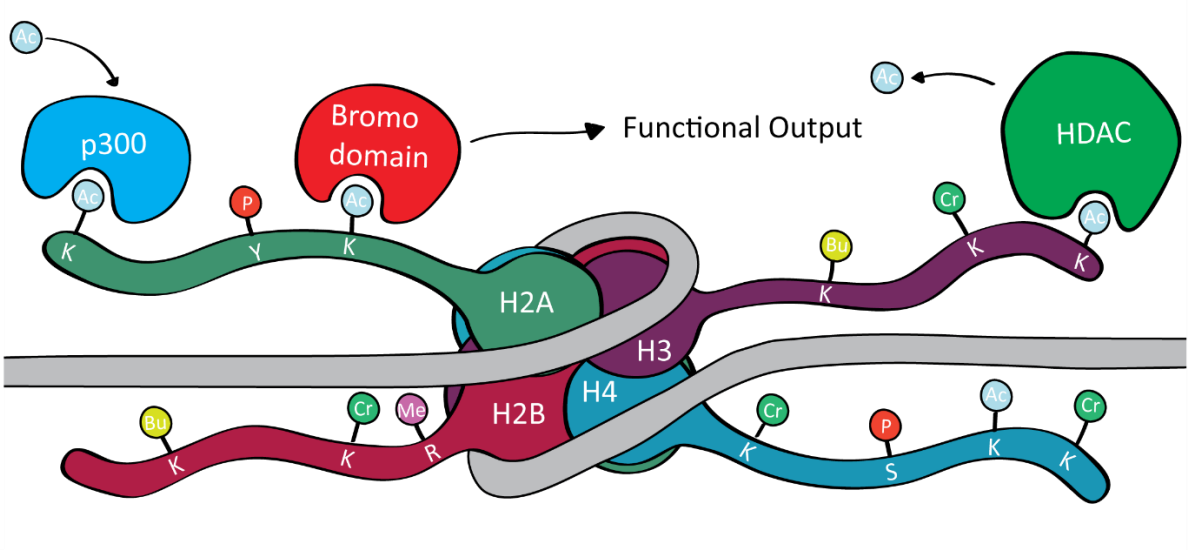

Figure 1.1. The nucleosome

The nucleosome is composed of an octamer of H2A, H2B, H3 and H4 histones which wrap 147 base pairs of DNA. Histones have an N-terminal region which can be extensively modified, for example with acetylation (Ac), phosphorylation (P), Butyrylation (Bu), Crotonylation (Cr) and methylation (Me). P300 is an acetyltransferase, bromodomains specifically recognise acetyl-groups and histone deacetylases (HDAC) remove them.

1.1.3 Histone modifications are linked to gene transcription and chromatin conformation

Due to their close contact with DNA, histone post-translational modifications (hPTM) are involved in DNA packaging and regulation of gene expression. Modifications to the core region of histones influence nucleosome stability, whilst modifications to lateral surface and histone tails change the association with DNA and interact with specific binding proteins. Histone tails are extensively modified with a range of chemical groups leading to the suggestion that this creates its own language with specific sets of modifications providing a 'code' for reader proteins to bind. Many specific hPTM binding proteins include chromatin remodelling enzymes which open or compact certain regions of the genome, transforming chromatin from a static to a dynamic structure. These enzymes use ATP as an energy source to enable the sliding or displacement of whole nucleosomes to neighbouring regions

to make the underlying DNA sequence more accessible (Tang *et al.*, 2010). Chromatin remodelling enzymes are both diverse and abundant in the cell with approximately one remodelling complex per 10 nucleosomes (Längst and Manelyte, 2015). Their targeting and regulation are finely tuned by multiple subunits that exist in complex with the catalytic subunit. These include histone and DNA binding modules which coordinate the nucleosome remodelling activity. A major family of ATP dependent chromatin remodellers are the SWI/SNF complexes which in humans includes the BAF and PBAF complexes (Tang *et al.*, 2010). Whilst some modifications are associated with euchromatin and others with heterochromatin, it is still unclear if these modifications are the direct cause or the consequence of changes to gene expression (Howe *et al.*, 2017). Despite their widely reported gene regulatory role and ability to act as binding platforms for factors involved in transcription or associated chromatin remodelling, it is still an unsolved issue whether changes to histone modifications occur prior or subsequently to the activation or repression of gene expression. This may limit our interpretation of studies on these epigenetic switches, but it does not negate their potentially important role in cellular processes.

1.1.4 Histone methylation

Histone methylation can occur as mono-, di- or tri- methylation depending on if there are one, two or three methyl groups added to the histone residue (Martin and Zhang, 2005). Methylation does not change the electronic charge of the histone but functionality is conferred by the binding of proteins which can distinguish between sites of methylation and number of methyl groups (Martin and Zhang, 2005; Musselman *et al.*, 2014). Histone methylation is associated with both active and repressive chromatin (Black *et al.*, 2012). Methylation of H3 lysine 9 (H3K9), H3K27 and H4K20 are associated with gene repression, whilst methylation of H3K4, H3K36 and H3K79 are associated with active genes (Hyun *et al.*, 2017). Different methylation states can have different distributions along the chromatin. H3K4me1 is present at enhancers, H3K4me2 at the 5’ end of transcribing genes and H3K4me3 at promoters of active and poised genes (Santos-Rosa *et al.*, 2002; Heintzman *et al.*, 2007; Mikkelsen *et al.*, 2007; Kim and Buratowski, 2009). A single methyltransferase, Set1, is responsible for all H3K4 methylation in yeast and it has 6 human homologs SET1A, SET1B and MLL1-4 (Shilatifard, 2012). H3K4 methylation is correlated with transcription but it is still unclear whether the addition of methylation preceeds changes to gene expression and how methyltransferase complexes are recruited to the histone (Howe *et al.*, 2017; Hyun *et al.*, 2017). Interestingly, mutations in MLL/KMT2 family of H3K4 methyltransferases increase likelihood of various types of cancer (Rao and Dou, 2015). H3K27 methylation is a paradym repressive modification and its misregulation is also associated with tumorigenesis (Hyun *et al.*, 2017). For example, higher levels of the H3K27 methyltransferase EZH2, a

polycomb group protein, was associated with increased progression of prostate cancer and worse survival rates (Varambally *et al.*, 2002). Since this study, EZH2 has been linked to other types of cancer and associated with alterations in cell migration, growth and invasion, resulting in the development of inhibitors against this enzyme (Bracken *et al.*, 2003; Kleer *et al.*, 2003; Velichutina *et al.*, 2010; McCabe *et al.*, 2017). H3K27 and H3K4 methylation can occur at the same sites, creating regions that are poised for activation. Switching between active, poised and repressed states is important in embryonic stem cells for differentiation into various cell types and enrichment of H3K4 and H3K27 methylation at the same sites was shown to be important in this process (Barski *et al.*, 2007; Mikkelsen *et al.*, 2007; Vastenhouw and Schier, 2012). Intriguinly, the H3K27 demethylase UTX/KDM6A and the H3K4 methyltransferase ALR/MLL2 are subunits of the same multi-subunit complex, enabling interaction between these two methylation marks (Issaeva *et al.*, 2007). Methylation of H3K9 is an important mark of silenced transcription and heterochromatin (Barski *et al.*, 2007). The G9a-GLP heterodimer can add mono- and di-methylation to H3K9 at euchromatic regions and then spread this mark to nearby nucleosomes to establish a repressive region. This mechanism is required for Oct3/4 and nanog silencing in embryonic stem cells to enable differentiation, which may explain why H3K9 methylation is often misregulated in cancer (Bittencourt *et al.*, 2014; Casciello *et al.*, 2015). H3K36 methylation occurs along the gene body and is thought to prevent erroneous initiation of transcription (Wagner and Carpenter, 2012). This mark is also implicated in inhibiting PRC2 mediated methylation of H3K27 to prevent the spread of a repressive chromatin environment and is involved in multiple pathways that repair damage to DNA (Pfister *et al.*, 2006; Fnu *et al.*, 2011; Kassam *et al.*, 2013).

1.1.5 Histone acetylation

1.1.5.1 The discovery of histone acetylation and its regulatory proteins

Histone acetylation and phosphorylation were discovered within four years of each other in 1959 and 1963 respectively (Fischer *et al.*, 1959; Phillips, 1963). However, due to technical challenges in studying acetylation, phosphorylation was the main focus for many years and was found to be a central regulator of signal transduction pathways, metabolism and other cellular processes (Verdin and Ott, 2015). Protein acetylation has now been identified in a diverse array of organisms from bacteria to humans and is linked to gene regulation (Allis and Jenuwein, 2016). It frequently occurs in structured domains and in highly conserved proteins such as metabolic enzymes, chaperones and ribosomes. This is in contrast to phosphorylation, which is often in unstructured regions of rapidly evolving proteins, giving insight into how the functions of these hPTMs may differ (Choudhary *et al.*, 2014). At least 22 histone acetyltransferases (HAT, also known as lysine acetyltransferase or KAT) have been identified which group into the GCN5, p300/CBP and MYST families. A large number of HDACs have been

identified which are grouped into class I (HDAC1-3 and HDAC8), class II (HDAC4-7 and HDAC9), class III sirtuins (SIRT1-7) and class IV (HDAC11). Classes I, II and IV HDACs share a similar structure and are zinc dependent whilst the class III SIRT use a distinct mechanism and rely on NAD+ as a cofactor (Choudhary *et al.*, 2014). HATs or HDACs are often present in multi-domain complexes which influence their activities, specificities and targeting to specific sites (Shahbazian and Grunstein, 2007). CBP, p300 and GCN5 all have bromodomains that read acetyl-groups to enable them to recognise specific sites on chromatin and coordinate transcription. In the human genome, 61 bromodomains are encoded, of which 29 have been characterised (Filippakopoulos *et al.*, 2012). Plant homeodomain and YEATS domain containing proteins have also been found to be acetyl readers (Lange *et al.*, 2008; Li *et al.*, 2014). Interestingly, most HATs and acetyl-binding domain-containing proteins are found predominantly in the nucleus (Choudhary *et al.*, 2014).

1.1.5.2 The diverse roles of histone acetylation

Histone acetylation is associated with regions of active transcription and is thought to act through two main mechanisms (Choudhary *et al.*, 2014). Acetylation neutralises the positively charged lysine to reduce attraction towards the negatively charged DNA, enabling loosening of the chromatin. Acetylation of histone tail residues also allows the recruitment of specific proteins, such as those involved in transcription or chromatin remodelling (Allis and Jenuwein, 2016). Histone acetylation is thought to be important for the recruitment or stabilisation of the SWI/SNF complex to enable chromatin remodelling, for example as part of double strand break repair (Hassan *et al.*, 2001; Agalioti *et al.*, 2002; Ogiwara *et al.*, 2011). During this process, the general transcription factor TFIID makes multiple contacts with the DNA and chromatin to stabilise its interaction with the promoter and facilitate formation of the preinitiation complex. TFIID binding is enabled by multiple subunits, TBP binds the TATA box on the DNA, TAF3 binds H3K4me3 and TAF1 can bind acetylated histones (Krasnov *et al.*, 2016). In fact, the mouse homolog of TAF1 Brdt, an essential factor for male genome programming in meiotic and haploid cells, requires hyperacetylation of H4 at both lysines 5 and 8 to be able to bind (Morinière *et al.*, 2009; Gaucher *et al.*, 2012). In addition, the presence of H3K4me3, TATA box and H3K14ac were found to have synergistic effects on binding, demonstrating the combinatorial nature of these protein binding sites (van Nuland *et al.*, 2013). In yeast, the HAT Sas2, establishes an increasing gradient of H4K16ac away from the telomeres, whilst Sir2 removes H4K16ac to generate a compact chromatin environment at the telomere (Kimura *et al.*, 2002). Interestingly, H4K16ac is associated with DNA damage repair and senescence (Dang *et al.*, 2009; Li *et al.*, 2010; Sharma *et al.*, 2010; Krishnan *et al.*, 2011).

H3 and H4 acetylation have different effects on the stability of the nucleosome. H3 acetylation was found to make the nucleosome more susceptible to salt induced dissociation whilst H4 acetylation

counteracted this (Gansen *et al.*, 2015). Broad H3/H4 acetylation renders a region permissive to the action of cellular machinery involved in transcription and chromatin modulation but activation of gene expression often requires targeted acetylation at the promoters of genes (Eberharter and Becker, 2002). Furthermore, acetylation at different residues of the histone tail can have different functions. This could be because different enzymes are responsible for their addition, recognition and removal. For example, deletion of PCAF/GCN5 ablated H3K9ac whilst deletion of p300/CBP reduced H3K27ac/H3K18ac (Jin *et al.*, 2011). H4K12ac was found to increase in macrophage determined dendritic cells after chronic alcohol exposure. Use of a specific inhibitor for the HAT Tip60 reduced H4K12ac as well as upregulating cytokines such as ICAM, IL-6 and IL-10 (Parira *et al.*, 2017). Diacetylation of H4K5 and H4K12 occurs prior to nucleosome assembly and these modifications are therefore associated with newly assembled chromatin (Sobel *et al.*, 1995; Chang *et al.*, 1997). H3K27ac was shown to have a robust circadian rhythm along with H3K4me3, H3K9ac and recruitment of RNAPII (Takahashi, 2015).

1.1.5.3 The control, distribution and function of H4K8 acetylation

H4K8ac is relatively under-studied compared to other acetyl-marks. However, it is associated with active genes and various functions have been attributed to this modification. In a study which profiled 39 different acetylation and methylation marks in CD4+ T cells, H4K8ac was found to be elevated in the promoter and transcribed regions of active genes along with H4K5, H4K12 and H4K16 acetylations. Acetylations of H3K18 and H3K27, amongst others, were mainly associated with transcription start sites. Interestingly, H4K8ac associated with around 12 % of enhancers, compared to 17 % for H3K27ac and 32 % for H3K4me1 (Wang *et al.*, 2008). A more recent study found that H4K8ac and H4K16ac were associated with transcription start sites (TSS) in embryonic stem cells at active genes that also contained H3K27ac, but with a slightly broader distribution. H3K27ac, H4K8ac and H4K16ac were correlated, with the tightest association being between acetylation at H4K8 and H4K16. Contrastingly, H4K5 and H4K12 acetylation were depleted around the TSS (Hayashi-Takanaka *et al.*, 2015). Fascinatingly, Li *et al.* (2019) showed that both H4K8ac and H3K27ac are found at a novel class of super enhancers, a genomic feature that is implicated in tumourigenesis and is also marked by H3K4me3. GCN5/PCAF is responsible for acetylation of H4K8 (Kuo *et al.*, 1996; Cieniewicz *et al.*, 2014). During the initiation of human IFN-β transcription, the enhanceosome recruits GCN5 resulting in acetylation of H4K8 and H3K9. H4K8ac is required for SWI/SNF binding, whilst H3K9ac, H3K14ac and H3S10 phosphorylation mediate TFIID binding (Agalioti *et al.*, 2002; Ford and Thanos, 2010). A study of Ras-mediated transformation of normal cells into cancerous cells found that the HAT Tip60 increased in Ras-transformed cells along with global upregulation of H4K8ac and H4K12ac. In another investigation, H2BK5, H2BK15, H3K9, H3K18, and H4K8 acetylations were increased upon Response

Gene to Complement-32 knockdown, a gene associated with the progression of colon cancer (Vlaicu *et al.*, 2010). Additionally, H4K8ac has been shown to be a major regulator of transcription changes mediated by chromatin during the life cycle of *Plasmodium falciparum* and was associated with both euchromatin and heterochromatin. H4K8ac was the most responsive to HDAC inhibitors of the H4 acetylations tested (Gupta *et al.*, 2017).

1.1.5.4 The functions of non-histone acetylation

Acetylation of non-histone proteins can also influence transcription. Tat is a HIV protein that is rate limiting for viral replication. The non-acetylated form binds to the HIV RNA stem loop structure of the transactivating response element, which results in increased RNA polymerase processivity. Acetylated Tat instead binds to the transcriptional co-activator PCAF, which promotes association of Tat with RNA polymerase II and HIV gene transcription (Dorr *et al.*, 2002; Mujtaba *et al.*, 2002). Acetylation can influence protein function by changing the subcellular location of that protein (Drazic *et al.*, 2016). This is because the subcellular localisation domain of a protein often contains lysine residues (Choudhary *et al.*, 2014). Lysines are actually one of the most frequently modified amino acids and can accommodate many different types of hPTM (Choudhary *et al.*, 2014). For example, glyceraldehyde-3-phosphate dehydrogenase catalyses an intermediate step in glycolysis in the cytoplasm, converting glyceraldehyde-3-phosphate into 1,3-bisphosphoglycerate. It can translocate to the nucleus, as a result of acetylation of three lysine residues by PCAF, to regulate transcription and DNA repair (Ventura *et al.*, 2010). Finally, acetylation can also change enzymatic activity as many residues present in the catalytic active sites are lysines. This can have opposing effects. For example, acetylation of acyl-CoA synthetase short chain family member 1 (ACSS1) is inactivating whilst phosphoglycerate mutase 1 (PGAM1) acetylation enhances its activity. SIRT HDACs counteract this acetylation. SIRT3 removes acetyl groups from ACSS1, whilst when glucose is restricted SIRT1 is upregulated to deacetylate PGAM1. As PGAM1 is an enzyme involved in glycolysis, acetylation may be used to modulate enzyme activity in a feedback mechanism to respond to changing conditions. A further interesting point is that p300/CBP can be autoacetylated, an activity which appears to be dependent on its dimerization and is reversed by SIRT2 (Choudhary *et al.*, 2014).

1.1.6 Histone modifications mark regulatory elements

Promoters and enhancers are sequences of DNA that enable gene expression by providing binding sites for transcription factors and transcriptional machinery. Promoter regions are upstream of the TSS and are the site of binding for RNA polymerases and transcription factors (Voet and Voet, 2011). Unlike prokaryotes which have a distinct sequence motif of TATAAT at around -10 and TTGACA at -35 positions from the TSS (Harley and Reynolds, 1987), the architecture of eukaryotic promoter regions

is more complex. Enhancers are found in non-coding regions of the genome, outside genes and in introns, and act to facilitate or enhance gene expression. For example, a typical β-globin gene contains two upstream elements, in addition to a promoter, which are bound to transcription factors and required to achieve normal levels of expression of β-globin (Voet and Voet, 2011). Enhancers can be many kilobases away upstream or downstream from the gene they regulate and also lack a consensus sequence. Hundreds of thousands of enhancer regions have been identified, far more than the around 20,000 protein-encoding human genes, but not all were found to have enhancer function in transgenic assays. Many of these regions were identified due to their sequence conservation but these could have alternative functions to enhancers or play a role in a different stage of development to the time points that were assayed (Pennacchio *et al.*, 2015).

There is increasing evidence to suggest that promoters and enhancers have a defined chromatin state which can be used to identify them in different cell types and under different conditions. Heintzman *et al.* (2007) profiled different histone modifications by chromatin immunoprecipitation (ChIP) at promoters and enhancers. They identified that both contain a nucleosome depleted region and are enriched for histone acetylation and H3K4 methylation. In a pioneering study, H3K4me1 was found to be a hallmark of distal enhancer elements, whilst H3K4me3 defined promoter regions (Heintzman *et al.*, 2007). Current evidence still suggests that enhancers have high H3K4me1 and promoters have high H3K4me3 (Sharifi-Zarchi *et al.*, 2017), but the situation is in fact more nuanced as H3K4me1 is also at large 5' portions of actively transcribed genes (Calo and Wysocka, 2013), whilst H3K4me3 was found to mark active enhancers in developing T and B lymphocytes (Pekowska *et al.*, 2011). The distribution of H3K4me1 is broad in non-coding regions (Calo and Wysocka, 2013) and is thought to mark developmental enhancers in human or mouse embryonic stem cells prior to their activation (Creyghton *et al.*, 2010; Rada-Iglesias *et al.*, 2011; Zentner *et al.*, 2011).

It has been suggested that the presence of H3K27ac, which is typically combined with H3K4me1, distinguishes active from inactive enhancers (Bonn *et al.*, 2012; Zhu *et al.*, 2013; Andersson *et al.*, 2014). Interestingly, using H3K27ac containing enhancers enabled a better prediction of developmental state than using enhancers that contained only H3K4me1 (Creyghton *et al.*, 2010). Two-thirds of H3K27ac containing enhancers showed activity in transgenic assays (Nord *et al.*, 2013). Poised enhancers also exist which contain H3K27me3 and H3K4me1 but not H3K27ac (Rada-Iglesias *et al.*, 2011; Zentner *et al.*, 2011). Whilst these three modifications have been the particular focus for characterising these genetic elements, it is likely that other marks are also present. P300/CBP binding is associated with enhancers (Visel *et al.*, 2009; Creyghton *et al.*, 2010) and this enzyme can add acetyl-groups to H3K27 or H3K18 (Jin *et al.*, 2011). In addition, H3K9ac and histone crotonylation have been detected at putitative enhancers (Ernst *et al.*, 2011; Tan *et al.*, 2011).

1.1.7 The histone acylation family

Histone acetylation is now part of a growing group of hPTMs called histone acylations which are of interest due to their potential to bridge cellular metabolism and epigenetic regulation (Zhao *et al.*, 2017). The different structural properties, binding proteins and suggested functions of this family are shown in Table 1.1. Lysine acetylation (Kac), propionylation (Kpr) and butyrylation (Kbu), contain short saturated fatty acyl chains of 2, 3 and 4 carbons respectively (Zhang *et al.*, 2009). Lysine crotonylation (Kcr) is more rigid due to a double bond which gives it a flat planar structure (Tan *et al.*, 2011). They can be derived from the short chain fatty acids (SCFA) acetate, propionate, butyrate and crotonate. There are also the hydroxylated modification β-hydroxybutyrylation (Kβ-HBu); the acidic modifications of malonylation (Kmal), succinylation (Ksucc) and glutarylation (Kglu); the branched modification hydroxyisobutyrylation (Khib); and the aromatic benzoylation (Kbz) amongst others (Du *et al.*, 2011; Peng *et al.*, 2011; Z. Zhang *et al.*, 2011; Dai *et al.*, 2014; Tan *et al.*, 2014; Xie *et al.*, 2016; Huang, Zhang, *et al.*, 2018). In some cases, these hPTMs are only a few atoms different, for example crotonylation has two less methyl hydrogen atoms than butyrylation.

Modification	Structure	Properties	Writer	Reader	Eraser	Function
Acetylation Kac		Hydrophobic	p300 (CBP, p300), MYST (Tip60, MOF, MOZ, HBO1), GCN5 (GCN5, PCAF) [1]	Bromodomain (BRD2, BRD9, TAF1, CECR2), PHD (MOZ, DPF2) and YEATS (AF9, YEATS2) [2]	Zn^{2+} dependent (HDAC1-11), NAD^+ dependent (SIRT1-7) [3]	Involved in multiple biological processes including transcription regulation, cell differentiation, regulation of mitochondrial enzymes and organismal development. [4]
Propionylation Kpr	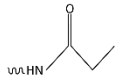	Hydrophobic	p300/CBP, PCAF, GCN5 , MOF, HBO1, MOZ [5]	Most BRDs (CECR2, BRD2-4,7,9, TAF1), MOZ, DPF2, AF9 YEATS2 [6]	SIRT1/2/3 [7]	Stimulates transcription *in vitro* and is enriched at promoters of active genes. Responsive to changes in metabolic state at popionyl-CoA levels. [8]
Butyrylation Kbu	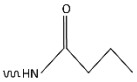	Hydrophobic	p300/CBP, PCAF, GCN5 [9]	TAF1(2), BRD7, BRD9, CECR2, MOZ, DPF2, AF9 YEATS2 [10]	SIRT1/2/3 [11]	Stimulates transcription *in vitro*. Involved in histone replacement during spermatogenesis. Prevents binding of testes specific gene expression driver BRDT. [12]
Crotonylation Kcr	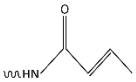	Hydrophobic	p300/CBP, MOF [13]	TAF1(2), AF9, YEATS2, MOZ, DPF2 [14]	HDAC1-3, SIRT1/2/3 [15]	Stimulates transcription *in vitro*, marks escapee genes during spermatogenesis. Link to pluripotency maintentance, cell cycle, DNA damage repair, cancer progression, HIV reactivation, kidney injury, depression and Alzheimer's disease. [16]
β-Hydroxybutyrylation Kβ-Hbu	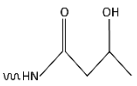	Polar	p300/CBP [17]	MOZ, DPF2 [18]	HDAC3, SIRT3 [19]	Associated with transcription activation. Involved in adaptation to cellular energy state including response to starvation and ketone body metabolism. Triggered by starvation and ketoacidosis. [20]
Malonylation Kmal	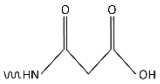	Acidic			SIRT5 [21]	Malonylation of yeast H2A leads to a defect in chromosome segragation. [22]
Succinylation Ksucc	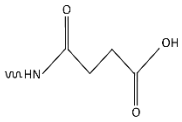	Acidic	p300/CBP, GCN5 [23]	GAS41 (YEATS) [24]	SIRT5-7 [25]	Hypersuccinylation results in defects in DNA repair. Responsive to dietary manipulation. [26]
Glutarylation Kglu	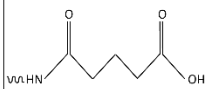	Acidic	p300/CBP [27]		SIRT5 [28]	Nutrient regulated, impacts metabolic processes and other mictochondrial functions. Upregulated in glutaric acidemia. [29]
2-Hydoxyisobutyrylation Khib	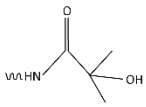	Branched Polar	p300, Tip60 [30]	MOZ, DPF2, YEATS2 [31]	HDAC1/2/3 [32]	Positively associated with gene expression. Marks escapee genes in post-meiotic sperm cells [33]
Benzoylation Kbz	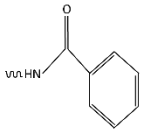	Aromatic Hydrophobic			SIRT2 [34]	Possibly a biproduct of using the food preservative sodium benzoate. [35]

Table 1.1. The histone acylation family

The structures, chemical properties, acyltransferases (writers), binding proteins (readers), deacylases (erasers) and functions currently attributed to many members of the histone acylation family are shown. [1] (Berndsen and Denu, 2008), [2] (Lange *et al.*, 2008; Filippakopoulos and Knapp, 2012; Li *et al.*, 2014), [3] (Choudhary *et al.*, 2014), [4] (Haberland *et al.*, 2009; Voss and Thomas, 2009; Allis and Jenuwein, 2016; Blasi *et al.*, 2016), [5] (Chen *et al.*, 2007; Montgomery *et al.*, 2014; Kebede *et al.*, 2017; Han *et al.*, 2018), [6] (Flynn *et al.*, 2015; Xiong *et al.*, 2016; Y. Li *et al.*, 2016; Zhang *et al.*, 2016; Zhao *et al.*, 2016), [7] (Feldman *et al.*, 2013), [8] (Kebede *et al.*, 2017), [9] (Chen *et al.*, 2007; Montgomery *et al.*, 2014; Goudarzi *et al.*, 2016; Kebede *et al.*, 2017), [10] (Flynn *et al.*, 2015; Xiong *et al.*, 2016; Y. Li *et al.*, 2016; Zhang *et al.*, 2016; Zhao *et al.*, 2016), [11] (Feldman *et al.*, 2013), [12] (Goudarzi *et al.*, 2016; Kebede *et al.*, 2017; S. Liu *et al.*, 2017), [13] (Sabari *et al.*, 2015; X. Liu *et al.*, 2017), [14] (Flynn *et al.*, 2015; Andrews *et al.*, 2016; Xiong *et al.*, 2016; Y. Li *et al.*, 2016; Zhang *et al.*, 2016; Zhao *et al.*, 2016), [15] (Madsen and Olsen, 2012; Bao *et al.*, 2014), [16] (Tan *et al.*, 2011; Sin *et al.*, 2012; Montellier *et al.*, 2012;

Sabari *et al.*, 2015; Ruiz-Andres *et al.*, 2016; S. Liu *et al.*, 2017; Fellows *et al.*, 2018; Jiang *et al.*, 2018; Abu-Zhayia *et al.*, 2019; Wang *et al.*, 2019; Wan *et al.*, 2019), [17] (Kaczmarska *et al.*, 2017), [18] (Xiong *et al.*, 2016), [19] (Zhao *et al.*, 2018; Zhang *et al.*, 2019), [20] (Xie *et al.*, 2016), [21] (Peng *et al.*, 2011), [22] (Ishiguro *et al.*, 2018), [23] (Wang *et al.*, 2017), [24] (Y. Wang *et al.*, 2018), [25] (Peng *et al.*, 2011; Park *et al.*, 2013; L. Li *et al.*, 2016), [26] (Tan *et al.*, 2014; L. Li *et al.*, 2016; Smestad *et al.*, 2018), [27-29] (Tan *et al.*, 2014), [30] (Huang, Luo, *et al.*, 2018; Huang, Tang, *et al.*, 2018), [31] (Xiong *et al.*, 2016; Zhao *et al.*, 2016), [32] (Dai *et al.*, 2014; Huang, Luo, *et al.*, 2018), [33] (Dai *et al.*, 2014) and [34-35] (Huang, Zhang, *et al.*, 2018).

1.1.8 Histone crotonylation and its role in transcription and cellular functions

Kcr was first identified by Tan and colleagues using unbiased mass spectrometry methods and is present in yeast, *C. elegans*, *D. melanogaster*, mouse and human, suggesting that it is evolutionarily conserved. Kcr occurs on all core histones at 28 different sites, and while some overlap with Kac sites, there are many sites where only Kcr occurs (Tan *et al.*, 2011). The precursor of crotonylation, crotonyl-CoA is around three orders of magnitude lower in concentration in the cytoplasm of HeLa S3 cells than acetyl-CoA, suggesting that crotonylation would be less abundant than acetylation in these cells (Sabari *et al.*, 2015). In line with this, our group found that crotonylation was present at H3K18 on around 2% of H3 histones in small intestinal crypt and colon compared to 20% of H3 histones containing acetylation at H3K18. Interestingly, H3K18cr in the colon always occurred with H3K23ac, suggesting an interaction between these two modifications (Fellows *et al.*, 2018). Despite its lower abundance than acetylation, crotonylation is therefore not a trace modification. Kcr was found to be mainly associated with active chromatin, including at TSS, putative enhancers, regions with higher H3K4me3 and is positively correlated with transcript levels (Hawkins *et al.*, 2010; Tan *et al.*, 2011; Fellows *et al.*, 2018). Interestingly, Sabari and colleagues found that p300 catalysed crotonylation could directly activate transcription of p53 to a greater extent than acetylation in a cell free assay (Sabari *et al.*, 2015). Together this evidence suggests that is associated with regions of active gene expression and could potentially be involved in their regulation.

Crotonylation has been linked to a growing number of cellular processes and disease states including the cell cycle, kidney injury, carcinogenesis, HIV reactivation and even depression (Ruiz-Andres *et al.*, 2016; S. Liu *et al.*, 2017; Fellows *et al.*, 2018; Jiang *et al.*, 2018; Wan, Liu and Ming, 2019). During spermatogenesis, spermatocytes undergo meiotic division to produce the haploid round spermatids which then form the highly specialised spermatozoa (Neto *et al.*, 2016). As part of this the single X chromosome is inactivated but some genes have been shown to escape this process (Yan and McCarrey, 2009). Tan *et al.* (2011) identified that the majority of genes with higher Kcr at the promoter in round spermatids than spermatocytes were activated after meiosis. These genes were more highly

expressed in adult mouse testes and were preferentially associated with the X and Y chromosomes. They suggested that Kcr marked a subset of genes that escape meiotic sex chromosome inactivation after meiosis, suggesting that it could sustain gene expression in a repressive environment (Tan *et al.*, 2011). This accumulation of Kcr at the TSS of sex linked genes was found to be dependent on RNF8, a DNA damage response factor involved in epigenetic reprogramming of escapee genes in post-meiotic spermatids (Sin *et al.*, 2012). Kcr was found to increase in a model of acute kidney injury at promoters of stress-induced genes, which also showed increased expression levels. Crotonate pre-treatment increased expression of these genes and was protective against acute kidney injury (Ruiz-Andres *et al.*, 2016). Our group identified that histone crotonylation is linked to the cell cycle, being upregulated in S and G2-M phase over G1 arrested cells. HDACs were implicated in the regulation of crotonylation during the cell cycle as the HDAC inhibitor MS725 prevented the downregulation of histone crotonylation that occured on G1 arrest (Fellows *et al.*, 2018). HDACs were also implicated in regulating crotonylation in hepatocellular carcinoma cell lines as upregulation of histone crotonylation occurred on HDAC1 or HDAC3 knock-down, reducing cell migration ability and suppressing proliferation. Histone crotonylation was upregulated in colon carcinoma, but reduced in hepatocellular carcinoma, suggesting that the levels of this modification in cancer are context dependent (Wan *et al.*, 2019). A different study found that H3K9cr was downregulated on UV or radiation induced DNA damage. This reduction was mediated by class I, II and IV HDACs, which have been previously shown to localise at sites of DNA damage and regulate histone acetylation to promote DNA double-strand break repair (Miller *et al.*, 2010; Abu-Zhayia *et al.*, 2019). In plants, acetylation, crotonylation and butyrylation at H3K9 have been shown co-occur at the promoters of a large number of active genes and are affected by submergence and starvation. H3K9ac appeared more responsive to these environmental changes than H3K9cr or H3K9bu (Lu *et al.*, 2018).

Histone crotonylation was recently implicated in the context of HIV, where immune cells with transcriptionally silent HIV-1 escape detection by the immune system. Kcr was found to mark the long terminal repeat in the HIV gene to regulate its transcription, in a mechanism mediated by Acyl-CoA synthetase short chain family member 2 (ACSS2). Promoting Kcr at the long terminal repeat of HIV led to reactivation of latent HIV and Kcr was proposed as a novel target in strategies for HIV eradication (Jiang *et al.*, 2018). Other recent evidence suggests that histone crotonylation is involved in Alzheimer's disease. NEAT1 was shown to regulate the transcription of endocytosis regulated genes involved in the clearance of β-amyloid by neuroglial cells. The accumulation of β-amyloid plaques in neural cells is thought to be involved in the neurodegeneration seen in Alzheimer's disease. NEAT1 was found to mediate increased H3K27ac but reduced H3K27cr, as a result of altering acetyl-CoA

generation, to regulate the expression of endocytosis related genes. NEAT1 interacted with p300/CBP resulting in autoacetylation of p300, which enhances its activity, and with the transcription factor STAT3, which bound H3K27ac but not H3K27cr (Wang *et al.*, 2019).

1.1.9 The function of other types of histone acylation

Chen *et al.* (2007) identified histone Kbu and Kpr as novel *in vivo* modifications. They suggested that as the precursors of Kbu and Kpr, butyryl-CoA and propionyl-CoA, are important metabolites and because these histone acylations cause distinct structural changes to the histone, that they are likely to have an important function in biological processes separate from that of other hPTMs (Chen *et al.*, 2007). Kbu and Kpr were associated with active chromatin in mouse liver and could promote gene expression of a chromatinized template in an *in vitro* transcription system (Goudarzi *et al.*, 2016; Kebede *et al.*, 2017). Butyrylation competed with acetylation at H4K5 and H4K8 to prevent binding of the testes specific transcriptional activator BRDT, resulting in delayed histone removal. Rapid turnover of acetyl and butyryl marks may result in dynamic association of BRDT with chromatin. This could facilitate the replacement of histone with the non-histone sperm-specific transition proteins and protamines, which occurs in late spermatogenesis and is dependent on BRDT (Goudarzi *et al.*, 2016). H4K8hib was also implicated in spermatogenesis as it showed more intense labelling in elongating spermatids than spermatocytes, similar to the pattern of H4K8ac. Both H4K8hib and H4K8ac were enriched at TSS of genes and preferentially associated with sex chromosomes, but H4K8hib was a better marker of transcriptional activity in round spermatids and spermatocytes than H4K8ac. Interestingly, nearly all sex-linked H4K8hib genes also had Kcr but none of them had Kac (Dai *et al.*, 2014).

1.1.10 Histone acyltransferases

The identification of acyl readers and modifiers for these novel histone acylations is important, as it enables researchers to learn more about their cellular functions. To investigate if known HATs have the capacity to use larger acyl chains, Simithy *et al.* (2017) used mass spectrometry to analyse the relative transfer of different acyl-CoAs by CBP, p300, GCN5 and PCAF on recombinant H3, and by MOF, Tip60 and NatA on recombinant H4. They found that most could use acetyl-, propionyl- and butyryl-CoA efficiently. The activity reduced with longer and more acidic acyl chain length with the exception of crotonyl-CoA which was least preferred due to its rigid and planar carbon-carbon double bond. PCAF and p300 had the highest crotonylation activities on H3. However, in equimolar competition assays, the HAT enzymes preferred to use acetyl-CoA (Simithy *et al.*, 2017). Other studies have shown that P300/CBP can add propionyl-, butyryl- and crotonyl-groups to histones and H3K18 was found to

be the dominant site of histone crotonyltransferase and HAT activity. (Chen *et al.*, 2007; Sabari *et al.*, 2015).

Many HATs exist in multi-subunit complexes which enhance catalytic activity and direct the enzyme to specific regions of the genome (Shahbazian and Grunstein, 2007). Whilst p300 does not require a helper protein it may require accessory proteins to restrict its access to unintended targets (Berndsen and Denu, 2008). Mutants of p300 and CBP with histone crotonyltransferase but not HAT activity were found to enhance transcription in a luciferase reporter assay relative to wild type p300/CBP. This was associated with increased histone crotonylation at promoters and recruitment of histone crotonylation readers (X. Liu *et al.*, 2017). The HAT enzymes GCN5 and PCAF can propionylate and butyrylate histones, although butyryl group transfer is less efficient than acetyl group transfer (Leemhuis, Packman, *et al.*, 2008; Ringel and Wolberger, 2016). It seemed that increasing acyl chain length was prohibitory to these enzyme's activity, as GCN5, PCAF, TIP60 and HBO1 showed no increase in histone crotonylation levels when they were transfected into cells (X. Liu *et al.*, 2017). MOF and its yeast homologue Esa1 can crotonylate histones *in vivo*. However, whilst Esa1 was shown to be responsible for the majority of histone crotonylation in yeast cells, it was p300/CBP that contributed to the bulk of crotonylation in human HeLa cells (X. Liu *et al.*, 2017).

1.1.11 Non-enzymatic acylation

The mechanism of acetylation by GCN5 involves deprotonation of a lysine residue, which enables it to act as a nucleophile towards the electrophilic group of the carbonyl-CoA. In fact, deprotonation of lysines is pH dependent and at alkaline pH, lysine acetylation can occur without GCN5 (Tanner *et al.*, 1999). Reproducing the high acetyl-CoA concentrations and alkaline pH found in the mitochondria was sufficient to cause non-enzymatic acylation of mitochondrial and non-mitochondrial proteins (Wagner and Payne, 2013). The high energy thioester bond in between the acyl and the CoA group is intrinsically reactive towards nucleophiles and thought to enable non-enzymatic acylation (Wagner and Hirschey, 2014). Interestingly, certain sites are more susceptible to non-enzymatic acylation, as incubation of recombinant H3 and H4 with supraphysiological levels of acyl-CoA resulted in more acylation at the globular and C-terminal domains of histones. Acidic acylations, such as Kmal and Kglu were the most easily transferred to histones in the absence of enzymes. In contrast, HATs preferred residues in the N-terminal tails of histones, which could be due to their increased accessibility relative to other residues on the histone (Simithy *et al.*, 2017). Therefore, cellular histone acylation may be a combination of both enzymatic and non-enzymatic acylation.

The stoichiometry, i.e. abundance relative to total available sites, of most cellular protein acetylation sites is low. In yeast, 86% of acetylation sites have less than 1% stoichiometry. The most abundant sites are on histones, HDAC and HAT complexes and transcription factors, supporting the role of action of regulatory enzymes at these sites (Weinert *et al.*, 2014). In has been proposed that non-enzymatic protein acylation could be due to the accumulation of intrinsically reactive metabolic intermediates in periods of stress to alter protein function and cellular homeostasis. This 'carbon stress' could function in a similar way to oxidative stress, in which reactive oxygen species are generated as an inherent part of metabolism and are prevented from accumulating in the cell by various mechanisms. One example of carbon stress is in diabetes, where the accumulation of aldehyde containing sugars in the blood causes non-enzymatic glycation and formation of advanced glycation end products which interfere with protein function and cellular signalling to promote disease pathophysiology, including cardiovascular and retinal complications. The NAD+ dependent SIRT HDACs have been implicated in metabolic homeostasis, resistance to stress and prolonging lifespan among other favourable cellular processes (Wagner and Hirschey, 2014). The loss or ablation of SIRT3 was shown to increase mitochondrial protein acetylation and lead to the acceleration or development of disease states including hearing loss, metabolic syndrome and cardiac hypertrophy (Hafner *et al.*, 2010; Someya *et al.*, 2010; Hirschey *et al.*, 2011). The effect of protein acetylation has been shown to be inhibitory, particularly for energy producing processes in the mitochondria (Ghanta *et al.*, 2013). Therefore, these novel protein modifications could be important for modulating protein function and metabolism in periods of cellular stress associated with disease states. Alternatively, accumulation of protein modifications could simply be a consequence of increased cellular stress.

1.1.12 Histone decrotonylases

1.1.12.1 The SIRT histone deacetylases

SIRT1-3 were found to catalyse the hydrolysis of lysine crotonylated peptides *in vitro* but only SIRT3 was found to have activity in cells. This study suggested that the HDAC and histone decrotonylase (HDCR) activity of these enzymes uses the same mechanism (Bao *et al.*, 2014). Contrastingly, another study in cells found that SIRT1 had both HDAC and HDCR activity, but no HDCR activity could be detected for SIRT2-5 and SIRT7 (Wei, Liu, *et al.*, 2017). This difference could be due to the varying sensitivities of the assays used, but these results do show that some SIRT enzymes have HDCR activity *in vivo*. Investigation of the structure of SIRT3 in complex with H4K5cr showed that it is present in a shallow binding pocket, stabilised by hydrogen bonding and aromatic/hydrophobic interactions. Much of the crotonyl side chain is exposed to the solvent which may explain the relatively low affinity, as determined by isothermal titration calorimetry (Bao *et al.*, 2014; Zhang *et al.*, 2016). Other SIRT

enzymes can use non-acetyl acylations. SIRT5 was shown using liquid chromatography/mass spectrometry to efficiently hydrolyse Ksucc or Kmal peptides (Du *et al.*, 2011). Using a flurorescent assay, SIRT5 was also shown to remove glutaryl groups, whilst other HDACs could not (Tan *et al.*, 2014). SIRT6 could efficiently remove myristoyl groups from H3K9 peptides and from tumour necrosis factor alpha with higher efficiency than acetyl groups, as monitored by liquid chromatography (Jiang *et al.*, 2013).

1.1.12.2 Class I, II and IV histone deacetylases

Initial comparison of the HDCR and HDAC capability of class I, II and IV HDAC enzymes in a fluorometric assay found that these enzymes had weak or no HDCR activity. The authors proposed that the inability of HDACs to decrotonylate histones could functionally distinguish acetylation from crotonylation which have common transferase enzymes (Tan *et al.*, 2011). However, whilst considerably lower than the HDAC activity, the HDCR activity of HDAC1, 2 and 3 in this assay was above that of background (Tan *et al.*, 2011). Another *in vitro* fluorometric assay of HDAC3 in combination with the NCoR1 complex showed that this enzyme did have HDCR activity *in vitro*. Although this was considerably lower than its HDAC activity, the authors commented that this was in the same range of efficiency as the deacetylase activity of HDAC8 and HDAC11 (Madsen and Olsen, 2012). A more recent study showed that the class I enzymes HDAC1, HDAC2, HDAC3 and HDAC8, but none of the class II or class IV enzymes, had decrotonylase activity in embryonic stem cells using an immunofluorescence approach (Wei, Liu, *et al.*, 2017). Knockdown of HDAC1/2/3 in combination by RNA silencing in cervical/uterine cancer HeLa S3 cells revealed a dramatic increase in histone crotonylation and acetylation whilst knockdown of SIRT1/3/5 in combination did not noticeably affect either modification (Wei, Liu, *et al.*, 2017). This suggests that class I HDACs are the major histone decrotonylases in cell culture.

Class I HDACs are found in multiprotein complexes, which in mammals are the Sin3, NuRD, CoREST and NCoR/SMRT complexes. These complexes are highly conserved and have been shown to function in distinct cellular processes including cell cycle regulation, maintenance of stem cell pluripotency and cellular differentiation (Hayakawa and Nakayama, 2011). Multi-subunit proteins have been described as molecular toolboxes, containing components involved in targeting, regulation of enzymatic activity and specificity as well as different chromatin modifying capabilities such as demethylation, deacetylation or chromatin remodelling. These complexes are not static, but can replace different domains to modulate their function in different contexts (Meier and Brehm, 2014). The complex of HDAC1/CoREST1/LSD1 was able to remove crotonyl-groups from fluorescein-tagged H3K18 peptides in addition to acetyl-groups from H3K18 and H4K16. Furthermore, genetic deletion of HDAC1/2 in embryonic stem cells substantially reduced H3K18ac and H3K18cr globally along with an 85%

reduction in decrotonylase activity and 54% reduction in deacetylase activity relative to control cells (Kelly *et al.*, 2018).

1.1.12.3 Cromodomain Y-like protein downregulates crotonylation

Chromodomain Y-like protein (CDYL) is a transcription corepressor, which reads H3K9me3 and H3K27me3, and interacts with the polycomb repressive complex 2 to propagate repressive marks along the chromatin (Vermeulen *et al.*, 2010; Y. Zhang *et al.*, 2011). CDYL contains an N-terminal chromodomain and a C-terminal enoyl-CoA hydratase/isomerase domain which can recruit HDAC1 and HDAC2 (Caron *et al.*, 2003). CDYL knock-out increased histone crotonylation in HeLa cells in 8 out of 36 sites on histones, suggesting CDYL has a role in crotonyl-group removal. CDYL could not decrotonylate histones but it could hydrate crotonyl-CoA, converting it to β-hydroxybutyryl-CoA. Whilst enoyl-CoA hydratase is more efficient, this enzyme is only mitochondrial, whilst CDYL is present in the nucleus. Transgenic mice with increased CDYL protein levels showed sperm defects and reduced fertility. The CDYL transgenic mice had reduced Kcr at promoters and reduced expression in round spermatids, but not spermatocytes (S. Liu *et al.*, 2017). As promoter Kcr was found previously to be higher in round spermatids than spermatocytes and marked genes that escaped sex chromosome inactivation (Tan *et al.*, 2011), this implicates regulation of Kcr by CDYL as an important process during spermatogenesis. In the brain, overexpression of CDYL in the prelimbic cortex increased social avoidance behaviours and reduced Kcr. This study found that CDYL represses the nerve growth factor VGF by changing Kcr and H3K27me3 at the promoter to inhibit structural synaptic plasticity and promote stress induced depression. Stress upregulated CDYL but not p300 or HDAC enzymes suggesting it has a unique role in induction of stress induced depression like behaviours (Y. Liu *et al.*, 2018).

1.1.13 Nucleosome turnover and histone acylations

Nucleosome turnover is essential for cell division as the chromatin must be disrupted to allow DNA replication and newly replicated DNA re-packaged into chromatin. As histones are removed from the DNA, histone chaperones play a key role in mediating histone recycling or delivery of new histones, to enable chromatin state reassembly after passing of the replication fork. New nucleosomes are made by first depositing a H3-H4 tetramer on the DNA, followed by two H2A-H2B dimers (Probst *et al.*, 2009). In addition, nucleosomes exhibit turnover at regulatory elements and turnover rates are highest at promoters and chromatin boundary elements (Dion *et al.*, 2007; Jamai *et al.*, 2007; Deal *et al.*, 2010; Radman-Livaja *et al.*, 2011). Therefore, the maintenance of chromatin marks on the nucleosome represents a significant challenge. Existing hPTMs are thought to promote new modifications on adjacent nucleosomes through the recognition of a reader protein, which recruits a

writer enzyme to catalyse transfer of the modification (Probst *et al.*, 2009). Histone acylations may facilitate nucleosome turnover as they destabilise the nucleosome by neutralising or adding a negative charge to the positively charged lysines (Barnes *et al.*, 2019). Nucleosome remodelling also provides an additional means to regulate hPTMs. In the case of H3K79 methylation, which is transferred to histones by DOT1L but lacks a known demethylase, nucleosome exchange enables erasure of the modification and establishment of varied states of methylation (Chory *et al.*, 2019). Additionally, the assembly of a new nucleosome can be a means to add modifications to a genomic region. Newly synthesised H3.1-H4 dimers are diacetylated at H4K5 and H4K12 which is mediated by the chromatin chaperone Asf1 and catalysed by the HAT RbAp46 in the cytoplasm (Jasencakova *et al.*, 2010). H3.1 and H3.3 are acetylated and methylated prior to assembly, which is thought to influence which final hPTMs are present in the nucleosome (Loyola *et al.*, 2006). Proteome analysis of Kcr upon p300 knockdown revealed that 11% of p300 targeted Kcr was outside the nucleus, consistent with the sub-cellular distribution of this acyltransferase (Huang, Wang, *et al.*, 2018). Therefore, nascent histone dimers or other substrates might be crotonylated or acetylated prior to nucleosome assembly, as an additional means of regulating these hPTMs.

1.1.14 Histone acyl readers

1.1.14.1 Bromodomains

Bromodomain containing proteins, of which there are 8 families in humans, are the most well-known acetyl-binders. Additionally, some bromodomains may require multiple adjacent modifications to be able to efficiently bind histones, meaning that different modifications could jointly recruit proteins to coordinate specific biological processes (Filippakopoulos *et al.*, 2012). To determine if they could also be crotonyl-readers, Andrews *et al*. (2016) conducted bromodomain pull down experiments and found that Kac- and Kpr-containing peptides bound specifically to bromodomains, but longer acyl groups did not interact or did only weakly, as in the case of TAF1 and BRD2 (Andrews *et al.*, 2016). However, close inspection of their supplementary data shows that binding of Kcr by TAF1 second domain (TAF1(2)) and both BRD2 domains, relative to Kac, was stronger than for p300 (Sabari *et al.*, 2015). A different study performed a more extensive study of 49 human bromodomains, using peptide arrays and isothermal titration calorimetry. Most human bromodomains only recognised Kac and Kpr, but TAF1(2) could recognise Kcr and Kbu with high affinity. Remarkably, considering the similarity of these modifications, BRD9 and CECR2 bound Kbu but not Kcr (Flynn *et al.*, 2015). The structure of BRD3(2) in complex with H3K18ac shows that the binding pocket is side-open and its shape blocks extension of the acyl chains meaning that Kbu and Kpr must protrude out of the side (Figure 1.2). Kcr, with its rigid double bond, can only fit into larger binding pockets such as that of TAF1(2) (Y. Li *et al.*,

2016). A structure of TAF1(2) in complex with H4K5cr peptide showed that the carbonyl oxygen of Kcr is hydrogen bonded to a conserved asparagine residue similar to Kac recognition and interaction is reinforced by hydrophobic/aromatic interactions. However, much of the pocket is made up of a network of hydrogen bonding interactions putting the crotonyl group in a less favourable environment (Zhang *et al.*, 2016). As all bromodomains strongly prefer Kac over Kcr, recognition of Kcr may not be the primary function of bromodomains.

1.1.14.2 YEATS domains

The YEATS domain family is thought to selectively bind Kcr with high affinity (Andrews *et al.*, 2016; Y. Li *et al.*, 2016; Zhang *et al.*, 2016; Zhao *et al.*, 2016). The YEATS family, named from the proteins Yaf9, ENL, AF9, Taf14 and Sas5, are an evolutionarily conserved group of proteins that in humans consist of ENL, AF9, GAS41 and YEATS2 and in yeast consist of Sas5, Taf14 and Yaf9. Many important chromatin remodelling and transcription complexes contain a YEATS domain (Schulze *et al.*, 2009). Whilst they all have a preference for Kcr, their site preferences and order of affinity to other acylations differ. AF9 prefers H3K9cr over H3K27cr and H3K18cr with affinities in the order of Kcr > Kpr > Kbu > Kac (Y. Li *et al.*, 2016). YEATS2 preferred H3K27cr over H3K4, H3K23 or H3K9cr and recognised acylated H3K27 peptides in the order of Kcr > Kbu > Khib > Kpr > Kac (Zhao *et al.*, 2016). YEATS domain proteins use a unique mode of recognition from that of SIRT HDACs, bromodomains or DPF domains (Figure 1.2a). The reader pocket is elongated and end open allowing full extension of the acyl-chain, as opposed to the side-open bromodomains and the end-dead DPF domains (Sabari *et al.*, 2017; Zhao *et al.*, 2017). Structures of human proteins AF9, TAF14 and YEATS2 showed the amide plane of the crotonyl group sandwiched between critical aromatic residues through π-π stacking which is stabilised by additional hydrophobic/aromatic interactions and hydrogen bonding (Figure 1.2b and c). Use of aromatic residues is common in proteins that recognise acetylation and methylation, for example, histone methyllysine recognition by HP1 uses a conserved cage of 3 aromatic residues. However, π-aromatic stacking, enabled by the crotonyl-group, has not been identified for any other groups of proteins (Andrews *et al.*, 2016). This could explain the preference of YEATS domains for Kcr. Kbu and Kpr can contribute to hydrophobic interactions but do not have the double bond required for π-electron conjugation, resulting in lower affinity. The planar double bond also makes the crotonyl group flatter and more able to fit in the narrow binding pocket. For the AF9 YEATS structure, authors identified that a phenylalanine side chain (F28) flips on Kcr insertion. As this residue is highly divergent within the YEATS family, they hypothesised that changes to this residue have been used to fine tune specificity (Y. Li *et al.*, 2016). Yeast protein Taf14 recognised H3K9cr using the same π-aromatic stacking mechanism and comparison with a structure of H3K9ac showed alternative conformations of a tryptophan residue (W81), indicating that Kac is bound in a different chemical environment with

reduced affinity. Taf14 has been identified as core component of the transcription factor complexes TFIID and TFIIF (Kabani *et al.*, 2005), suggesting a direct link between crotonylation and binding of polymerases (Y. Li *et al.*, 2016).

1.1.14.3 DPF domains

In an expansion of the functional potential of histone crotonylation, the double plant homodomain finger (DPF) domain containing proteins MOZ and DPF2 were found to prefer Kcr to other histone acylations in the order of Kcr > Kbu > Kpr > Kac > Kβ-HBu (Xiong *et al.*, 2016). MOZ/MORF are HAT paralogs known to be involved in leukemogenesis (Yang, 2015), whilst DPF1/2/3 are non-catalytic subunits of the BAF ATP dependent chromatin remodelling complexes, which have diverse roles in development and cancer (Wu, 2012). Both were previously identified to recognise H3K14 acetylation and influence gene expression (Xiong *et al.*, 2016). H3K14cr was preferred by MOZ and DPF over H3K14ac, or nucleosomes containing Kac or Kcr at other sites, implying that DPF domains have particular site specificity regardless of the type of acylation. Interestingly, a dual H3K14crK23cr peptide, which may increase hydrophobicity, enhanced the binding affinity by 1.6-fold suggesting sensitivity to nearby modifications. In contrast to bromodomains and YEATS domains, DPF domains have an end-dead pocket which uses hydrophobic interactions and hydrogen bonding to tightly encapsulate the crotonyl group without using π-aromatic stacking (Figure 1.2). DPF2 has a higher affinity for H3K14cr than MOZ, but a double mutant of an aspartate and arginine on MOZ to make it more like DPF2 increased the affinity threefold. H3K14cr was identified at the promoters of the MOZ target genes HOXA5, HOXA7 and HOXA9. Mutation of MOZ disrupted H3K14cr binding, resulting in increased H3K14cr at the nuclear periphery (Xiong *et al.*, 2016). Heterochromatin preferentially localises at the nuclear periphery and interactions with the nuclear envelope components such as lamin are thought to facilitate silencing (Arib and Akhtar, 2011). Therefore, MOZ could bind to H3K14cr on certain HOX genes and lead to translocation from the nuclear periphery to nuclear plasma to promote gene activation.

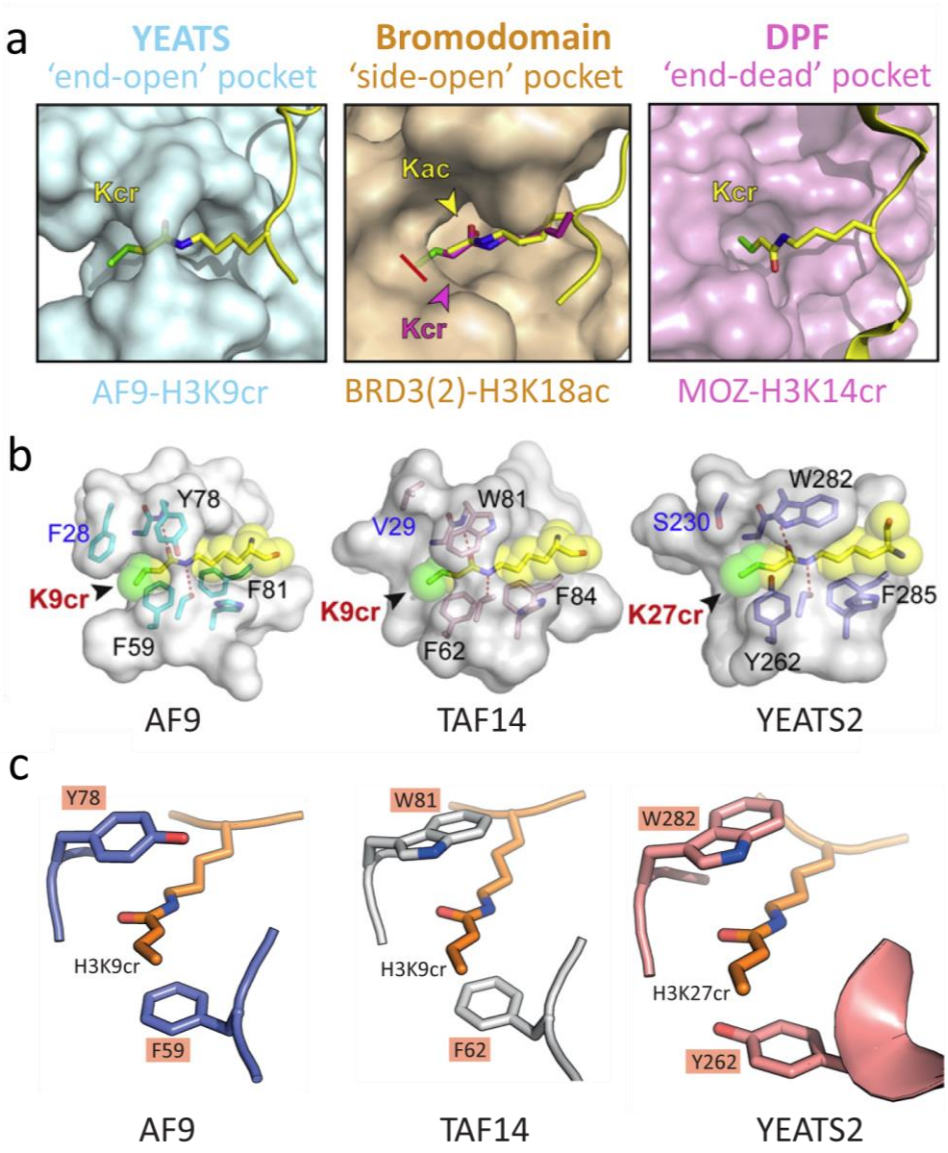

Figure 1.2. The molecular basis of histone acetylation and crotonylation recognition

a) Crystal structures of the reader pockets of YEATS domain (left, AF9 in complex with H3K9cr, protein database (PDB) code 5HJB), bromodomain (middle, BRD3 second bromodomain in complex with H3K18ac, PDB code 5HJC) and DPF domain (right, MOZ in complex with H3K14cr, PDB code 5B76). H3K18cr is modelled in the BRD3 structure in purple to show the steric clash. Histone peptides are shown as a yellow ribbon with the acyllysine side chain in stick mode and the extended hydrocarbon group of crotonyl in green. Nitrogen atoms are in blue and oxygen atoms in red. **b)** Comparison of the reader pockets of the YEATS domain containing proteins AF9 (left, in complex with H3K9cr, PDB code 5HJB), TAF14 (middle, in complex with H3K9cr, PDB code 5IOK) and YEATS2 (right, in complex with H3K27cr, PDB code 5IQL). Key residues forming the aromatic pocket of the proteins in turquoise, pink and purple. **c)** The residues involved in aromatic stacking interactions by the YEATS domain containing proteins AF9 (purple), TAF14 (grey) and YEATS2 (pink). These diagrams are from the same structures as in part b. Parts a and b are adapted from Zhao *et al.* (2017) and part c from Sabari *et al.* (2017).

1.1.15 Crotonylation on non-histone proteins.

Crotonylation was initially identified on histones in human cell lines and mouse sperm (Tan *et al.*, 2011) but has now been identified on thousands of non-histone proteins outside of the nucleus (Wei, Mao, *et al.*, 2017; Wu *et al.*, 2017; Xu *et al.*, 2017). One study found that crotonate treatment of HeLa cells enhanced Kcr on histone and non-histone proteins but did not affect Kac. In contrast, p300 overexpression increased both modifications on histone and non-histone proteins. Crotonate is likely to enhance Kcr by increasing crotonyl-CoA levels, allowing p300 to catalyse transfer of more Kcr to many types of protein. They identified 70 crotonylated proteins which was increased to 453 on crotonate treatment. Gene ontology revealed that the majority of these proteins are involved in DNA and RNA metabolism, as well as the cell cycle (Wei, Mao, *et al.*, 2017). Another study found that 40% of crotonylated proteins were in the cytoplasm, 27% in the nucleus and 13% in the mitochondria (Xu *et al.*, 2017). A third study, which identified the most crotonylated proteins, found a very similar distribution with 37.5% cytosolic, 27.4% nuclear and 13.5% mitochondrial crotonylated proteins (Wu *et al.*, 2017). They also found this was similar to the pattern of global proteome localisation suggesting that crotonylated proteins have broad distribution and biological functions. This study investigated the effects of suberoyl anilide hydroxamic acid (SAHA) treatment on Kcr in human lung carcinoma A549 cells, as they had previously found that SAHA treatment had upregulated Kac. On core histones, 24 out of 35 Kcr sites were upregulated, suggesting that class I and II HDACs are involved in Kcr regulation on these histones. Interestingly most sites on histone H1, the nucleosome linker histone, were slightly downregulated. This suggests that class I and II HDACs have no activity on this histone but there might be an indirect or non-specific effect of SAHA inhibition of HDACs, for example as a result of cellular stress. On non-histone proteins, 281 proteins were upregulated with roles identified in translation, transcription, gene expression and ribosome (GO and KEGG terms). The 41 downregulated proteins were implicated in cellular components of the endolysosome, lysosome lumen and vacuolar lumen compartments. KEGG pathway enrichment analysis identified carbon metabolism, pentose phosphate pathway and biosynthesis of amino acids and lysosome. Most of the up- and down-regulated proteins were in the cytoplasm and nucleus (Wu *et al.*, 2017). Whilst class I HDACs are mainly nuclear, class II HDACs can be nuclear or cytoplasmic (Haberland *et al.*, 2009). As many cytoplasmic proteins were crotonylated and known class II HDAC targets were found to have increased Kcr after SAHA treatment, it is possible that these enzymes have some HDCR activity (Wu *et al.*, 2017).

1.2 Metabolism

1.2.1 Metabolism is essential for life

Metabolism is essential for all living organisms as it enables breaking down food for energy, creating macromolecules from building blocks and breaking down waste. Despite a wide diversity of life on Earth, the underlying biochemical reactions are surprisingly similar. Simple building blocks such as amino acids and sugars are combined to create complex molecules that can store the information and energy required to sustain reproduction and evolution of species. For example, the eleven carboxylic acids of the tricarboxylic acid (TCA) cycle are common to all of life and are thought to have originated in a pre-enzymatic environment (Smith and Morowitz, 2004). Centred on this is carbon, which can serve as the backbone for complex structures as it can form multiple bonds with many other atoms and thus enables variety in biological macromolecules (Pace, 2001). Cellular metabolism can be grouped into either catabolic, breaking down, or anabolic, building up reactions. These chemical reactions are linked together to form multiple steps in a network of pathways, each catalysed by an enzyme that allows the reaction to occur at a physiological temperature and in a time frame that is useful to the cell. If a cell requires more energy, catabolic pathways are used to break down molecules into high energy intermediates such as NADH, which are used to generate ATP, the energy currency of the cell. When nutrients are limited this can include the breakdown of large macromolecules to maintain cellular homeostasis. If a cell requires certain proteins or nucleic acids to be made, for example during a period of proliferation, then a series of anabolic reactions will be used to generate the desired macromolecule from its building blocks. The metabolic requirements of each cell are determined by its environment and tissue type, but every cell must constantly perform multiple biochemical transformations to enable it to perform its functions (Metallo and Vander Heiden, 2013).

1.2.2 Metabolic regulation enables response to the environment

A cell's metabolism is a complex network of interconnected steps involving thousands of metabolites. This means that multiple food sources can be converted into the same central metabolite, which can then be used in multiple cellular functions. Metabolic network activity is determined by the concentrations of intermediates and the activity of the enzymes performing the reactions. This activity or flux is influenced by the genotype, epigenotype, signalling, inhibitor action and nutrient input (Reid *et al.*, 2017). Encoding multiple isoforms of enzymes, such as pyruvate kinase, allows alternative splicing to produce enzymes with properties that fulfil the needs of that tissue type. For example, pyruvate kinase isoform M1 (PKM1) has high activity and promotes use of pyruvate by the TCA cycle, whilst pyruvate kinase isoform M2 (PKM2) has lower activity and is regulated by various factors to

promote glucose to lactate conversion. Mis-regulation of PKM2 is thought to contribute to the altered glucose metabolism in cancer (Anastasiou *et al.*, 2012). The function and environment of a cell determines its metabolic requirements. For example, hepatocytes must be flexible in their choice of metabolic pathway in order to maintain energy intensive processes such as macromolecule synthesis and breaking down toxic molecules. Therefore, in a low glucose environment, the cell adapts by using fatty acid or amino acid catabolism to provide high energy intermediates for oxidative respiration (Metallo and Vander Heiden, 2013).

External cell signalling is also an important way to direct cellular metabolism. For example, release of the anabolic hormone insulin stimulates cells to uptake glucose, which is turned into glycogen for storage, whilst suppressing gluconeogenesis (Saltiel and Kahn, 2001). Metabolites can also act as signalling molecules, creating a direct and fast responsive feedback mechanism. Pyruvate kinase converts phosphoenolpyruvate (PEP) to pyruvate in the last step of glycolysis. Fructose-1,6-bisphosphate, an earlier stage intermediate of glycolysis, acts as an allosteric activator of pyruvate kinase to promote flux through the pathway (Jurica *et al.*, 1997). The abundance of a single metabolite is not always informative of the metabolic state of a cell as many regulatory systems detect the substrate/product ratio to maintain homeostasis. For example, adenosine monophosphate-responsive protein kinase (AMPK) senses the energy state of a cell by responding to the ATP/AMP and ATP/ADP ratios. It responds by phosphorylating many metabolic enzymes including glycogen synthase and acetyl-CoA carboxylase, to downregulate their activity (Hardie, 2011; Oakhill *et al.*, 2011). AMPK has also been found to prevent activation of SREBP1, a transcription factor involved in lipid metabolism (Li *et al.*, 2011). Thus, through short and long acting mechanisms, AMPK can increase glucose uptake and catabolic processes to generate ATP, whilst reducing anabolic processes which require ATP.

1.2.3 Chromatin modifications reflect cellular metabolism

Many of the epigenetic switches on chromatin are linked to the metabolic state of the cell because the enzymes that catalyse these modifications are mediated by the availability of substrates, cofactors and allosteric inhibitors which are important metabolic intermediates (Reid *et al.*, 2017). As chromatin modifications are involved in transcription regulation, this could allow the metabolic state of the cell modulate gene expression in response to changes in the metabolic requirements of the cell. The activities of cellular enzymes are controlled by their kinetic (k_m) and thermodynamic (k_d) properties relative to substrate concentration. Changes in metabolite (substrate) concentration are only relevant for enzyme activity when the concentration of the metabolites fluctuates close to the K_m of the enzyme. The ATP-dependent protein kinases catalyse histone phosphorylation, these include IKK and

AKT which phosphorylate H3S10 and ATR and ATM which phosphorylate H2A.X (S139) in mammals (Banerjee and Chakravarti, 2011; Locasale and Cantley, 2011). The concentration of ATP is in the millimolar range and far in excess of the enzyme's k_m, which is in the micromolar range, meaning that kinases would not be limited by substrate availability (Locasale and Cantley, 2011). Acetylation and methylation reactions often use substrates which fluctuate at a concentration in a similar range to the K_m of the enzyme, meaning that these modifications can be responsive to changes in metabolism such as the TCA cycle or methionine metabolism (Reid *et al.*, 2017). For example, the concentration range of acetyl-CoA in humans is 2 - 13 µM and yeast is 3 - 30 µM, whilst the K_m of the acetyltransferase GCN5 (also called KAT2A) is 0.62 µM and its yeast counterpart is 2.5 µM (Langer *et al.*, 2002; Cai *et al.*, 2011; Lee *et al.*, 2014). The concentration of S-adenosyl methionine in human erythrocytes was measured as 3.5 µM, whilst the K_m of human SUV39H1 and SET9 were 0.9 µM and 5.4 µM respectively with H3 (Oden and Clarke, 1983; Chin *et al.*, 2006). Some histone modifying enzymes use key metabolites, including SIRT HDACs which use NAD+, HATs which use acetyl-CoA and histone methyltransferases that use S-adenosyl methionine. In addition, metabolites such as S-adenosyl homocysteine, coenzyme A (CoA), 2-hydroxyglutarate, succinate and β-hydroxybutyrate (β-HBu) can act as competitive inhibitors of these enzymes. In one interesting study, limiting methionine supply to colon carcinoma cells was found to deplete S-adenosylmethionine and S-adenosylhomocysteine as well as reducing H3K4me3 abundance (Mentch *et al.*, 2015). As these metabolites are involved in many different pathways, the activity of these chromatin modifying enzymes integrates activity from across cellular metabolism and links it to histone and DNA modifications (Reid *et al.*, 2017). In parallel, changes in metabolite levels may alter gene expression which then leads to changes in histone modifications.

1.2.4 Multiple pathways influence histone acetylation

Acetyl-CoA is an abundant metabolite and is central to many different pathways. It is generated by the pyruvate dehydrogenase (PDH) complex after glycolysis, by thiolase in the beta-oxidation pathway and ketone body breakdown, and in the metabolism of some amino acids such as lysine and tryptophan (Voet and Voet, 2011). Figure 1.3 shows how it is central to many cellular pathways. It is thought that acetyl-CoA is a sensor of the metabolic state of the cell due to its central position in anabolic and catabolic pathways. It enables coupling to chromatin as histone acetylation is thought to be sensitive to the availability of acetyl-CoA in many different organisms (Takahashi *et al.*, 2006; Friis *et al.*, 2009; Wellen *et al.*, 2009; Cai *et al.*, 2011; Donohoe *et al.*, 2012). An interesting example of changes to acetyl-CoA levels influencing histone acetylation is in a model system known as the yeast metabolic cycle, where yeast are grown continually in a nutrient limited aerobic environment resulting

in synchronisation of oscillating oxygen consumption (Mellor, 2016). This involves switching between the oxidative phase, where mitochondrial respiration is highest, the reductive and building phase, where cell division occurs and the oxygen consumption begins to drop, and the reductive and charging phase which is quiescent-like and involves induction of stress and starvation genes. Acetyl-CoA levels are highly cyclical during this process, with peak levels coinciding with oxidative phase and induction of growth genes. A fascinating study showed that increased levels of acetyl-CoA on entry into the oxidative growth phase resulted in increased acetylation by Gcn5p-SAGA, specifically at genes that are important for growth. The authors suggested that the cell uses histone acetylation to coordinate the induction of growth when energy levels are high (Cai *et al.*, 2011). Further to this, the coregulation of histone acetylation, particularly at H3K18ac and H3K9ac, with key transcription factors Pip2 (fatty acid metabolism), Hfi1 (SAGA complex formation) and Xbp1 (carbohydrate and amino acid metabolism) was found be important for the regulation of gene expression in the yeast metabolic cycle using a multi-omic integrative approach (Sánchez-Gaya *et al.*, 2018).

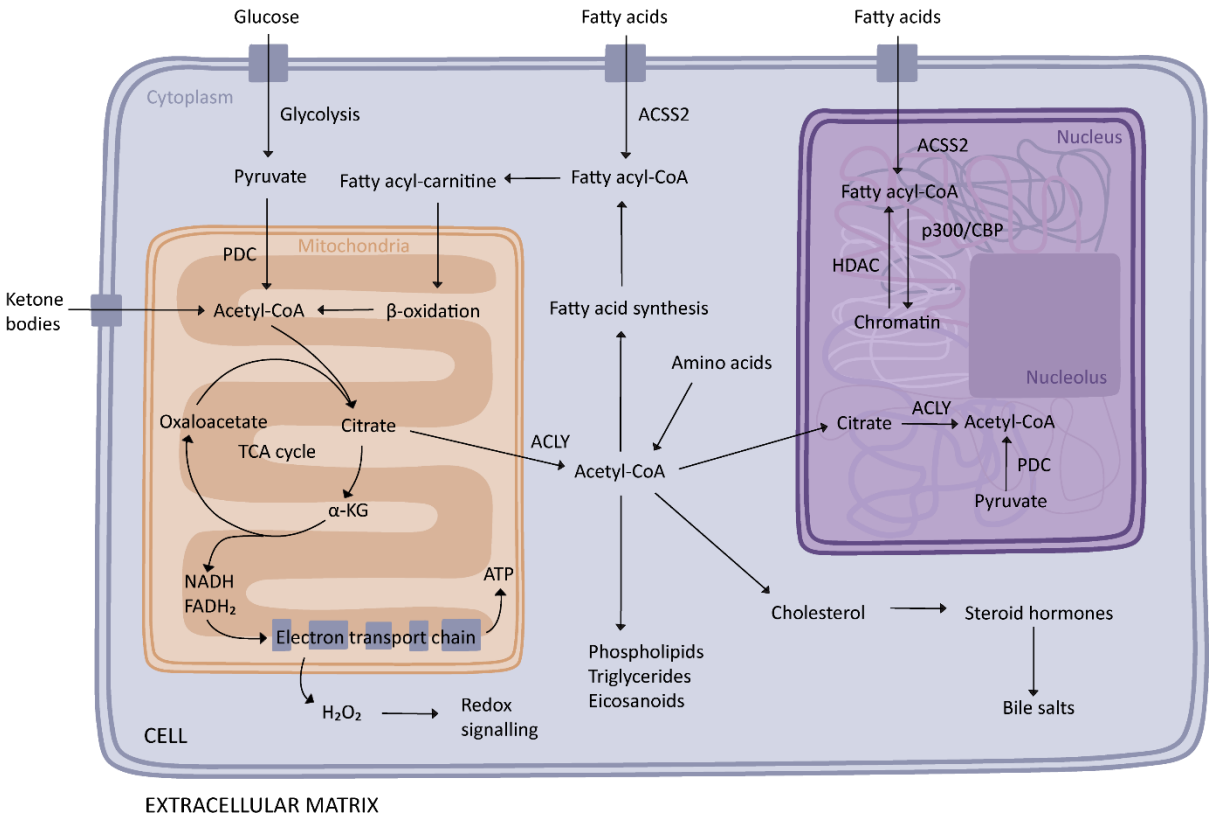

Figure 1.3. Acetyl-CoA is a central component of cellular metabolism

Acetyl-CoA is generated during glycolysis, ketone body breakdown, amino acid breakdown and in fatty acid beta-oxidation. It is used to generate the reduced intermediates NADH and $FADH_2$ in the TCA cycle which are used to generate ATP. It is also used to produce phospholipids, triglycerides, eicosanoids, cholesterol and longer chain fatty acids. The compartmentalisation of acetyl-CoA metabolism into mitochondria, cytoplasm and nucleus is because acetyl-CoA cannot pass through cell membranes. ACSS2 converts acetate into acetyl-CoA in the

cytoplasm and nucleus, which can be added onto chromatin by HATs. Acetyl-CoA can also be generated from pyruvate due to the PDH complex moonlighting into the nucleus.

1.2.5 Acetyl-CoA generation in different cellular compartments

Compartmentalisation is essential for proper cell function. For example, it enables highly degradative enzymes such as trypsin to be isolated to prevent cell damage. Whilst many inhibitors are allosteric, competitive inhibition is thought to predominate in metabolism, with inhibitors likely to be neighbours in metabolic networks and therefore are similar in structure. Additionally, central metabolites are more likely to be inhibitors. One of the main ways that this metabolic self-inhibition is alleviated is through compartmentalisation, which separates the enzymes from their inhibitors (Alam *et al.*, 2017). This could be why some processes such as fatty acid oxidation and the TCA cycle occur in the mitochondria whilst others like glycolysis occur in the cytoplasm. Acetyl-CoA is generated in the cytoplasm by glycolysis, and also in the mitochondria by pyruvate decarboxylation and β-oxidation of fatty acids (Figure 1.3). However, it cannot pass through intracellular membranes due to its high energy thioester bond. At the entry point of the TCA cycle, acetyl-CoA is converted by citrate synthase into citrate, which can be transported out of the mitochondria. Citrate can then be converted back to acetyl-CoA by cytoplasmic ATP citrate lyase (ACLY) (Voet and Voet, 2011).

ACLY also exists in the nucleus in mammalian cells enabling the generation of nuclear acetyl-CoA (Wellen *et al.*, 2009). Silencing of ACLY was found to reduce histone acetylation in HCT116 colon carcinoma cells with reduced expression of genes involved in glucose uptake and metabolism. This could be rescued by supplementation of acetate at higher than physiological concentrations, an effect mediated by ACSS2 which converts acetate to acetyl-CoA (Wellen *et al.*, 2009). Acetate can flow freely from the cytoplasm into the nucleus through the nuclear pore complex (Moore *et al.*, 1975). Nuclear ACSS2 recycles acetate released by HDACs into acetyl-CoA which can be used to produce histone acetylation (Wellen *et al.*, 2009). This recycling has been shown to prevent loss of histone acetylation during nutrient limitation and hypoxia, as ACSS2 expression and nuclear localisation increases (Bulusu *et al.*, 2017). The importance of these mechanisms for cell fate was demonstrated by silencing ACLY in 3T3-L1 preadipocytes, which prevented the increase in histone acetylation normally seen on differentiation to adipocytes. This was rescued by supplementation of acetate, which could increase histone acetylation in the ACLY silent cells (Wellen *et al.*, 2009).

Fascinatingly, mitochondrial inhibition reduced cytoplasmic citrate levels but did not change histone acetylation (Yi *et al.*, 2011) suggesting an alternative source of nuclear acetyl-CoA. Several metabolic enzymes have been identified in the nucleus and are thought to transiently relocate there in periods of cellular stress (Boukouris *et al.*, 2016). PKM2, which is highly expressed in cancer, has been shown

to translocate to the nucleus when human cancer cells were stimulated by epidermal growth factor (EGF). PKM2 phosphorylated proteins using PEP, rather than ATP, as the phosphoryl group donor, resulting in the generation of nuclear pyruvate (Vander Heiden *et al.*, 2010; Gao *et al.*, 2012; Yang *et al.*, 2012). A different study found that the PDH complex, which converts pyruvate to acetyl-CoA, translocated to the nucleus during cell cycle progression and increased histone acetylation at H3K9 and H3K18, which are known to be important for entry into S phase (Cai *et al.*, 2011), as well as levels of other S phase progression markers. This was facilitated by the heat shock protein Hsp70 and could be induced by growth factors or mitochondrial inhibition (Sutendra *et al.*, 2014). These studies suggest that cellular stress can induce an alternative method of acetyl-CoA generation in the nucleus to facilitate cellular responses.

1.2.6 Histone acetylation and metabolism in cancer

Changes to metabolism are a hallmark of carcinogenesis (Hanahan and Weinberg, 2011; Ward and Thompson, 2012) and metabolic-epigenetic interactions play an important role in cellular transformation. The source of acetyl-CoA and the functional effects of histone acetylation are context dependent. In cell culture where cells are rapidly proliferating, the majority of histone acetylation is derived from glucose (Evertts *et al.*, 2013; Lee *et al.*, 2014). Contrastingly, introduction of the medium chain fatty acid octanoate resulted in an increase in histone acetylation in immortalized hepatocytes (alpha mouse liver 12). Using isotope tracing and proteomics, the authors demonstrated that the majority of acetylation was lipid-derived, even in the presence of excess glucose (McDonnell *et al.* 2016). Cancerous cells use glycolysis instead of the more energy efficient oxidative phosphorylation, even in the presence of oxygen, known as the Warburg effect (Warburg, 1956; Vander Heiden *et al.*, 2009). In colon carcinoma cells, low doses of butyrate inhibited growth and increased histone acetylation, an effect attributed to the lack of butyrate metabolism and subsequent accumulation to concentrations where it acted as an HDAC inhibitor. When the Warburg effect was prevented by low glucose concentrations, butyrate instead promoted growth, despite also increasing histone acetylation. This was in an ACLY dependent manner suggesting metabolism of butyrate to generate acetyl-CoA. High doses of butyrate inhibited growth in either context. This could be because the amount of butyrate exceeded the capacity of cells (without the Warburg effect) to metabolise it, allowing it to exist in high enough concentrations to act as an HDAC inhibitor. Interestingly, HDAC inhibition and butyrate metabolism/HAT activation upregulated different sets of target genes, the first being enriched for cell-proliferative genes and the second for anti-apoptotic genes. The authors suggested that these two mechanisms of butyrate action are additive, with the ACLY-dependent

mechanism acting first to upregulate gene expression and the ACLY-independent (HDAC mediated) mechanism acting to maintain gene expression at higher butyrate doses (Donohoe *et al.*, 2012).

1.2.7 Metabolism influences histone acylations by generating acyl-CoAs

1.2.7.1 Crotonyl-CoA generation as part of beta-oxidation and lysine metabolism

Fatty acid β-oxidation in the mitochondria breaks down long chain fatty acids by removing two carbons in each cycle until two molecules of acetyl-CoA are left. The last cycle is shown in Figure 1.4. Short chain acyl-CoA dehydrogenase (ACAD) converts butyryl-CoA to crotonyl-CoA, then enoyl-CoA hydratase coverts it to β-hydroxybutyryl-CoA which is then turned into two acetyl-CoA molecules by thiolase (Schulz, 1991). Interestingly, ACAD deficient mice had increased lysine butyrylation as a result of butyryl-CoA accumulation. However, the study looked generally at lysine butyrylation and did not examine if butyrylation increased on histones (Pougovkina *et al.*, 2014). Another source of crotonyl-CoA results from the breakdown of some amino acids. An intermediate step in the saccharopine pathway, which metabolises lysine, tryptophan and 5-hydroxylysine; involves the conversion of glutaryl-CoA to crotonyl-CoA by glutaryl-CoA dehydrogenase (Besrat *et al.*, 1969). However, this enzyme is present in the mitochondrial matrix (Lenich and Goodman, 1986). It is unclear how non-acetyl acyl-CoAs leave the mitochondria as the CoA group prevents their transport across cellular membranes. Whilst generation of acyl-CoAs by beta-oxidation and the TCA cycle, which generates malonyl- and succinyl-CoA, is thought to contribute to mitochondrial protein acylation; some have suggested that these high energy metabolites are used up in the mitochondria before they can accumulate in sufficient quantities in the cytoplasm or nucleus (Sutendra *et al.*, 2014).

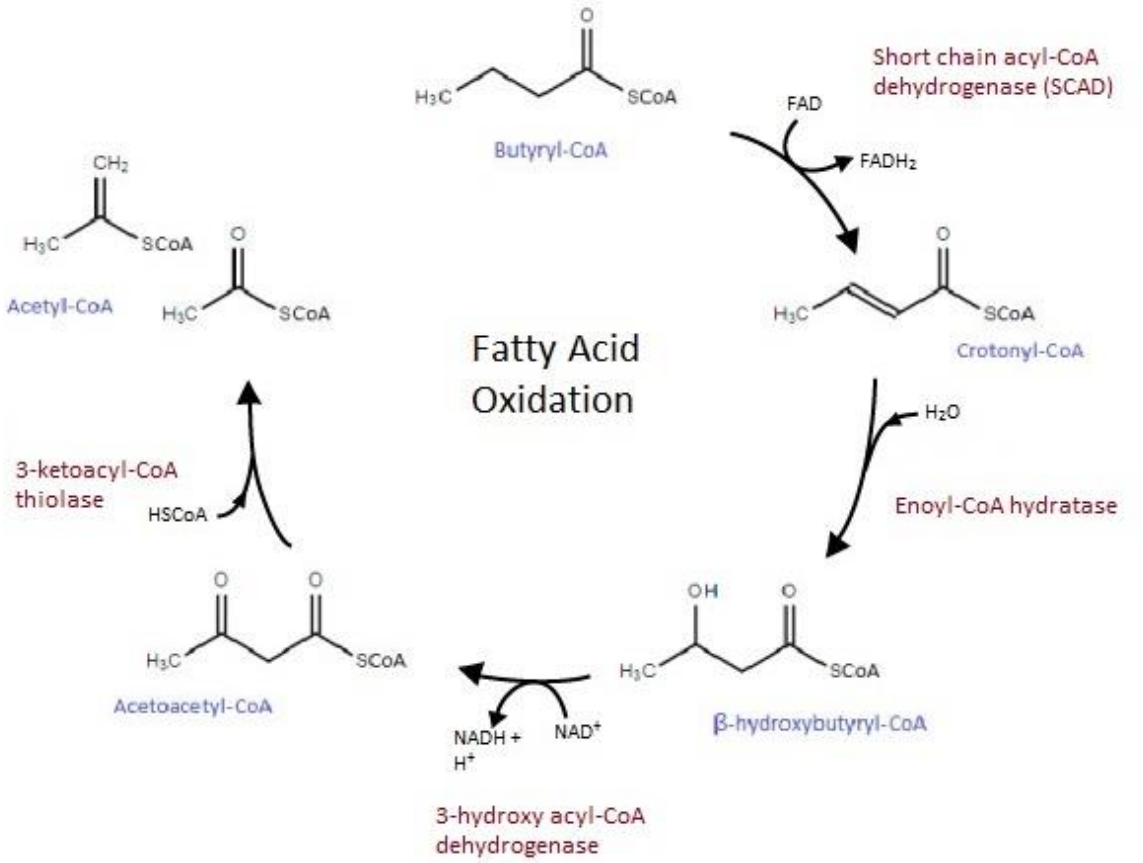

Figure 1.4. The last cycle of fatty acid β-oxidation

Fatty acid β-oxidation removes two carbons from CoA activated fatty acids in each cycle. In the last cycle, butyryl-CoA is converted into crotonyl-CoA, to β-hydroxybutyryl-CoA, then to acetoacetyl-CoA and finally to two molecules of acetyl-CoA.

1.2.7.2 Crotonyl-CoA generation during fatty acid synthesis

Fatty acid synthesis occurs in the cytoplasm and uses acetyl-CoA and malonyl-CoA to generate long chain fatty acids. This is catalysed by fatty acid synthase, a multi-enzyme complex that uses an acyl carrier protein (ACP) to shuttle intermediates to different catalytic sites. Malonyl- and acetyl-groups are transferred from CoA to ACP and joined to form acetoacetyl-ACP. Then in the reverse of β-oxidation, acetoacetyl-ACP is converted to β-hydroxybutyryl-ACP, then to crotonyl-ACP and finally to butyryl-ACP. The cycles of carboxylative reactions continue to build up the fatty acid, two carbons at a time (Voet and Voet, 2011). As this occurs in the cytoplasm, intermediates could be easily shuttled off to the nucleus or attached to newly formed nucleosomes in the cytoplasm. This is an anabolic process which requires energy, which could mean that it occurs in a different cellular context to beta-oxidation or lysine breakdown, i.e. during conditions of plentiful energy rather than nutrient input and energy production, with the drive being to produce lipids for storage or cellular structures.

1.2.7.3 Crotonyl-CoA production from crotonate

Histone crotonylation has been shown to be sensitive to the addition of crotonate to the media of HeLa S3 cells, which increased intracellular crotonyl-CoA and crotonylation at core histones in a dose-dependent manner. The abundance of histone crotonylation was not influenced by acetate treatment (Tan *et al.*, 2011; Sabari *et al.*, 2015). ACSS2 can convert acetate to acetyl-CoA in mammalian cells but was also found to use larger acyl chains such as propionate *in vitro* (Frenkel and Kitchens, 1977). ACSS2 knock-down reduced the effect of crotonate treatment on histone crotonylation. This suggests that ACSS2 could convert crotonate to crotonyl-CoA *in vivo* to contribute to the pool of nuclear crotonyl-CoA used for histone crotonylation. In fact, ACSS2 knock-down reduced histone crotonylation even without addition of crotonate to the media, suggesting basal levels of crotonyl-CoA and histone crotonylation are maintained by an endogenous source of crotonate (Sabari *et al.*, 2015). It is unclear at present what the source of this cell-generated crotonate is. Whilst histone crotonylation was responsive to crotonate, histone acetylation did not change on acetate treatment. The lack of change in histone acetylation is, at first, surprising because acetate is converted into acetyl-CoA by ACSS2 and histone acetylation is known to be responsive to acetyl-CoA levels (Takahashi *et al.*, 2006; Friis *et al.*, 2009; Wellen *et al.*, 2009; Cai *et al.*, 2011; Donohoe *et al.*, 2012). However, this could be because the pool of acetyl-CoA is already large and indeed in a previous study acetate only increased histone acetylation levels in ACLY-depleted cells (Wellen *et al.*, 2009). The pool of crotonyl-CoA in cells is small compared to acetyl-CoA, and is below the K_m of p300, meaning that environmental fluctuations might have a greater proportional effect on the crotonyl-CoA pool than the acetyl-CoA pool.

Crotonyl-CoA can compete with acetyl-CoA for p300 as modifying the relative amounts of acetyl-CoA and crotonyl-CoA in an *in vitro* p300 catalysed reaction dictated the relative amounts of the respective modifications (Sabari *et al.*, 2015). This means that changes to the relative abundance of acetyl- and crotonyl-CoA could influence histone acetylation and crotonylation abundance *in vivo*. To test if changing the ac-CoA/cr-CoA ratio in cells could influence their respective modifications Sabari and colleagues knocked-down ACLY or PDHE1α, which is a critical subunit of the PDH complex. Both ACLY and PDHE1α knockdown reduced histone acetylation but increased histone crotonylation. As the intracellular crotonyl-CoA concentration is low relative to acetyl-CoA and the relative concentration of crotonyl-CoA and acetyl-CoA could influence p300 activity *in vitro*, they suggested that lowering acetyl-CoA concentrations by ACLY or PDHE1α knockdown might reduce competition between acetyl-CoA and crotonyl-CoA for p300, enabling more p300 mediated crotonyl-transfer to the histone (Sabari *et al.*, 2015).

1.2.8 The relative abundance of acyl-CoAs

Relative to acetylation, other acylations are less abundant. Kpr, Kbu, Kcr, Kβ-HBu, Kmal, Ksucc and Kglu, had low abundances of 1-5% relative to total acylation levels, whereas Kac was in the range of 15-30% in HeLa and myogenic cells (Simithy *et al.*, 2017). The abundance of different histone acylations was found to show a strong positive correlation with the cellular levels of their acyl-CoA donors. Myogenic differentiation in which myoblasts fuse to form multinucleated cells, resulted in significantly decreased levels of Kac, Kpr, Kbu, Kmal, Ksucc and Kglu, whilst Kcr increased. Correspondingly, acetyl-, propionyl-, butyryl-, malonyl-, and succinyl-CoA levels decreased but crotonyl- and glutaryl-CoA did not change (Simithy *et al.*, 2017). The reduction in other acyl-CoAs may have freed up HAT enzymes such as p300 to transfer more crotonyl-CoA to histones, resulting in more crotonylation without changing crotonyl-CoA levels. Therefore, the abundance of a particular histone acylation may be sensitive to not just the abundance of its acyl-CoA, but also the ratio of many acyl-CoAs in different cellular pools. In the nucleus, histone acylation abundance is a result of the balance of HAT and HDAC activities. Sensing metabolite ratios is a common feature of metabolism as it provides more information on the metabolic state than a single metabolite. For example, the acetyl-CoA:CoASH ratio in the nucleus is glucose sensitive which can impact histone acetylation levels (Lee *et al.*, 2014). Additionally, as some histone acetylation marks have very fast turnover (Zheng *et al.*, 2013), which could also be true for crotonylation, this could allow rapid adjustment to gene expression to accommodate changing metabolic state. The active mark H4K3me3 has fast turnover and was shown to be globally depleted in yeast when growth conditions changed (Radman-Livaja *et al.*, 2010; Zheng *et al.*, 2014). However, this could be because nucleosome turnover was found to be higher around the TSS of actively transcribed genes in yeast and Drosophila (Dion *et al.*, 2007; Deal *et al.*, 2010). Whilst H3K4me3 is highly associated with active genes, very little transcription changes when H3K4me3 is removed and therefore it may not directly trigger gene expression (Clouaire *et al.*, 2012; Howe *et al.*, 2017). Therefore, the situation is likely to be more complex and requires further investigation.

1.2.9 Metabolism, histone crotonylation and gene expression

Sabari *et al.* (2015) studied the macrophage response to lipopolysaccharide (LPS) in which p300 recruitment is required to facilitate histone acetylation and chromatin remodelling. LPS activated genes were divided into two groups; pre-activated genes had p300, H3K18ac and H3K18cr before stimulation, whereas de novo activated genes acquired this on LPS stimulation. Only the de novo activated genes were sensitive to crotonate pre-treatment, which showed increased H3K18cr but decreased H3K18ac at those genes. This was accompanied by increased gene expression and secretion

of inflammatory proteins. In contrast, pre-activated genes were minimally affected. The effects of crotonate on de novo gene activation were dependent on ACSS2 as knockdown of this gene reduced de novo mRNA levels (Sabari *et al.*, 2015). A further study showed that crotonate-mediated enhancement of gene expression is dependent on the crotonyl-reader AF9 containing a fully functional YEATS domain. AF9 localisation to chromatin was higher for the LPS stimulated genes that were sensitive to crotonate pre-treatment (Y. Li *et al.*, 2016). AF9 may exert its effects by reading non-histone crotonylation in addition to histone crotonylation, as other YEATS domains are known to bind non-histone acetylation. For example, Yaf9 can bind acetylation on the non-histone protein Eaf1 in the fungal pathogen *Candida albicans* (X. Wang *et al.*, 2018).

1.2.10 Metabolism and histone β-hydroxybutyrylation

During starvation the liver produces ketone bodies, such as β-HBu, which are released into the blood stream to be used as an energy source (Laffel, 1999). Treatment of cells in culture with heavy labelled β-HBu followed by mass spectrometry analysis found 28 sites of the previously unidentified Kβ-HBu on histones. Additionally, cell culture treatment with β-HBu produced a dose dependant increase in Kβ-HBu as a result of cell culture treatment, but no change was seen in Kac. Using ChIP-sequencing (ChIP-seq) they found H3K9β-HBu to be enriched at TSS and correlated with the active mark H3K4me3. Mice were starved or fed normally for 48 hours and ChIP-seq and RNA-sequencing (RNA-seq) performed on extracted livers. It was found that β-hydroxybutyrylation increased as a result of starvation and many of the pathways most enriched for H3K9β-HBu were also the pathways with the greatest up-regulation of gene expression (Xie *et al.*, 2016). These results show that Kβ-HBu can respond to changes β-HBu concentrations in cell culture and to dietary changes, which could potentially be true for other histone acylations.

1.3 Gut microbiota

1.3.1 The importance of the gut microbiota

Communities of symbiotic microorganisms exist in all multicellular organisms and are thought to have been important in their evolution (Ley *et al.*, 2008). In humans, microorganisms exist on most mucosal surfaces, including those of the skin, eyes, mouth, lungs, gut and vagina. They are thought to regulate the function of the digestive, immune, neural and homeostatic systems amongst others (Brestoff and Artis, 2013; Sommer and Bäckhed, 2013). The gut microbiota is the most bacteria dense and diverse community of micro-organisms in the body (Ley *et al.*, 2006). The latest estimates suggest that there are around 38 trillion gut bacteria in humans, similar to the number of cells in the average human

body (Sender *et al.*, 2016). Due to the diversity of bacterial species, there are thought to be 100 times more genes in the gut bacteria than human genes in our genome (Ley *et al.*, 2006), a large number of which are involved in energy production and metabolism (Gill *et al.*, 2006). This provides exciting potential for the genome of the microbiota to adapt to the needs of its constituents and the host far more rapidly than the host genome is able to (Musso *et al.*, 2011). The gut microbiota exists in a symbiotic relationship with the host. The microbiota is in an equilibrium that allows the coexistence of beneficial and harmful bacteria, with the spread of pathogenic bacteria prevented by large numbers of commensal bacteria and the action of the immune system (Blaser and Kirschner, 2007; Flint *et al.*, 2012).

1.3.2 The structure of the gut

The gastrointestinal tract is a hollow tube stretching from the mouth to the anus. After food passes through the oesophagus, the stomach initially stores food and begins the digestive process. Next, the small intestine is the main site of digestion and absorption, followed by the colon which salvages water and electrolytes, and compacts the stool, which is stored in the rectum (Thompson, 2010). In humans the gastrointestinal tract is around 5 meters, although this varies considerably between individuals. The surface area is much larger with latest estimates suggesting an area of around 32 meters squared (Helander and Fandriks, 2014). Whilst the mouse gut surface area is much smaller, at 1.4 meters squared, the body surface area to intestinal surface area is very similar to humans, suggesting that the mouse is a good model for studying gut biology (Casteleyn *et al.*, 2010).

The large surface area of the gut is due to villi and microvilli which enable efficient absorption of nutrients from the diet. In the small intestine, the epithelial layer of cells lining the lumen are invaginated to form finger like projections called villi and pocket-like structures called crypts. In the colon there are crypts but not villi (Clevers and Batlle, 2013). The intestinal epithelium is constantly renewing, with stem cells in the base of the crypt generating new cells which move through the transit amplifying compartment, the differentiating zone and finally up to the top of the villi where they are lost by anoikis (apoptosis induced by loss of contact between epithelial cells) into the gut lumen. Various specialised cells exist in the epithelium, as shown in Figure 1.5. The small intestine contains a single diffuse layer of mucus which is not attached to the epithelium and contains some bacteria. The colon contains inner and outer mucus layers. The inner mucus layer is compact, attached to the epithelium and is normally free from bacteria. The outer mucus layer is diffuse with an undefined border and provides a habitat for intestinal bacteria. The colon microbiota is larger and more diverse than that of the small intestine (Hansson, 2012). The lamina propria is a thin layer of connective tissue which supports the epithelial cell niche (Powell *et al.*, 2011). Semi-distinct communities of bacteria

exist in different sections of the intestine which vary in physiology, flow rate, substrate availability, host secretion, pH and oxygen tension (Flint *et al.*, 2012).

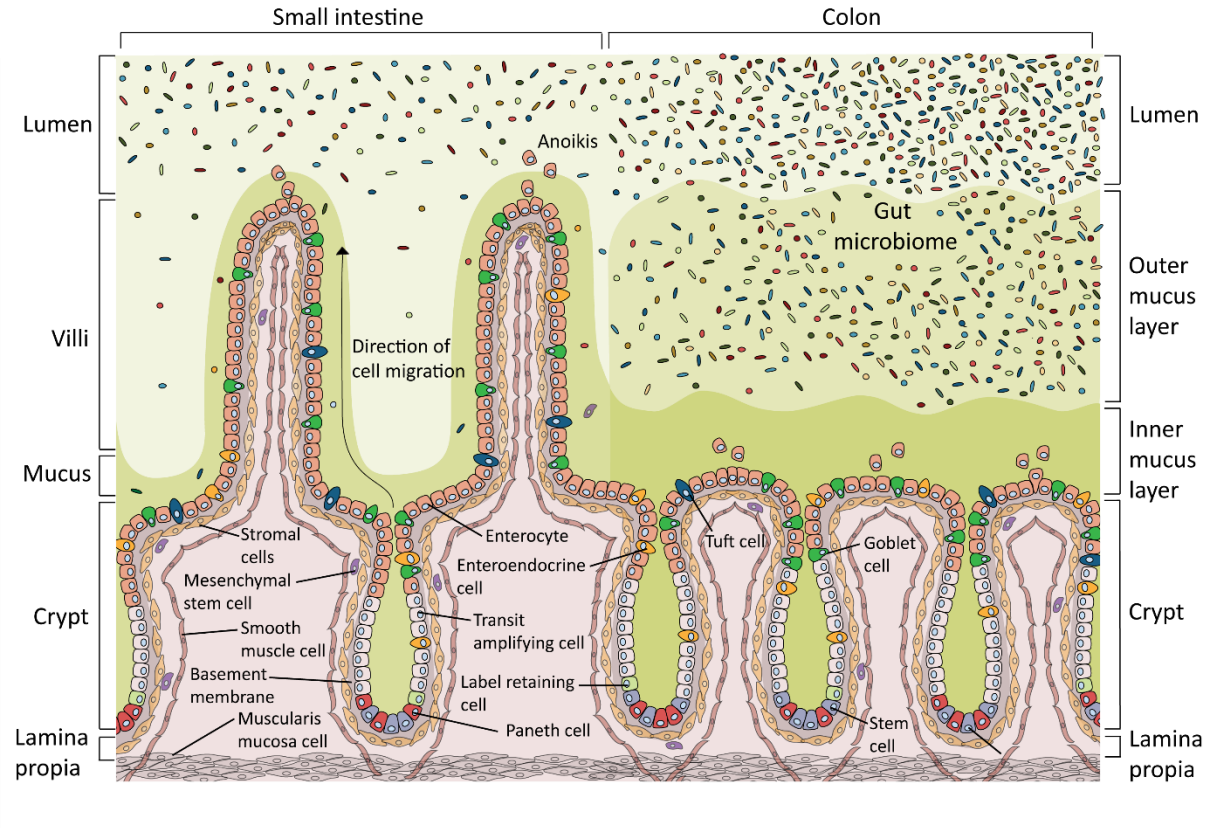

Figure 1.5 The structure of the small intestine and colon

The small intestine contains crypts and villi whilst the colon only has crypts. Stem cells in the base of the crypt are supported by Paneth cells and label retaining cells. Paneth cells secrete antimicrobial proteins and support the stem cells; label retaining cells are paneth cell precursors; transit amplifying cells are proliferative and lineage committed to become enterocytes, which are the absorptive cells; goblet cells secrete mucus; enteroendocrine cells secrete hormones and tuft cells secrete prostanoids and opioids. Cells differentiate as they move up from the crypt and are lost into the lumen by anoikis. There is a higher density of microbes in the colon than the small intestine.

1.3.3 Microbiota development through life

The gut microbiota changes substantially throughout the duration of an organism's life and is thought to play an important part in its development (Kundu *et al.*, 2017). In the first few months, an infant receives microbes from the mother's breast milk, resulting in large numbers of *Bifidobacteria*, which are well suited to process milk oligosaccharides. Once solid food is introduced the complexity of the microbiota gradually increases, something that coincides with the rapid development of the immune system over the first three years of life. As humans grow to adulthood, the gut surface area increases,

allowing for more environmental niches and is accompanied by increased microbial richness, a key indicator of gut microbiota health (Kundu *et al.*, 2017). Some species are commonly detected in most adult faecal samples, but there seems to be a wide variability in bacteria species between adult individuals (Flint *et al.*, 2012). It has been suggested that there is some redundancy between species and a functional core is shared between the majority of individuals. This core community is thought to buffer stresses and restore the original composition of the microbiota, resulting in substantial stability over time (Turnbaugh and Gordon, 2009; Rajilic-Stojanovic *et al.*, 2013).

1.3.4 The effect of diet on microbiota composition

Particular components of the diet are known to stimulate polysaccharide utilizing bacteria to increase butyrate production, either directly or through cross-feeding (Louis and Flint, 2009). For example, low carbohydrate diets in obese human males produced a reduction in *Roseburia/E. Rectale* species with a corresponding decrease in butyrate concentration in the faeces (Duncan *et al.*, 2007). The butyrate producing *Roseburia*/*Eubacterium Rectale* species and *F. prausnitzii* have been found to prefer lower pH values of around 5.5, rather than 6.5, with highest butyrate production but reduced acetate concentrations at pH 5.5 (Walker *et al.*, 2005). Interestingly, the pH alters the relative abundance of protonated and ionized forms of SCFAs, which influences its absorption as the ionized form cannot diffuse into the cell (Cook and Sellin, 1998). Comparing the microbial faeces of children in Burkino Faso, which have a high fibre diet, and those of children in Italy on a high fat and protein diet, revealed that higher fibre diets produce an enrichment for *Bacteriodetes* and depletion of *Firmicutes* species. Children in Burkino Faso also had higher levels of SCFAs, including specific species which were involved in the utilisation of xylan and cellulose (De Filippo *et al.*, 2010). An interesting study tested the stability of the microbial community on dietary change in human volunteers and found that consumption of either an animal-based or a plant-based diet over a short period could dramatically change the structure of the microbiota (David *et al.*, 2014). However, another study which measured the microbiota on sourdough and white bread containing diets in humans, saw greater inter-individual variability than differences between diet (Korem *et al.*, 2017). Studies using galacto-oligosaccharide or inulin supplementation saw an increase in *Bifidobacteria* species and *F. prausnitzii* relative to other community members, but not all subjects responded (Ramirez-Farias *et al.*, 2009; Davis *et al.*, 2011).

1.3.5 The microbiota increases host energy harvest from the diet

The microbiota plays a key role in energy harvest from food as it digests resistant macromolecules that would be otherwise excreted, into small molecules which can be used by host cells to produce ATP. Bacteria produce a variety of metabolites including small organic acids, bile acids, choline

metabolites and lipids (Nicholson *et al.*, 2012). In particular, colonocytes rely on butyrate as its main energy source using β-oxidation, rather than glycolysis, to produce acetyl-CoA for the TCA cycle and mitochondrial respiration. As colonocytes occupy a large surface area and have a high turnover (2-5 days), the intestines would be a major sink for glucose and deprive other tissues if it were not for this microbial derived energy source (Stappenbeck *et al.*, 1998; Kaiko *et al.*, 2016). Germ-free mice were found to consume more food than conventionalised germ-free mice or conventionally raised mice, but are leaner and are more protected against an insulin-resistant state (Backhed *et al.*, 2004). Germ-free mice were also found to have lower NADH/NAD+ and ATP levels in the colon but not in the liver, kidney, heart or testes compared to conventionally raised mice (Donohoe *et al.*, 2011). Transcriptome and proteome analysis identified downregulation of enzymes involved in butyrate metabolism as the most affected pathway in colonocytes of germ-free mice, along with reduced TCA cycle functioning and oxidative phosphorylation. Butyrate administration rescued oxidative phosphorylation and the energy state of germ-free mice, along with reduced autophagy (Donohoe *et al.*, 2011).

1.3.6 Production of SCFAs by the gut microbiota

The fermentation of indigestible oligo- and poly-saccharides by gut bacteria results in the production of SCFAs of which the most abundant are acetate, propionate and butyrate. These exist in high concentrations from 70-140 mM in the proximal colon to 20-70 mM in the distal colon (den Besten *et al.*, 2013). The ratio of acetate to propionate to butyrate is estimated to be 20:1:4 ratio in the ileum and changes to a 3:1:1 ratio in the colon and faeces (Cook and Sellin, 1998; Flint *et al.*, 2012). Other SCFAs including isobutyrate (C4), valerate (C5) and hexanoate (C6) also exist in concentrations 5-10% of total SCFAs (Cook and Sellin, 1998). Much of the acetate and propionate produced by the microbiota is released into the portal circulation and is made available for other tissues, including the liver which uses 70% of acetate and 30% of propionate (den Besten *et al.*, 2013). Colonocytes use 70-90% of microbial derived butyrate in preference to acetate or propionate (Cook and Sellin, 1998). Crotonate may also exist in the colon, as it is an intermediate in anaerobic metabolism and certain *Clostridium* species have been shown to been able to utilize it (Bader *et al.*, 1980; Guccione *et al.*, 2010). Additionally, crotonate was identified in the faeces of miniature Dachshunds, where it was present at a concentration around three times less than butyrate (Igarashi *et al.*, 2017). This suggests that crotonate exists in the gut lumen, but as it is usually not tested there is little evidence of its presence in the gut in different organisms or on different diets.

Butyrate producing bacteria in the gut are strict anaerobes and the majority belong to distinct families within the *Firmicutes* phylum, although members of *Bacteriodetes* and *Actinobacteria* phyla have been identified to be potential butyrate producers (Vital *et al.*, 2014). In fact, the diversity of butyrate

producers has led them to be considered as a functional group, rather than a single phylogenetic one (Rivière *et al.*, 2016). The two most abundant butyrate-producing bacteria are *F. prausnitzii and E. rectale*, which were present in 8 % of next generation sequences in obese human males and in up to 14 % of the phylogenetic core in normal weight individuals, as determined by 16S rRNA gene sequencing of faecal samples (Louis and Flint, 2009; Tap *et al.*, 2009; Walker *et al.*, 2011, 2014). Whilst they use comparable pathways for butyrate synthesis, *E. rectale* is flagellated and can use a range of dietary fibres, whilst *F. prausnitzii* is not flagellated and has a limited capacity to use dietary polysaccharides, meaning that these bacteria sit in distinct ecological niches (Flint *et al.*, 2012). These bacteria colonize the mucosal layer of the gut, as opposed to the luminal layer, making their metabolic products easily accessible to the colonocytes (Van Den Abbeele *et al.*, 2013). Interestingly *F. prausnitzii* has been shown to be cross fed by *Bifidobacterium* species which supplies them with acetate and lactate (Ferreira-Halder *et al.*, 2017). This indicates that treatments targeted at some groups of bacteria may indirectly influence others. For example, prebiotics such as inulin-type fructans can stimulate *Bifidobacteria* species but can also have beneficial effects related to butyrate producers (Rivière *et al.*, 2016). Both *Bifidobacteria* species and *F. prausnitzii* are reduced in patients with inflammatory bowel disease and colorectal cancer suggesting that they play a key role in intestinal function (Rivière *et al.*, 2016).

1.3.7 Crosstalk between the microbiota, intestinal epithelium and immune system

There is substantial cross-talk between different elements of the gut. Intestinal epithelial cells (IEC) form a physical barrier, release mucus, sense bacterial signals and secrete antimicrobial peptides, cytokines and chemokines to modulate the behaviour of the bacteria and immune cells (Roda *et al.*, 2010; Gallo and Hooper, 2012). It has been suggested that IECs can modulate the adhesion of bacteria to the mucus and to the IECs, to increase the competitive advantage of certain microbes (McLoughlin *et al.*, 2016). In turn, immune cells release cytokines to regulate epithelial permeability, IEC proliferation and antimicrobial peptide secretion (Dahan *et al.*, 2007). The microbiota plays a critical role in development and maturation of both innate and adaptive immunity, to maintain immune cell homeostasis (Kabat *et al.*, 2014). SCFAs are involved in mediating the cross-talk between IECs, microbiota and the immune system. For example, SCFAs activate the G-protein coupled receptors GPR43 and GPR109a to induce the production of IL-18 by IECs, a pro-inflammatory cytokine that is involved in repair and maintenance of epithelial integrity (Singh *et al.*, 2014; Macia *et al.*, 2015). SCFA administration in humans promoted the expression of anti-microbial peptides such as LL37 by IECs and reduced inflammation in response to infection (Raqib *et al.*, 2006, 2012; Sunkara *et al.*, 2012).

SCFAs have been found to have both immune stimulating and anti-inflammatory effects, the reason for which is still unclear (Corrêa-Oliveira *et al.*, 2016). SCFAs and gut function

The pleiotropic effects of SCFAs in the gut, including acting as modulators of intestinal pH, cell volume, ion transport, proliferation, differentiation and gene expression may be because they have multiple modes of action (Cook and Sellin, 1998). They can be converted to acyl-CoAs which are intermediates in important metabolic processes, act as epigenetic regulators by inhibiting HDACs and influence signalling through the G-coupled protein receptors GPR43, GPR41 and GPR109A (Corrêa-Oliveira *et al.*, 2016). In addition to passive diffusion of protonated SCFAs, the solute carriers Slc16a1 and Slc5a8 actively transport SCFAs across the cellular membrane from the intestinal lumen into the IEC cytosol (Cook and Sellin, 1998; den Besten *et al.*, 2013). Interestingly, butyrate is potent HDAC inhibitor and propionate inhibits HDAC nearly as effectively, but acetate inhibits it only weakly, therefore these SCFAs may induce different cellular responses in some contexts (Candido *et al.*, 1978; Cousens *et al.*, 1979).

A fascinating study demonstrated how the structure of the gut enables butyrate to influence certain cell types differently. Butyrate was found to inhibit proliferation of cultured primary intestinal stem cells via HDAC inhibition, but not via GPCR stimulation. The suppressive effect of butyrate was in part mediated by foxo3, a negative cell cycle regulator. Colonocytes in the upper regions of the crypt metabolise butyrate and use it for oxidative phosphorylation, which is ACAD dependent. The breakdown of butyrate by colonocytes results in titration of butyrate down the crypt with highest concentrations at the top down to much lower concentrations at the base, which protects the stem cells (Kaiko *et al.*, 2016). In fact, butyrate concentrations in the crypt base have been estimated to be much lower than that of the lumen, at 50-800 µM (Donohoe *et al.*, 2012). Acetate and propionate did not inhibit stem cells and passed through the epithelial barrier for use by other tissues (Kaiko *et al.*, 2016).

SCFA metabolism by colonocytes may be important for establishing the oxygen gradient that exists in the gut, as antibiotic mediated reduction of the microbiota diminished hypoxia. The oxygen concentration decreases from the O_2 rich lamina propria to the hypoxic colon lumen, where many anaerobic bacteria live, with the colonic epithelium functioning at a pO_2 well below that of other tissues (He *et al.*, 1999). Despite this low oxygen abundance, butyrate was found to promote its own metabolism in IECs by stimulating pyruvate dehydrogenase kinases which inhibit the PDH complex and suppress glycolysis (Blouin *et al.*, 2011). Butyrate has also been found to activate AMPK in colonic cell lines and AMPK is known to inhibit the Warburg effect and suppress tumour growth (Donohoe *et al.*, 2011; Elamin *et al.*, 2013; Faubert *et al.*, 2013). SCFA mediated oxygen consumption lowers pO_2 in the

gut and results in stabilisation of hypoxia inducible factor (HIF), a transcription factor that mediates maintenance of barrier integrity amongst other things (Kelly *et al.*, 2016). Interestingly, HIF stabilisation is protective against colitis (Karhausen *et al.*, 2004), and may be one of the reasons why butyrate has been successful in some cases to treat colitis, which is a disease characterised by inflammation of the colon. Interestingly *F. prausnitzii* is stimulated by low oxygen conditions suggesting that it exists in a niche that involves exposure to some oxygen, such as in the mucin layer, closer to the IECs (Flint *et al.*, 2012).

1.3.8 SCFAs and disease

The gut microbiota has been implicated in a wide range of diseases including cardiovascular disease, obesity, diabetes, malignancy, inflammatory bowel diseases and even neurodegenerative disorders (Musso *et al.*, 2011; Borre *et al.*, 2014; Shreiner *et al.*, 2015). Dietary fibre has been shown to reduce the risk of colon cancer and inflammatory bowel diseases, but the mechanism involved is unclear. As fermentation of fibre produces SCFAs, these have been under intense study for their potential therapeutic benefits but the results have been variable. In one study SCFA irrigation of patients with diversion colitis resulted in the disappearance of symptoms, but another study saw no benefit (Harig *et al.*, 1989; Guillemot *et al.*, 1991). In a rat model of cancer, it was demonstrated that only dietary fibre that increased the concentration of butyrate in the distal colon was protective against colon cancer (McIntyre *et al.*, 1993). Another study found that the ratio of SCFAs may be important, as comparing polyp/colon cancer patients with normal controls showed a higher abundance of acetate and a lower abundance of butyrate relative to total SCFA concentration (Weaver *et al.*, 1988). Butyrate may be protective because of its differential effect on normal and malignant cells. It was found to induce apoptosis and inhibit proliferation in cancer cell lines, but withdrawal of butyrate induced apoptosis in normal pig colonocytes (Hague *et al.*, 1993; Luciano *et al.*, 1996). This could be due to the differences in metabolism between normal and malignant cells (Vander Heiden *et al.*, 2010), as butyrate promotes growth (or has no effect) on non-cancerous cells but inhibits proliferation in cancer cells undergoing the Warburg effect (Donohoe *et al.*, 2012). Butyrate may have a context dependent effect in colon cancer. In a study of mice with a tumour suppressor gene and mismatch repair gene mutation, butyrate feeding promoted tumourigenesis (Belcheva *et al.*, 2014). In contrast, mice deficient in the butyrate receptor GRP109a were susceptible to colon cancer (Singh *et al.*, 2014). A reduction in butyrate producers has been identified in patients with inflammatory bowel disease and colorectal cancer (Rivière *et al.*, 2016). In addition, dietary fibre mediated increase in butyrate concentration in the distal colon is protective against colorectal cancer (Cook and Sellin, 1998). In regards to energy homeostasis, increased SCFA production has been found to exert anti-obesity and

anti-diabetic effects, but other evidence suggests that overproduction of SCFAs in the bowel can lead to obesity (Sanna *et al.*, 2019). An interesting recent study suggested that a shift in microbial pathways towards butyrate production increased insulin production, but did not affect type 2 diabetes risk. In contrast, a shift towards propionate production and increased propionate in the faeces did not change insulin production, but reduced the risk of type 2 diabetes (Sanna *et al.*, 2019). *C. difficile* infections often follows disruption to the normal gut microflora, for example due to antibiotics, resulting in damage to the epithelium and inflammation of the colon (Napolitano and Edmiston, 2017). A fascinating recent study found that administration of butyrate, or treatments that increase butyrate, protected against *C. difficile* by attenuating intestinal inflammation and improving barrier function in mice, an effect dependent on stabilisation of HIF1 in the colon (Fachi *et al.*, 2019).

1.4 Objectives of this study

My overall aim of the thesis is to shed new light onto the symbiotic microbiota-host crosstalk in the gut by elucidating mechanisms through which the microbiota may affect metabolism, epigenetic state and gene expression in the intestinal epithelium. My hypothesis is visualised in Figure 1.6. I propose that metabolites, generated by the microbiota from the diet may direct the use of metabolic pathways in the IECs to enable energy generation. Changes to cellular metabolism would in turn influence histone modifications, by changing substrate availability or enzyme activity, to alter chromatin state. I will focus on histone acetylation and crotonylation as they are known to respond to the availability of acetyl-CoA and crotonyl-CoA, which are derived from multiple sources including microbial generated SCFAs. Whilst many histone crotonylation sites and interacting proteins have been identified, much less is understood about how it is influenced by cell metabolism and the microbiota. As these hPTMs are implicated in regulation of gene expression, I suggest that microbiota induced changes to histone acetylation and crotonylation would in turn influence gene expression and enable the microbiota to effect IEC function in a reversible and dynamic manner.

I will therefore examine how histone crotonylation and acetylation are influenced by changes to the microbiota and the mechanism by which this occurs. I aim to:

- Test if SCFAs can influence histone crotonylation or acetylation in colon carcinoma cells and organoids.
- Determine whether SCFAs can influence histone acylations through inhibition of HDACs
- Find out if HDACs have the capacity to use longer crotonyl- or butyryl-modifications.
- Test if high fibre diets can increase SCFA concentrations in the gut and find out how this influences histone acylations in IECs.
- Investigate the effects of antibiotics treatment on SCFA concentrations and histone acylations in IECs.
- Find out whether ACAD deficient mice have an altered response to high fibre diet or antibiotics treatment.
- Characterise certain histone crotonylation and acetylation marks that are linked to the microbiota, in colon and liver.

- Determine how antibiotics treatment changes gene expression in the colon and how this is linked to histone modifications.

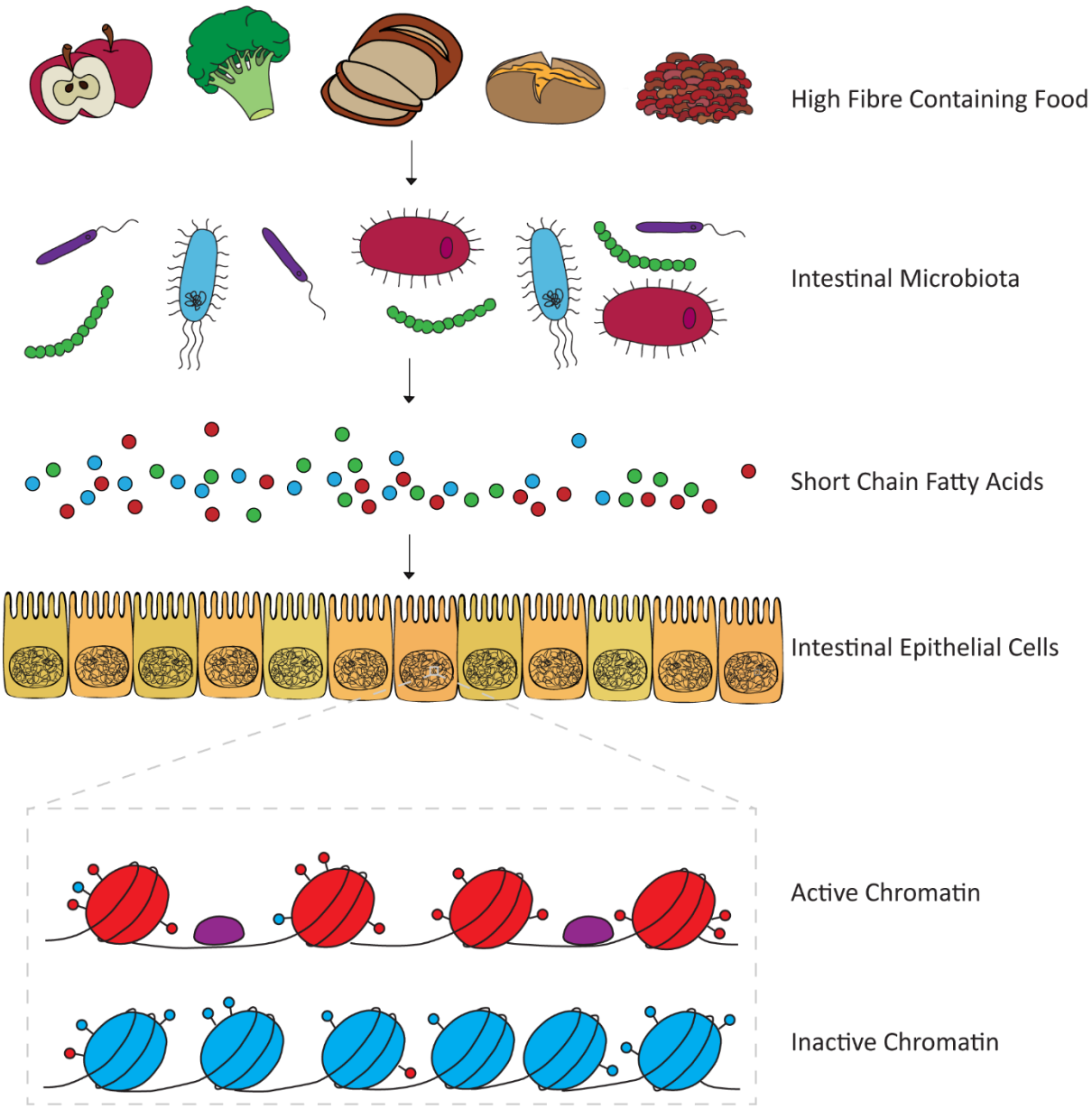

Figure 1.6. Hypothesis: SCFA induced changes to chromatin mediate the interaction between the microbiota and intestinal epithelial cells

The microbiota digests dietary fibre containing foods such as apples, broccoli, rye bread, potatoes and beans to produce SCFAs. These microbial metabolites are an important energy source for intestinal epithelial cells that influence their metabolism and chromatin state. Changes to modifications on the nucleosome enables transition from a more closed and inactive state (blue) to an open active state (red), which enables transcriptional machinery (purple) to bind. Microbiota derived SCFAs may influence histone modifications.

2

2 Materials and Methods

2.1 Antibodies

Anti-crotonyl-histone H3 lys18 (anti-H3K18cr, PTM-517), anti-butyryl-histone H3 lys18 (anti-H3K18bu, PTM-306), anti-hydroxybutyryl-histone H3 lys18 (anti-H3K18β-HBu, PTM-1292), anti-crotonyl-histone H4 lys8 (anti-H4K8cr, PTM-522) anti-butyryl-histone H4 lys8 (anti-H4K8bu, PTM-311), anti-lysine crotonyl (anti-Kcr, PTM-501) and anti-lysine acetyl (anti-Kac, PTM-101) were from PTM biolabs. Anti-acetyl-histone H3 lys18 (anti-H3K18ac, ab1191), anti-acetyl-histone H4 lys8 (anti-H4K8ac, ab15823), anti-crotonyl-histone H4 lys8 (anti-H4K8cr, ab201075) and anti-histone H3 (anti-H3, ab1791) were from abcam. Anti-HDAC1 (05-100, Clone 2E10) was from millipore, anti-HDAC2 (sc9959, C-8) was from SantaCruz and anti-HDAC3 (BD61124) was from BD Biosciences. Anti-rabbit IgG horseradish peroxidase (HRP) linked whole antibody (anti-rabbit, NA934-1ml) was from GE healthcare. Anti-mouse IgG HRP linked whole antibody (anti-mouse, 401215) was from Calbiochem.

2.2 *In vitro* experiments

2.2.1 Peptide assay

95% pure and lyophilized H3K18-crotonyl or -acetyl peptides were obtained from BioGenes. Sequences were TGGKAPR-Lys(Crotonyl)-QLATKAA-EDA-Biotin (Peptide 60556.1) and TGGKAPR-Lys(Acetyl)-QLATKAA-EDA-Biotin (Peptide 60555.1). EDA is a spacer amino acid sequence. H3K18cr and H3K18ac peptides were diluted in HDAC assay buffer (25 mM Tris-HCl pH 7.5, 50 mM KCl, 1 mM $MgCl_2$ and 1 µM $ZnSO_4$) and incubated with 0.12 µM HDAC1 or buffer alone for 2 hours at 30 °C, followed by stopping at 95 °C for 1 minute. In the following experiment 0.12, 0.06, 0.03 or 0.015 µM HDAC1 was incubated with the peptide for different time intervals up to 60 minutes.

2.2.2 HDAC assay with recombinant acylated histone H3

The activity of recombinant HDAC1, HDAC2 and HDAC3/NcoR1 were assayed using acetylated, crotonylated or butyrylated recombinant histone H3 as described in full in the appendix (section 8.1). The full protocol was published in Bio-protocols (Fellows and Varga-Weisz, 2018). In brief, 5.65 µM recombinant histone H3 was combined with 87 µM acyl-CoA and 0.66 µM recombinant p300 catalytic domain, in a buffer containing 50 mM Tris-HCl, 50 mM KCl, 0.1 mM EDTA, 0.01% Tween 20, 10% glycerol and 1 mM DTT. It was then incubated for 2 hours at 30 °C followed by stopping at 65 °C for 5 minutes. A 1:3 dilution of the reaction mix was made in a buffer containing 25 mM Tris-HCl pH 7.5, 50 mM KCl, 1 mM $MgCl_2$ and 1 µM $ZnSO_4$. A series of reactions were set up with the reaction mix and a 1:2 serial dilution of recombinant HDAC enzyme starting with 0.25 µM HDAC1, 0.18 µM HDAC2 or 0.45 µM HDAC3/NCoR1 for 2 hours at 30 °C, followed by stopping the reaction at 95 °C for 1 minute. After mixing 1:1 with 2x laemmli buffer and 2-mercaptoethanol, reactions were analysed by western blotting using anti-Kcr or anti-H3K18ac antibodies as described in section 2.6.2. For inhibitor tests, crotonylated H3 or acetylated H3 were incubated with constant 0.12 µM HDAC1 and a 1:2 serial dilution of inhibitor, starting at 200 nM trichostatin A (TSA), 50 mM crotonate or 10 mM butyrate. Reactions were analysed by dot blotting. For enzymatic assays, 0.03 µM HDAC1 was incubated with 1.41, 0.94, 0.71, 0.57 and 0.47 µM acetylated or crotonylated H3 for 0, 0.5, 1, 2, 4 and 10 minutes in triplicate. Reactions were analysed by dot blotting by spotting in quadruplicate on nitrocellulose membrane followed by blotting with anti-Kcr and anti-H3K18ac as described in section 2.6.2. Spots were quantified using image J and the raw intensity value divided by zero time point for each substrate concentration to give relative values. Multiplying by the starting substrate concentration converted the image intensity to substrate concentration, which was plotted against time and a linear regression fitted for the first 30 sec or first 1 min of the reaction, as appropriate. The initial rate was plotted against substrate concentration in GraphPad Prism Version 7 software and the analysis tools used to calculate K_m, V_{max}, and K_{cat}. For assays testing HDAC1 histone acylation, recombinant H3.1 and a 1:2-fold serial dilution of crotonate, acetate or butyrate starting at 50 mM was incubated with 0.11 µM HDAC1 or without HDAC for 2 hours at 30 °C. Reactions were analysed by western blotting using anti-H3K18ac/bt/cr, as described in section 2.6.2.

2.3 Colon carcinoma cell experiments

2.3.1 Defrosting cells

Human colon carcinoma (HCT116) cells were a gift from Simon Cook's lab (Babraham Institute) who obtained them from Bert Vogelstein, John Hopkins University, Baltimore. HCT116 cells are not part of

a list of frequently misidentified cell lines, as listed by the International Cell Line Authentication Committee (ICLAC). A frozen ampule of HCT116 cells was rapidly thawed in a 37 °C water bath and added dropwise to a sterile 15 ml tube containing 5 ml prewarmed media (DMEM with pyruvate, 4.5 g/L glucose, 10% foetal bovine serum (FBS, heat inactivated), 100 units/ml penicillin and 100 µg/ml streptomycin). After spinning at 1000 x*g* for 5 minutes, media was removed and cells resuspended with 10 ml fresh media. Cells were counted with a haemocytometer and a phase contrast microscope, seeded to 0.75-1 million cells per ml in a T75 flask and incubated at 37 °C with 5% CO_2. Media was changed after 24 hours and cells were passaged after 48 hours.

2.3.2 Passaging HCT116 cells

Media was removed from a T75 flask containing HCT116 cells at 60-80% confluency and put in a 50 ml tube. Cells were washed with 5 ml of phosphate buffered saline (PBS). 2 ml of prewarmed trypsin-EDTA 0.05 % solution with phenol red was added and incubated at 37 °C for 2 minutes. The flask was tapped firmly and dissociation confirmed under the microscope. Trypsinised cells and a 5 ml wash of the flask with fresh media were transferred to the 50 ml tube and spun 1000x*g* for 5 minutes. Cells were resuspended in 10 ml fresh media and the appropriate volume added to a prewarmed T75 flask with 12 ml media. For three days of culture, a 1:15 dilution was used and for four days of culture, a 1:20 dilution was used.

2.3.3 HCT116 cell treatment

A homogeneous solution of HCT116 cells was prepared in prewarmed media and seeded in 6 well plates at a density of 200,000 cells per well (3 ml per well). After around 24 hours, when the cells were around 20-40% confluent, the desired amount of compound was added and plate was swirled to mix. 24 hours after treatment the cells were harvested as quickly as possible to prevent loss of histone modifications. Each well was washed with 1 ml PBS, followed by incubation with 300 µl trypsin-EDTA solution at 37 °C for 2 minutes. The solution was transferred to a 1.5 ml tube with 900 µl fresh media and the mix was used to wash the well. Cells were spun at 4 °C, 425x*g* for 5 minutes. After removing the media, cells were resuspended in cold 500 µl PBS and spun again. Cells were then resuspended in 30 µl RT PBS and 30 µl of 1x laemmli buffer without β-mercaptoethanol and immediately put at 95 °C for 5 minutes. After cooling samples were frozen at -20 °C or prepared for western blot immediately as described in section 2.6.1.

2.3.4 HCT116 cell chromatin preparation

Two or three T75 flasks containing HCT116 cells at 60-80% confluency and typically 15-20 million cells were used per ChIP. Treatment was with 5 mM crotonate for 24 hours prior to harvest. Cells were trypsinised, collected in 50 ml tubes and resuspended in 10 ml RT PBS, as described for passaging. Cells were fixed in 10 ml of PBS with 1% methanol free formaldehyde for 10 minutes at room temperature (RT) with gentle agitation. After quenching with 0.125 M glycine for 5 minutes, cells were spun at 480x*g* and 4 °C for 5 min. 100x stock of protease inhibitor cocktail was made by dissolving one tablet of EDTA-free protease inhibitor cocktail (PIC, Sigma) in 500 µl H_2O. The cell pellet was resuspended in HCT116 ChIP lysis buffer (150 mM NaCl, 25 mM Tris-HCl pH8, 5 mM EDTA, 0.1% triton, 1% SDS) supplemented with protease inhibitors (10 mM sodium butyrate, 1 mM PMSF and 1x PIC) at a ratio (v/v) of 75-100 µl buffer to 10 µl approximate pellet volume. After incubation for 10 minutes on ice, sonication was performed in a water-cooled Biorupter (Diagenode) at high power, 30 seconds on and 30 seconds off for 12-15 cycles, to obtain fragment sizes of 200-500 base pairs (bp). The sonicated material was transferred to a 1.5 ml tube, incubated for at least 30 minutes on ice and then spun at 28,000x*g* and 4 °C for 10 minutes. After putting the supernatant in a fresh tube, sonication test tubes were prepared with 5 µl sonicated chromatin, 74 µl elution buffer (0.1 M $NaHCO_3$ and 1% SDS) and 20 mg/ml 1 µl proteinase K. These tubes were incubated in a thermomixer for 2 hours at 65 °C and 300 rpm followed by purification with the Qiagen polymerase chain reaction (PCR) purification kit, eluting in 30 µl. 500 ng was run on a 1.5% agarose gel at 120V and 250 mA for 40 minutes to verify fragment size distribution. ChIP was performed as described in section 2.7.3.

2.4 Organoid experiments

2.4.1 Small intestinal organoid establishment

Before starting, 24 well tissue culture plates were prewarmed and phenol-free matrigel was thawed on ice. After killing mice with CO_2 and cervical dislocation, the small intestine was dissected and fat removed. The intestine was flushed with cold PBS using a 1000 µl pipette and opened longitudinally. The villi were scraped off gently using a coverslip and the intestine cut into 2 to 4 mm pieces with scissors. Five times, the pieces were shaken vigorously for 1 minute in a 50 ml tube with cold PBS and supernatant discarded until the supernatant was only a bit cloudy. The pieces were incubated on ice whilst shaking with 2 mM EDTA in PBS for 30 minutes. The remaining villi were removed by shaking vigorously for 10 seconds and incubating with 5 mM EDTA in PBS for a further 30 minutes. After another short shake, the solution was passed through a 40 µM strainer to remove large pieces and

spun at 425x*g* for 5 minutes. The pellet was resuspended in 2 ml of cold PBS, transferred to a 1.5 ml tube and spun again. The crypts were then resuspended in 100% red-phenol free matrigel (BD Biosciences, 50 µl per 100-200 crypts) and seeded in 50 µl drops in the prewarmed 24 well plate. After 30 minutes incubating at 37 °C to polymerise the matrigel, 500 µl complete small intestine growth media was added to each well containing advanced DMEM/F12 (Sigma), 2 mM Glutamax (Invitrogen), 10 mM HEPES (Gibco), 100 U/ml penicillin/streptomycin (Invitrogen), 1 mM N-acetyl-cysteine (Sigma), 1× B27 supplement (Invitrogen), 1× N2 supplement (Invitrogen), 50 ng/ml mouse EGF (Peprotech), 100 ng/ml mouse Noggin (Peprotech), and 10% human R-spondin-1-conditioned medium from R-spondin-1-transfected HEK293T cells (Cultrex). RT PBS was added to unused wells to reduce evaporation. Medium was changed after 24 hours and then every two to three days. Organoids were passaged after six to eight days.

2.4.2 Colon organoid establishment

After killing mice with CO_2 and cervical dislocation, the colon was dissected, opened longitudinally and rinsed three to four times in a petri dish with cold Hank's balanced salt solution (HBSS) without Ca^{2+} or Mg^{2+}. The colon was cut into 2-5 mm pieces, transferred to a 15 ml tube containing cold Dulbecco's PBS and pieces washed three times by pipetting them up and down with a 0.1% bovine serum albumin (BSA) coated 10 ml pipette, letting the pieces sink and replacing the solution. Colon pieces were incubated on ice with shaking and 5 mM EDTA in HBSS for 35 minutes. Pieces were washed three times, by pouring off the solution and adding fresh HBSS. 3ml fresh HBSS was added and the pieces pipetted up and down three times with a coated 5 ml pipette, then the solution was transferred to a fresh, BSA coated 15 ml tube. This was repeated twice to get as many crypts as possible. The tube was spun at 600x*g* and 4 °C for 5 minutes, then pellet resuspended in 500 µl cold PBS and transferred to a 1.5 ml tube. After another spin, the pellet was resuspended in 100% thawed matrigel and 50 µl drops prepared in a 24 well plate, which was incubated at 37 °C for 30 minutes. 500 µl prewarmed complete colon growth medium was added to each well containing advanced DMEM/F12 (Sigma), 2 mM Glutamax (Invitrogen), 10 mM HEPES (Gibco), 100 U/ml penicillin/streptomycin (Invitrogen), 1 mM N-acetyl-cysteine (Sigma), 1× B27 supplement (Invitrogen), 1× N2 supplement (Invitrogen), 50 ng/ml mouse EGF (Peprotech), 100 ng/ml mouse Noggin (Peprotech), 10% human R-spondin-1-conditioned medium from R-spondin-1-transfected HEK293T cells (Cultrex), 50% wnt3a conditioned medium from L Wnt-3A cells (ATCC CRL-2647), 10 µM Y-27632 (Rock-inhibitor) and 500 µg/ml primocin. Media was changed after 24 hours to growth media without primocin and then every two to three days with growth media without Y-27632 or primocin. Organoids were passaged every six to eight days.

2.4.3 Organoid passage

When there were 4-16 wells of organoids, media was removed from a three-quarters of the wells with an aspirator leaving just the matrigel drop. A 1000 µl pipette was used to disrupt the Matrigel in all of the wells. Then, the remaining quarter media was used to collect all of the cells and matrigel in a 15 ml tube on ice. 1 ml cold PBS was used to wash four wells and was also transferred to the 15 ml tube which was made up to 12 ml with cold PBS. With one or two wells the same procedure was applied, but all media and matrigel were transferred to a 1.5 ml tube and 500 µl cold PBS used to wash the wells. The tube was submerged in ice and incubated for 30 minutes to let the matrigel thaw. After spinning at 4 °C and 600xg for 5 minutes, media and as much matrigel as possible was removed. If organoids were still spread through the matrigel, fresh PBS was added and the tube spun at 800x*g* for 5 minutes. Organoids were disrupted in 300 µl cold basal medium with a 200 µl pipette for about 5 minutes until the organoid specks were only just visible. After spinning again at 600x*g* and 4 °C for 5 minutes, media was removed and cells resuspended in 25 µl media and 25 µl 100% Matrigel per well required. Typically, two or three times more wells were made than the number collected for passaging, so that there was a 1:2 or 1:3 dilution of the organoids. After incubating at 37 °C for 30 minutes, 500 µl complete colon or small intestine growth media was added with rock inhibitor (colon only). PBS was added to unused wells.

2.4.4 Organoid treatment

48 hours after seeding organoids, media was changed to complete growth media containing the desired concentration of the treatment. Four wells were used per condition to ensure that enough material was obtained. After 48 hours with the treatment, the organoids were harvested. Media was removed and each well washed with 500 µl cold PBS. 250 µl cell recovery solution was added to each well and left on ice for 3 minutes. Drops were disrupted with a 1000 µl pipette and transferred to a 15 ml tube for each condition. 250 µl cell recovery solution was used to wash four wells, which was also transferred to the 15 ml tube. Tubes were incubated on ice for 30 minutes, made up with cold PBS and spun at 600x*g* and 4 °C for 5 minutes. After washing with 5 ml cold PBS, the cell pellet was resuspended in 500 µl PBS, transferred to a 1.5 ml tube and spun again. The pellet was resuspended in 30 µl PBS and 30 µl 1x laemmli sample buffer then boiled at 95 °C for 5 minutes. After cooling, organoid extracts were either frozen at -20 °C or processed immediately for western blot as described in section 2.6.1.

2.5 Mouse experiments

2.5.1 Mouse experiments at the Babraham Institute

Untreated mice for the ChIP-seq experiments, for establishing organoids and for crotonate treatment were housed at the Babraham Institute Biological Service Unit. All experimental protocols at Babraham Institute were approved by the Babraham Research Campus local ethical review committee and the Home Office (PPL 80/2488 and 70/8994). All mice were C57BL/6 adult males, were kept in specific pathogen-free conditions and fed ad libitum. Crotonate was added at 0, 10 or 50 mM to the drinking water for two weeks for the crotonate treatment experiment.

2.5.2 High fibre diet and antibiotic treatment of mice

The antibiotics treatment and high fibre diet experiments were performed at the University of Campinas. Male C57BL/6, Balb/c or Balb/c ByJ mice at age 8–12 weeks were provided by the Multidisciplinary Centre for Biological Investigation and all the experimental procedures were approved by the Ethics Committee on Animal Use of the Institute of Biology, University of Campinas (protocol number 3742-1). The Balb/c and Balb/c ByJ strains (JAX stock #001026) were obtained from the Jackson Laboraroty, USA in 2013. Mice received 200 µl of a mixture of antibiotics (5 mg/ml of neomicin, 5 mg/ml of gentamicin, 5 mg/ml of ampicillin, 5 mg/ml of metronidazole, and 2.5 mg/ml of vancomycin, Sigma Aldrich) daily for 3 days by gavage. The weight of the animals was monitored throughout the experiment. The high fibre diets were given for one month with the control diet based on the AIN93M diet (Reeves *et al.*, 1993), with 5% of cellulose and with inulin and pectin diets containing 5% of cellulose and 10% of inulin or pectin. At the end of treatment period, faeces were collected and snap-frozen in liquid nitrogen. After that, the animals were anesthetized using a mix of ketamine and xylazine (300 and 30 mg/kg, respectively) and the blood was collected by cardiac puncture. The blood was maintained at RT for 30 min and then centrifuged (3000×*g*, 8 min). The serum was collected and frozen at −80 °C. After euthanizing the animals by cervical dislocation, the entire intestine was harvested and the small intestine, colon, colon contents and cecum were isolated. Mice of the same age and breed were randomly put in the experimental groups. The order of samples from groups was mixed on collection. Sample size is reported in exact numbers and no samples are excluded from the analysis. No blinding was conducted.

2.5.3 Determination of faecal bacterial load

Stool samples were collected on the third day after treatment by gavage with a mix of antibiotics or PBS. Bacterial load estimation was performed by the Marco Vinolo group as described in Fellows *et al.* (2018). Fifty milligrams of the samples were used for extraction of the microbial genomic DNA using the Invitrogen™ PureLink™ Microbiota DNA purification kit (Thermo Fisher Scientific). The concentration and purity of the DNA was assessed using a NanoDrop spectrophotometer. The samples were quantified by real time PCR in a 96 well format in the Applied Biosystems 7500 real time PCR system using SYBR™ green master mix (Thermo Fisher Scientific). Primers were against the 16S rRNA gene in *Eubacteria* and the sequences were ACT CCT ACG GGA GGC AGC AGT (sense) and ATT ACC GCG GCT GCT GGC (anti-sense). A standard curve was generated using extracted genomic DNA from *Escherichia coli* grown *in vitro* to determine the faecal bacterial load. Results were normalised to the untreated condition.

2.5.4 Short chain fatty acid measurement

Short chain fatty acid (SCFA) concentration in the colon lumen or serum was determined by gas chromatography coupled to mass spectrometry. Sample preparation and analysis was conducted by the Caroline Marcantonio Ferreira laboratory as published in Bio-protocols (Ribeiro *et al.*, 2018). I performed statistical analysis with t-tests, one-way ANOVA or two-way ANOVA using the GraphPad Prism statistical analysis functions as appropriate. Prior to running the analysis, I checked that the data met the assumptions for parametric tests. Interpretation of resulting p-values took into account the variability and distribution of the pool of data from which the samples were taken.

2.5.5 Butyrate treatment of germ-free mice

The germ-free butyrate treatment was performed by José Luís Fachi. Experiments with germ-free (microbiota-free) animals were with Swiss mice aged 6-10 weeks old at the Department of Microbiology, Institute of Biological Science of the Federal University of Minas Gerais. Treatment was for one week with 150 mM butyrate in the drinking water.

2.5.6 Dietary restriction of mice

The dietary restriction of mice was performed by the group of Linda Partridge, in accordance with the recommendations and guideline of the Federation of the European Laboratory Animal Science Association (FELASA), with all protocols approved by the Landesamt für Natur, Umwelt und Verbraucherschutz, Nordrhein-Westfalen, Germany (reference numbers: 8.87-50.10.37.09.176).

Parental animals were received from Charles River Laboratories (Lyon, France) and animals used in this study were 5-month old female F1 hybrid mice (C3B6F1), generated by mating C3H/HeOuJ females with C57BL/6 N males. All mice were fed commercial rodent chow (ssniff R/M-H autoclavable, ssniff Spezialdiäten GmbH, Soest, Germany) and were provided with acidified water ad libitum. The food uptake of ad libitum-fed animals was measured weekly and dietary restriction was applied by feeding the animals 40% less food. Adult-onset treatment was started at the age of 12 weeks in a stepwise manner, by reducing food amounts fed to dietary restricted animals by 10% each week until the 40% reduction was reached. At the age of 5 months, which corresponded to 2 months of treatment, mice were killed by cervical dislocation and organs were immediately harvested and flash-frozen. On the day they were killed, tissue samples were collected in a 3 h time-window in the morning prior to the regular feeding of mice.

2.5.7 Tissue collection and extract preparation for western blot

Dissected colons or small intestines were cut open longitudinally and washed in PBS. A 1 cm piece was cut, dried briefly on a paper towel and flash frozen. For the liver, a 3-5 mm section of the largest lobe was cut and flash frozen. A pestle, mortar and two small spatulas were chilled on dry ice. Tissue pieces were ground to a fine powder and transferred to a 1.5 ml tube. Quickly, 500 µl of 1x laemmli buffer was added and mixed by a combination of pipetting and vortexing. Immediately after, the tube was boiled at 95 °C for 5 minutes. Samples were frozen at -20 °C or prepared immediately for western blotting.

2.6 Western Blotting

2.6.1 Cell sonication and quantitation

HCT116 cell or organoid extracts in a 60 µl volume were sonicated briefly (two to three seconds) with a probe sonicator. Tissue extracts from mouse or colon liver with 500 µl volume were sonicated in two bursts of four seconds. Sterile water was sonicated for a few seconds in between each sample to wash the probe. Tubes were then spun at 13,000x*g* and RT for 10 minutes to remove bubbles and pellet debris. Supernatants were only transferred to fresh tubes for the tissue extracts, as a pellet did not form with cell culture extracts. A 1:5 or 1:10 dilution was made in 1x laemmli sample buffer and protein amount of a 1:5 or 1:10 dilution of sample quantitated using the EZQ kit, with a two-fold serial dilution of ovalbumin in 1x laemmli sample buffer as the standard. Protein concentration of the original sample was then used to prepare 20-30 µl solutions of 1.25 µg/µl in 1x laemmli buffer. This was mixed 1:1 with 2x laemmli sample buffer containing 5% (v/v) 2-mercaptoethanol.

2.6.2 SDS-PAGE electrophoresis, dot blot and immunoblotting

For western blot, 2.5-5 µg of cell or tissue extracts in laemmli buffer containing 2-mercaptoethanol were loaded onto pre-cast bis-tris 4-12% gradient gels (Expedeon), according to the EZQ quantitation, along with 5 µl pre-stained protein marker. Gels were run at 80-150 V, 250 mA for 1-1.5 hours. After rinsing the gel in 1x tris-glycine-SDS (Bio-Rad), the gel was assembled in a semi-dry transfer machine with blotting paper and nitrocellulose membrane soaked in transfer buffer (20% methanol, 50 mM tris, 40 mM glycine). Protein was transferred to the membrane for 45 minutes at 15 V, 270 mA.

The dot blot or western blot membrane was rinsed briefly in tris buffered saline (TBS) with tween-20 (TBS-T, 50 mM tris, 150 mM NaCl and 0.05% tween 20) and blocked with 3% BSA in TBS-T pH 7.5 (TBS-T BSA) whilst on a rolling platform for 1-2 hours. Incubation with 5 ml of the desired primary antibody was overnight in TBS-T BSA followed by washing with TBS-T. After re-blocking with 15 ml TBS-T BSA, incubation with 5 ml secondary antibody in TBS-T BSA was for 1 hour followed by washes with TBS-T. ECL was added to the membranes, which were sandwiched between transparent acetate sheets and sealed with autoclave tape in a cassette. Exposure was conducted in a dark room with x-ray film and an automatic developer. The bands from scanned western blot images were quantitated using ImageJ. The intensity of the background was subtracted from band intensity. Next, band intensity was normalised to the intensity of a reference blot, either anti-H3, anti-H4 or anti-laminB1. Normalised band intensity was plotted in GraphPad Prism (version 7 or 8), relative to the control or average of the control group. For experiments with multiple replicates per group, t-tests, one-way ANOVA or two-way ANOVA were performed using the GraphPad Prism statistical analysis functions as appropriate. Prior to running the analysis, we checked that the data met the assumptions for parametric tests. Interpretation of resulting p-values took into account the variability and distribution of the pool of data from which the samples were taken.

2.7 ChIP-seq and ChIP-quantitative PCR

2.7.1 Mouse colon chromatin preparation

Mice for antibiotics treatment experiments were anesthetized in Brazil using isoflurane followed by cervical dislocation. Mice used in control only H4K8ac ChIP-seq were sacrificed in the UK by exposure to CO_2 followed by cervical dislocation. Dissected colons were opened longitudinally and washed three times with ice cold HBSS without Ca2+/Mg2+. Colons were cut into 3-5 mm pieces and epithelium dissociated by incubating on ice with 30 mM EDTA/HBSS at 60 oscillations per minute for 1 h. 50 ml tubes containing tissue pieces were shaken vigorously by hand (2–3 shakes/second) for 5 min followed by an additional 10 min on ice with EDTA/HBSS and further

shaken by hand for 5 min. Solutions were poured through a 70 µM cell strainer to remove mucus and sub-mucosa. The extracted cells were pelleted at 480 x g at 4 °C for 10 min, resuspended in 5 ml ice cold PBS then re-pelleted at 480 x g at 4 °C for 5 min. For the control colon H4K8ac ChIP (Figure 5.13) and antibiotics treated colon H4K8ac ChIP (Figure 5.20), three colons were combined per replicate. Cells were fixed in 10 ml of PBS with 1% methanol free formaldehyde for 10 min at RT with gentle agitation. After quenching with 0.125 M glycine, cells were spun at 480 x g and 4 °C for 5 min.

If sonicated immediately, the cell pellet was resuspended in 5 ml PBS and transferred to a 15 ml polystyrene tube before being spun again as before. If it was to be sent from Brazil to the UK, the cell pellet was resuspended in 1.2 ml PBS and transferred to a 1.5 ml tube before being spun again as before. Then the supernatant was removed and cell pellets flash frozen in liquid nitrogen. Two EDTA free PIC tablets (Sigma, 11836170001) were dissolved in 1 ml water for a 100x solution. Frozen pellets or fresh material were resuspended in lysis buffer (50 mM Tris-HCl pH8, 10 mM EDTA, 1% SDS) supplemented with protease and HDAC inhibitors (10 mM sodium butyrate, 1 mM phenylmethylsulfonyl fluoride (PMSF) and 1x PIC) at a ratio (v/v) of 75-300 µl buffer to 10 µl approximate pellet volume. After incubation for 10 min on ice, sonication was performed in a water-cooled Biorupter (Diagenode) at high power, 30 sec on and 30 sec off for 12-15 cycles to obtain fragment sizes of 200-500 bp. The sonicated material was transferred to a 1.5 ml tube, incubated for at least 30 min on ice and then spun at 28,000 x g and 4 °C for 10 min. A 5 µl aliquot of the chromatin was digested in elution buffer (0.1 M NaHCO3 and 1% SDS) using 0.25 mg/ml proteinase K for 2 h at 65 °C under constant shaking at 300 rpm (Eppendorf ThermoMixer® comfort). DNA purification was with the Qiagen PCR purification kit, eluting in 30 µl. 500 ng was run on a 1.5% agarose gel at 120V and 250 mA for 40 min to verify fragment size distribution. If the chromatin was not sufficiently sonicated, fresh SDS was added and the samples sonicated again (up to 40 cycles in total).

2.7.2 Mouse liver chromatin preparation

Mice were killed by exposure to CO_2 and cervical dislocation. The largest lobe of the liver was dissected, chopped into small pieces, placed in a 1.5 ml tube and flash frozen in liquid nitrogen. The pieces were ground to a powder using a pestle and mortar on dry ice and transferred to a fresh 15 ml polystyrene tube. The powder was resuspended in PBS with 1% methanol free formaldehyde, supplemented with protease inhibitors and incubated with gentle agitation for 10 minutes at RT. Glycine was added to 0.125 M final concentration and the solution spun at 850x*g* and 4 °C for 5 minutes. The cells were washed with 10 ml cold PBS containing protease inhibitors and then

resuspended in 5 ml cell lysis buffer (85 mM KCl, 0.5% IGEPAL (NP40), 5 mM HEPES pH 8.0 and protease inhibitors) and incubated on ice for 15 minutes, mixing every few minutes. Material was centrifuged at 3000x*g* for 5 minutes, supernatant removed, 75-100 µl nuclear lysis buffer (10 mM EDTA, 50 mM Tris-HCl pH 8.0, 1% SDS and protease inhibitors) added for every 10 µl pellet volume and tubes incubated on ice for 10 minutes. Sonication was performed in a water-cooled Biorupter (Diagenode) at high power, 30 seconds on, 30 seconds off for 15-20 cycles to obtain fragment sizes of 200-500 bp. The sonicated material was transferred to a 1.5 ml tube, incubated for at least 30 minutes on ice and then spun at 16,000x*g* and 4 °C for 10 minutes. After putting the supernatant in a fresh tube, good sonication was verified by the same method as for the colon.

2.7.3 Chromatin immunoprecipitation

The DNA concentration of the proteinase-K-digested sonication test was measured using the Qubit™ dsDNA high sensitivity assay kit (Thermo Fisher Scientific, catalogue number Q32851) and used to estimate sonicated chromatin concentration. 100 µg was used for the H4K8cr ChIP, 25 µg for the H4K8ac ChIP and 5 µg for the Kcr ChIP. The chromatin was diluted 5-10 times (v/v) in ChIP dilution buffer (1% triton, 1.2 mM EDTA, 16.7 mM Tris-HCl pH 8.0 and 167 mM NaCl) supplemented with protease inhibitors. When ChIP reactions were performed on multiple samples, each was made up to the same total volume. 2.5 µg of antibody was used for H4K8cr, 1 µg for H4K8ac and 2 µg for Kcr. Chromatin and antibody were incubated on a rotating wheel overnight at 4 °C. 5 µl protein A/G magnetic beads (Millipore) per 1 µg antibody were washed in 30 volumes of ChIP dilution buffer, in respect to the bead volume used. The supernatant was separated on a magnetic rack and removed, then the chromatin-antibody mix was used to resuspend the beads. Chromatin-antibody-bead mix was incubated for 3 hours on a rotating wheel at 4 °C. Beads were washed once with low salt buffer (0.1% SDS, 1% triton, 2 mM EDTA, 20 mM Tris-HCl pH 8.0 and 150 mM NaCl), twice with high salt buffer (same as low salt apart from using 500 mM NaCl) and once with TE (1 mM EDTA, 10 mM Tris-HCl pH 8.0). Kcr ChIPs were washed three times with high salt buffer. Washes were performed by spinning briefly at low acceleration, removing the supernatant on a magnetic rack on ice, adding 800 µl of the required buffer and inverting well to mix before incubating for 5 minutes at 4 °C on a rotating wheel. After the last wash, the magnetic beads were resuspended in 200 µl elution buffer and incubated in a thermomixer at 65 °C and 1100 rpm for 30 minutes. The supernatant was separated on a magnetic rack and transferred to a clean tube. An input was prepared for each biological replicate by taking 1% of the volume used for ChIP, and made up to 200 µl in elution buffer. 8 µl of 5 M NaCl was added to ChIP and input samples for a final concentration of 190 mM and incubated at 65 °C and 300 rpm overnight. 2 µl of 20 mg/ml proteinase K was added and sample incubated for 2 hours at 65

°C, 300 rpm. DNA purification was performed with the Qiagen PCR purification kit eluting in 40 µl and DNA concentration determined using the Qubit high sensitivity DNA assay kit.

2.7.4 ChIP qPCR and data analysis

Purified ChIP or input DNA was prepared with nuclease free water and SYBR® green PCR master mix (applied biosystems) allowing 0.3 ng per reaction. The master mixes and 300 nM primer were loaded on a 384 well plate in triplicate. The run was performed on a BioRad CFX384 quantitative PCR (qPCR) system, with 10 minutes initial denaturation at 95 °C, then 45 cycles of 15 seconds at 95 °C and one minute at 62 °C, followed by detection and a melt curve. To get ΔCq, triplicates were averaged, outliers removed and the Cq values subtracted by the input Cq value minus log(2)100 (adjusting from 1% to 100%). To get percentage input, 2^-ΔCq value was multiplied by 100 and the resulting value adjusted according to the different volumes used in the qPCR master mix. Fold enrichment was determined by dividing by at least one negative target and values were plotted in GraphPad Prism version 8. For the antibiotics treated qPCR experiments, fold enrichment was calculated by dividing each value by the geometric mean of the negative targets (adam23, cys1 and slc4a5). Data were log transformed prior to analysis when there was a scale related increase in variability. GraphPad Prism was used to perform two-way ANOVA and pairwise comparisons with Holm-Sidak's correction (to give adjusted p-values and generate volcano plots). Fold enrichment for each target was plotted using GraphPad Prism version 8.

2.7.5 ChIP Library preparation

PEG solutions were prepared with 2.5 M NaCl, 10 mM Tris HCl-pH8, 1 mM EDTA, 0.05 % Tween 20, and 15.75%, 22.5% or 27% PEG 8000 and filtered at 20 µM. 40 µl Seramag beads (SpeedBeads, carboxylate modified, Sigma Aldrich) were washed twice with 2 ml TE and then mixed well with 2 ml of either 15.75%, 22.5% or 27% PEG solution for 7%, 10% or 12% final concentration respectively. For each ChIP or input sample, 6 ng of purified DNA was made up to 50 µl with 10 mM Tris-HCl pH8. The NEB Ultra II DNA library prep kit (E7645S) was used to perform the end prep and adaptor ligation steps. Adaptor was diluted 1:25 in 10 mM Tris-HCl pH8 and 10 mM NaCl. Size selection was performed with Seramag beads in 7% PEG to remove large fragments, and then using Seramag beads in 12% PEG to remove small fragments. This was done by adding 3.5 µl H_2O and 80 µl beads with the 7% PEG solution to the 96.5 µl mix with USER enzyme from step 2.6 in the Ultra II manual. After mixing and incubating for 10 minutes at RT, the 100 µl supernatant was transferred to fresh tubes with 80 µl beads in the 7% PEG solution and 100 µl H_2O. After mixing well and incubating for 10 minutes at RT, the supernatant was transferred to fresh tubes with 27.9 µl H_2O and 80 µl beads in the 12% PEG

solution. After mixing thoroughly and incubating for 10 minutes at RT, the supernatant was discarded and the beads washed twice with 300 µl 80% ethanol. Beads were airdried to remove all ethanol and resuspended in 16 µl Tris-HCl pH8. After mixing well and incubating for 5 minutes at RT, the eluate was transferred to a fresh tube. PCR ligation was performed according to the Ultra II kit (section 4 in the manual) with 8 cycles of denaturation and annealing/extension. Index primers were from NEB set 1 or 2 (E7335S or E7500S) and chosen according to their barcode differences. After ligation, two clean-ups of the PCR reaction mix were performed to remove adaptor dimers, using beads with 10% PEG solution. 50 µl of ligation mix was made up to 100 µl with H_2O and 80 µl beads with 10% PEG added. After mixing well and incubating for 10 minutes at RT, the supernatant was discarded and beads washed with 200 µl 80% ethanol. After airdrying the beads were resuspended in 102 µl Tris-HCl pH8, mixed and incubated for 5 minutes at RT. 100 µl eluate was transferred to a fresh tube with 80 µl beads with 10% PEG. The clean-up was repeated, eluting in 15 µl (with 1 µl dead volume).

To determine library quality and average bp, the prepared libraries were loaded undiluted or at 1:2 dilution onto a high sensitivity DNA chip along with reagents from the Aligent high sensitvitiy DNA kit according to manufacturer's instructions and analysed with a bioanalyser agilent 2100 system. Libraries were quantitated using the NEB library quantitation kit (E7630S) performing 1:10,000 and 1:100,000 dilutions of the library and using a Biorad CFX96 or CFX384 to perform the run.

2.7.6 ChIP-Seq and bioinformatic analysis

H4K8ac HCT116, H4K8ac colon, H4K8ac liver ChIP-Seq libraries were sequenced on a HiSeq2500, 50 bp Paired End sequencing mode, by the Babraham Sequencing Facility. H4K8ac ABX colon and Kcr ABX colon ChIP-seq libraries were sequenced on a BGISeq500 in a 50 bp single end sequencing mode by BGI. The H3K18cr colon ChIP-seq data set was previously published (Fellows et al., 2018) and is available at GEO under the accession number GSE96035. Downstream processing was performed by Babraham Bioinformatics Facility using the clusterflow fastq_bowtie2 pipeline, comprising adapter and quality trimming using trim galore v0.6.0 using default paired end parameters followed by mapping to the mouse GRCm38 genome assembly using bowtie2 v2.3.2 using options --no-unal --no-mixed --no-discordant –X 1200. For the paired end H4K8ac and H3K18cr to single end Kcr comparison, only the first read of the paired end data was mapped, to avoid mapping biases between single end and paired end data. Mapped reads were imported into SEQMONK (version 1.44.0) for data exploration and analysis. For single end data, reads were extended by 300 base pairs.

Probes were generated around TSS +/- 500 bp, were running windows of 500 bp or were generated using the MACS peak caller in SEQMONK (Zhang *et al.*, 2008). Probes over MACS peaks were generated

using the feature probe generator selecting MACS peaks generated of each ChIP replicate, normalised to the largest data store linear read count quantitated and deduplicated. Enrichment normalisation of quantitations were performed on ChIP samples between the 5-20th and 90-98th percentiles, depending on the cumulative distribution plot. Regions with high input were excluded. For the comparison of H4K8ac ChIP with gene expression levels in Figure 5.12d, annotation tracks of gene expression percentile bins from the HCT116 RNA-seq (described below) were used to generate probe lists of the H4K8ac ChIP-seq data set with probes generated over TSS (+/- 500 bp) for either the input or the combined replicates of the ChIP samples. Gene ontology analysis was performed using the Panther statistical overrepresentation test and Panther GO-slim biological process (Mi *et al.*, 2019). Terms containing more than 1000 genes in the reference list or depleted terms relative to the reference list were removed. For comparison of H4K8ac in liver and colon in Figure 5.13, only the 25-30 terms with the highest enrichment were used to simplify the plot. Fold enrichment against negative log10 of the adjusted failure discovery rate (FDR) was plotted in R using the ggplot2 package. Venn diagrams were generated in R using the venneuler package or with meta-chart.com, counting each gene or promoter that contained a MACS peak once. For Figure 5.15b, each MACS peak was counted separately. Pie charts were generated in Excel, counting each gene, promoter or regulatory element that contained a MACS peak once. For Figure 5.13e, each MACS peak was counted separately. The mouse candidate cis regulatory element track was generated by the Zhiping Weng laboratory of 8-week adult male CB57BL/6 mouse colon (accession number was ENCFF387SAQ) from ENCODE (Davies *et al.*, 2011; Dunham *et al.*, 2012). The ChIP-seq data were compared to the colon regulatory element track as the equivalent liver regulatory element track had the same number of elements and boundaries, although the classification of elements does differ (the Zhiping Weng laboratory, 8-week adult male CB57BL/6 mouse liver, accession number ENCFF290EVU).

For the comparison of H4K8ac, H3K18cr or Kcr with gene expression levels in Figure 5.15e, annotation tracks of gene expression percentile bins were generated using control samples from the colon ABX RNA-seq data set (described below) and used to create probe lists of the ChIP-seq data sets with probes generated over TSS (+/- 500 bp). The Limma statistical test (Smyth, 2004) was performed on H4K8ac and Kcr ABX ChIP-seq data and used to generate the differentially crotonylated probe list. Only probes overlapping genes were exported. In excel, the probe list was deduplicated keeping only one MACS peak per gene. The MACS peak with the highest absolute fold change was kept. For Rara and Fgfr2, which had MACS peaks in both up and down lists, both MACS peaks per gene were kept. Volcano plots were generated on averaged and log transformed data. For the XY plots in Figure 5.18c and Figure 5.19, lists of Kcr MACS peaks (deduplicated to keep the most changing peak for each gene) were merged with RNA-seq genes in R and plotted in Excel. Figure 5.18c had only significantly changing Kcr

MACS peaks against differentially expressed genes. Figure 5.19 was Kcr MACS peaks (one per gene) against all expressed genes (excluding unobserved values). Two-tailed Chi-squared tests with Yate's correction were performed using GraphPad QuickCalcs 2x2 contingency table and the total number of expressed genes of 13607 (determined from the RNA-seq data set excluding unobserved probes). For Figure 5.20e and f, probes were generated +/- 500 bp of TSS and log2 transformed. Scatter plots are of the ChIP replicate set against combined H4K8ac and Kcr inputs. For Figure 5.21, H4K8ac or Kcr data was linearly quantitated over MACS peaks that changed significantly in Kcr between treatments and enrichment normalised. Values less than 1 (due to the normalisation) were set to 1 and log2 fold change between the average of antibiotics and control groups calculated. The graph was plotted in R, with points coloured by the group in either data set that contained the most reads.

2.7.7 Chromatin state analysis

ChIP-seq data from 8-week old adult mouse liver (C57BL/6), generated by Bing Ren, was downloaded from ENCODE. The accession numbers of the aligned BAM files were ENCFF380FAM (H3K4me1 replicate 1), ENCFF087XCZ (H3K4me1_2), ENCFF538SCQ (H3K4me3_1), ENCFF262ALD (H3K4me3_2), ENCFF734PDO (H3K27ac_1), ENCFF726OSP (H3K27ac_2), ENCFF803QFK (H3K27me3_1), ENCFF254XUS (H3K27me3_2), ENCFF591CDW (H3K36me3_1), ENCFF730GII (H3K36me3_2), ENCFF515GCB (input_1) and ENCFF465JMB (input_2). H3K27me3 ChIP-seq data from 10 to 12-week old adult mouse colon was generated by Lo *et al.* (2017) and is available at GEO under the accession GSE82181 (Lo *et al.*, 2017). H3K27ac and H3K4me1 ChIP-seq data from 5-week old adult mouse colon was generated by Qin *et al.* (2018) and is available at GEO under the accession GSE99670 (Qin *et al.*, 2018). No publically available H3K36me3 data for adult mouse colon could be found. Due to incompatibility issues between the mm10 aligned ENCODE ChIP-seq files and the GRCm38 H4K8ac ChIP-seq files, Simon Andrews ran a script to remove the 'chr' labels from the mm10 ENCODE bam files. ChIP-seq BAM files were filtered to a minimum mapping score of 20 and ChIP replicates were merged using SAM tools. Merged BAM files were converted to genome-wide binary enrichments at 200 bp intervals using the 'BinarizeBed' ChromHMM function (version 1.12) (Ernst and Kellis, 2012). A few different models for a range of overall ChromHMM states were derived using the 'LearnModel' function (version 1.12), before a 6-state model was deemed optimal for both colon and liver data sets. Fold enrichments across all 6 states of the ChromHMM model for a number of genomic features were calculated and plotted using the 'OverlapEnrichment' ChromHMM function (version 1.12) (Ernst and Kellis, 2012).

2.8 RNA-seq

2.8.1 Preparation of RNA lysates from mouse colon

Dissected colons were flushed gently three times with PBS, cut longitudinally and then cut into 0.5 cm pieces. The pieces were washed three times in a falcon tube by adding 10 ml 1x HBSS with 5% FBS (HBSS-FBS). 30 ml HBSS-FBS was added and tubes incubated at 37 °C for 1 hour with inverting and vortexing every 10 minutes for a few seconds. The solution was passed through a 70 µM cell strainer and spun at 840x*g*, 4 °C for 10 minutes. Cell pellets were resuspended in HBSS-FBS and a 1:20 dilution counted. 2 million cells were transferred to a fresh tube and spun at 840x*g*, 4 °C for 10 minutes. To prepare the lysis buffer, 19.8 ml of lysis buffer from PureLink RNAna mini kit (Ambion-Life technologies) was mixed with 200 µl β-mercaptoethanol. After a wash with cold PBS, the cell pellet was resuspended in 600 µl lysis buffer, vortexed for a few seconds and frozen at -80 °C.

2.8.2 RNA isolation

RNA was isolated from mouse colon epithelium at RT using the Qiagen RNeasy micro kit as described here. All steps were carried out with low bind tubes and pipette tips at RT. 200 µl of RNA lysate was mixed with 333 µl RNAse free water, 1667 µl RLT buffer and 1500 µl of 70% ethanol. After mixing, 750 µl of solution was added to a RNeasy MinElute column, spun at 8000x*g* for 15 seconds and flow through discarded. This was repeated three times until all solution had been passed through. After each spin, flow through was discarded. 350 µl RW1 buffer was added, centrifuged as before and flow through discarded. 10 µl of 1x DNase I was cautiously mixed with 70 µl of RDD buffer and added to the column for a 15 second spin. The step with RW1 was repeated and another 80 µl of DNase/RDD mix was added to the centre of the column and spun followed by another spin with 350 µl RW1. 500 µl of RPE was added and centrifuged at RT, 8000x*g* for 15 seconds and then 500 µl of 80% ethanol was added and spun at RT, 8000x*g* for 2 minutes. The collection tube was changed and tubes centrifuged for a further 5 minutes with the lid left open. The collection tube was changed again to a 1.5 ml tube, 53 µl (3 µl lost on column) of 45 °C water was added and the tube centrifuged for 1 minute at 13,000x*g*. The quality of the RNA was assessed by loading 1 µl onto an RNA chip along with reagents from the Agilent RNA 6000 Pico kit according to manufacturer's instructions and analysed with a bioanalyser Agilent 2100 system.

2.8.3 RNA library preparation

RNA library preparation was prepared using the NEBNext Ultra RNA library prep kit for Illumina (E7420S) according to section 1 of the instruction manual using the poly(A) mRNA magnetic isolation

module with a few modifications. Sections from the manual are referenced with the 'm' prefix to distinguish from sections in this document. The first strand reaction buffer and random primer mix were prepared as described in section m1.1. To perform the isolation, fragmentation and priming, 100 ng of RNA from each isolated RNA sample was made up to 50 µl with RNAse free water and put on ice. Section m1.2 was followed exactly as described in the manual without performing any adjustment for insert sizes larger than 200 nt. Care was taken to mix each sample the same number of times. Actinomycin D stock solution was prepared in nuclease free water at 5 µg/µl concentration, unused aliquots were frozen at -20 °C (stable for one month, protected from light). This stock solution was diluted 1:50 in nuclease free water and used immediately. Directional first strand cDNA synthesis was performed by adding murine RNase inhibitor, ProtoScript II reverse transcriptase and 5 µl of 0.1 µg/µl actinomycin D to the fragmented and primed mRNA (section m1.3). Second strand synthesis was performed as described in section m1.4 but the water volume was reduced as the samples had a volume of 21.5 µl rather than 20 µl.

Size selection was performed using Seramag beads as follows. Seramag bead solutions of 10% and 12% PEG were prepared by combining 2.5 M NaCl, 10 mM Tris HCl pH 8.0, 1 mM EDTA, 0.05% Tween 20 with 22.5% or 27% of PEG 8000 respectively and filtered at 20 µM. Then, 40 µl of Seramag beads (Sigma Aldrich) were washed twice in 1x TE and resuspended in 2 ml of either 22.5% or 27% PEG solution to give final PEG concentrations of 10% and 12% respectively. RT beads were vortexed and 80 µl of the 12% solution added to 80 µl of second strand cDNA synthesis reaction mix (section m1.4) along with 20 µl water. After pipetting ten times to mix and incubating for 10 minutes at RT, tubes were spun briefly and put on a magnetic rack for 5 minutes. The supernatant was discarded and beads washed twice with 200 µl 80% ethanol (prepared fresh). Ethanol was removed and the remainder air-dried taking care not to over-dry (when the beads crack). The bead pellet was resuspended in 60 µl 0.1x TE, mixed well, incubated for 5 minutes at RT, spun briefly and put on a magnetic rack for 5 minutes. 56 µl of eluate was transferred to a fresh 0.2 ml tube.

The end prep of the cDNA library (section m1.6) and adaptor ligation (section m1.7) were prepared according to the NEBNext manual. The seramag protocol was performed a second and third time by adding 80 µl 10% PEG and 13.5 µl (second) or 0 µl (third) water to the solution from the previous step. Beads were eluted in 103 µl (second) or 23 µl (third) of Tris-HCl pH8 and 100 µl or 20 µl respectively taken for the following step. After the third seramag bead purification, PCR library enrichment was performed (section m1.9A) with 15 cycles of annealing/extension and NEBNext oligos for Illumina from NEB set 1 or 2 (E7335S or E7500S). The seramag bead purification was performed a fourth time by adding 80 µl of 10% PEG and 50 µl water to the PCR mix. After ethanol wash, the DNA was eluted

in 24 µl of Tris-HCl pH8, taking 1 µl for bioanalyser with the Agilent DNA high sensitivity kit and 20 µl for sequencing.

2.8.4 RNA sequencing and data analysis

RNA-Seq libraries were sequenced on a HiSeq2500 in a 50 bp Single End sequencing run, by the Babraham Sequencing Facility. Downstream processing by the Babraham Bioinformatics Facility used the clusterflow fastq_hisat2 pipeline, comprising adapter and quality trimming using trim galore v0.6.0 using default single end parameters followed by mapping to the mouse GRCm38 genome guided by gene models from Ensembl release 70 using hisat2 v2.1.0. Hisat2 mapping parameters were --dta --sp 1000, 1000. Exploration and analysis of RNA-seq data was performed with SEQMONK (version 1.44.0). Data was imported as RNA-seq data with a minimum mapping quality of 20. Read counts were quantified at the gene level with the seqmonk RNA-seq quantitation pipeline. Differential expression analysis was performed using the DESeq2 count-based method (Love *et al.*, 2014). Hierarchical clustering was performed on DESeq2 hits. The DESeq2 hit list was exported from SEQMONK, annotating with exactly matching genes, and volcano plots made in Excel using log transformed, averaged data. Gene ontology analysis was performed using the Panther statistical overrepresentation test and Panther GO-slim biological process (Mi *et al.*, 2019). The background list was generated from the same data set, excluding the unobserved values, to give 13607 genes. Depleted terms relative to the background list and those containing more than 1000 genes in the background list were removed. Gene ontology plots were generated in R using the ggplot2 package.
HCT116 RNA sequencing and analysis

For the comparison to HCT116 cell H4K8ac ChIP-seq, the DMSO controls of an RNA-seq data set on HCT116 cells, previously generated by Claudia Stellato, were used. RNA was isolated from HCT116 cells (four biological replicates) as described in section 2.8.2. Library preparation was performed from 500 ng of RNA as described in section 2.8.3. Illumina Tru-Seq adaptors were used and library amplification was performed with the KAPA PCR Amplification kit (KAPA, Cat. KK2501) using 14 cycles. Libraries were sequenced on a HiSeq2500 sequencer (Illumina) according to the manufacturer's instructions. Sequencing reads were adaptor trimmed using Tim Galore! (version 0.4.2) and mapped to the human (GRCh38) reference genome with HiSAT2 (version 2.0.5). Analysis of RNA-seq was performed with SEQMONK version 1.44.0 on filtered reads with a MAPQ score of >60 for uniquely mapped reads. Read counts were quantified by the SEQMONK RNA-seq pipeline, quantifying only probes with at least one read. Probe values were corrected for transcript length and were divided into percentile bins according to their average expression levels of four replicates.

3

3 Short chain fatty acids influence the abundance of histone acylations in cell culture and are regulated by class I histone deacetylases

3.1 Introduction

Histone acylations are a rapidly growing family of modifications which includes the extensively studied acetylation and newly identified modifications crotonylation and butyrylation (Tan *et al.*, 2011). Histone acylations are thought to promote gene expression and are found at many of the same positions on the histone (Tan *et al.*, 2011; Sabari *et al.*, 2015). These histone modifications are of particular interest as their precursors are important metabolic intermediates, creating a mechanism for changes to metabolism to influence gene expression. Acetyl-CoA is at the centre of multiple metabolic pathways including glycolysis, beta-oxidation, tricarboxylic acid cycle, ketone body metabolism and amino acid metabolism; whilst crotonyl-CoA and butyryl-CoA are produced during beta-oxidation. In addition, ACSS2 can convert SCFAs such as acetate, butyrate and crotonate into their respective acyl-CoAs in the cytoplasm or nucleus (Frenkel and Kitchens, 1977; Wellen *et al.*, 2009). In the intestine, SCFAs are a major energy source for IECs and are provided in abundance by the intestinal microbiota. The acyltransferase p300/CBP can add acetyl-, butyryl- and crotonyl-groups to protein lysines including those on histones. This histone acyl-transfer is responsive to the relative abundance of acetyl-CoA and crotonyl-CoA, as reducing acetyl-CoA concentrations by ACLY or PDHE1α knockdown can promote histone crotonylation and reduce acetylation (Sabari *et al.*, 2015). In addition, Sabari *et al.* (2015) demonstrated that crotonate could increase intracellular crotonyl-CoA concentration resulting in upregulation of histone crotonylation but not acetylation in a uterine/cervical tumour cell line (HeLa S3). Histone crotonylation has been shown to activate gene expression to a greater extent than histone acetylation and it is recognised by the YEATS domain, a structurally distinct domain from the acetyllysine reading bromodomain (Zhao *et al.*, 2017). The NAD+ deacetylases SIRT1-3 and the Zn^{2+} dependent HDAC3/NCoR1 have been shown to have decrotonylase activity (Madsen and Olsen, 2012; Bao *et al.*, 2014). But other HDAC enzymes including HDAC1 and HDAC2 have been found not to have decrotonylase activity (Tan *et al.*, 2011). The opposing action of

transfer and removal enzymes provides the potential for rapid changes to metabolism to influence histone acylations and the use of different specific binding proteins would enable coupling to acylation type-specific gene expression programs. In this chapter, we investigate how SCFAs influence histone crotonylation and acetylation and identify that these modifications are regulated, at least in part, by class I HDACs.

3.2 Results

3.2.1 Antibody specificity tests

Western blot analysis of acylated recombinant histones revealed that anti-Kcr recognised crotonylated-H3 but not acetylated-H3, whilst anti-H3K18ac recognised acetylated-H3 but not crotonylated-H3 (Figure 3.1a). Analysing tissue extracts by western blot showed that anti-H3K18cr and anti-H3K18ac recognised only a single band (Figure 3.1b). In western blot, histone H3 tends to run at a higher molecular weight. For example, anti-H3 (ab24834) recognises a band at around 18 kDa when H3 has a predicted molecular weight of 15 kDa. Anti-Kcr is specific to protein lysine crotonylation rather than only histone crotonylation, but the strongest bands ran at a speed consistent with them being histone H3 and H4. Anti-Kcr was also previously validated by other groups studying histone crotonylation (Tan *et al.*, 2011; Bao *et al.*, 2014; Sabari *et al.*, 2015).

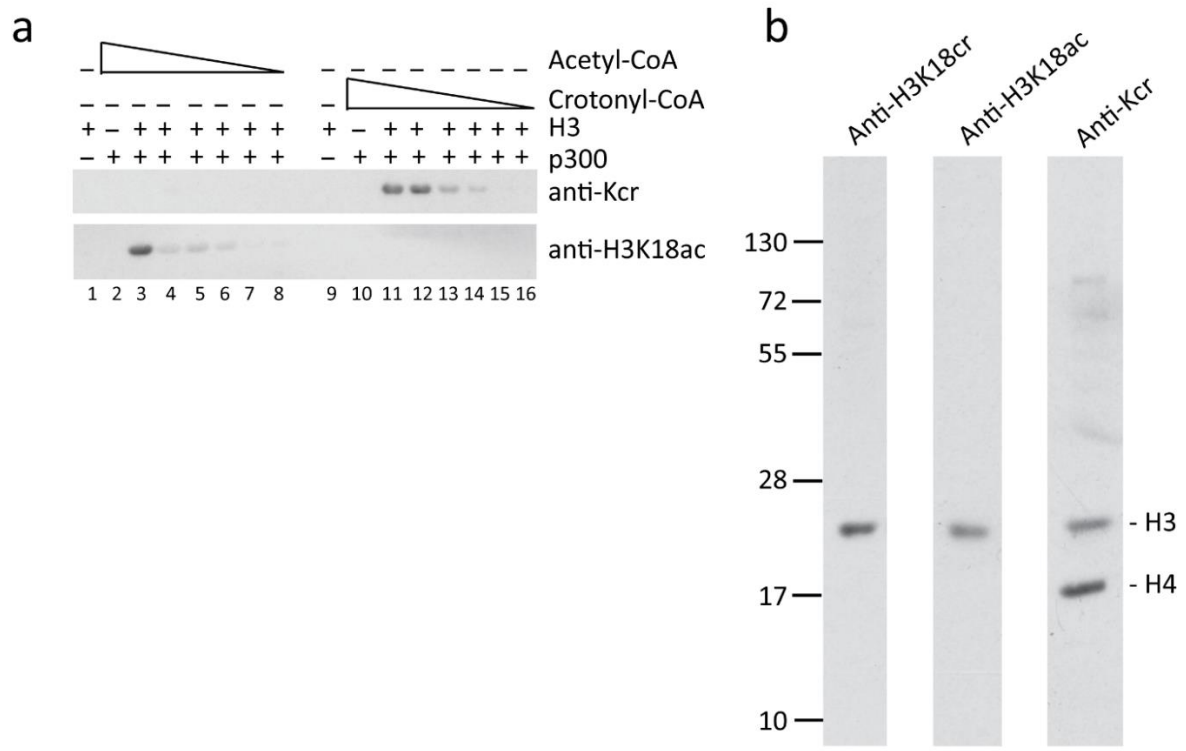

Figure 3.1. Crotonyllysine and acetyllysine antibody specificity tests

(a) Recombinant histone H3 was either acetylated or crotonylated with acetyl-CoA or crotonyl-CoA at a concentration of 100 µM, 50 µM, 25 µM, 12.5 µM, 6.25 µM or 3.13 µM (lanes 3-8 and 11-16). 100 µM was used for reactions 2 and 10. Reactions were incubated with the recombinant catalytic domain of p300 and analysed by western blot using the specified antibodies. **(b)** The anti-H3K18cr, anti-H3K18ac and anti-Kcr antibodies detect primarily histone modifications in colon extracts as tested by western blot. Migration positions of molecular weight markers are on the left in kDa.

3.2.2 The effect of SCFAs on histone crotonylation in cell culture

To investigate how different nutrients influence histone acylation in intestinal cells, we used a colon carcinoma cell line (HCT116) as many conditions could be tested with ease. SCFAs can be converted into their CoA activated form by ACSS2 and these acylated-CoAs are substrates for histone modifying enzymes. As crotonate treatment of HeLa S3 cells was previously shown to promote histone crotonylation (Sabari *et al.*, 2015), we added it to the media of HCT116 cells and tested how crotonylation changed (Figure 3.2a). The western blots are shown in Figure 3.2a and the combined quantitations are shown in Figure 3.2b-c. Experiments 1a and 1b are technical repeats of western blotting on the same cell extracts (Figure 3.2b). Experiments 1, 2, 3 and 4 are biological repeats on independently cultured cells, with the quantifications for experiment 1 being the average of the technical repeats (Figure 3.2c). H3K18cr increased above 20 mM in experiment 1 and at 10 mM in experiment 2 (Figure 3.2b and c). No changes were seen in experiments 3 and 4, but these only tested concentrations up to 5 mM. From these experiments, it appears that crotonate does not affect histone crotonylation at concentrations of 5 mM and below. Crotonate may promote histone crotonylation above 10 mM, but further experiments with more biological replicate conditions are required to test this. We also tested the effects of β-HBu treatment of HCT116 cells by western blotting (Figure 3.3a). The combined quantitations of two biological repeat experiments showed only very small changes in H3K18cr, suggesting that β-HBu does not influence histone crotonylation even at 20 mM (Figure 3.3b).

Acetate, propionate and butyrate exist in high concentrations in the colon lumen, reaching concentrations of as much as 70 mM on certain diets (Topping and Clifton, 2001). As they are physiologically important, we tested the effect of these SCFAs on histone crotonylation. When acetate was added to colon carcinoma cells, H3K18cr, Kcr H3 and Kcr H4 were reduced to different extents (Figure 3.4). H3K18cr showed the biggest decrease whilst Kcr H3 decreased only slightly. It is clear from these experiments that acetate does not increase histone crotonylation. A third repeat experiment would enable statistical testing to determine if these reductions are significant. Future experiments should run repeat conditions on the same blot. This would allow treatment conditions to be normalised to the average of the control conditions, rather than to a single control value, to allow

for variability. Propionate treatment of colon carcinoma cells did not change H3K18cr at concentrations up to 1 mM but promoted a striking increase in H3K18cr above 5 mM in two biological repeat experiments (Figure 3.5a and b). When butyrate was added to the media of colon carcinoma cells, it promoted H3K18cr at 0.5 and 1 mM in four biological repeat experiments and to a greater extent at 5 mM in two of those experiments (Figure 3.6a and b).

To see if the effects of crotonate and butyrate on crotonylation were additive, butyrate and crotonate were added in combination at different concentrations (Figure 3.7a and b). With a constant concentration of 1 mM crotonate, an increase was seen in H3K18cr from 0.5 to 5 mM butyrate in two biological repeat experiments. The 5-fold increase in H3K18cr at 5 mM butyrate and 1 mM crotonate was similar to the 5.6-fold increase seen in H3K18cr with 5 mM butyrate alone (Figure 3.7 and Figure 3.6). The reverse, of 5 mM crotonate and 1 mM butyrate, produced only a 3.8-fold increase in H3K18cr. Whilst crotonate alone only promoted H3K18cr at concentrations above 10 or even 20 mM (Figure 3.2), when combined with 1 mM butyrate, an increase could be seen at concentrations as low as 0.5 mM crotonate. This suggests that crotonate and butyrate together have an additive effect on H3K18cr, but also that butyrate is a more effective promoter of crotonylation than crotonate in colon carcinoma cells (Figure 3.2 and Figure 3.6).

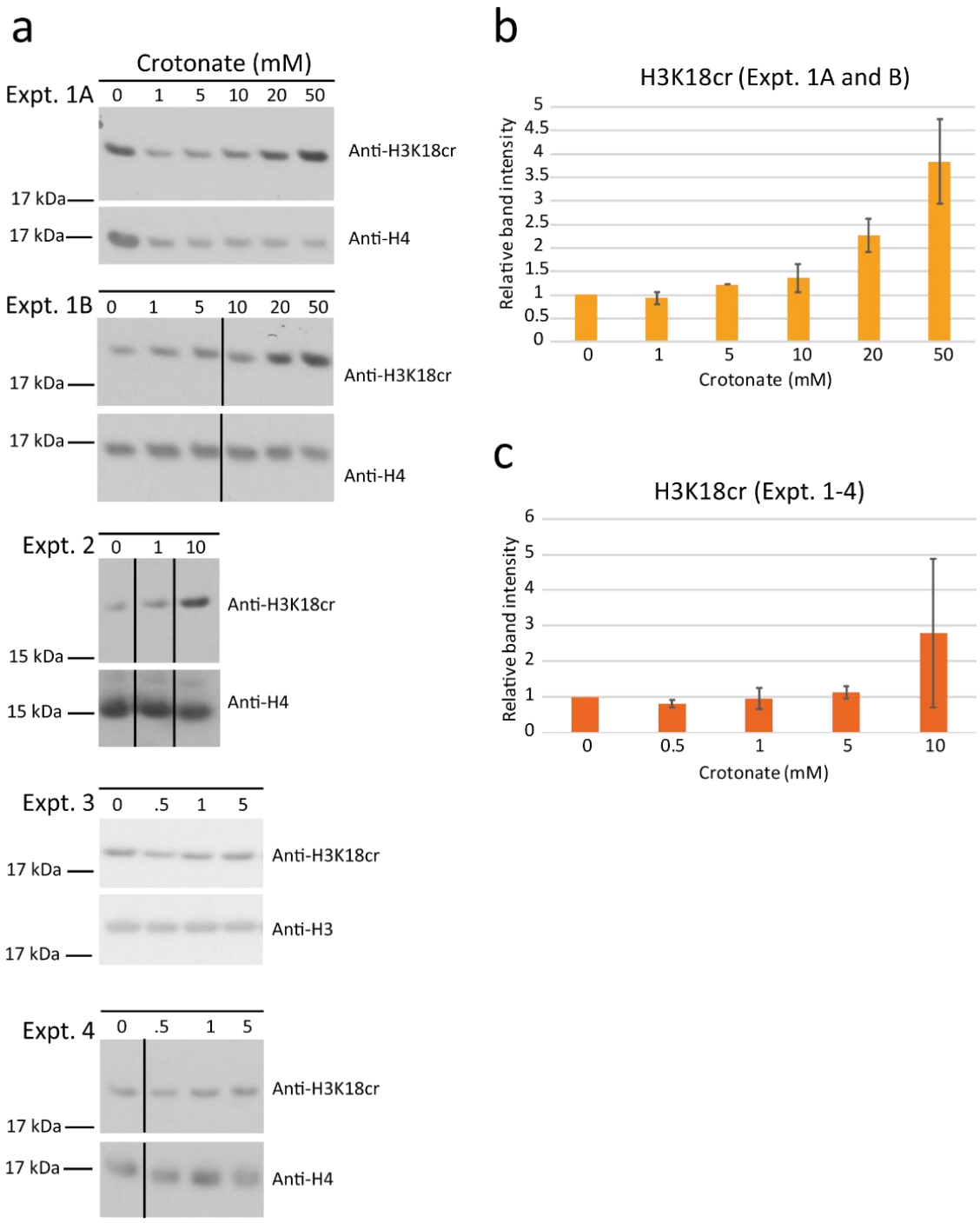

Figure 3.2. The effect of crotonate on histone crotonylation in colon carcinoma cells

Crotonate was added to the medium of colon carcinoma cells for 24 hours and whole cell extracts were analysed by western blotting using anti-H3K18cr. **(a)** Western blot images from two technical repeats of experiment 1 and the biological repeats of experiments 2-4. **(b-c)** Band quantifications of biological repeat experiments relative to the H3 or H4 blot and the untreated group. Where there are at least two repeats for a condition in the western blots, the average of band quantifications is shown with error bars as standard deviation. All concentrations are in millimolar.

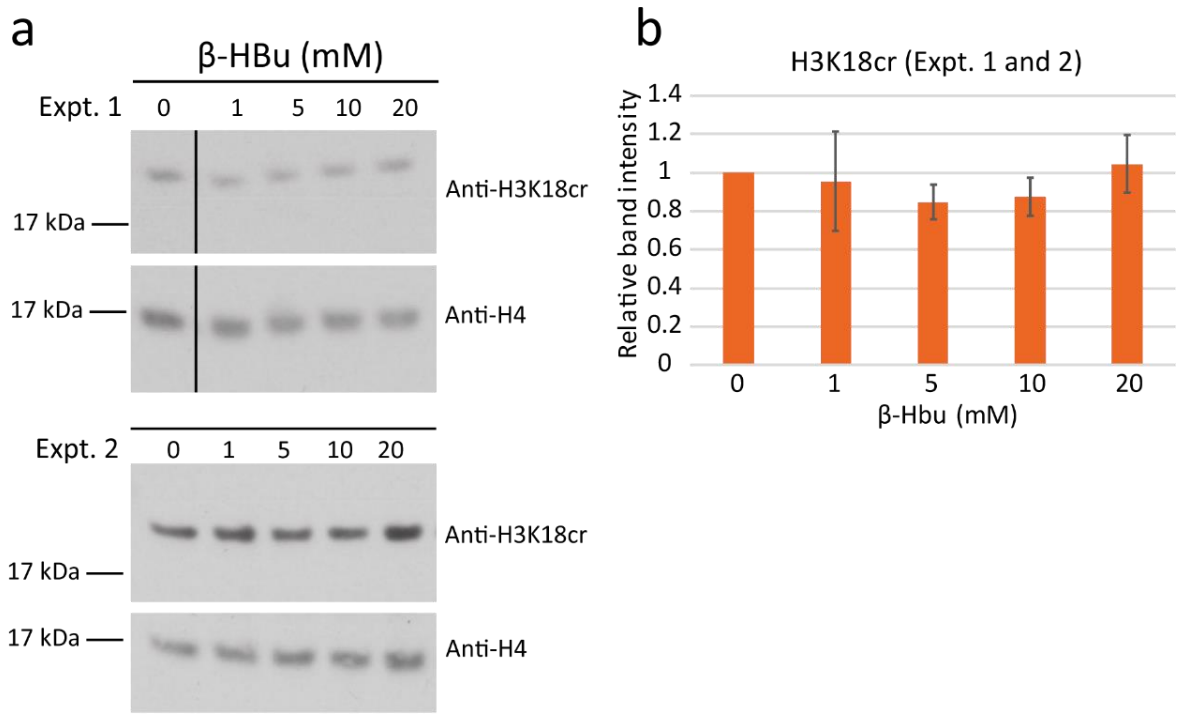

Figure 3.3. β-HBu does not promote crotonylation in colon carcinoma cells

β-HBu was added to the medium of colon carcinoma cells for 24 hours and whole cell extracts were analysed by western blotting using the anti-H3K18cr antibody. **(a)** Western blot images from two biological repeat experiments. **(b)** Band quantification is shown relative to the H4 blot and the untreated group. The average of band quantifications from the two experiments is shown with error bars as standard deviation. All concentrations are in millimolar.

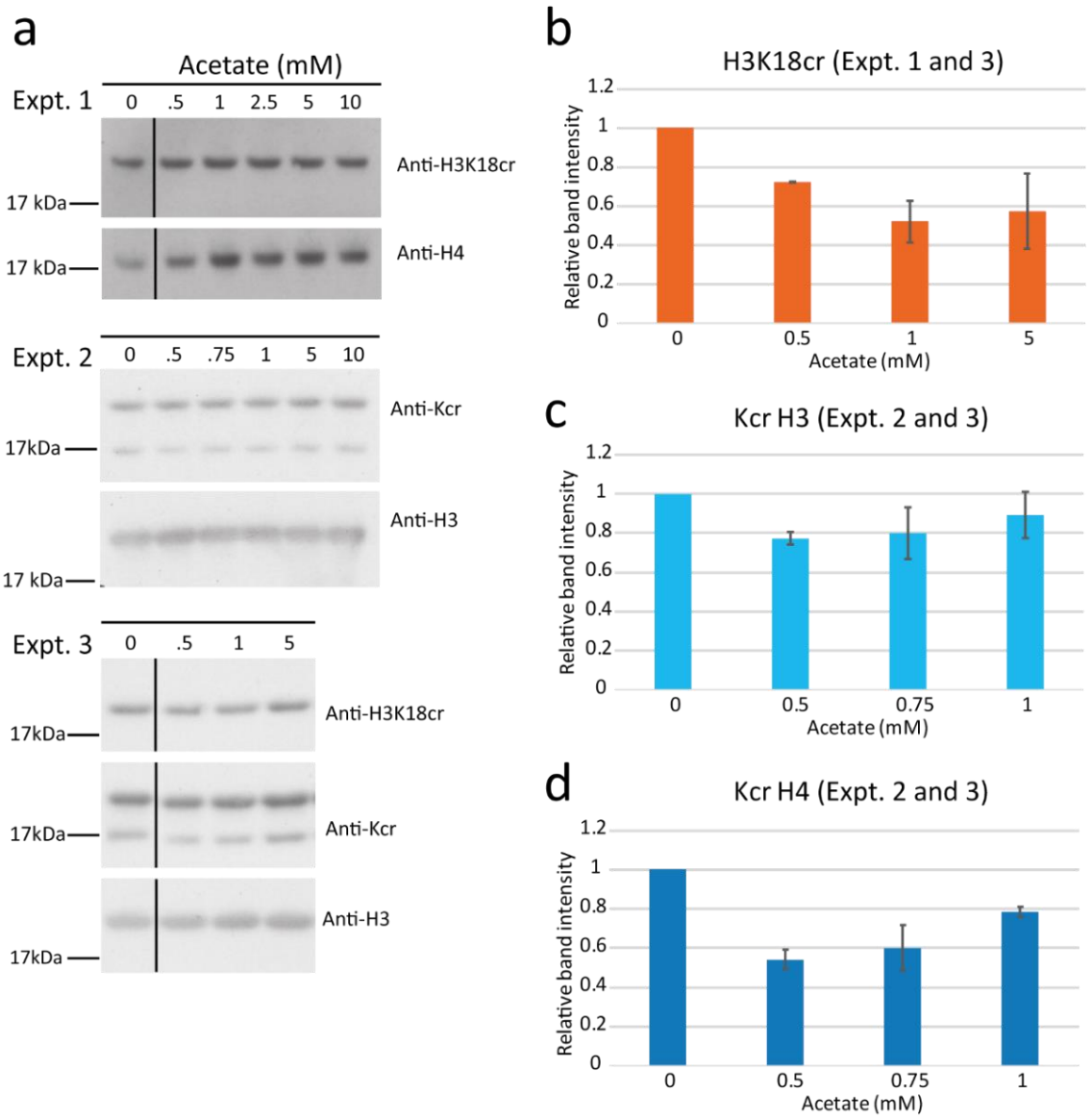

Figure 3.4. Acetate does not promote histone crotonylation in colon carcinoma cells

Acetate was added to the medium of colon carcinoma cells for 24 hours and whole cell extracts were analysed by western blotting using the specified antibodies. **(a)** Western blot images from three biological repeat experiments. **(b-d)** Band quantification was relative to the H3 or H4 blot and the untreated group. The H3 and H4 bands of the anti-Kcr blot were quantified separately and are shown on different graphs. Where there are at least two repeats for a condition in the western blots, the average of band quantifications is shown with error bars as standard deviation. All concentrations are in millimolar.

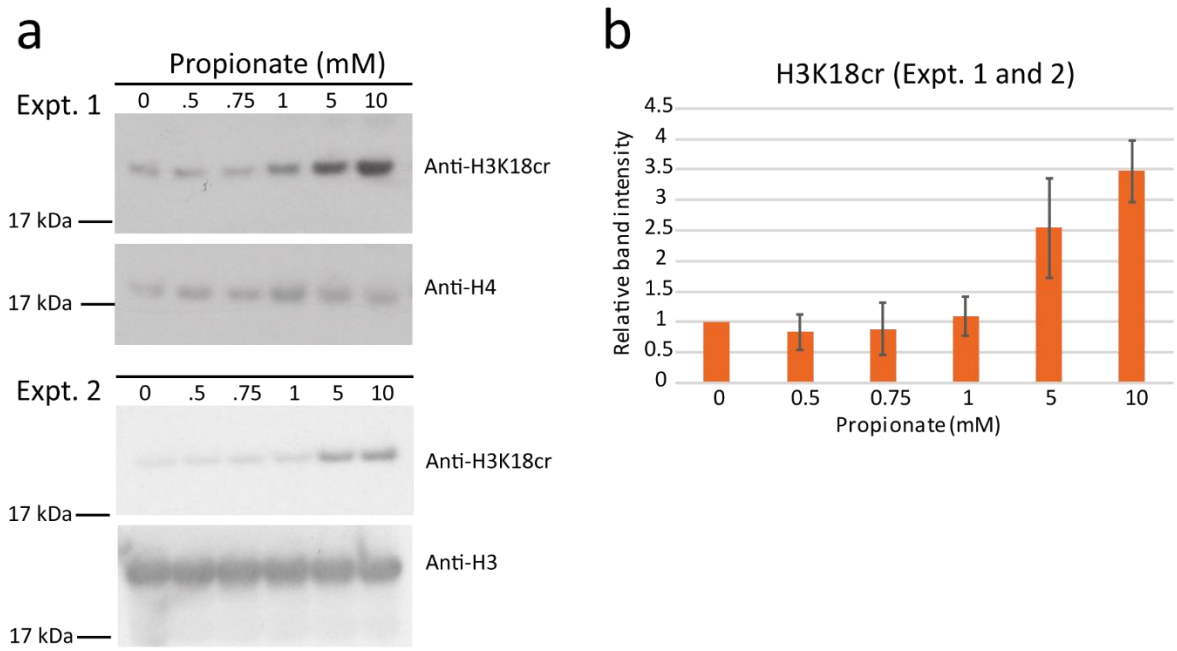

Figure 3.5. Propionate promotes crotonylation in colon carcinoma cells

Propionate was added to the medium of colon carcinoma cells for 24 hours and whole cell extracts were analysed by western blotting using the specified antibodies. **(a)** Western blot images from two biological repeat experiments. **(b)** Band quantifications are relative to the H3 or H4 blot and normalised to the untreated group. The average of band quantifications from two biological repeats is shown with error bars as standard deviation. All concentrations are in millimolar.

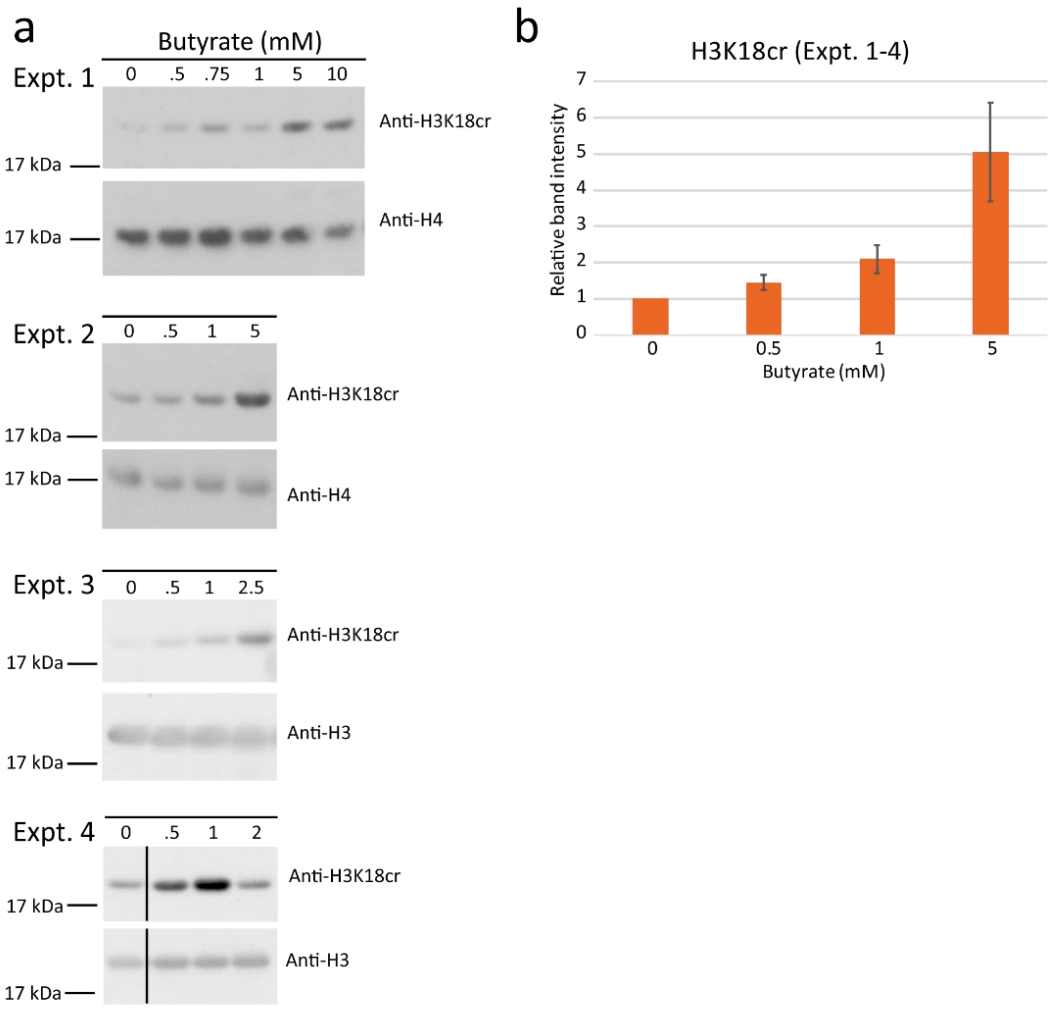

Figure 3.6. Butyrate promotes histone crotonylation in colon carcinoma cells

Butyrate was added to the medium of colon carcinoma cells for 24 hours and whole cell extracts were analysed by western blotting using the specified antibodies. **(a)** Western blot images from four biological repeat experiments. **(b)** Band quantifications are relative to the H3 or H4 blot and normalised to the untreated group. Where there are at least two repeats for a condition in the western blots, the average of band quantifications is shown with error bars as standard deviation. All concentrations are in millimolar.

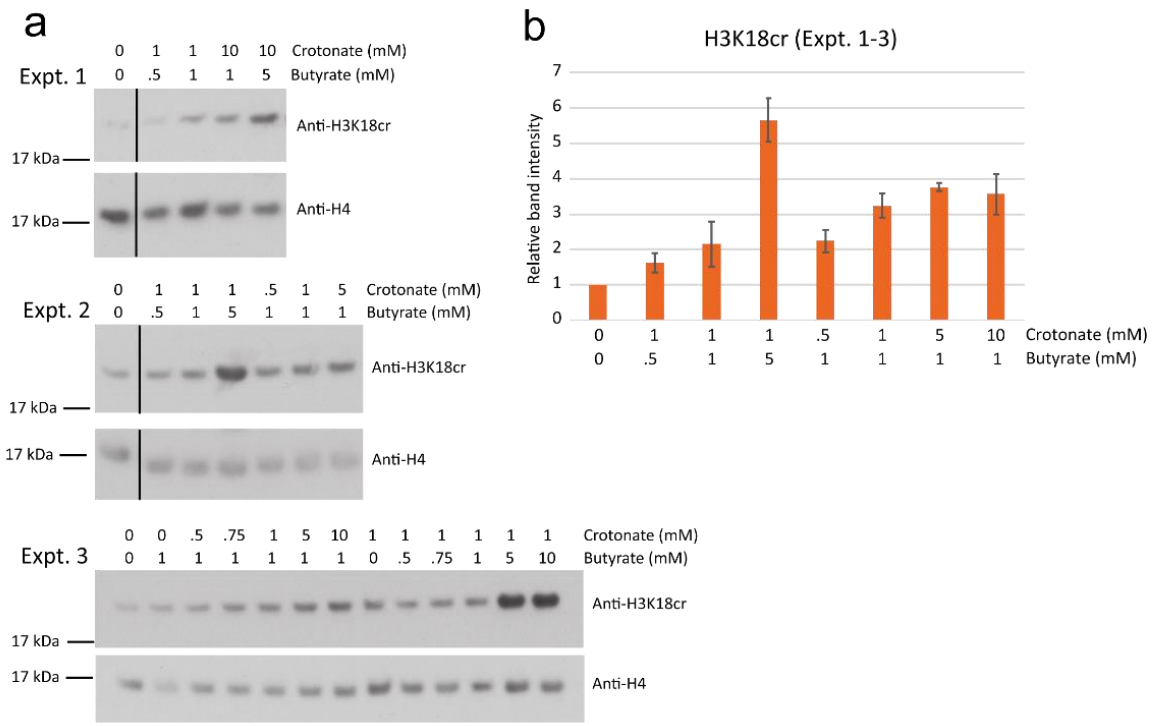

Figure 3.7. The combined effects of crotonate and butyrate on crotonylation in colon carcinoma cells

Butyrate and crotonate were added in combination to the medium of colon carcinoma cells for 24 hours and whole cell extracts were analysed by western blotting using the specified antibodies. **(a)** Western blot images from three biological repeat experiments. **(b)** Band quantifications are relative to the H3 or H4 blot and normalised to the untreated group. Where there are at least two repeats for a condition, the average of band quantifications is shown with error bars as standard deviation. All concentrations are in millimolar.

3.2.3 The dynamics of histone crotonylation response to crotonate and butyrate treatment in cell culture

For chromatin state changes to reflect changes in nutrient availability, histone crotonylation would need to change rapidly so that the cell could respond quickly to changing conditions. We therefore tested the timescale over which crotonylation of histones occurs when crotonate or butyrate is added to the medium of colon carcinoma cells. When crotonate was added, H3K18cr showed a time-dependent increase over 8 hours that was consistent between two technical repeat experiments (Figure 3.8a). 20 mM crotonate was used because an initial test with 10 mM showed no change, although 10 mM treatments were not tested any further. A time-dependent increase in H3K18cr was also seen when butyrate was added to the cell culture medium, and was around 2-fold higher after 1 hour in three technical repeat experiments (Figure 3.8c). The increase was not significant when tested by repeated measures one-way ANOVA with pairwise comparisons. The lack of significance may be because the increase in band intensity relative to the control varied between technical repeats; this

can be easily influenced by small changes in the control. However, an increase of 2-fold or greater was reached in all three repeats suggesting that crotonylation is promoted by butyrate over a timescale of 0.25 to 8 hours. In an initial test of removing crotonate to decrease crotonylation, HCT116 cells were cultured with 10 mM crotonate for 24 hours followed by washing out the SCFA and harvesting the cells at regular intervals. A rapid decrease was seen when crotonate was removed from the cell culture media, although further experiments are required to verify this (Figure 3.8b). These results suggest that histone crotonylation is a dynamic modification, but biological repeat experiments rather than technical repeats would make this conclusion more robust.

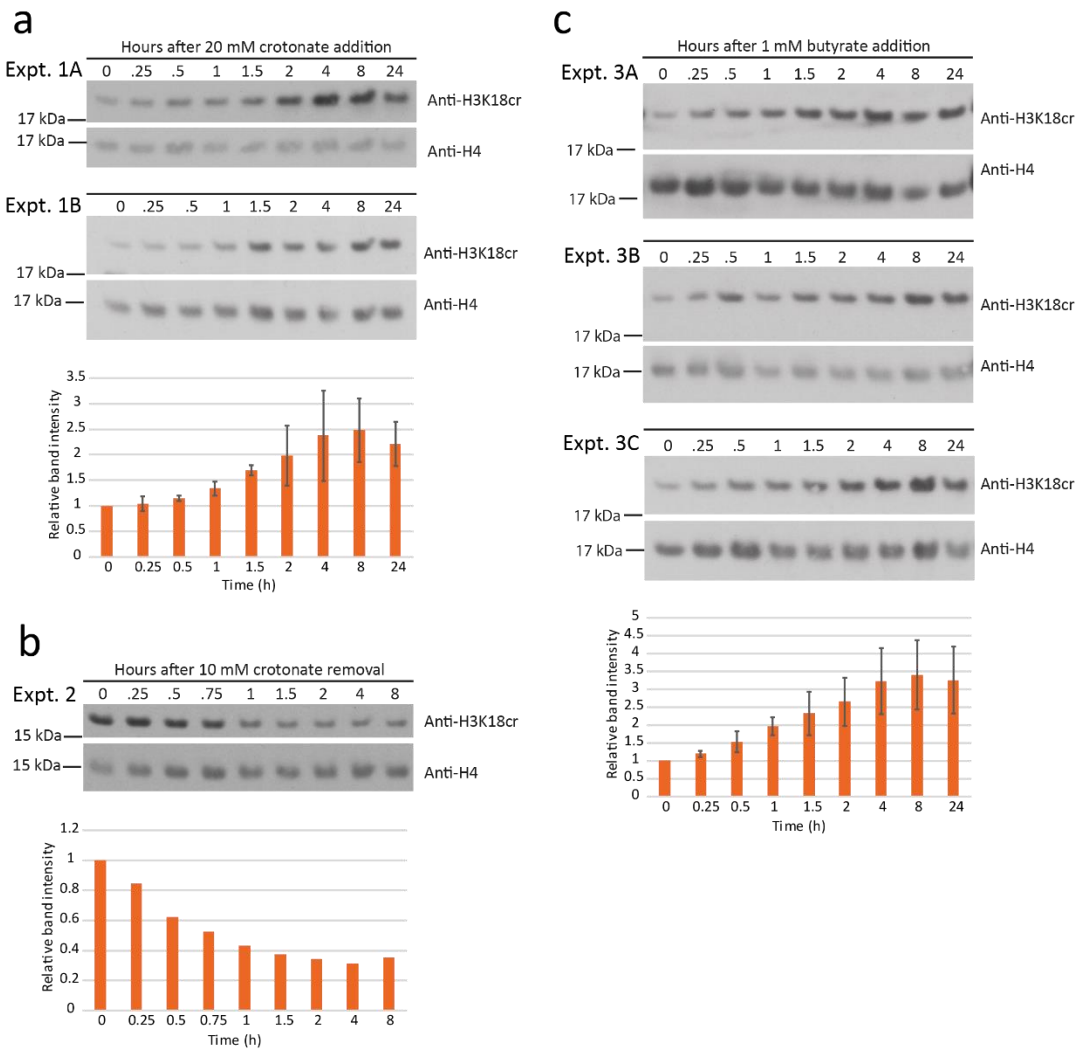

Figure 3.8. Histone crotonylation changes dynamically in response to crotonate and butyrate

SCFAs were added to the medium of colon carcinoma cells for the specified time and whole cell extracts were analysed by western blotting using the specified antibodies. Band quantification was normalised to the H4 band intensity and to the untreated group. Where technical repeats were performed, the average band intensity is shown with error bars as standard deviation. **(a)** 20 mM crotonate was added to the medium of HCT116 cells for up to 24 hours followed by harvesting and preparation of whole cell extracts. **(b)** 10 mM crotonate was added

to the medium of HCT116 cells for 24 hours and then washed out at specified time points up to 8 hours. **(c)** 1 mM butyrate was added to the medium of HCT116 cells for up to 24 hours.

3.2.4 The effects of SCFAs on histone acetylation in colon carcinoma cell culture

Adding acetate to ACLY knock-down cells was found to promote histone acetylation (Wellen *et al.*, 2009), therefore we added acetate to HCT116 cell culture media and tested changes to histone acetylation by western blot. There was no change in H3K18ac or H4K8ac in two biological repeat experiments (Figure 3.9). As butyrate and propionate promoted histone crotonylation in colon carcinoma cells, we hypothesised that they might promote histone acetylation, as metabolism of these SCFAs can generate acetyl-CoA. Butyrate treatment increased H3K18ac at 0.5 and 1 mM in two biological repeat experiments but did not consistently change H4K8ac (Figure 3.9). Butyrate treatment did not produce a clear increase in H4K8ac; perhaps this modification is regulated in a different manner to H3K18ac. Crotonate did not change either H4K8ac or H3K18ac. It is interesting that acetate, which is closest in chemical structure to acetylation, did not upregulate H3K18ac but butyrate did. In cell culture, acetyl-CoA levels are high and the metabolism of SCFAs may not produce a large fold increase in acetyl-CoA above steady-state levels that result in changes to histone acetylation. Donohoe *et al*. (2012) demonstrated that carcinoma cells grown in plenty of glucose do not metabolise butyrate to any great extent as glycolysis is the predominant pathway, thus allowing butyrate to accumulate in the cell. Butyrate, but not acetate, can act as a HDAC inhibitor (Cousens *et al.*, 1979), which could explain why butyrate promoted H3K18ac.

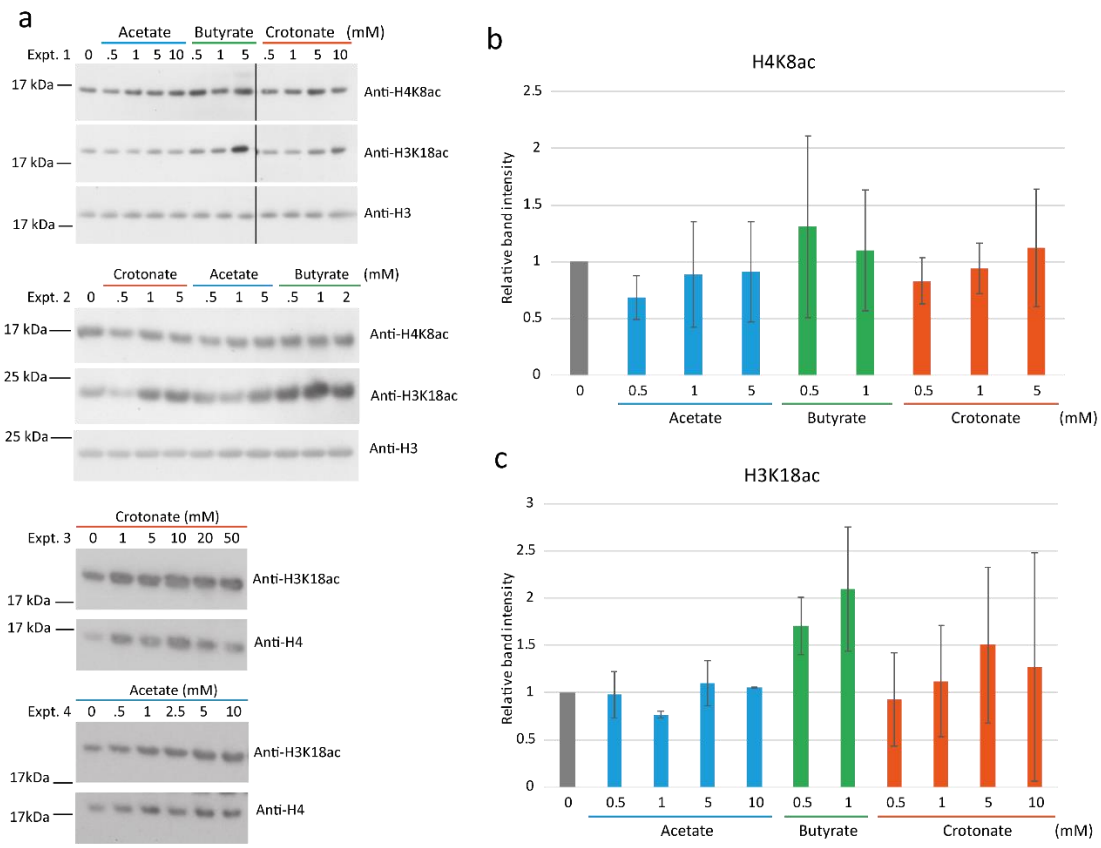

Figure 3.9. The effect of acetate, butyrate and crotonate on histone acetylation in colon carcinoma cells

SCFAs were added to the medium of colon carcinoma cells for 24 hours and whole cell extracts were analysed by western blotting using anti-H4K8ac and anti-H3K18ac. **(a)** Western blot images from four independent experiments. The black lines on the blots in experiment 1 indicate where some n=1 conditions have been spliced out. **(b-c)** Band intensity relative to the quantified bands of the H3 or H4 blot and normalised to the untreated group. Where there are at least two repeats for a condition in the western blots, the average band intensity is shown with error bars as standard deviation.

3.2.5 The effects of SCFAs on histone crotonylation in intestinal organoid culture

Carcinoma cells by their nature are prone to mutations and are grown in conditions that select for highly proliferative cells. Additionally, malignant cells frequently have altered metabolism. Therefore, we chose to test the effect of SCFAs on gut organoid cultures which are a more representative system. Mouse small intestinal or colon stem cells are collected and grown with the required growth factors in a 3D gel where they organise into 'mini-guts' that mimic the gut structure, consisting of a lumen, buds reflecting the crypt zone and differentiated cell types. As these are derived from healthy adult mice, the cells contain a genome with few mutations. We added crotonate or butyrate to the medium of small intestinal organoids and tested changes to H3K18cr by western blot (Figure 3.10). 10 mM

crotonate treatment produced a 2.8-fold average increase in H3K18cr. The fold change between experiments was quite variable with the standard deviation from 1.8- to 3.5-fold for H3K18cr. This variability in fold change in H3K18cr was also seen when HCT116 cells were given 10 mM crotonate (Figure 3.2), with standard deviation from 1- to 5-fold. This could be due to differences in the intensity of the control or small variations in the H3 or H4 normalisation blot. 1 mM butyrate increased H3K18cr but β-HBu did not change H3K18cr in two biological repeat experiments, which reproduces what was seen in colon carcinoma cells. To determine if these fold-changes are significant, and to account for small variations in the control group, four repeats of each condition should be compared in the same western blot.

The colon contains a larger and richer microbiota, resulting in the generation of more SCFAs than the small intestine. We therefore wanted to confirm if SCFAs promoted histone crotonylation in colon organoids, particularly as the growth conditions are not the same as for small intestinal organoids. When crotonate was added to the media of colon organoids, it produced a dose-dependent increase Kcr H3 and H3K18ac in two biological repeat experiments (Figure 3.11a and b). Although the 0.5 and 1 mM conditions were similar to the untreated group, 5 mM crotonate clearly increased Kcr H4 in two experiments. Butyrate increased Kcr H4 and possibly also Kcr H3. 5 mM butyrate increased H3K18ac but this was not repeated and 1 mM either did not change or slightly decreased H3K18ac. These experiments suggest that crotonate and butyrate can promote histone crotonylation in colon and small intestinal organoids, in agreement with the results seen in colon carcinoma cells. However, further experiments are required to make sure that these conclusions are robust and to determine at what concentration a significant increase is seen.

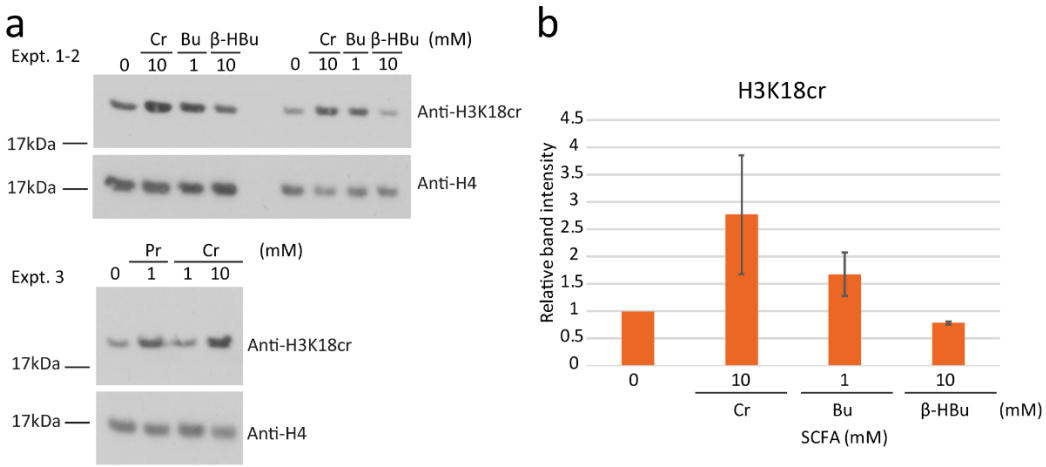

Figure 3.10. The effects of crotonate, butyrate and β-HBu on crotonylation in small intestinal organoids

SCFAs were added to the growth medium of small intestinal organoids for 48 hours. Whole cell extracts were then prepared and analysed by western blotting using the specified antibodies. **(a)** Western blot images from

three biological repeat experiments. **(b)** Band quantification relative to the H3 or H4 band intensity and normalised to the untreated group. Propionate (Pr), crotonate (Cr), butyrate (Bu) and β-HBu. Average band intensity is shown with error bars as standard deviation when there are at least two repeats for a condition.

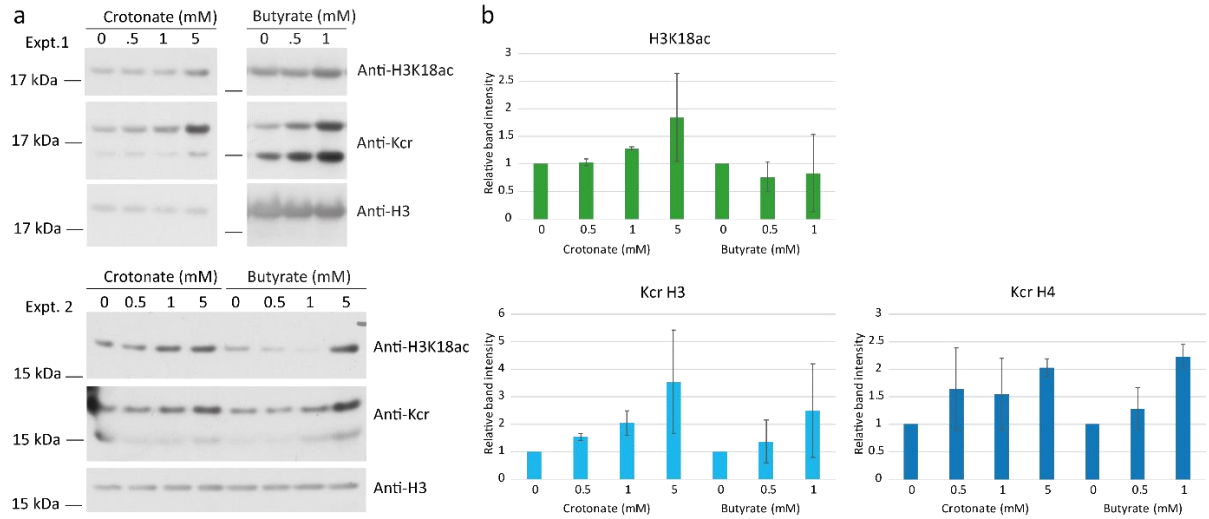

Figure 3.11. Crotonate and butyrate promote histone crotonylation in colon organoids

SCFAs were added to the medium of colon organoids for 48 hours and whole cell extracts were analysed by western blotting using the specified antibodies. **(a)** Western blot images from two biological repeat experiments. **(b)** Band quantification is relative to the anti-H3 band intensity and the untreated group. Average band intensities are shown with error bars as standard deviation where there are at least two repeats for a condition.

3.2.6 Non-butyrate HDAC inhibitors promote histone acetylation and crotonylation

It is difficult to elucidate the mechanism of the effect of butyrate on histone acylations as it can act on the cell through multiple pathways. However, other HDAC inhibitors exist which have a distinct structure and are not precursors to metabolic intermediates. To compare the effect of HDAC inhibition on histone crotonylation and acetylation, we added TSA, SAHA or butyrate to the media of colon carcinoma cells and analysed whole cell extracts using specific crotonyl and acetyl antibodies. As shown in Figure 3.12, all of these HDAC inhibitors promoted both acetylation and crotonylation in three biological repeat experiments. For butyrate, this is in agreement with the experiments in Figure 3.6 and Figure 3.9 which also saw that butyrate could promote Kcr and H3K18ac. As seen from the quantifications of band intensity, this occurred in a dose-dependent manner with the highest concentrations of TSA, SAHA and butyrate producing a significant increase in Kcr H4 relative to the untreated group (Figure 3.12). There was also a significant increase compared to the control in Kcr H3 for the highest concentrations of TSA and butyrate, but no significant changes in H3K18ac. The

western blots show a clear dose-dependent increase in H3K18ac in each experiment with all inhibitors tested. So the lack of significance may be because experiment 1 shows different fold changes to experiments 2 and 3 resulting in variability in the band quantifications. The clearest example of this is for 0.2 µM TSA which produces low acetylation and crotonylation for experiment 1 but is increased relative to control in experiments 2 and 3. These experiments suggest that non-butyrate HDAC inhibitors can promote histone crotonylation and the striking consistency between experiments 2 and 3 suggests that these effects are biologically relevant.

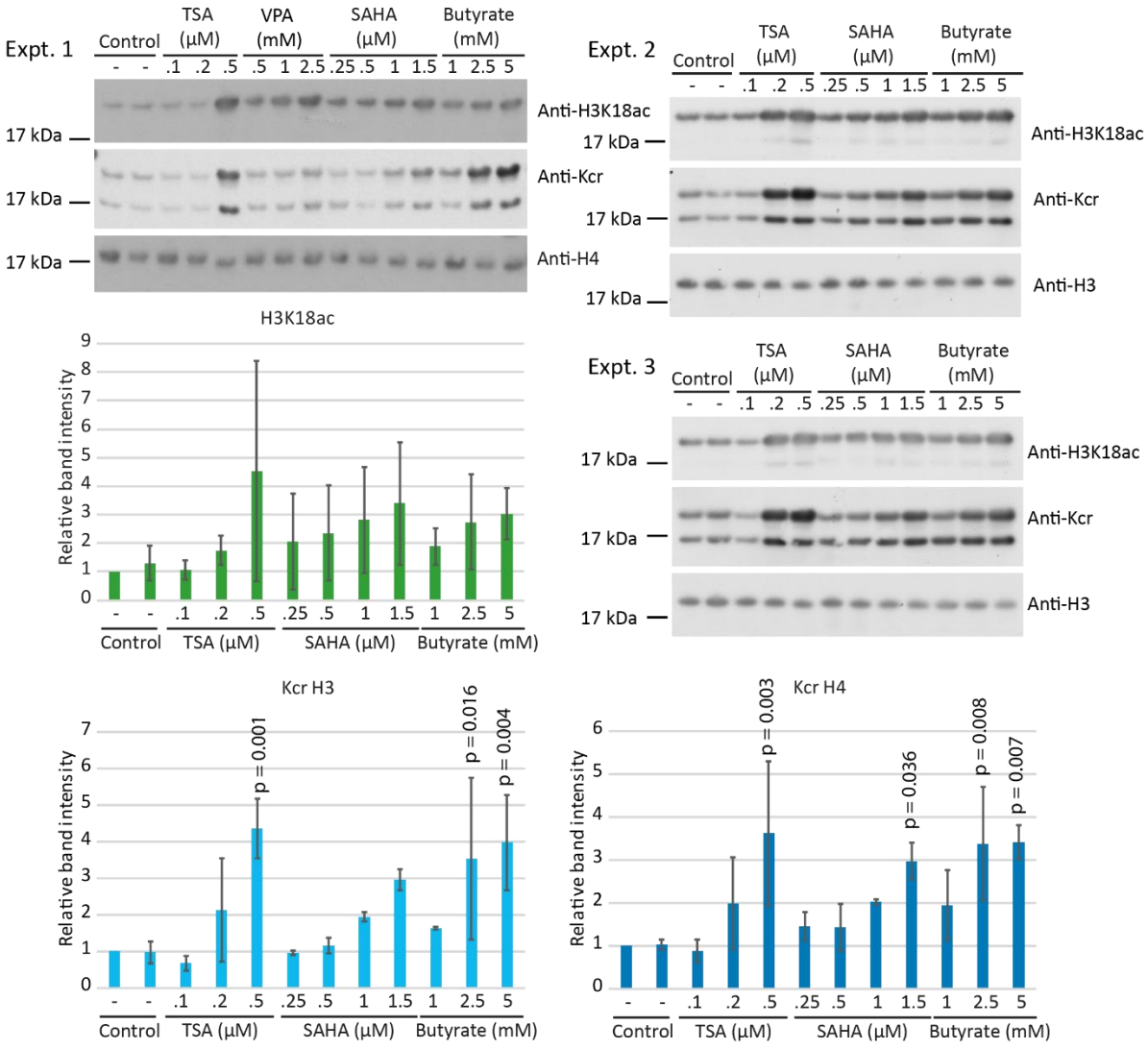

Figure 3.12. HDAC inhibitors promote histone acetylation and crotonylation in HCT116 cells

HCT116 cells were treated with the indicated amounts of TSA, SAHA or butyrate for 24 hours. Three biological repeat experiments are shown. The first control group is untreated, the second control group was treated with 0.5% DMSO which was also in all of the treatment conditions. Western blot was performed with anti-H3K18 acetyl, anti-Kcr and anti-H4 or anti-H3. Quantified bands are shown below the blot relative to H4 band intensity and the first control group. Graphs show the average relative band intensities from the three repeats with error

bars as standard deviation. One-way ANOVA was performed with pairwise comparisons and the p values of significant pairwise comparisons are shown on the graph.

3.2.7 HDAC1 can remove crotonyl-groups from H3 histones but not H3 peptides.

As we have shown, inhibition of HDACs in cell culture promoted crotonylation as well as acetylation but it was not known if HDACs could act directly by decrotonylating the histone or if these changes occurred through an indirect method where increased histone acetylation promoted histone crotonylation. Prior to our study, some evidence did exist to suggest that HDACs could use larger acyl chains. One study using a fluorogenic crotonylated H4 peptide found measureable activity with HDAC3/NCoR1 but no other HDAC enzymes (Madsen and Olsen, 2012). We incubated different amounts of biotinylated acetyl or crotonyl H3K18 peptides with or without HDAC1 for 2 hours at 30 °C. HDAC1 reaction mixes were spotted in quadruplicate onto nitrocellulose membranes and western blot with anti-H3K18cr or anti-H3K18ac performed. The dot blot shows that there was no difference between the reactions with HDAC1 or without HDAC1 for either substrate (Figure 3.13a). To further test the ability of HDAC1 to remove acetyl- or crotonyl-groups from H3 peptides, we tested different amounts of HDAC1 and different durations of the reaction with an intermediate concentration of acylated peptide (4 μM). No changes in spot intensity could be seen, although high background in some places of the blot did make this more difficult to interpret (Figure 3.13b). Quantifications of the 60 and 100 nM HDAC1 timecourses, which had low background, were compared to zero time (the 0 nM HDAC1 and 60-minute conditions without high background). There was a slight reduction in acetyl-peptide from 1 to 60 minutes, but the zero time was the lowest. The crotonyl-peptide reactions revealed an equally inconclusive picture.

HDAC1 may be able to remove acetyl- and crotonyl-groups from these H3 peptides with other reaction conditions, but we saw no convincing evidence of removal in our initial tests. Therefore, we performed a preliminary test with acylated recombinant histone H3. The recombinant catalytic domain of the acyltransferase p300 and acetyl-CoA, butyryl-CoA or crotonyl-CoA were used to acylate recombinant histone H3.1 *in vitro*. The resulting acylated histone was then tested against HDAC1, HDAC2 or HDAC3-NCoR1. The NCor1 protein is required for the full HDAC3 activity (You *et al.*, 2013). The reaction mixes were analysed by western blot with specific antibodies. The acyltransferase reaction by p300 was successful as there is a strong H3K18ac, H3K18bu or H3K18cr band without any HDAC (Figure 3.14). The highest concentration of each HDAC was sufficient to remove all (or nearly all) of the acetylation, crotonylation and butyrylation. Strikingly, even the lowest concentration of HDAC1 (0.03 μM) was sufficient to remove almost all H3K18cr despite it being strongly present in the control group.

Whilst these experiments suggested that class I HDACs could remove crotonyl- and butyryl-groups from histones, we did not have repeats for each condition. Additionally, these reactions were incubated for 2 hours to ensure that the reaction had gone to completion, but we did not know how quickly the acyl-group removal had been. We chose to focus on HDAC1 as it appeared to be the most effective decrotonylase out of the three enzymes tested. A time course experiment was performed, incubating HDAC1 with crotonyl-H3 or acetyl-H3 for different durations. After 60 minutes, a significant reduction could be seen in H3K18ac with HDAC1 in three repeat experiments (Figure 3.15). Interestingly, decrotonylation by HDAC1 was faster, with a significant reduction in the modification after just 10 minutes in three experiments.

To fully assess whether HDAC1 has comparable decrotonylation efficiency to deacetylation, a kinetic assay must be performed with repeats of different substrate concentrations to determine reaction constants. This is because enzymes can have a residual or promiscuous activity which can be detected *in vitro* but may not occur to any functional extent *in vivo* (Khersonsky and Tawfik, 2010). We performed *in vitro* enzymatic assays by incubating a constant concentration of HDAC1 with different concentrations of crotonyl-H3 or acetyl-H3 for different durations to plot a substrate rate curve that enables estimation of V_{max}, K_m and K_{cat}. V_{max} describes the maximum rate that is possible with a given enzyme concentration. K_m is the Michaelis constant and describes the substrate concentration required to achieve half maximal rate. This constant gives a measure of how effective the enzyme is with lower substrate concentrations. Finally, K_{cat} is the turnover number, as in the number of molecules of substrate turned over to product per unit time, and gives a measure of the enzyme's efficiency with that substrate. Reactions were performed in triplicate with multiple concentrations of acetyl-H3 or crotonyl-H3 and different time points. The reactions were dot blotted in quadruplicate and western blot performed followed by spot quantification using image J. The result in Figure 3.16 shows that deacetylation can reach a higher maximal rate and is around 2.5 times more efficient than decrotonylation. However, the fact that the K_{cat} of decrotonylase activity is only 2.5-fold lower than the K_{cat} of deacetylation suggests that it is not a residual activity of this enzyme. Interestingly the K_m of the decrotonylase reaction is lower than that of the deacetylase reaction meaning HDAC1 can act efficiently on lower concentrations of crotonyl-H3 compared to acetyl-H3. This difference in K_m may be because the V_{max} of deacetylation is higher. At 0.25 µM of acetyl-H3 or crotonyl-H3, the rate of decrotonylation and deacetylation are very similar, between 0.4 and 0.5 µM/min. This kinetic study demonstrates that HDAC1 has a similar capacity to remove crotonyl groups as it does to remove acetyl groups.

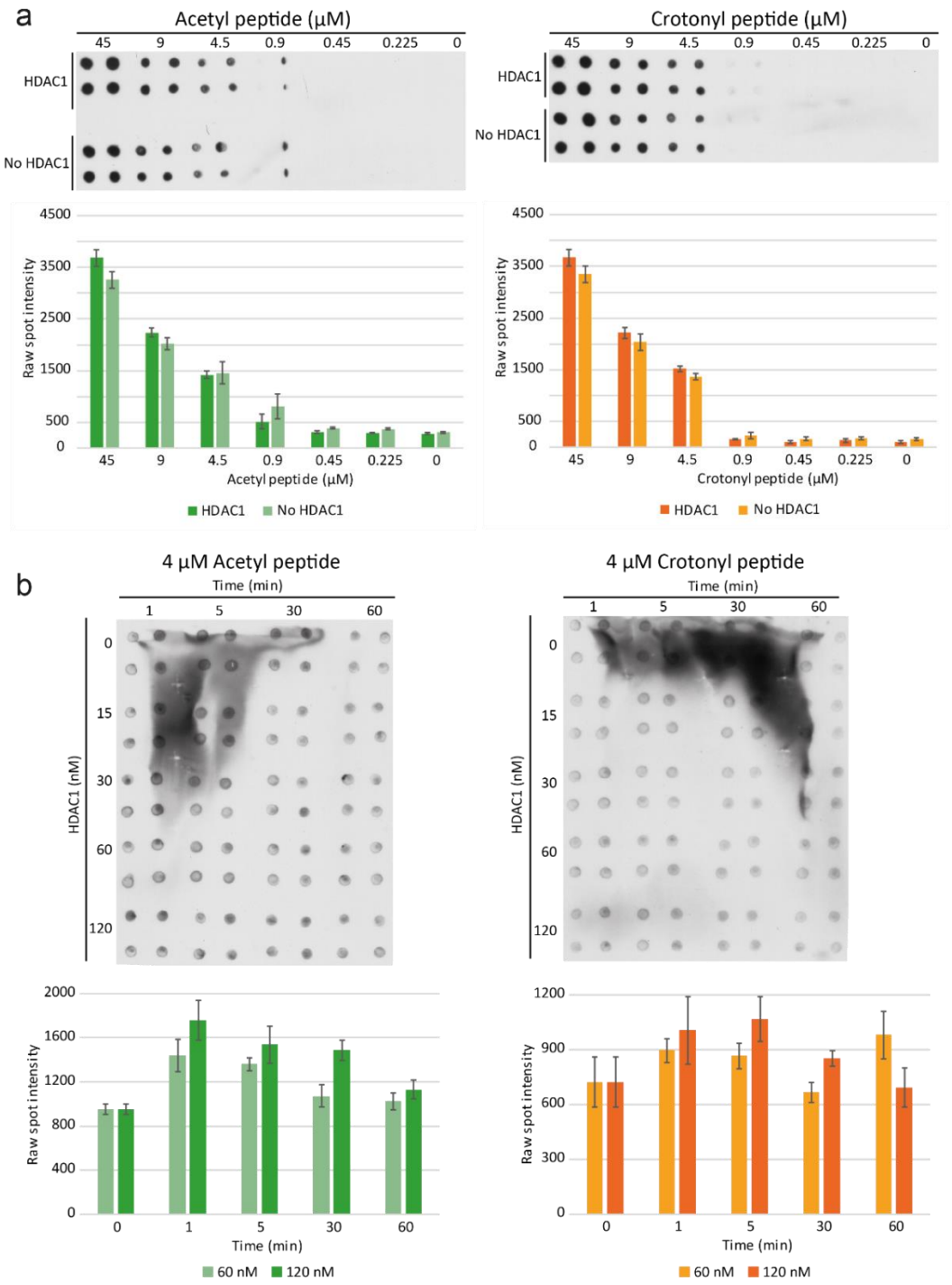

Figure 3.13. Removal of acyl groups from biotinylated peptides by HDAC1

(a) The specified concentration of acetyl- or crotonyl-H3 peptide was incubated with 0.12 μM HDAC1 or without HDAC1 for two hours followed by spotting onto nitrocellulose membrane and performing western blot with anti-H3K18ac or anti-H3K18cr. The quantifications are shown as an average of the spot intensity of four replicate spots with error bars as standard error. **(b)** 4 μM acetyl- or crotonyl-H3 peptide was incubated with the specified amount of HDAC for the specified duration, followed by spotting onto nitrocellulose membrane and performing western blot with anti-H3K18ac or anti-H3K18cr. The quantifications are shown as an average of the

quadruplicate spots with error bars as standard error of the mean. The zero time quantifications are of the 0 nM HDAC1 and 60 minute reactions without background.

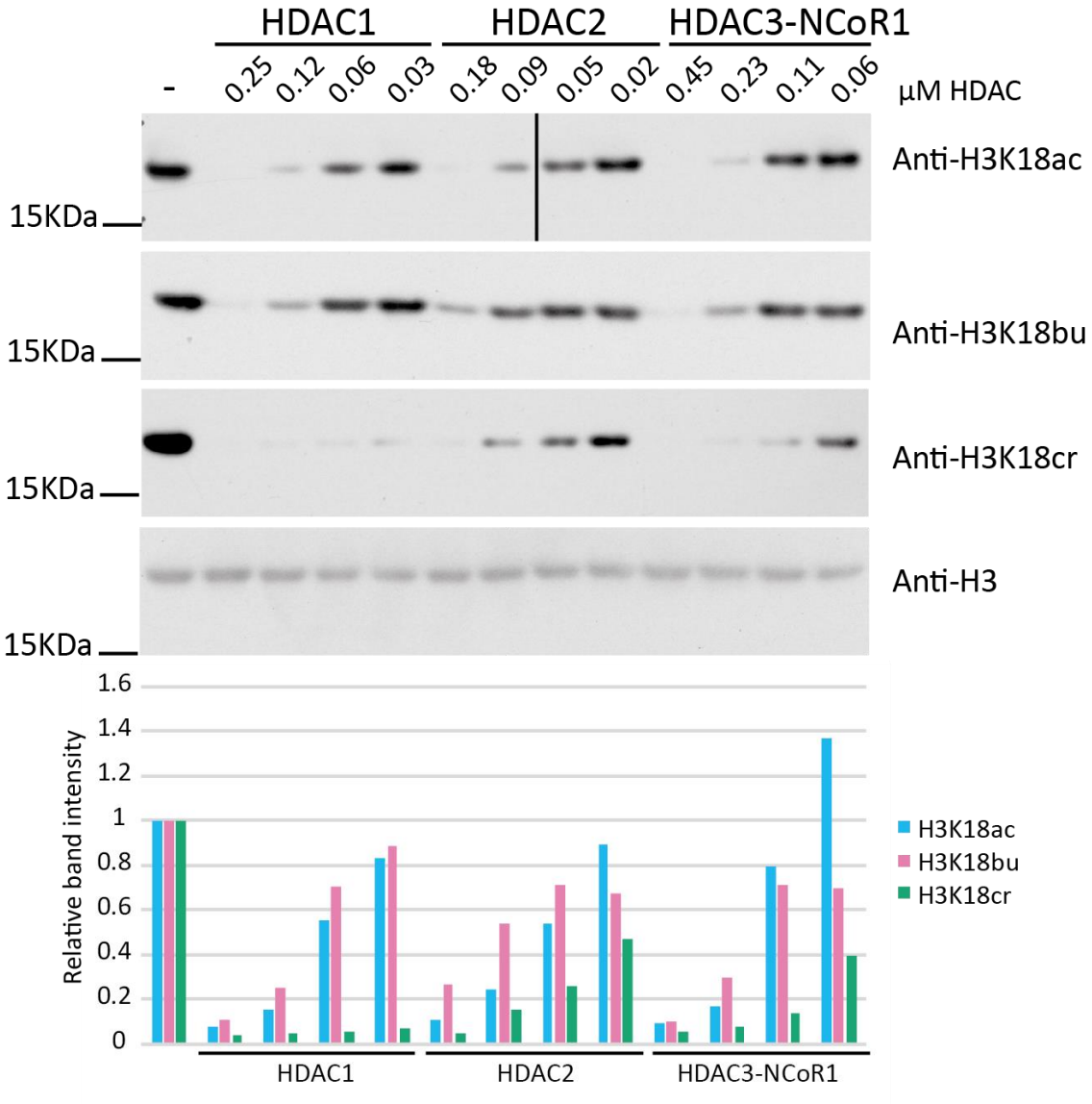

Figure 3.14. Histone deacetylation, debutyrylation and decrotonylation by HDAC1, HDAC2 or HDAC2/NCoR1

5.65 µM histones were acetylated, butyrylated or crotonylated *in vitro,* using the relevant acyl-CoA and recombinant p300, and then subjected to removal of the modification by the indicated HDACs at the specified concentrations. Western blot was performed with antibodies against H3K18 acetyl, butyryl or crotonyl depending on the acyl-H3 substrate in the reaction. A representative anti-H3 blot is shown for one set of reactions to show that the protein loading is equal. Band quantifications are shown below using image J and are relative to the H3 band intensity and the reaction without HDAC.

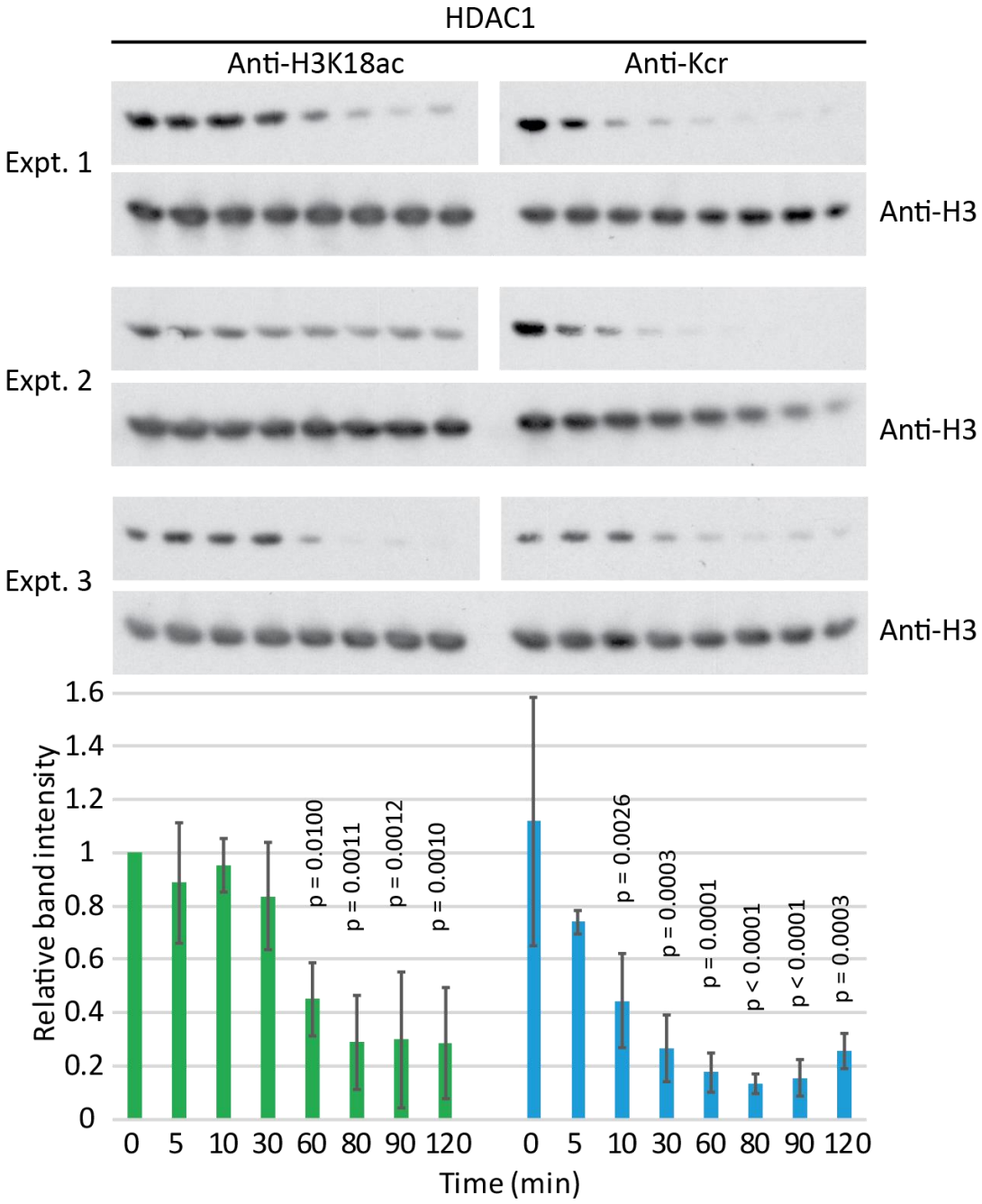

Figure 3.15. HDAC1 decrotonylation occurs over a similar timescale to deacetylation

Recombinant acetylated or crotonylated histone H3 (5.65 µM) was incubated with 0.12 µM HDAC1 for the specified time and stopped reactions were analysed by western blot using anti-pan-crotonyllysine or anti-H3K18 acetyllysine. A separate gel was run and blotted for anti-H3 to measure protein loading. Quantifications were normalised to H3 band intensity and are shown relative to the start reaction. The HDAC1 quantifications are an average of three separate experiments with error bars as standard deviation. One-way ANOVA was performed which was significant with a p value of 0.0001 for H3K18ac and < 0.0001 for Kcr. Comparisons were performed between each timepoint at the start reaction and significant p values are shown on the graph. Western blots were performed by Szabina Balázsi and Zoltán Hajnády and I performed the data analysis.

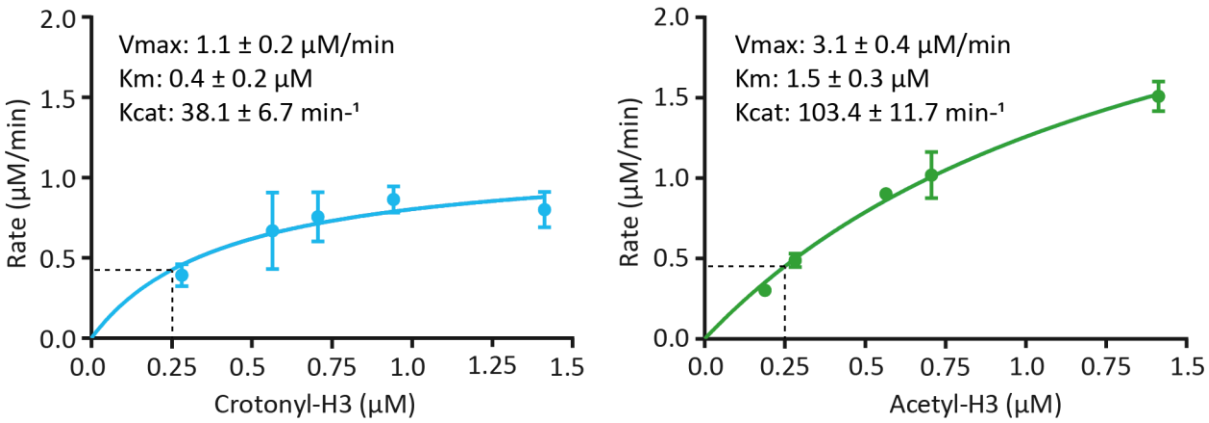

Figure 3.16. Comparitive kinetics of HDAC1 decrotonylation and deacetylation

5.65 µM histones were crotonylated or acetylated using recombinant p300 and crotonyl or acetyl-CoA. Acylated histones were subjected to removal of the modification by 0.03 µM HDAC1 for different lengths of time and different initial substrate concentrations. Samples were analyzed by dot blotting using antibodies against H3K18cr and H3K18ac. Initial rates of reaction were determined by plotting substrate removal over time. Kinetic parameters V_{max}, K_m, and K_{cat} are shown on the graph, error bars are standard error of the mean, $n = 3$.

3.2.8 The effect of HDAC inhibitors on decrotonylation and deacetylation

Having confirmed that HDAC1 is an efficient decrotonylase, we then tested if different HDAC inhibitors could prevent decrotonylation as well as deacetylation *in vitro*. After recombinant H3 acylation using p300, we added HDAC1 and different concentrations of TSA or butyrate to see if this would prevent acyl-group removal. Whilst crotonylation was completely removed without inhibitor, a reduction in removal of crotonylation could be seen as the dose of TSA or butyrate increased in two experiments (Figure 3.17a and b). In one experiment, the highest dose of TSA or butyrate produced a level of crotonylation similar to that of the positive control without any HDAC1, whilst in the other the final level was less than the control. Reassuringly, TSA and butyrate could also reduce removal of acetylation as expected. As butyrate and TSA could inhibit both activities, this suggests that HDAC1 may use the same active site for both deacetylation and decrotonylation reactions. As for the treatments of cells with inhibitors (Figure 3.12), TSA was more potent than butyrate as much lower concentrations were required to achieve maximum inhibition. We also found that crotonate could reduce deacetylase and decrotonylase activity of HDAC1 (Figure 3.17c), although the extent of inhibition of deacetylation was quite variable between the two experiments. The concentrations of butyrate, crotonate and TSA used in cell culture to promote histone acetylation and crotonylation (Figure 3.2, Figure 3.6 and Figure 3.12), are very similar to the concentrations able to inhibit HDAC1 activity *in vitro* (Figure 3.17). These experiments suggest that TSA, butyrate and crotonate can inhibit

decrotonylation by HDAC1 but variability between some experiments makes it hard to determine at what concentration this occurs. Performing these experiments again with additional repeats will enable determination of inhibition constants, such as the concentration required to achieve half maximal inhibition for both HDAC1 activities.

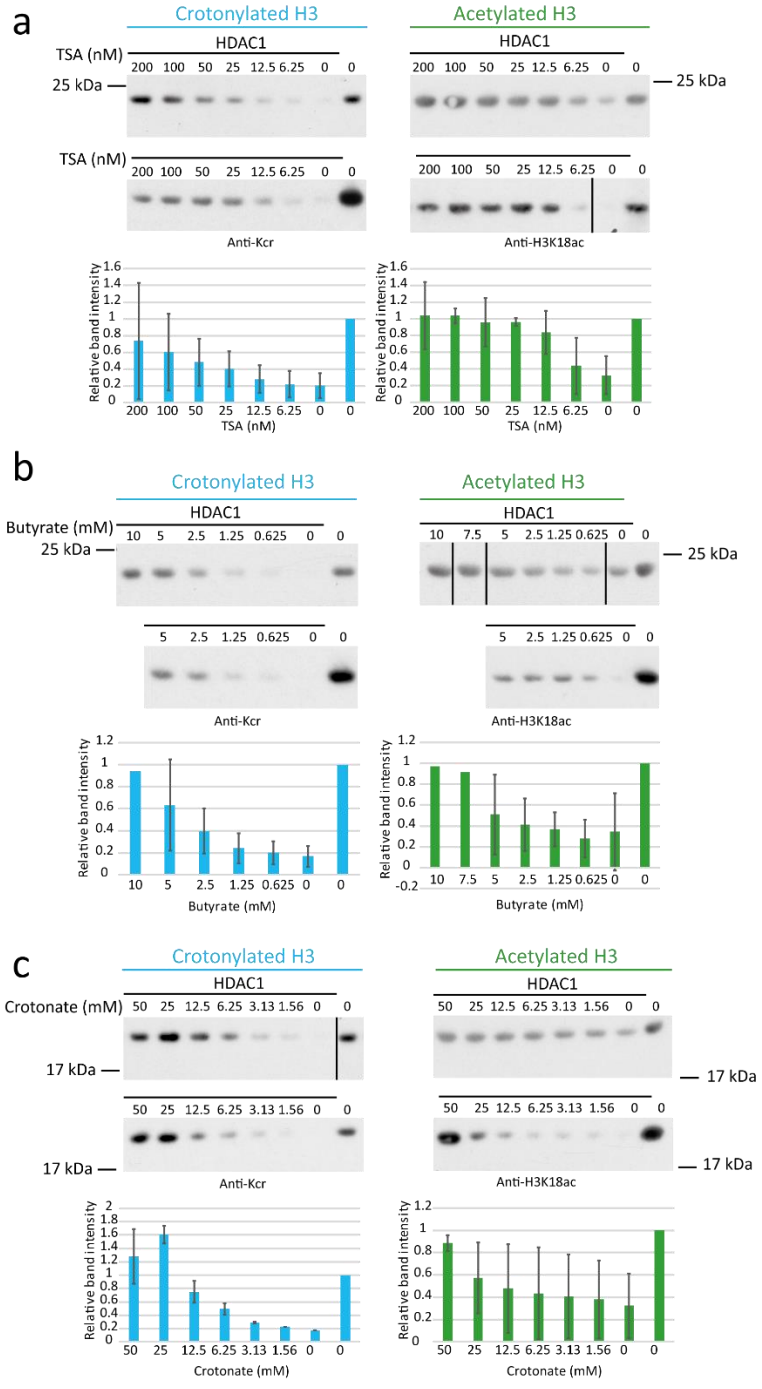

Figure 3.17. TSA, butyrate and crotonate inhibit decrotonylation and deacetylation by HDAC1

Recombinant acetylated or crotonylated histone H3 was incubated with 0.12 µM of HDAC1 and different concentations of TSA, butyrate and crotonate as specified above. Western blot was performed using anti-Kcr against the crotonyl-H3 reactions and anti-H3K18ac against the acetyl-H3 reactions. Band quantifications are

the average of two independent experiments each normalised to the condition without HDAC1. Error bars are standard deviation. Black lines on blots are where miss-loaded samples were spliced out or the order of samples was rearranged (b). These experiments were performed with some help from Szabina Balázsi and Zoltán Hajnády.

3.2.9 HDAC1 can use crotonate as a substrate to transfer crotonyl groups to histones

One interesting thing that we noticed from Figure 3.17c is that at 25 mM crotonate the level of histone crotonylation was slightly higher than the control where no HDAC1 or crotonate was added to the crotonyl-H3 protein solution. This did not happen in the acetyl-H3 assay with HDAC1 and crotonate. Could additional crotonyl groups be transferred from crotonate to the histone during the reaction? HDAC1 deacetylation generates acetate in the nucleus (Bulusu *et al.*, 2017), so it is likely HDAC1 decrotonylation generates crotonate. This reaction has the potential to reverse with higher concentrations of product. Alternatively, non-enzymatic transfer of crotonyl-groups from crotonate could occur. Studies have shown that non-enzymatic acylation of protein lysines can occur due to high acyl-CoA concentrations and an alkaline pH (Wagner and Hirschey, 2014). Therefore, we performed an *in vitro* assay in which reactions with recombinant H3 and different concentrations of crotonate were incubated with HDAC1 or without HDAC1 for 2 hours (Figure 3.18). Reactions were analysed by dot blot. We observed a dose-dependent increase in histone crotonylation with crotonate in the presence of HDAC1 in two repeat experiments. Histone crotonylation did not change when HDAC1 was absent, although this should be repeated to verify the result (Figure 3.18). It is possibile that crotonate transfer is non-enzymatic but dependent on the concentration of protein in the reaction. However, HDAC1 is at a concentration of 0.18 µM, compared to 5.65 µM histone H3.1, meaning that the change in protein concentration without HDAC1 is small. To control for this in future experiments, 0.18 µM BSA could be used for the no-HDAC control. This result suggests that this was an enzymatic transfer of the crotonyl group by HDAC1 and highlights the reversible nature of HDAC1 decrotonylase activity. However, as concentrations of crotonate as high as 50 mM are unlikely to exist in the cell, HDAC1 probably does not have crotonyltransferase activity *in vivo.*

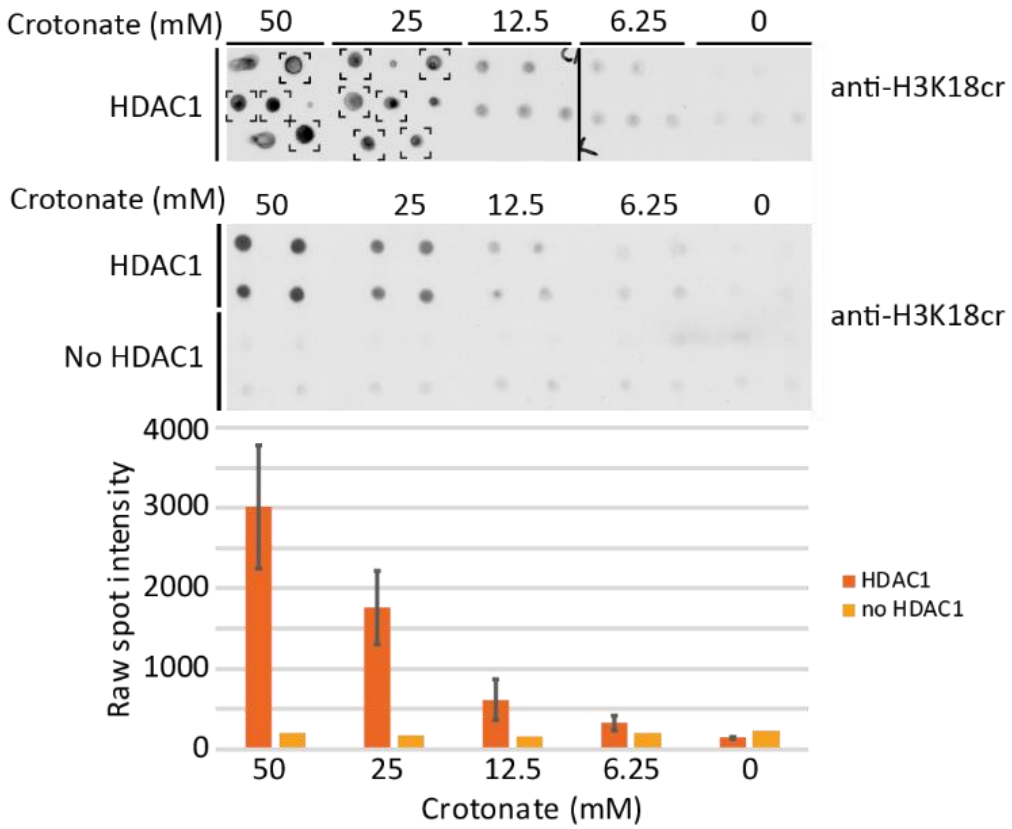

Figure 3.18. HDAC1 can use crotonate as a substrate to decrotonylate histones

Recombinant H3 was incubated with different concentrations of crotonate and a constant concentration of HDAC1 or no HDAC1. Dot blot of two independent repeats of the reactions with HDAC1 and one repeat without HDAC1. Spot intensity was averaged for each reaction. For HDAC1 reactions, quantifications are the average of combined reaction spots and error bars are the standard deviation of the two repeats. Squares around spots indicate the spots that were used in the quantifications as some spots were miss-loaded.

3.3 Discussion

3.3.1 HDAC1 is an efficient histone decrotonylase

We found that treating HCT116 cells with HDAC-inhibiting TSA or SAHA resulted in promotion of histone crotonylation as well as histone acetylation, suggesting that HDACs could be involved in histone decrotonylation. Preliminary tests suggested that HDAC1 was ineffective against short H3 acetyl- or crotonyl-peptides but HDAC1-3 could remove acyl-groups from recombinant H3. Using a kinetic assay, we identified for the first time that HDAC1 has a similar capacity to remove crotonyl groups as it does to remove acetyl groups. The K_m of HDAC1 with the acetylated H3 was 1.5 ± 0.3 µM, higher than the K_m of 0.4 ± 0.2 µM with crotonylated H3, suggesting that HDAC1 is responsive to low concentrations of crotonyl-H3. The maximum rate and efficiency (V_{max} and K_{cat}) of deacetylation was

around 3 times higher than decrotonylation, indicating a higher maximal capacity with the acetyl substrate but also that the decrotonyl activity is not a trace activity of the enzyme.

The only previous kinetic analysis of HDAC decrotonylase activity was of HDAC3/NCoR1 with a fluorescent crotonyl H4 peptide. The K_m was 19 µM ± 15, suggesting that HDAC3 is less responsive to low substrate concentrations. However, the turnover was much higher as the K_{cat} was 0.18 ± 0.06 min^{-1}, compared to HDAC1 which was 38.1 ± 6.7 min^{-1} (Madsen and Olsen, 2012). As both the enzyme (HDAC1 or HDAC3/NCoR1) and substrate (H3-crotonyl or fluorescent-crotonyl) are different, it is unclear whether this difference in efficiency is due to the enzyme or the substrate. K_m values of HDAC1 determined with different acetylated fluorescent or tritiated substrates vary considerably from 0.68 to 78 µM (Hoffmann *et al.*, 1999; Wegener *et al.*, 2003; Schultz *et al.*, 2004; Halley *et al.*, 2011; Henkes *et al.*, 2012). The properties of the substrate may influence HDAC efficiency and therefore using the physiological substrate, as we have done here, may be important for determining true *in vivo* activity. That said, this assay only provides estimates of kinetic parameters, as substrate concentration could not be determined directly. HDAC enzymes are part of multisubstrate complexes *in vivo* which influence substrate specificity and enzyme rate. A subsequent study to our work found that a ternary complex of HDAC1, CoRest and LSD1 could hydrolyse H3K18cr peptides (Kelly *et al.*, 2018). In their study, the HDAC1 complex could use H3K18cr peptides suggesting that only HDAC1 alone requires the full histone H3 and emphasing the importance of the complex in regulating substrate specificity. The assay we have developed would enable investigation of how different complexes change the kinetic parameters of various enzymes, provided that the complex could be produced recombinantly.

Whilst this work was in revision, another study was published showing that the class I enzymes HDAC1, HDAC2, HDAC3 and HDAC8 have decrotonylase activity in embryonic stem cells using an immunofluorescence approach (Wei, Liu, *et al.*, 2017). They treated cervical/uterine cancer HeLa S3 cells, with TSA and saw also a large increase in histone crotonylation. Interestingly there was only a modest increase with the SIRT inhibitor, nicotinamide. Knockdown of HDAC1/2/3 using RNA silencing revealed a dramatic increase in histone crotonylation and acetylation, whilst knockdown of SIRT1/3/5 did not noticeably affect either modification (Wei, Liu, *et al.*, 2017). In combination with our results, and the findings by Madsen *et al.* (2012) and Kelly *et al.* (2018), this provides strong evidence that class I HDACs are major histone decrotonylases in cell culture and may also be *in vivo.*

3.3.2 The therapeutic potential of HDAC inhibitors

HDAC inhibitors have important therapeutic potential particularly in the treatment of cancer. HDACs are upregulated or misregulated in various cancer types and are associated with increased

proliferation and poor prognosis (Yoon and Eom, 2016). The HDAC inhibitor SAHA has been licensed to treat cutaneous T cell lymphoma, but the responses of different cancer types to HDAC inhibitors have been varied (Bojang and Ramos, 2014). The explanation for this could be in part due to the action of HDACs on non-acetyl histone acylations, as we found that treatment of cells with SAHA or other HDAC inhibitors upregulated histone crotonylation in addition to acetylation. This novel finding that class I HDACs are decrotonylases suggests that drugs which were previously developed to target histone acetylation may have wider effects than anticipated. As HDAC inhibitors can prevent both deacetylation and decrotonylation, these enzymes may use the same active site for both reactions making it difficult to design selective inhibitors. However, we found that TSA inhibited the deacetylation reaction of HDAC1 at lower doses than the decrotonylation reaction *in vitro*. These dose-dependent divergences in the effect of TSA on deacetylation or decrotonylation suggests that there might be differences in how HDAC1 uses either substrate. Excitingly, Wei *et al.* were able to mutate HDAC1 so that it retained HDCR activity but lost HDAC activity. Expression of this HDAC1 mutant in HeLa cells could repress transcription of several housekeeping genes to the same levels as wild type HDAC1, demonstrating the importance of histone crotonylation in gene regulation (Wei, Liu, *et al.*, 2017). The structural differences between wild type HDAC1 and the HDAC1 mutant could be exploited to generate inhibitors targeting only one activity. These more specific inhibitors may have fewer side effects or a more potent therapeutic action.

3.3.3 The effect of SCFAs on histone crotonylation on colon carcinoma cells and organoids

We show that butyrate and propionate treatment can upregulate histone crotonylation in a dose-dependent manner in colon carcinoma cells. The effect of butyrate treatment on histone crotonylation was rapid, occurring within two hours of treatment. Our results also suggest that crotonate can promote histone crotonylation, in agreement with a previous study that found crotonate treatment could promote histone crotonylation in cervical/uterine carcinoma cells (Sabari *et al.*, 2015). Further experiments are required to demonstrate this conclusively in colon carcinoma cells, as 10 mM crotonate promoted crotonylation in some experiments but not others. Interestingly, butyrate and propionate seemed to be more effective than crotonate at promoting histone crotonylation in colon carcinoma cells as concentrations of 1-5 mM butyrate or propionate could promote crotonylation as opposed to 10-20 mM crotonate. However, β-HBu did not change crotonylation and acetate even slightly decreased crotonylation. The effects of acetate, butyrate, propionate and β-HBu were reproducible across two or more blots. In particular, butyrate promoted histone crotonylation at H3K18cr in colon carcinoma cells in four independent experiments. However, the fold changes at particular concentrations were variable.

We showed that butyrate and crotonate could also promote histone crotonylation in mouse small intestinal and colon organoids. These increases were seen in two or more experiments. In particular, 10 mM crotonate produced a significant increase in crotonylation in small intestinal organoids, but there was some variability in fold-change between the three experiments. Additionally, the concentrations of SCFA used in organoid culture were similar to those used in colon carcinoma cells, but did not result in the same fold changes. This may be because repeat experiments, for either HCT116 cells or organoids, were run on separate blots and so normalisation to the control group had to be done to compare them. This meant that small variations in the intensity of the control group resulted in larger variations in fold change. Whilst overall crotonate and butyrate appear to promote crotonylation in organoids, in some cases only one or two repeats were performed for a particular treatment concentration making the confidence in the conclusion less high. If fewer concentrations of each treatment were tested, more repeats could be included on the same blot to reduce technical variability and determine if the fold change observed is significant.

3.3.4 The effect of SCFAs on histone acetylation in colon carcinoma cell and organoid culture

Our finding that acetate, which can be directly converted into acetyl-CoA by ACSS2, did not promote histone acetylation in HCT116 cells is curious. This could be because acetyl-CoA levels are already high as it is an abundant metabolite and is central to many metabolic pathways (Pietrocola *et al.*, 2015). Previous studies found that acetate could rescue histone acetylation but this was only when important metabolic enzymes were knocked down such as ACLY, which is a major source for nuclear acetyl-CoA (Wellen *et al.*, 2009). Acetyl-CoA concentration has been measured in the range of 2-13 µM in human gliobastoma and hematopoietic cell lines (Lee *et al.*, 2014), and in HCT116 cells was around 50 µM (X. Liu *et al.*, 2018, pre-print). The K_m of human lysine acetyltransferases is typically lower, for example KAT2A (GCN5) and P/CAF have K_m values of 0.62 µM and 0.28 µM respectively for acetyl-CoA with histone H3 (Langer *et al.*, 2002; Leemhuis, Nightingale, *et al.*, 2008). Therefore, further increasing acetyl-CoA concentration with acetate treatment may not influence acetyltransferase activity. Our results suggest that butyrate can promote acetylation at H3K18 in HCT116 cells, and may also do in colon organoids although further experiments are required to verify this. We are confident that the change we see is due to modulation of acetylation as the H3K18ac antibody did not recognise crotonylation in our specificity test. There seems to be no requirement for the structure of the SCFA to match that of the histone acylation type, so how do these SCFAs influence histone acylation abundance?

3.3.5 What is the mechanism by which SCFAs promote histone crotonylation in colon carcinoma cells and organoids?

Whilst butyrate was more potent than crotonate in HCT116 cells, these SCFAs had a similar effect on histone crotonylation in organoid culture. Our current hypothesis is that because fatty acid metabolism is higher in organoids, as they do not undergo the Warburg effect, HDAC inhibition is less dominant and promotion of crotonylation is dependent on acyl-transfer to the histone. Therefore, crotonate and butyrate would have similar effects as they each contain one acyl-group. In HCT116 cells, butyrate is not metabolised as these cells rely on glycolysis rather than beta-oxidation for energy (Vander Heiden *et al.*, 2009; Donohoe *et al.*, 2012). Therefore, it can accumulate to a level where it functions as an HDAC inhibitor and results in hyperacetylation (Donohoe *et al.*, 2012). Our *in vitro* assays revealed that butyrate can inhibit HDAC1 decrotonylation at lower concentrations than crotonate can. We suggest that in HCT116 cells, butyrate is a more effective upregulator of histone crotonylation than crotonate because HDAC inhibition is dominant and butyrate is a more potent HDAC inhibitor (Donohoe *et al.*, 2012). This may also explain why butyrate could promote histone acetylation in HCT116 cells, as it can inhibit HDACs, whilst acetate does not.

The regulation of histone crotonylation by butyrate is dynamic in HCT116 cells, occurring within two hours of treatment. The opposing actions of p300/CBP and HDAC1-3 in the nucleus may allow histone acetylation and crotonylation to fluctuate dynamically in response to the changing environment. The abundance of each acylation would then depend on the balance between crotonyltransfer and decrotonylation. An increase in acyl-CoA would cause more transfer to histones by p300 but with HDAC1-3 continually removing acyl groups from lysines, a return in acyl-CoA to basal levels would mean that histone acylation would shift to reflect this. This rapid change could mean that regulation of crotonylation is through modulation of enzymatic activity, for example by changing substrate availability, rather than requiring synthesis of new enzymes which would take more time. To test this, a western blot could be performed to test how the abundance of key enzymes involved in regulating crotonylation, such as ACAD, ACSS2, p300 or HDAC1, change over time after crotonate treatment. If their abundance is constant, then changes to crotonylation are likely to be due to changes in enzyme activity. Knock-down of these enzymes, followed by SCFA treatment, would also help us understand which mechanism is used in HCT116 cells and organoids. For example, if butyrate treatment no longer promoted histone crotonylation in HDAC1-knockdown HCT116 cells it would suggest that HDAC1 inhibition is the main mechanism involved. Heavy label tracing using ^{13}C versions of butyrate, propionate and crotonate combined with mass spectrometry analysis of histone proteins would be a useful method to determine how important acyl-transfer to the histone is in the promotion of

crotonylation by SCFAs. It will be interesting to see whether this differs substantially between colon carcinoma cells and organoids. There is some evidence that HDACs can remove crotonyl groups from non-histone proteins as SAHA treatment changed the abundance of crotonylated proteins across cellular compartments (Wu *et al.*, 2017). Crotonylated non-histone proteins identified in mass spectrometry analysis are involved in many cellular processes including nucleic acid metabolism, RNA processing, DNA recombination, chromosome organisation and translation (Wu *et al.*, 2017). As non-histone lysine acetylation has been shown to alter protein function (Tang *et al.*, 2008), this should be taken into consideration when analysing the effects of SCFAs on cell function. The identification of class I HDACs as decrotonylases suggests that this modification is not simply metabolic noise, but is modulated by specific enzymes in a regulated manner. Basal crotonyl-CoA levels are low compared to acetyl-CoA, meaning that changes to cell metabolism could cause greater fold changes to histone crotonylation and result in a greater sensitivity to certain aspects of cellular metabolic state than acetylation. As histone crotonylation is linked to gene regulation, it provides a mechanism for gene expression to rapidly respond to changing metabolic state.

Whilst these results in colon carcinoma culture and organoids are interesting, further work is needed to confirm these findings and apply them to the whole organism. The *in vivo* system is much more complex with immune cells, mucus layer, gut bacteria, gut transit times and diet composition having the potential to alter the effects that SCFAs have on coloncyte epigenetic state. Additionally in the gut, differentiated colonocytes metabolise butyrate to protect the stem cells at the crypt base (Kaiko *et al.*, 2016). However, in the gut organoid system the stem cells are on the outside and directly exposed to the culture medium. Importantly, SCFAs are thought to be derived from the intestinal microbiota so manipulation of microbiota and dietary composition is critical to be able to develop our understanding of this system and improve therapies to treat disease. The influence of diet composition and microbiota on colonocyte histone acylation and gene expression will be addressed in subsequent chapters.

4

4 The effect of diet on histone acylations in mouse colon

4.1 Introduction

In the gut, microorganisms ferment long chain carbohydrates from the diet and release SCFAs such as butyrate, acetate and propionate (Cook and Sellin, 1998; Flint *et al.*, 2012; den Besten *et al.*, 2013). Butyrate is the major energy source for colon epithelial cells, whilst much of the acetate and propionate produced is released into the portal circulation and used by the liver (den Besten *et al.*, 2013). Dietary fibre, including cellulose, inulin and pectin, are derived from plant materials and are resistant to degradation by enzymes encoded in the mammalian genome. The wide diversity and high metabolic capability of bacteria in the gut means that a much greater range of complex molecules can be harvested for their energy (Gill *et al.*, 2006; Ley *et al.*, 2006). The presence of microorganisms is thought to have occurred early in the evolution of multi-cellular organisms as it confers a distinct advantage in digestion, immune development and protection from pathogens (Ley *et al.*, 2008). In addition to the symbiosis between bacteria and their host, there are also beneficial interactions between bacteria. Different bacterial species have varying capacities to break down resistant molecules from the diet and many rely on cross-feeding of intermediate molecules from other bacteria for their energy. An example of this is the butyrate producing *F. prausnitzii* which benefits from lactate and acetate production by *Bifidobacteria* species (Rivière *et al.*, 2016).

SCFAs are important for gut health as they are modulators of intracellular pH, cell volume, ion transport, proliferation, differentiation, gene expression and apoptosis (Cook and Sellin, 1998). In particular, butyrate is thought to protect against colon cancer and inflammation (Cook and Sellin, 1998; Ferreira-Halder *et al.*, 2017). However, it is important to note that SCFAs have been found to have both pro- and anti-inflammatory effects in different studies, possibly because they influence so many aspects of gut function (Corrêa-Oliveira *et al.*, 2016). In a previous study, supplementation of fibre to the diet of rats increased total SCFA levels and histone acetylation. Interestingly, butyrate levels were highest in the 5 and 10% wheat bran groups but cell proliferation was lowest compared to the 0 and 20% groups (Boffa et al., 1992). In the last chapter, our experiments suggested that

butyrate could upregulate histone crotonylation in cell culture and this may be through inhibition of HDACs. Therefore, supplementation of fibre to increase luminal SCFAs could influence host epithelial cell histone crotonylation as well as histone acetylation. In this chapter, we will test the effects of modulating fibre content in conventional mice and SCFA supplementation in both conventional and germ-free mice. We predict that these will promote histone acylations in intestinal epithelial cells. We will also test dietary restriction, which we hypothesise will reduce histone acylations as there would be less substrates for microbial fermentation.

4.2 Results

4.2.1 Dietary restriction, crotonate and butyrate treatment do not change histone crotonylation or acetylation

As SCFAs are derived from the diet, we first tested the effect of dietary restriction on histone acetylation and crotonylation in liver and colon. However, no difference could be seen in histone crotonylation or acetylation in either tissue (Figure 4.1). Possibly, there was sufficient fibre present in the restricted diet to maintain SCFA concentrations in the colon lumen and serum meaning that these histone acylations did not change. Our previous results suggested that crotonate could promote histone crotonylation in both colon carcinoma cells and colon organoids (Figure 3.2, Figure 3.8, Figure 3.10 and Figure 3.11). Therefore, we added crotonate to the drinking water of mice and tested histone crotonylation in colon extracts by western blot to see if it increased. We observed a downward trend in histone crotonylation with increasing dose, but this was not statistically significant (Figure 4.2). H3K18cr ChIP-qPCR on small intestinal crypts from the same mice found that H3K18cr associated with the promoters of *Klf11* and *Klf13* genes did increase in this modification on the 10 mM and 50 mM treatments (Figure 4.3). Possibly, changes to histone crotonylation do occur at many genes but are not large or widespread enough to see using western blot, which looks at global changes to hPTMs.

Crotonate treatment was performed on mice fed a normal chow diet and containing a healthy microbiota, meaning that the steady-state level of microbial derived SCFAs may have been high already. To eliminate the supply of SCFAs by the endogenous microbiota, we tested how microbiota-free mice responded to butyrate treatment. We showed previously that butyrate could upregulate histone crotonylation in colon carcinoma cells and organoids (Figure 3.6, Figure 3.10 and Figure 3.11). However, there was no difference in histone crotonylation as a result of butyrate treatment in the colon or small intestine (Figure 4.4). One possibility is that butyrate was absorbed as it passed along the small intestine and colon, meaning that it never reached high concentrations in any part of the gut. Additionally, the mice were drinking freely, meaning that water (and therefore butyrate)

consumption may have varied between mice, resulting in more variability between biological replicates within a group.

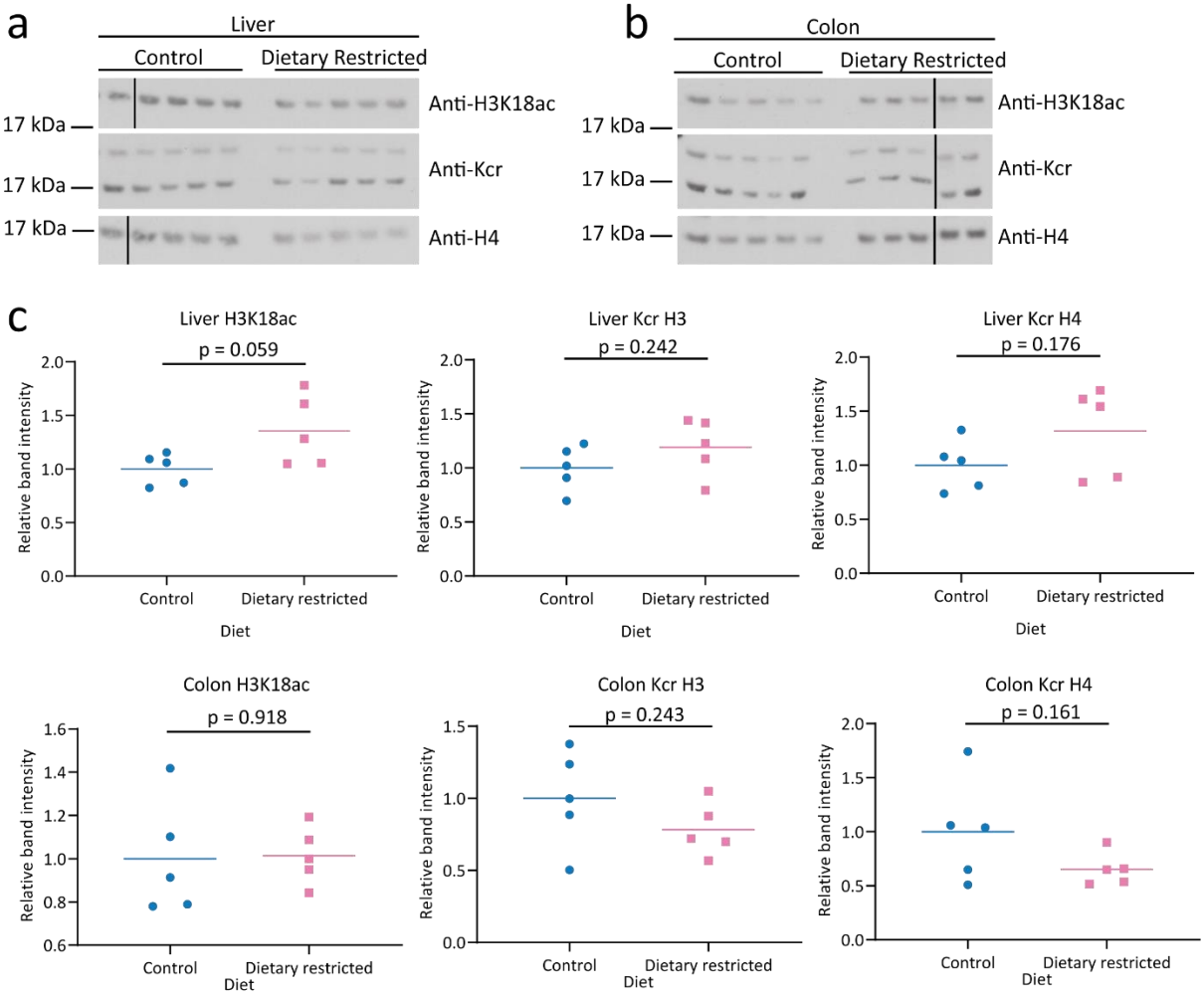

Figure 4.1. Dietary restriction does not change histone crotonylation or acetylation in liver or colon

Western blots of liver **(a)** and colon extracts **(b)** from mice given a standard chow diet (control) or a restricted diet and probed with anti-H3K18ac, anti-pan-crotonylation (Kcr) and anti-histone H4. **(c)** Quantifications of western blot bands was performed using image J, normalised to H4 band intensity and are shown relative to average of the control group. Statistical analysis used an unpaired t-test with a threshold p-value of 0.05, all were not significant and p values are shown on the graphs, n=5.

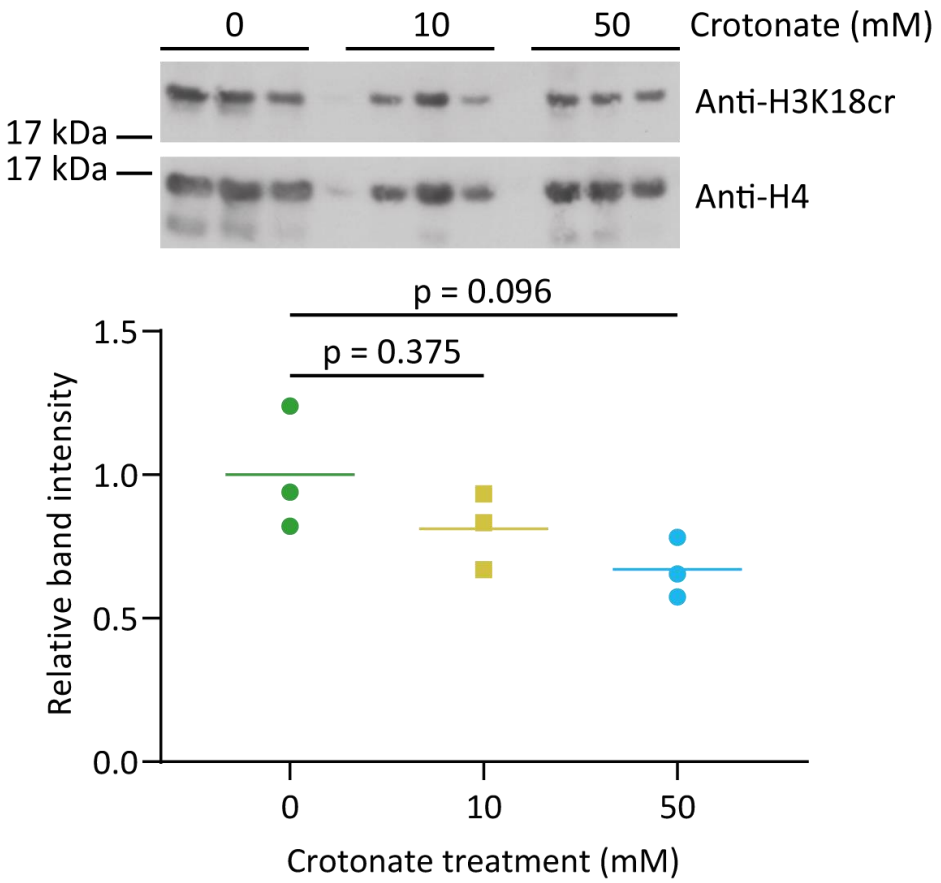

Figure 4.2. Crotonate treatment does not change histone crotonylation in the small intestine

Western blots using anti-H3K18cr or anti-histone H4 of small intestinal extracts from wild type BL6 mice given 0, 10 or 50 mM crotonate in their drinking water for two weeks. Band quantification is shown below relative to H4 and the average of the 0 mM group. The overall difference between the groups was not significant ($p = 0.11$) as tested by one-way ANOVA. The pairwise comparison between 0 mM and 10 or 50 mM is shown on the graph. Multiple testing correction used the Holm-Sidak method, n=3.

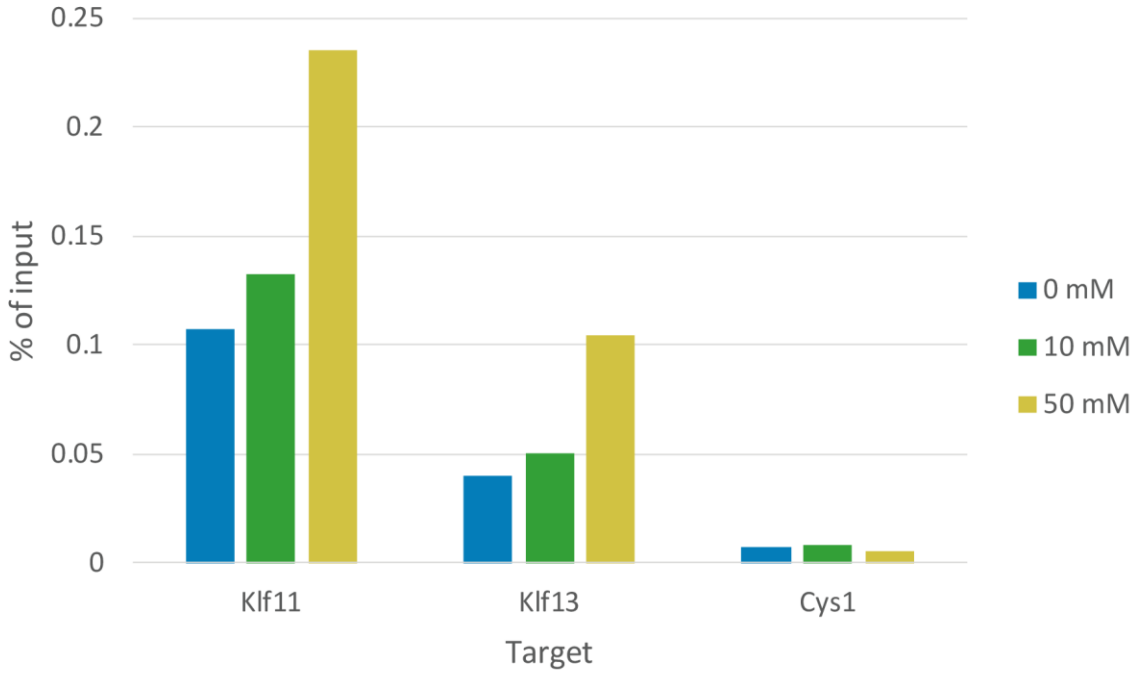

Figure 4.3. H3K18cr ChIP-qPCR on small intestine of crotonic acid fed mice

Wild type BL6 mice were fed 0, 10 or 50 mM crotonate for two weeks followed by ChIP of small intestinal crypts against H3K18cr. This was followed by real time qPCR of two candidate genes, *Klf11* and *Klf13*, as inferred from previous H3K18cr ChIP-seq data from our group, as well as *Cys1* as a negative control. A two-fold enrichment of H3K18cr, relative to 0 mM, was seen at 50 mM in both *Klf11* and *Klf13*. This experiment was performed by Payal Jain.

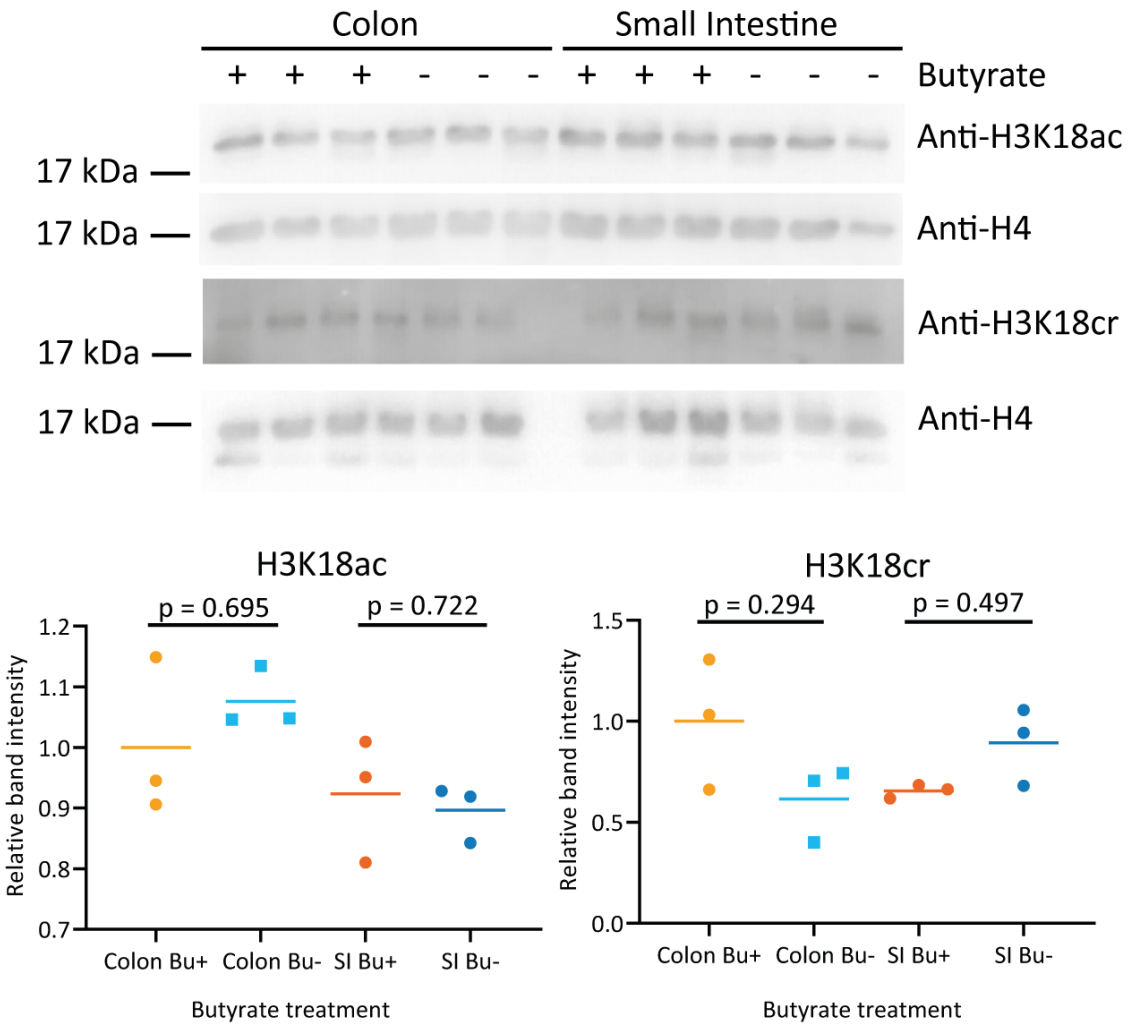

Figure 4.4. Butyrate treatment of microbiota-free mice does not change histone crotonylation or acetylation
Western blots and quantifications of colon or small intestine extracts from germ-free mice probed with specified antibodies. Mice were given 150 mM butyrate in their drinking water for one week. Quantifications are relative to the H4 loading control and the average of the butyrate treated colon group. Labels are butyrate (Bu), small intestine (SI), treated (+) and control (-). One-way ANOVA was used to determine that the overall differences between groups were not significant. Pairwise comparisons are shown on the graph, with multiple testing correction using the Holm-Sidak method, n = 3.

4.2.2 The effect of high fibre diet on histone acetylation, histone crotonylation and HDAC abundance in conventionally raised mice

As the gut microbiota ferments dietary fibre to produce SCFAs, we sought to increase colonic luminal SCFAs by increasing the fibre content of the diet and investigated how this affected histone acylations. For one month, mice were given a normal chow diet containing 5% cellulose (the control) or chow diet supplemented with either 10% inulin or 10% pectin. We expected the enriched fibre diets to increase

histone acylations, but found that diets supplemented with 10% inulin or 10% pectin did not significantly increase histone acetylation or crotonylation in any of three independent experiments relative to the control diets (Figure 4.5). Instead, crotonylation and acetylation either decreased or stayed the same in a manner that was not consistent across experiments. Inulin reduced H3K18ac in both experiment 1 and 3, but these two experiments differed in their effects on histone crotonylation. On the pectin supplemented diet, H3K18ac was significantly reduced in experiment 3 and Kcr was significantly reduced in experiment 1. However, no significant changes could be seen in acetylation or crotonylation in experiment 2.

To see if the high fibre diets had increased SCFA concentrations, we measured acetate and butyrate concentrations in the serum (Figure 4.6). Previous studies have found that blood acetate concentrations in human and murine blood range from 25 to as much as 600 μM (Richards *et al.*, 1976; Tollinger *et al.*, 1979; Rémésy *et al.*, 1980; Pomare *et al.*, 1985; Davies *et al.*, 2011; Tumanov *et al.*, 2016). Over both experiments, serum acetate showed a statistically significant increase ($p = 0.0006$) from 50±16 μM on the cellulose 5 diet to 232±34 μM on the pectin 10 diet, with inulin 10 at an intermediate concentration between the two (169±28 μM). This is similar to a previous study in human subjects which saw an increase from ~50 μM to 96±12 μM plasma acetate after giving a 20 g pectin diet (Pomare *et al.*, 1985). In contrast, no increase was seen in butyrate serum concentrations. Instead, butyrate significantly decreased from 108±10 μM on the cellulose 5 diet to 88±5 μM on the inulin 10 diet. Both of these concentrations are higher than previously measured plasma or serum butyrate concentrations in mice or human of 3-8 μM (Wolever and Chiasson, 2000; Nishitsuji *et al.*, 2017). The low serum concentration of butyrate is thought to be due to high absorption of microbial generated butyrate by colonocytes (Topping and Clifton, 2001). However, in another study 100 μM butyrate was recorded in the portal vein of rats (Rémésy *et al.*, 1980). SCFA measurements are often variable between studies which is thought to be due to differences in diet and the extent of fermentation by the microbiota (Topping and Clifton, 2001). The changes to histone acylations are more similar to the changes in serum butyrate rather than serum acetate. Experiment 2 showed no change in butyrate and also no change in histone acylations on either diet. In experiment 1, butyrate decreased on the inulin diet, which matches the decreases seen in histone acetylation and crotonylation (Figure 4.5 and Figure 4.6). This could mean that it is butyrate rather than acetate that influences histone acetylation and crotonylation in the gut, but this would require further investigation.

We also tested the effect of these high fibre diets on HDAC abundance, as HDAC2 levels were previously shown to be affected by butyrate (Kramer *et al.*, 2003) and could be the mechanism for the effects of SCFAs on histone acylations. Figure 4.7 shows western blots of HDAC1, HDAC2 and HDAC3 abundance in colon extracts from three independent experiments. Quantifications below are shown

for each experiment separately, rather than combined, as the fold change was much higher in experiment 2 due to substantial changes in the lamin B1 normalisation blot. HDACs and lamin B1 may be more susceptible to degradation than histones due to their higher molecular weight. The effect of inulin and pectin diets on HDAC abundance was not consistent between experiments (Figure 4.7). In experiments 1 and 2, HDAC1-3 increased significantly on the inulin diet. In experiment 3, HDAC1 and HDAC3 remained the same, whilst HDAC2 decreased on the inulin diet. The pectin diet significantly reduced HDAC2 and HDAC3 in experiment 1 and HDAC2 in experiment 3. But HDACs remained the same or increased in the other blots. The expectation was that changes to HDAC abundance would be in the opposite direction to histone acylation changes, as HDACs remove acetylation and crotonylation from histones. However, whilst the increase in HDAC1 or HDAC2 abundance on the inulin diet in experiment 1 was matched by a reduction in histone acetylation and crotonylation (Figure 4.5 and Figure 4.7), the decrease in HDAC2 and HDAC3 abundance with pectin diet in experiment 1 was not matched by an increase in histone acylations (Figure 4.5 and Figure 4.7).

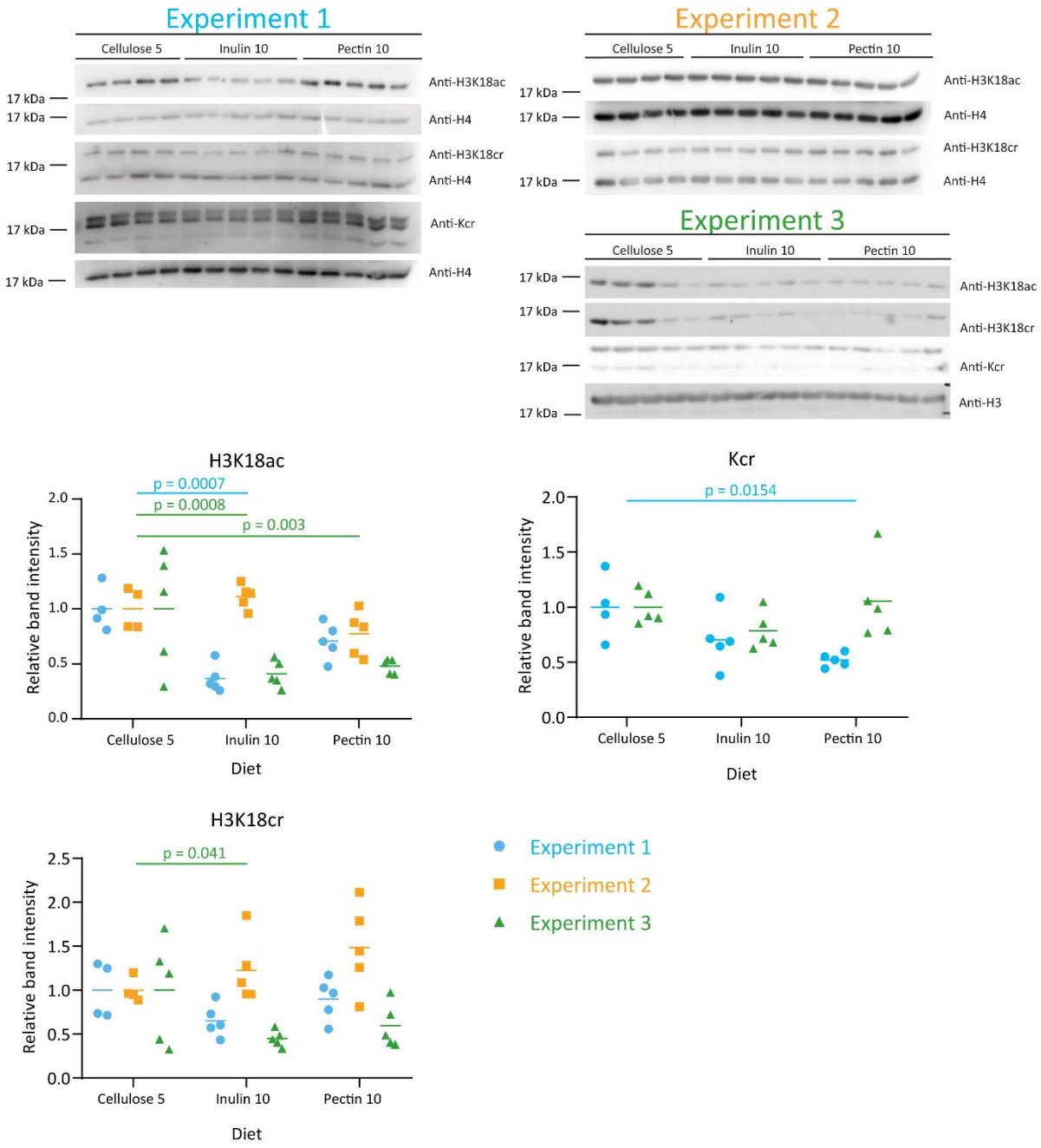

Figure 4.5. High fibre diet does not increase histone crotonylation or acetylation

Western blots on colons from mice given a standard chow diet containing 5% cellulose (cellulose 5), chow with added 10% inulin (inulin 10) or chow with added 10% pectin (pectin 10). Three independent experiments were performed with five mice in each group, for some blots only four cellulose 5 samples were loaded due to a limited number of wells in the gel. Quantifications were normalised to H3 or H4 band intensity and are shown relative to the average of the cellulose 5 group. Two-way ANOVA was performed with pairwise comparisons between each diet within an experiment. Overall, there was a significant difference between both diet, experiment and an interaction between the two for H3K18ac ($p = 0.0002$, $p = 0.0011$ and $p = 0.0037$). There was a significant difference between experiment for H3K18cr ($p = 0.0004$) and for Kcr there was a significant difference between experiments and a significant interaction between experiment and diet ($p = 0.0281$ and $p =$

0.0425). Significant differences in the pairwise comparisons between diets for each experiment, are shown on the graphs in the colour of the relevant experiment. Multiple testing correction used the Holm-Sidak method, n = 5.

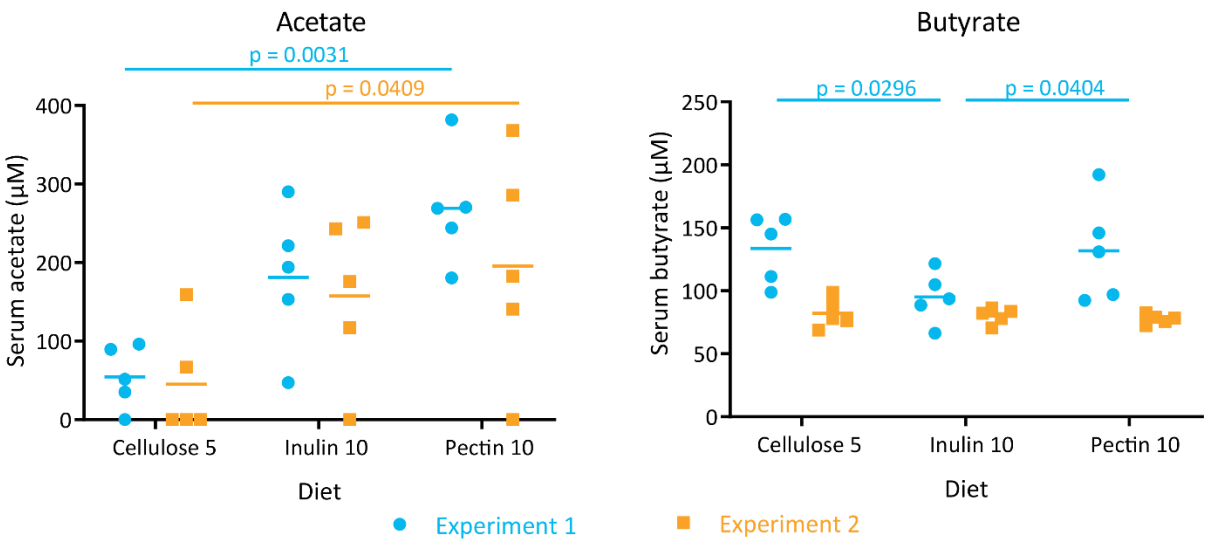

Figure 4.6. High fibre diet increases acetate but not butyrate in serum

Acetate and butyrate were measured in the serum by gas chromatography from mice given a standard chow diet containing 5% cellulose (cellulose 5), chow with added 10% inulin (inulin 10) or chow with added 10% pectin (pectin 10. Two-way ANOVA statistical tests were conducted using diet and experiment as the variables, with pairwise comparisons between diets within an experiment. Values of zero were below detectable levels. For acetate there was a significant difference between diets but no difference between experiments. For butyrate there was a significant difference between experiments; experiment 1 had significant differences between diets but experiment 2 had no differences between diets. Significant pairwise comparisons between diets are shown on the graph, with multiple testing correction using the Holm-Sidak method, n = 5.

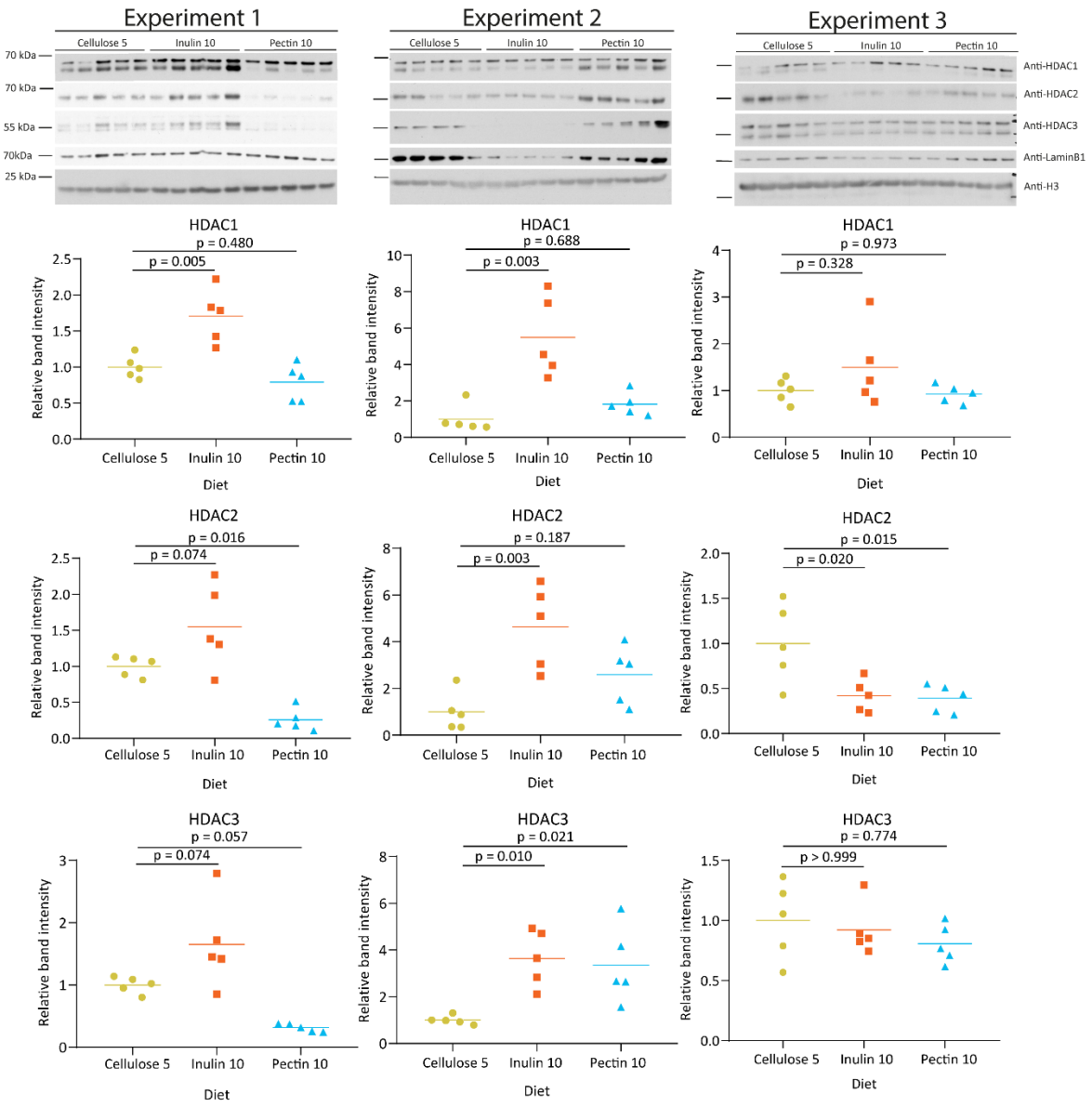

Figure 4.7. High fibre diet does not cause consistent changes in class I HDACs

Western blots of colon extracts from mice given a standard chow diet containing 5% cellulose (cellulose 5), chow with added 10% inulin (inulin 10) or chow with added 10% pectin (pectin 10) using the specified antibodies. Three independent experiments were performed with five mice in each group. Quantifications of HDAC band intensity were normalised to the lamin B1 band intensity which has a similar molecular weight to the HDACs. Quantifications of all bands are shown relative to the average of the cellulose 5 group to make the three experiments easier to compare. One-way ANOVA was performed which gave a significant effect of diet overall for all except HDAC1 and HDAC3 in experiment 3. Pairwise comparisons between cellulose 5 and the high fibre diets are shown on the relevant graph. Holm-Sidak's multiple testing correction was applied, n = 5.

4.2.3 The effect of high fibre diet on histone acylations in wild type or ACAD deficient mice

A further experiment was conducted, comparing a normal diet (5% cellulose) to diets with 10% inulin supplement. This was performed with wild type mice and also those with a deficiency in ACAD, to see if an absence of short chain fatty-acyl CoA dehyrogenation would change how histone acylations are influenced by the high fibre diet. Band quantifications from wild type and ACAD deficient mouse colons are shown on the same graph and the effect of diet compared together using two-way ANOVA because almost no differences were seen in histone acylations between the wild type and ACAD deficient mice when cellulose and inulin diets were compared directly (Figure 4.8). The effect of inulin diet on histone acylations was broadly consistent between wild type and antibiotics treated mice (Figure 4.9). A reduction was seen on inulin diet in H4K8ac, H3cr and H4cr in both wild type and ACAD deficient mice (Figure 4.9). Additionally, a significant increase was seen in HDAC2 in wild type mice on the inulin diet ($p = 0.006$), although this was not observed in the ACAD deficient mice ($p = 0.962$). The differences in the effect of high fibre diet on histone acylations between experiments 1, 2 and 3 in wild type BL6 mice (Figure 4.5), could be due to differences in their microbiotas because they were housed at different time periods in the same facility. Wild type and ACAD deficient mice were all cohoused as part of the same experiment and would therefore have more similar microbiotas, which could explain why a high fibre diet had a more consistent effect between groups of mice in this experiment (Figure 4.9). Whilst each histone acylation was similar between wild type and ACAD deficient mice, there were differences between histone acylations. For example, H4K8ac and Kcr decreased whilst H4K8cr did not change. Importantly, and in contrast to our hypothesis, high fibre diet did not increase histone acetylation or crotonylation in any of these experiments but stayed the same or decreased.

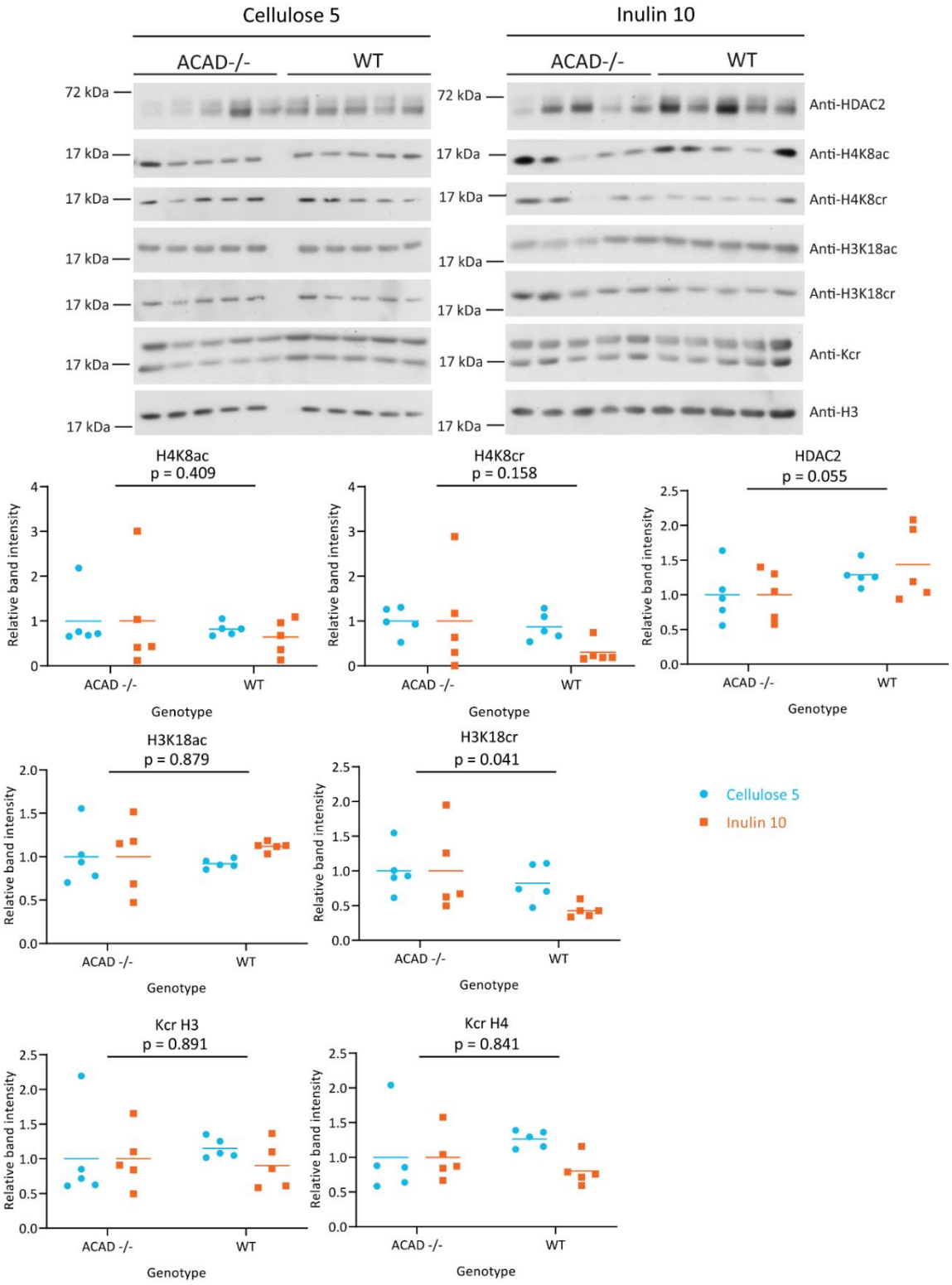

Figure 4.8. No difference is seen between ACAD -/- and wild type mice on different diets

Wild type mice or those with a deficiency in ACAD were given a normal chow diet with 5% cellulose (cellulose 5) or a diet with added 10% inulin (inulin 10) and extracts of colons investigated by western blot using the specified antibodies. Quantifications are shown relative to the histone H3 loading control and cellulose 5 condition. Two-way ANOVA was performed with both ACAD -/- and WT and a threshold p value of 0.05. P values of the effect

of genotype are shown on the graph. There was no significant effect of diet or an interaction between diet and genotype for any of the blot quantifications, n = 5.

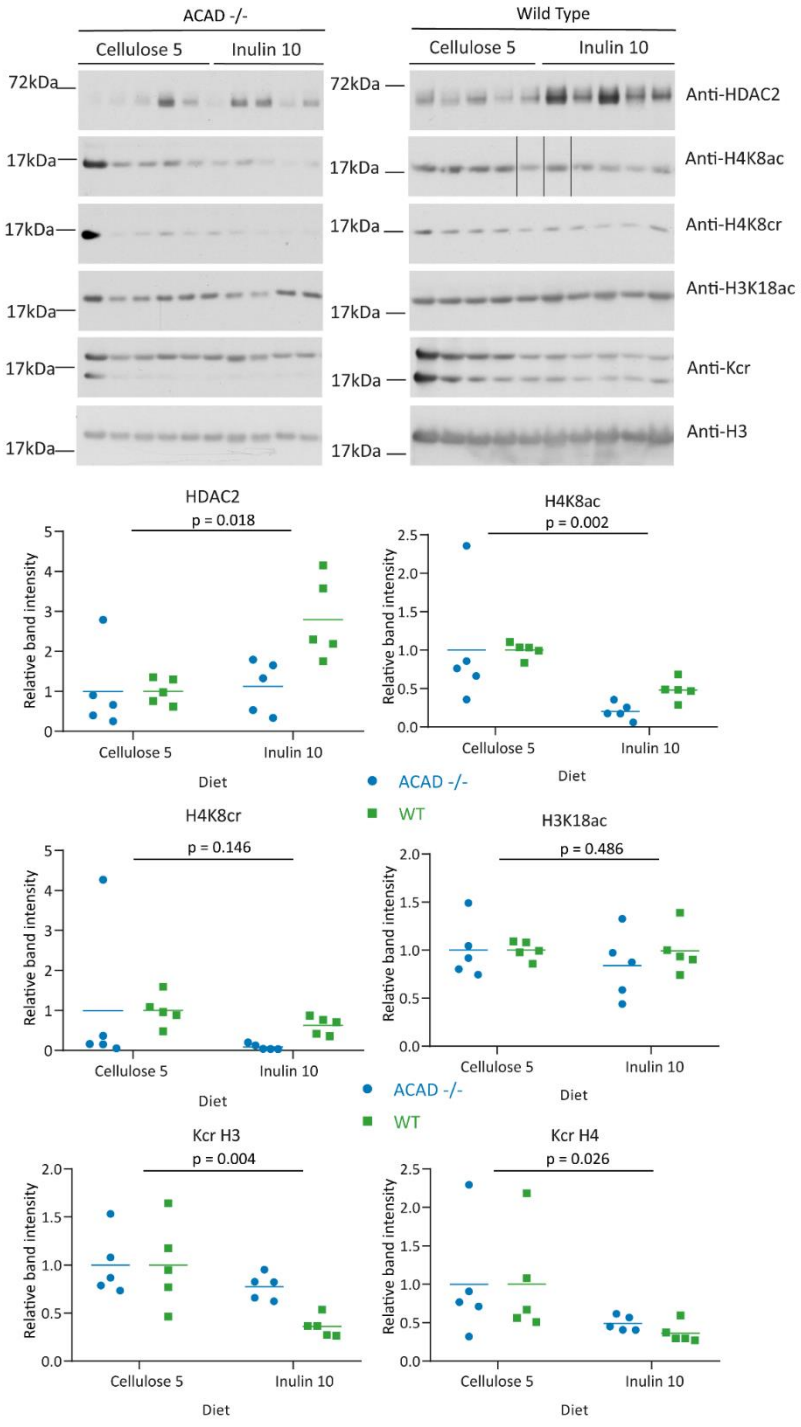

Figure 4.9. The effect of high fibre diet on HDAC2 and histone acylations in wild type or ACAD deficient mice

Wild type mice or those with a deficiency in ACAD were given a normal chow diet with 5% cellulose (cellulose 5) or a diet with added 10% inulin (inulin 10) and extracts of colons investigated by western blot using the specified antibodies. The lines on the blot show where the order of the bands was changed to match other blots due to problems with loading the gel. Quantifications are shown relative to the histone H3 loading control and cellulose

5 condition. Two-way ANOVA was performed with ACAD -/- and WT. The effect of diet is shown on each graph. HDAC2 also gave a significant effect of genotype and significant interaction between diet and genotype, n = 5.

4.2.4 Diet supplementation with 25% inulin increases butyrate concentrations in the colon

Increasing the fibre content of the diet did not yield consistent effects on histone acetylation but this could be because changes in butyrate concentration in the serum on 10% inulin or 10% pectin were small (Figure 4.6, experiment 1) or did not change (Figure 4.6, experiment 2) compared to the control diet. To see if further increasing the fibre content of the diet could impact SCFA concentrations, we performed an initial test measuring SCFA concentrations on more diets with two biological repeats for each. Statistical testing was not performed as there were only two replicates. The inulin 10 and pectin 10 diets had higher colon luminal acetate concentrations than cellulose 5 (Figure 4.10), a similar pattern to that in Figure 4.6. Propionate only showed an upward trend for inulin 10. Only 25% inulin produced a clear increase in colon luminal butyrate concentration (Figure 4.10), which could explain why no change in butyrate was seen previously with 10% inulin.

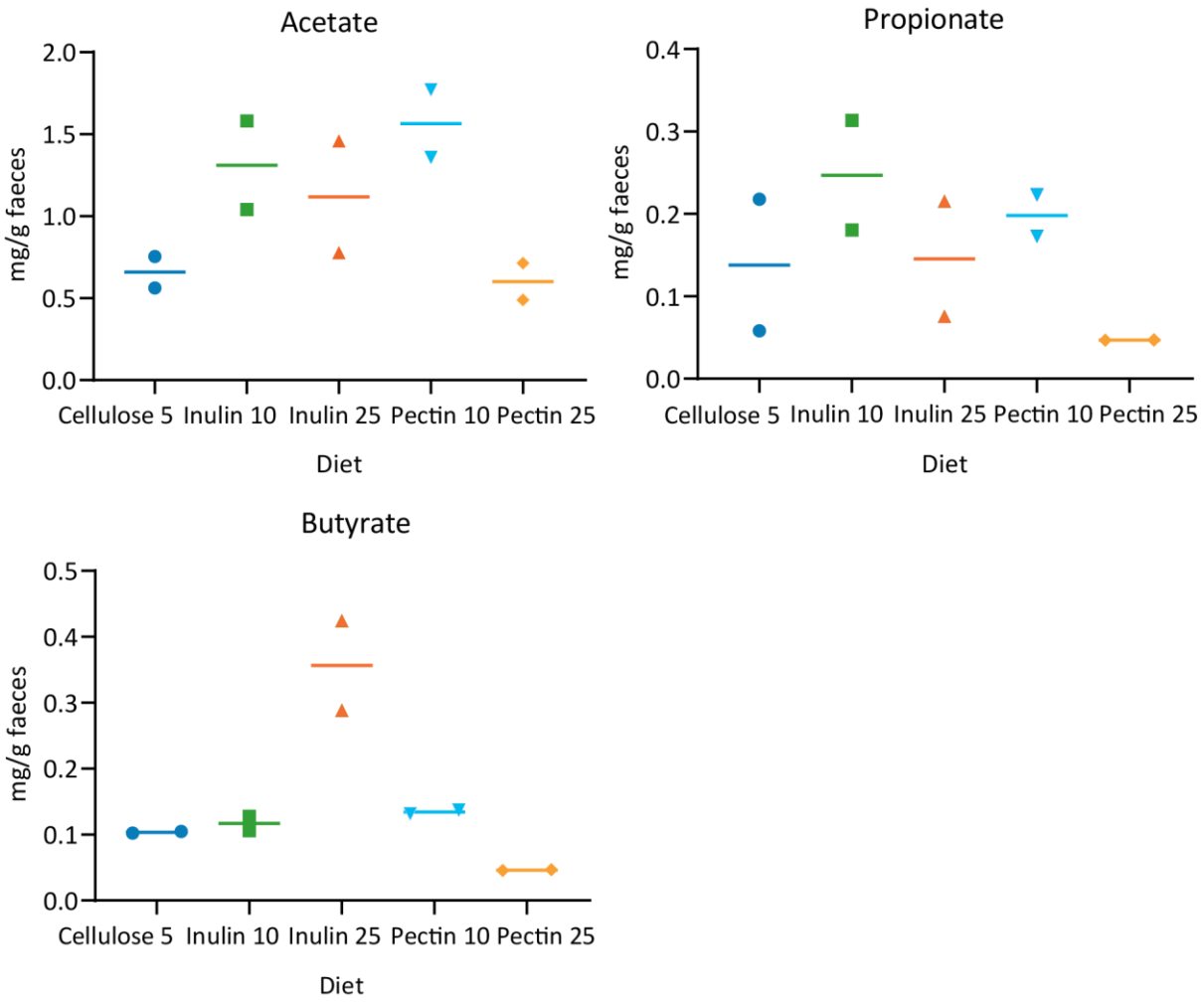

Figure 4.10. 25% inulin supplementation increases butyrate concentration

Acetate, propionate and butyrate were measured in luminal colon content of mice given different diets using gas chromatography, n = 2. SCFA measurement was performed by Caroline Marcantonio Ferreira's group.

4.2.5 Fibre free diet reduces histone acylations in conventional mice

As 25% inulin significantly increased butyrate concentration in the colon lumen (Figure 4.10), we tested supplementing 25% inulin to the diet. In addition, we tested a no fibre condition, as the control diet contains 5% cellulose, to see if there would be a bigger difference in histone acylation relative to the high fibre diet. Cellulose is a resistant polysaccharide that might be used in microbial fermentation, resulting in high SCFA concentrations in the colon lumen. The 25% inulin supplemented diet significantly reduced H4 crotonylation relative to the 5% cellulose diet, whilst other modifications did not change (Figure 4.11). This was similar to the reduction in histone acetylation and crotonylation with inulin supplementation seen in some of our previous experiments. Many acylations did change in the same way as a result of inulin treatment between different experiments. H3K18ac reduced on inulin 10 in experiment 1 (Figure 4.5), H3K18cr reduced on inulin 10 in experiment 2 (Figure 4.5),

H4K8ac and Kcr reduced on inulin 10 in Figure 4.9, and H4K8cr, H3K18ac and Kcr H4 reduced on inulin 25 in Figure 4.11. Not every acylation changed in each experiment, but we can conclude that inulin supplementation does not increase histone acylations relative to the cellulose 5 diet in our hands. Only H3K18ac showed a significant increase between no fibre and inulin 25, which were both lower than the cellulose 5 diet. The diet without fibre reduced H3K18ac, H4K8bu and H4K8cr relative to cellulose 5 but did not significantly change Kcr or H4K8ac. This agrees with our hypothesis that removing fibre would reduce histone acylations. Perhaps, SCFA levels are already high in the cellulose 5 treated mice, so we only see reductions in histone acylations when fibre is removed from the diet, but no increase when fibre is added to the diet. These more consistent effects on histone acylations of no fibre, compared to inulin or pectin supplementation, may also be because they are less dependent on the species composition of the microbiota. However, further experiments with no fibre are necessary to determine if this is a robust effect.

SCFA measurements of the colon content of these mice show that there was a statistically significant increase in acetate and propionate on the 25% inulin diet (Figure 4.12). Although a preliminary test of the effect of different high fibre diets on SCFA concentrations produced a striking increase in butyrate on the 25% inulin diet (Figure 4.10), in Figure 4.12 the concentration of butyrate on the 25% inulin diet is similar to the 5% cellulose diet. There is a significant decrease in butyrate in the no fibre diet whilst acetate and propionate do not change. The changes to butyrate concentration correlate better with the changes in histone acylations than the changes to acetate and propionate. Inulin 10 reduced serum butyrate and H3K18ac in experiment 1 (Figure 4.5 and Figure 4.6), whilst no fibre diet reduced colon luminal butyrate and H3K18ac, H4K8ac and H4K8cr (Figure 4.11 and Figure 4.12). However, further experiments are required to determine if fibre-derived butyrate is the cause of changes to histone acylations. We have not seen consistent effects of increasing the fibre content of the diet on butyrate concentration. Whilst inulin 10 reduced serum butyrate in experiment 1 it did not change in experiment 2 (Figure 4.6). Additionally, an inulin 25 diet increased colon luminal butyrate in an initial test (Figure 4.10), but did not significantly change colon luminal butyrate in the subsequent experiment (Figure 4.12). Therefore, further experiments are required to understand the variation between results.

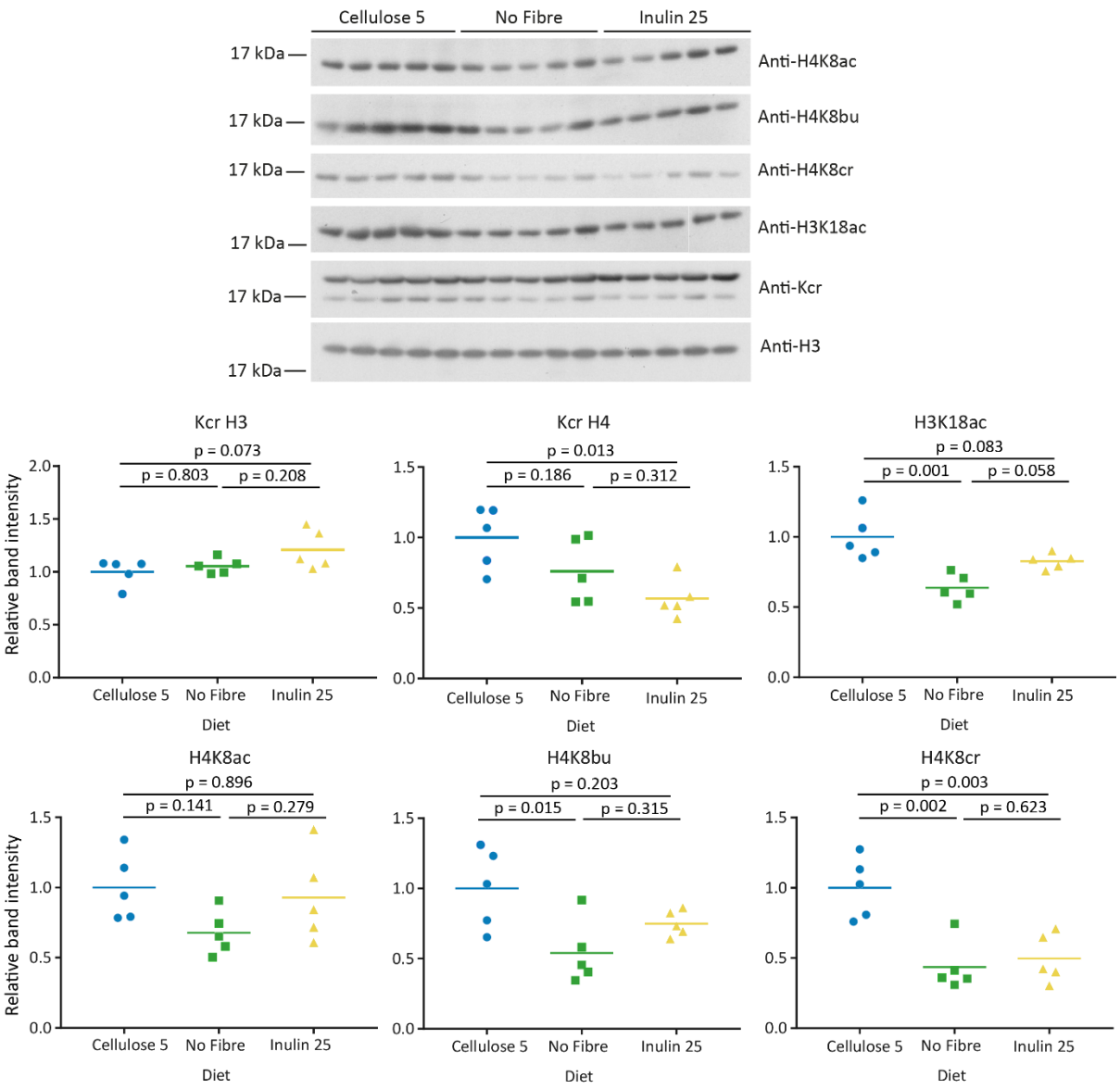

Figure 4.11. The effect of no fibre diet on histone crotonylation, acetylation and butyrylation in mouse colon

Western blots of colons from mice given a normal chow diet containing 5% cellulose (cellulose 5), chow diet without cellulose (no fibre) or chow diet plus 25% inulin (inulin 25) probed with the specified antibodies. Each lane is the colon extract from a separate mouse. Quantifications of western blot bands are shown relative to the anti-histone H3 loading control and the average of the cellulose 5 condition. One-way ANOVA was performed, H4K8cr and Kcr H4 had a significant effect of diet overall (p = 0.0009 and p = 0.0169 respectively). P values of pairwise comparisons between the diets are shown on the graph, the threshold p value was 0.05. Multiple testing correction used the Holm-Sidak method, n = 5.

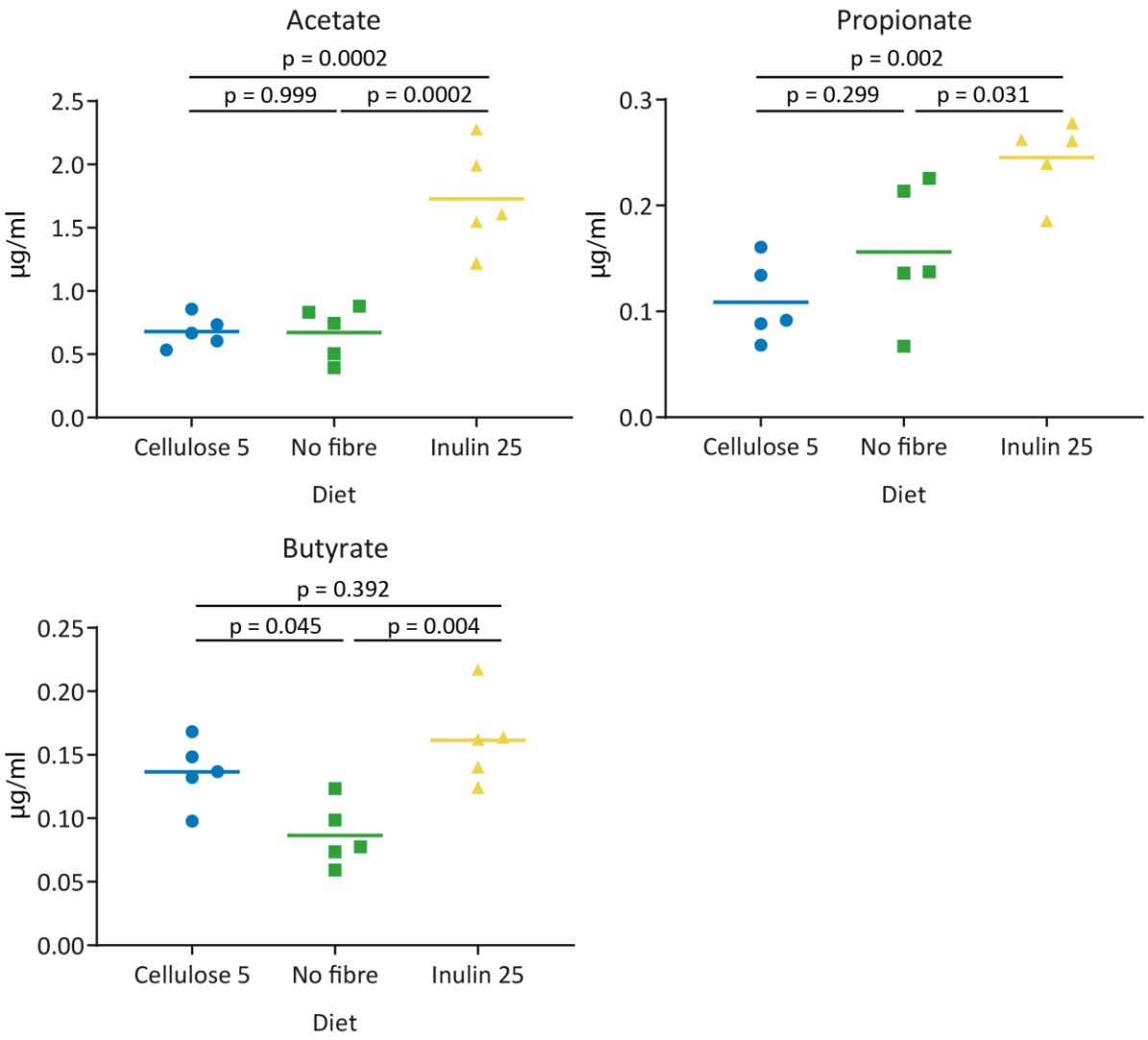

Figure 4.12. Changes to acetate, propionate and butyrate in the colon lumen of mice on different diets

Acetate, propionate and butyrate were measured in the luminal colon content by gas chromatography. One-way ANOVA was performed and the overall effect of different diets on acetate, propionate or butyrate was significant. Pairwise comparisons between diets are shown on the graphs with a threshold p value of 0.05, multiple testing correction used the Holm-Sidak method, n = 5.

4.3 Discussion

4.3.1 The effect of dietary fibre on histone acylations in mouse colon

We found that removing all fibre (including cellulose) from the diet produced a reduction in some acetyl- and crotonyl-marks, as well as a slight decrease in luminal butyrate concentration. However, increasing the fibre content of the diet either decreased or did not change histone crotonylation and acetylation abundance in mouse colon in multiple independent experiments. This was in contrast to

our hypothesis, as we had anticipated that more fibre would enable increased generation of SCFAs. However, whilst we observed increases in acetate and propionate on 10 or 25 % inulin, there were no increases in butyrate. A previous study found that 10% inulin shifted the relative production of SCFAs from acetate to propionate and butyrate, and increased total SCFA concentrations in rat caecum. However, in this study there was no linear correlation between the total SCFA concentrations and percentage of inulin, as SCFA levels were lower with 20% than with 10% inulin (Levrat *et al.*, 1991). This suggests that the relationship between dietary fibre and SCFA levels in the healthy gut may be more complex.

4.3.2 Differences in microbiota between mice could contribute to variation in the response to high fibre diets

The differences between experiments could be due to differences in gut microbiota composition between these mice. We observed more consistent changes to histone acetylation and crotonylation between ACAD deficient mice and wild type mice on high fibre diets. As ACAD deficiency did not change histone acylation abundance, the similarity of effect could be because mice were cohoused and therefore had more similar microbiotas. The environment is a key contributor to the composition of the microbiota and it has been well documented that mice can vary substantially in their microbiota between facilities due to differences such as water acidity, bedding and food. The inoculum that a mouse receives from its mother is a key factor in establishing the microbiota and cohousing of unrelated mice can result in similar microbiota. Additionally, mice can even differ in their microbiota within a facility (Goodrich *et al.*, 2014). We chose to use mice with enriched microbiota relative to standard laboratory mice which are specific or pathogen free (SOPF) and have low microbiota diversity. This was because the generation of SCFAs from fibre by the microbiota is dependent on particular species, such as those present in *Clostridium* clusters, which may be less prevalent in low microbiota diversity mice. Furthermore, the generation of some SCFAs, in particular butyrate, relies on cross-feeding between microbial species and therefore will be enhanced by greater diversity. Whilst this diversity may be important to observe the full effects of fibre supplementation, it also results in high inter-individual variability in microbiota composition which is known to influence the response to dietary manipulation and can make interpretation of the results difficult (Flint *et al.*, 2012).

4.3.3 Microbial adaptation and the other potential effects of fibre in the gut

Another component of this study is that high fibre diets were given for one month in our experiments, which means that the microbiota may adapt to this different diet. An interesting study found that a

short-term changes to diet, involving switching from a plant-based to animal-based diet in humans, could dramatically alter adult microbial community structure, although another study found that the microbiota differed more between people than diet (David *et al.*, 2014; Korem *et al.*, 2017). As bacterial metabolites modulate the composition of the microbiota (Ferreira-Halder *et al.*, 2017), an increase in SCFA concentrations could have resulted in a compensatory change in the abundance or diversity of gut bacteria. In these experiments with high fibre diets we do not know how the relative abundance of different bacterial species changed. Furthermore, fibre can influence many components of gut physiology. Fibre is known to influence water absorption, gut transit times, cholesterol and glycaemic levels and trap potentially harmful substances, in addition to promoting fermentation by the gut flora. Whilst different types of fibre can differently influence gut motility, in general it is associated with increased frequency of bowel movements (Dhingra *et al.*, 2012). SCFA concentrations in the gut are a balance of microbial production and colonocyte absorption. Shortened gut transit may mean that SCFA concentrations are not able to accumulate as much and could counter balance the effect of adding increased SCFA substrate. Further studies could test shorter periods of dietary manipulation to reduce microbial adaptation. Additionally, more steps should be taken to standardise the microbiota between experiments and the composition of key bacterial species monitored using 16S rRNA sequencing. This needs to be understood if the knowledge gained is to be applied to humans, which are considerably more variable in their microbiota composition.

4.3.4 Which SCFA is responsible for changes to histone acetylation and crotonylation?

In the high fibre diet experiments, changes to histone acylations seemed to be linked to changes in butyrate rather than acetate or propionate. This suggests that the actions of butyrate producing bacteria could be the drivers for changes to histone acylations. In chapter 3, butyrate and propionate but not acetate could upregulate histone crotonylation in cell culture. Butyrate is mainly metabolised in colon cells whereas acetate and propionate are metabolised in the liver and other organs. This raises the exciting possibility that changes to the abundance of butyrate producing bacteria differentially affect histone acylations in colonocytes rather than changes to acetate producing bacteria. Therefore, addition of a diet or probiotic that promotes butyrate production could also promote histone acylations. This may be complicated avenue to investigate as there is much cross-feeding between bacteria in the gut lumen. An interesting further study could test transplantation of butyrate generating bacteria, such as *E. rectale* which can use complex polysaccharides, into germ-free mice. This would reduce inter-experimental variability and enable more direct assessment of the effect of butyrate on histone acylations in mouse colon.

4.3.5 How do histone acylations relate to the effects of fibre SCFAs on gut health?

Fibre is thought to protect against colon cancer (McIntyre *et al.*, 1993; Cook and Sellin, 1998; Topping and Clifton, 2001; Aune *et al.*, 2011). However, the beneficial effects of fibre may be dependent on the composition of the microbiota and its ability to ferment fibre into SCFAs. The presence of fibre in the diet has been studied in relation to the presence of different microbial species and biomarkers of health (Flint *et al.*, 2012), but has not been investigated in relation to the presence of histone modifications in the colon. We observed that changing the fibre content of the diet can influence histone acetylation and crotonylation, but we did not see any increases in these hPTMs with higher fibre doses. However, we have observed reductions in histone acetylation and crotonylation with reducing fibre dose. The pleiotropic effects of SCFAs are thought to be due to their multiple modes of action on intestinal cells. GPCR activation has been linked to energy homeostasis, HDAC inhibition to apoptosis and metabolism of butyrate to cell proliferation (Donohoe *et al.*, 2012; Corrêa-Oliveira *et al.*, 2016; Kaiko *et al.*, 2016). Histone acylations may couple fibre and SCFAs to their effects on gut function and health, but whether this is a consistent interaction and under what circumstances this occurs remains unclear.

5

5 Antibiotics induced microbial depletion influences histone acylations and gene expression in mouse colon

5.1 Introduction

The partnership between the microbiota and host is important for host digestion, immune development and defence against pathogens. The molecular mechanisms of this interaction are poorly understood but rapidly improving techniques have enabled research into the effects of the microbiota to progress and the microbiota have now been implicated in various diseases (Lynch and Pedersen, 2016). A key part of microbiota-host interactions are the biproducts of microbial metabolism which can influence host metabolism and epigenetic state. Microbiota-derived epigenetic modulators include folate which is essential for DNA methylation, succinate which inhibits histone demethylases and butyrate which is a histone acylation precursor and HDAC inhibitor (Crider *et al.*, 2012; Xiao *et al.*, 2012; Koh *et al.*, 2016). As host epigenetic state can regulate diverse sets of cellular functions, it is essential to determine how the epigenome responds to the microbiota in the context of the intestine.

There is some evidence that changes to the microbiota can influence histone modifications and gene expression in intestinal epithelial cells. Colonization of germ-free mice was shown to promote histone acetylation and SCFA supplementation of germ-free mice could partially match histone acetylation and methylation patterns of conventional mice (Krautkramer et al., 2016). Zarrinpar *et al.* (2018) observed reductions in SCFAs in the gut lumen, changes to microbial metabolic pathways and dysregulation of metabolic genes in the caecum. In this chapter, we will investigate how antibiotic treatment influences histone crotonylation, acetylation, butyrylation and hydroxybutyrylation in the colon. In addition to testing how global levels of histone acylations change, we plan to investigate what the distribution of some of these modifications is across the genome and how it changes in response to depletion of the microbiota. Our group previously showed that H3K18cr is abundant in intestinal epithelial cells and is associated with TSS and H3K4me3 (Fellows et al., 2018). However, we still do not know the distribution of other crotonyl marks such as H4K8cr or Kcr and how they relate

to genomic elements such as enhancers and promoters. In addition, no studies so far have investigated how crotonylation or acetylation change at specific sites in response to depletion of the microbiota. To provide a direct comparison to H4K8cr we plan to investigate H4K8ac, a mark which has been linked to cancer progression, male germline programming and transcriptional changes in the lifecycle of *Plasmodium falciparum* (Morinière *et al.*, 2009; Vlaicu *et al.*, 2010; Gaucher *et al.*, 2012; Sánchez-Molina *et al.*, 2014; Gupta *et al.*, 2017). However, little is known about the distribution of H4K8ac in colon and liver, both microbial metabolite-influenced tissues. Therefore, we will profile H4K8ac in these tissues, determining if it is related to enhancers or promoters and whether it changes in response to microbial depletion by antibiotic treatment.

5.2 Results

5.2.1 Antibiotic treatment reduces histone acylations

In chapter 4, we observed that the no fibre diet showed a significant reduction in many histone acylations, which could be due to the reduction in butyrate concentration in the colon lumen. We hypothesised that depleting the microbiota by antibiotic treatment would have a similar effect to removing fibre in that it would reduce the production of SCFAs and may therefore reduce abundance of histone acylations. We performed two independent experiments where mice were gavaged for three days with a mixture of antibiotics to deplete the microbiota. 16S sequencing of faecal samples confirmed that the gut bacterial load had been reduced (Figure 5.1) and SCFA measurements in serum and colon lumen showed a clear reduction in acetate, propionate and butyrate concentrations (Figure 5.2). Western blotting of colon extracts showed that many histone acylations were significantly reduced, as can be seen from the blots (Figure 5.3). The quantifications of band intensity relative to H3 loading from both experiments are shown on the same graph (Figure 5.4). In particular, H4K8cr showed a strong reduction in both experiments on antibiotics treatment, with a p value of 0.0004 from the two-way ANOVA test. H4K8ac, H4K12ac, H3K18cr and Kcr H4 were also significantly reduced but H4K8bu, H3K18ac and Kcr H3 did not significantly change. HDAC abundance was also tested, showing a significant upregulation in HDAC2, but not HDAC1 or HDAC3. In a previous chapter, preliminary data suggested that HDAC2 could remove acetyl and crotonyl-groups from histones *in vitro* (Figure 3.14). This could explain the reduction in histone acylations on antibiotics treatment. Interestingly, H3K18β-HBu increased significantly. Potentially, it could respond to a different set of cues to the other histone acylations tested here.

These results were interesting, particularly the striking reduction in H4K8cr suggesting a sensitivity to the microbiota. But there was variability in histone modification levels between mice on the same

treatment, meaning that we wanted to perform a further experiment to make sure that these changes were biologically relevant. Kcr H3 produced a slight reduction which was potentially interesting but the change overall was not significant. A power calculation revealed that the statistical test was underpowered and for the effect size observed here, more samples would be required to achieve enough power to reach significance. Therefore, a further experiment was performed with the BL6 mice but with more biological replicates in each group. As in Figure 5.3 and Figure 5.4, a significant reduction was seen in H4K8cr, H4K8ac, H4K12ac and Kcr H4 (Figure 5.6 and Figure 5.6). This time, H3K18ac and Kcr H3 were also reduced significantly. Interestingly, the effect of antibiotic treatment on H4K8ac was more pronounced compared to the experiments in Figure 5.3 and Figure 5.4, whilst H4K8cr was less. It seems that the direction of the change is consistent between experiments but the degree of difference and significance varies. This could simply be due to technical differences in how the experiment was performed. In this experiment, we also observed significant reductions in H4K16ac, H3K9ac and Kac H4, whilst Kac H3 was borderline significant ($p = 0.0502$). This suggests that the effect of antibiotics treatment is not limited to H4K8ac or H4K12ac but broadly affects many acetyl marks. However, we cannot rule out that some other histone acetyl marks may not change particularly as the effects on Kac were less pronounced. In conclusion, in three independent experiments, histone crotonylation and acetylation show a clear reduction on antibiotics treatment.

To see if antibiotics treatment reduced more than just histone acetylation and crotonylation, we also tested how paradym histone methylation marks changed. Figure 5.6 shows that whilst a downward trend was observed in the active mark H3K4me3, this was not significant. No significant changes were observed for the repressive H3K9me2, H3K9me3 or H3K27me3 which showed a slight upward trend. As histone methylation marks are not thought to be influenced by SCFAs, this suggests that the effect of antibiotics treatment on histone acetylation and crotonylation could be due to changes in SCFA concentrations. However, we cannot conclusively state this as the abundance of other histone methyl marks or the gut luminal concentrations of other microbial metabolites such as folate have not yet been tested.

The effect of antibiotic treatment on HDAC abundance was also investigated. HDAC2 did not change, in contrast to the previous experiments with antibiotics (Figure 5.3 and Figure 5.4), whilst HDAC1 decreased slightly (Figure 5.6). We would expect a reduction in HDAC1 abundance to increase histone acetylation and crotonylation, but they decrease. Furthermore, the changes to HDAC1 and HDAC2 are not consistent between the experiments in Figure 5.3 and Figure 5.6. This result, in combination with the inconsistent changes to HDAC abundance on high fibre diet suggests that this is not the main mechanism for SCFAs to change histone acylations.

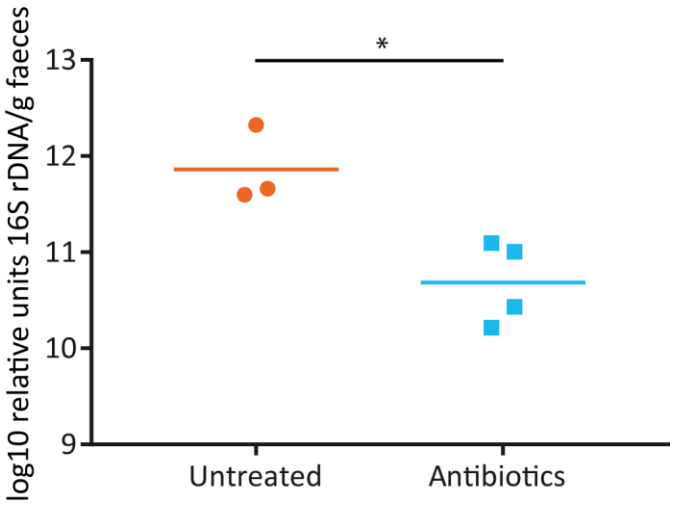

Figure 5.1. Antibiotic treatment in mice reduces gut bacterial load

Bacterial load of mouse faecal samples was determined by qPCR pf 16S rDNA and is expressed as relative amount of bacterial DNA per gram of faeces. Faecal samples were from mice used in experiment 2 (Figure 5.3). Bacterial load estimation was performed by Marco Aurelip Ramirez Vinolo's group.

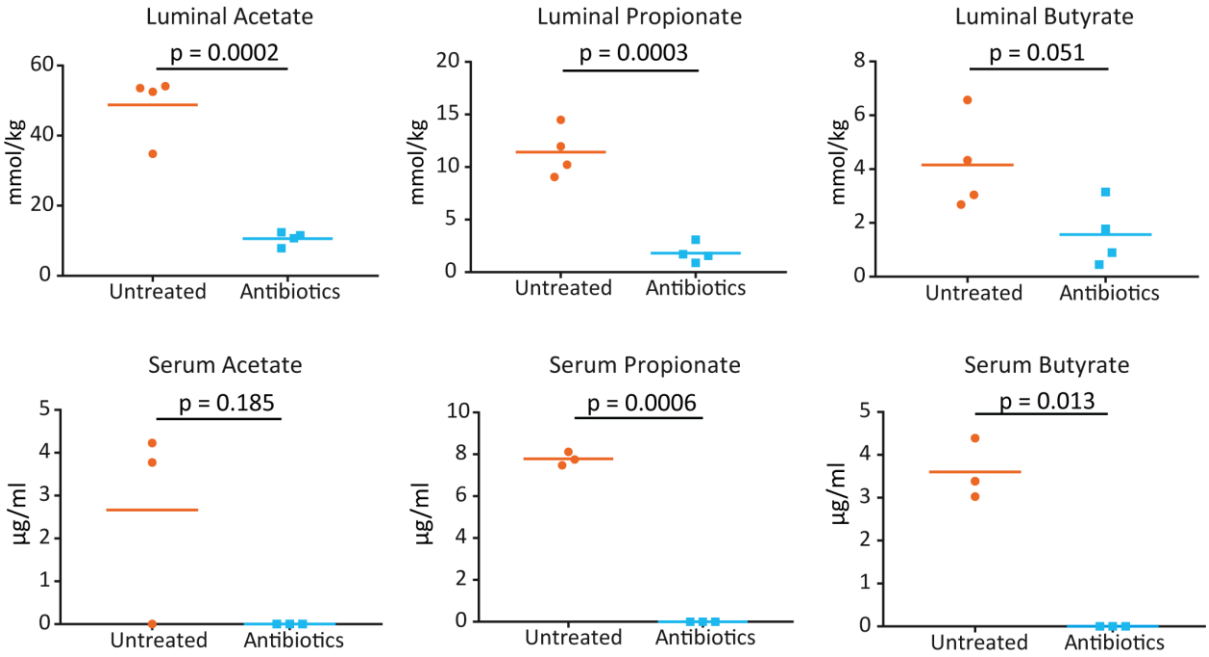

Figure 5.2. Antibiotic treatment in mice reduces luminal and serum SCFA concentrations

SCFA concentrations in the colon luminal content and serum of mice from experiment 2 (Figure 5.3) were measured using gas chromatography (n≥3). Unpaired t-tests were conducted for luminal measurements and one sample t-tests for serum measurements (due to values of zero), both with a threshold p value of 0.05. Values of zero were below detectable levels. SCFA measurements were conducted by Caroline Marcantonio Ferreira's group.

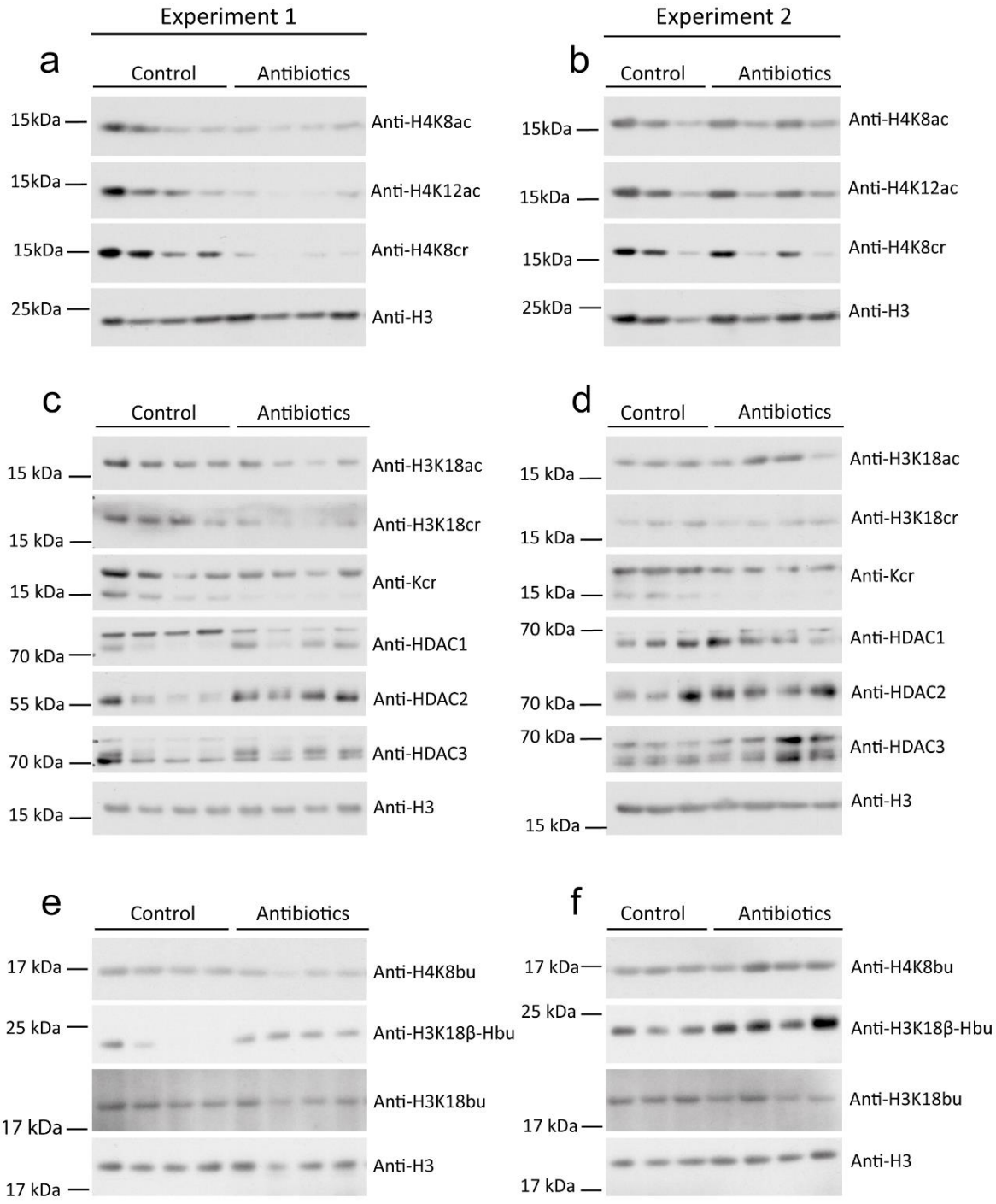

Figure 5.3. Antibiotic treatment reduces histone acylations in mouse colon

Mice were gavaged with a mixture of antibiotics for three days followed by western blotting of mouse colon extracts using the specified antibodies. Two independent experiments (experiment 1 in parts a, c and e and experiment 2 in parts b, d and f) are shown with three or four mice per condition. Blots are grouped into different parts based on the relevant H3 normalisation blot.

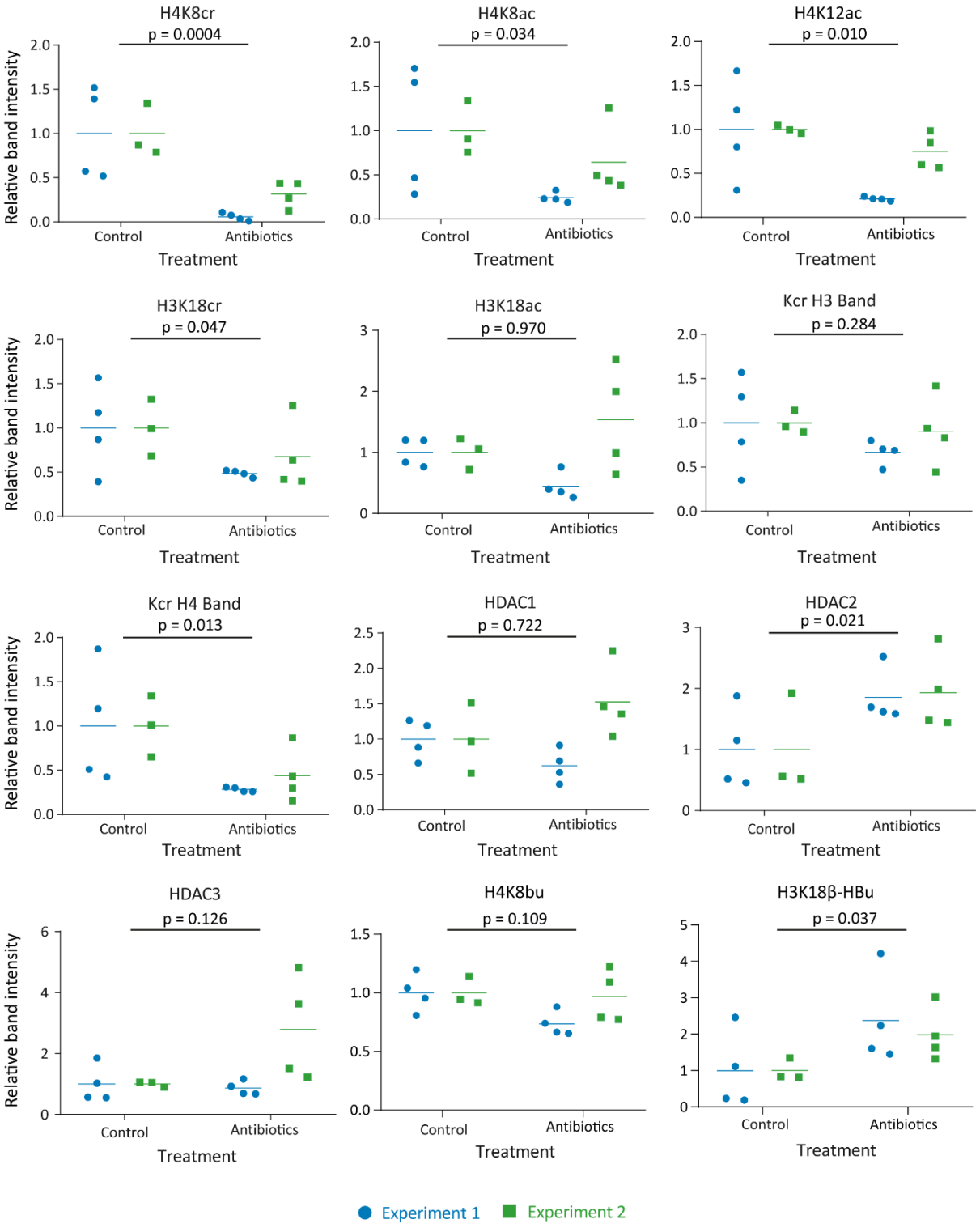

Figure 5.4. Quantifications of western blots on antibiotics treated mice

The western blots from Figure 5.3 were quantified and plotted relative to the histone loading control and the average of the control group. The anti-H3K18bu blot was not quantified due to high background. Both experiments are shown on the same graph and two-way ANOVA was performed using experiment and treatment factors, p values of the effect of treatment are indicated on the graphs. There was no statistically significant

difference between experiments, meaning that antibiotics treatment had the same effect on all histone modifications or HDAC abundances in both experiments, except HDAC3.

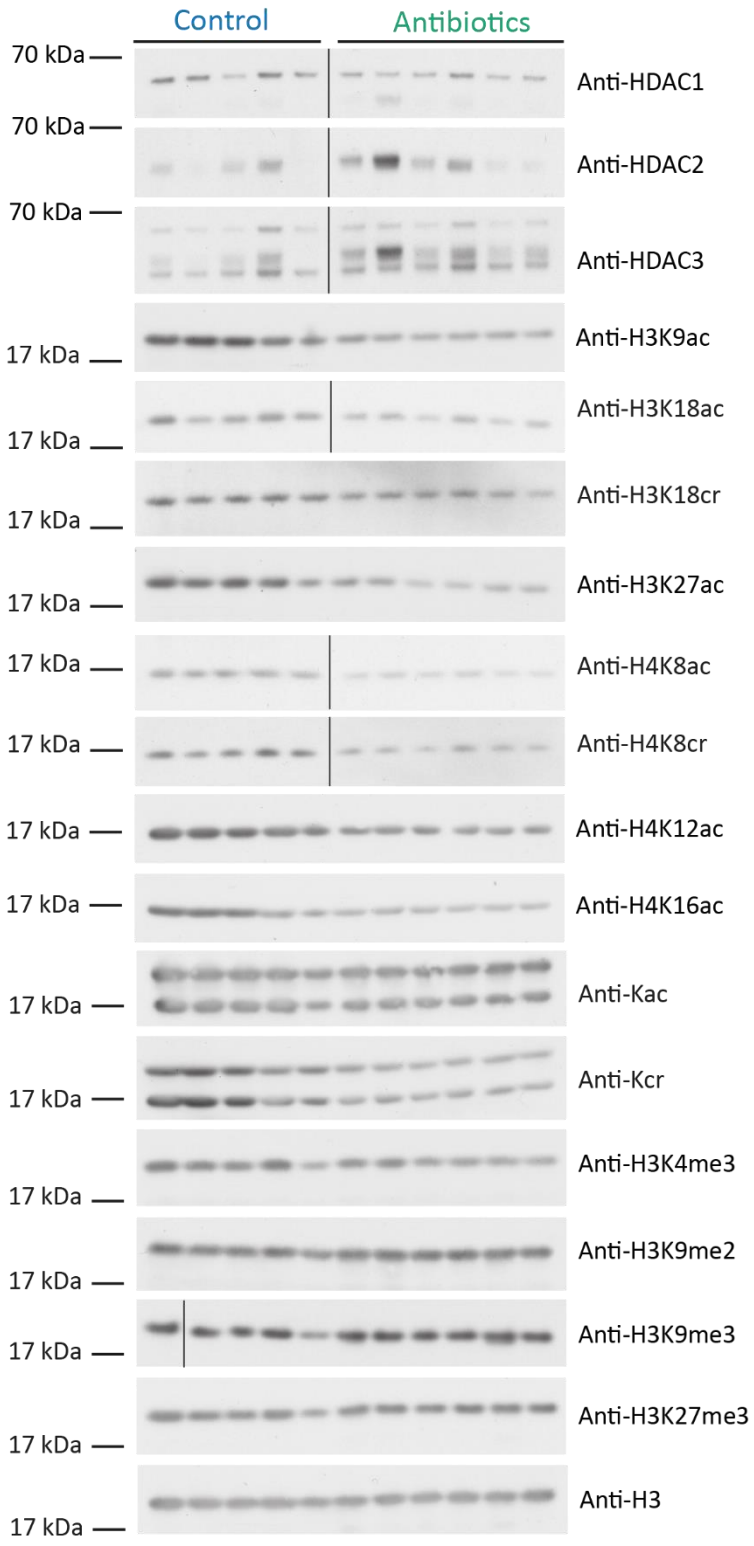

Figure 5.5. Antibiotics treatment reduces histone acetylation and crotonylation but not methylation in mouse colon

Mice were gavaged with PBS or a mixture of antibiotics. Five mice were used in the untreated group and six mice in the antibodies treated group. Western blots of mouse colon extracts probed with the specified antibodies. The black lines indicate where a band was spliced out due to a problem with one of the samples.

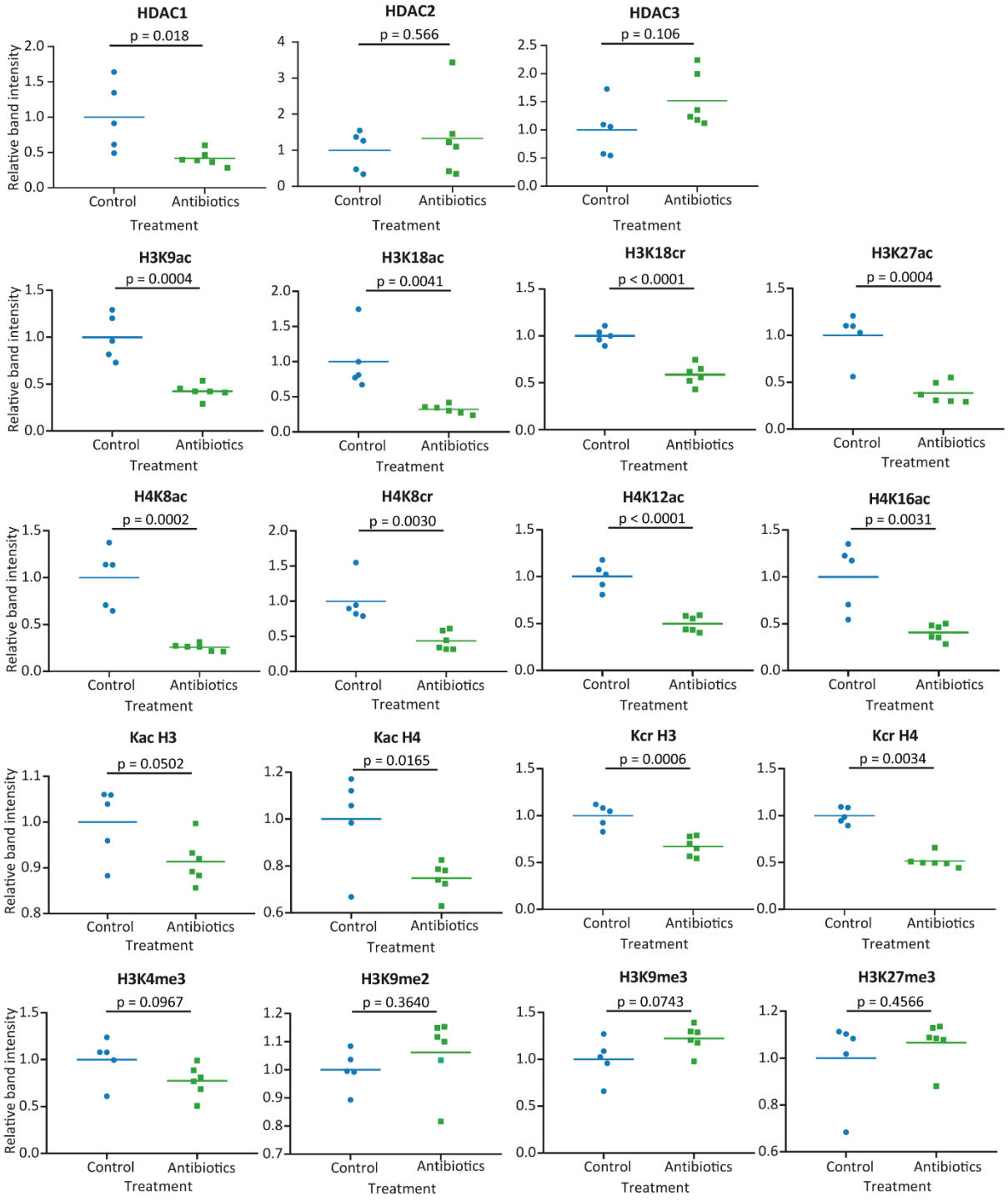

Figure 5.6. Quantifications of western blots on antibiotics treated mice

Mice were gavaged with PBS or a mixture of antibiotics. Five mice were used in the untreated group and six mice in the antibodies treated group. Quantifications of the blots in Figure 5.5 relative to the histone loading control

and the average of the control group. Unpaired t-tests were performed and the p values are shown on the graphs. The p value threshold for significance was 0.05.

5.2.2 The effect of antibiotic treatment on histone acylations in colon organoids

Whilst the effect of antibiotics treatment on histone acetylation and crotonylation in mice may be due to the reduction in luminal bacterial content and subsequent reduction in SCFAs, it is also possible that the antibiotics themselves can have an effect. We planned to treat colon organoids with the same mixture of antibiotics as those used to gavage the mice. The dose used to treat mice was high, but we could not be sure how much the concentration had been diluted by the stomach and small intestine during transit. Therefore, we performed an initial test of different concentrations of the antibiotics mix whilst keeping the ratio between the antibiotics the same and monitoring the organoids to check that they were still growing well. Figure 5.7 shows western blotting of colon organoid extracts using different acyl antibodies. Antibiotics treatment did not change H3K18ac or Kcr H3. Treatment increased H4K8cr but only at the A3 condition. There was no linear relationship between antibiotics concentration and H4K8ac, H3K18cr or Kcr H4 as the modification was lower with higher antibiotic doses (A1 and A2) than lower antibiotic doses (A3 and A4), but was lowest in the untreated condition (A0). Therefore, whilst antibiotics treatment produced a reduction in histone crotonylation and acetylation in the mouse colon, in colon organoids there is no linear change in these modifications because of treatment (Figure 5.7). However, although there are no dose-dependent changes to histone acetylation or crotonylation, antibiotics treatment does influence their abundance in this experiment. As this experiment was only performed once, further experiments are required to determine if the antibiotics themselves can influence these histone modifications. The *in vivo* situation is much more complex. Antibiotics are diluted in their transit through the gastrointestinal tract and may be modified by host and microbial enzymes. Furthermore, the colon contains thick mucus layers, which could protect the colonocytes from the immediate effects of antibiotics and the crypt structure further protects stem cells, which in colon organoids are directly exposed to the media. Therefore, to assess whether antibiotics can influence histone modifications in colonocytes *in vivo,* antibiotics should be used to treat germ free mice to eliminate the effects of the microbiota.

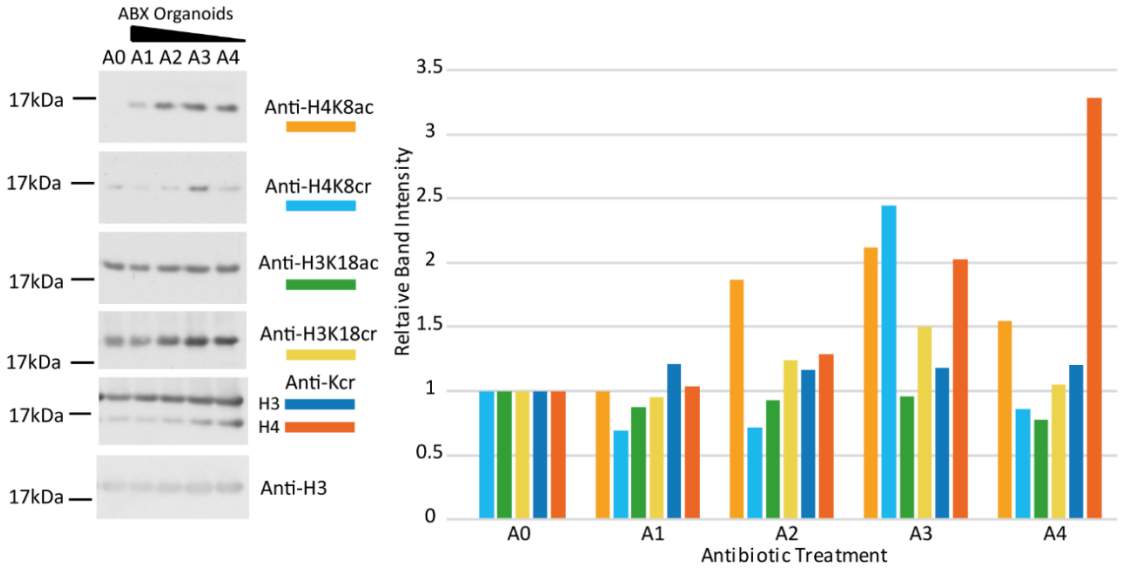

Figure 5.7. The effect of antibiotics treatment of colon organoids on histone acylations

Colon organoids were treated with a mix of antibiotics in the same ratio as that used in the mouse. A0 is without antibiotics, and A1 is with 500 µg/ml metronidazole, 250 µg/ml vancomycin hydrochloride, 500 µg/ml ampicillin sodium salt, 500 µg/ml neomycin sulphate and 500 µg/ml gentamicin. Concentrations decrease two-fold stepwise from A1 (500/250 µg/ml), to A2 (250/125 µg/ml), to A3 (100/50 µg/ml) and finally to A4 (50 or 25 µg/ml). Western blots of whole organoid extracts were analysed by western blot using the specified antibodies. Quantification is shown to the right with background subtracted and relative to anti-H3 blot and the A0 condition. For the anti-H4K8ac blot, quantifications are relative to the A1 condition as no band was visible for A0. The anti-Kcr blot was quantitated separately as H3 and H4 bands.

5.2.3 Antibiotic treatment reduces histone acylations in Balb/c mouse colon but the effect of treatment is not changed by ACAD deficiency

We were interested in the mechanism by which antibiotic treatment reduced histone acylations. ACAD catalyses the conversion of butyryl-CoA to crotonyl-CoA as part of the beta-oxidation pathway and would be important in the metabolism of butyrate to histone crotonylation. When mice were treated with antibiotics, both the wild type and ACAD deficient mice showed significant reductions in all histone acetylation, crotonylation and butyrylation marks tested in the colon (Figure 5.8). These results seen in Balb/c mice are consistent with those seen in BL6 mice (Figure 5.3, Figure 5.4, Figure 5.5 and Figure 5.6). We then ran the western blots with the order switched around, to compare ACAD deficiency with wild type in control mice or in antibiotics treated mice. No clear differences could be seen from the western blots of colon extracts (Figure 5.9) and two-way ANOVA of the band quantifications confirmed that the effect of genotype was not significant (Figure 5.9). This agrees with the comparison of ACAD deficient mice and wild type mice between mice on the same diet, where no

effect of genotype could be observed in the control diet or with 10% inulin supplementation (Figure 4.8).

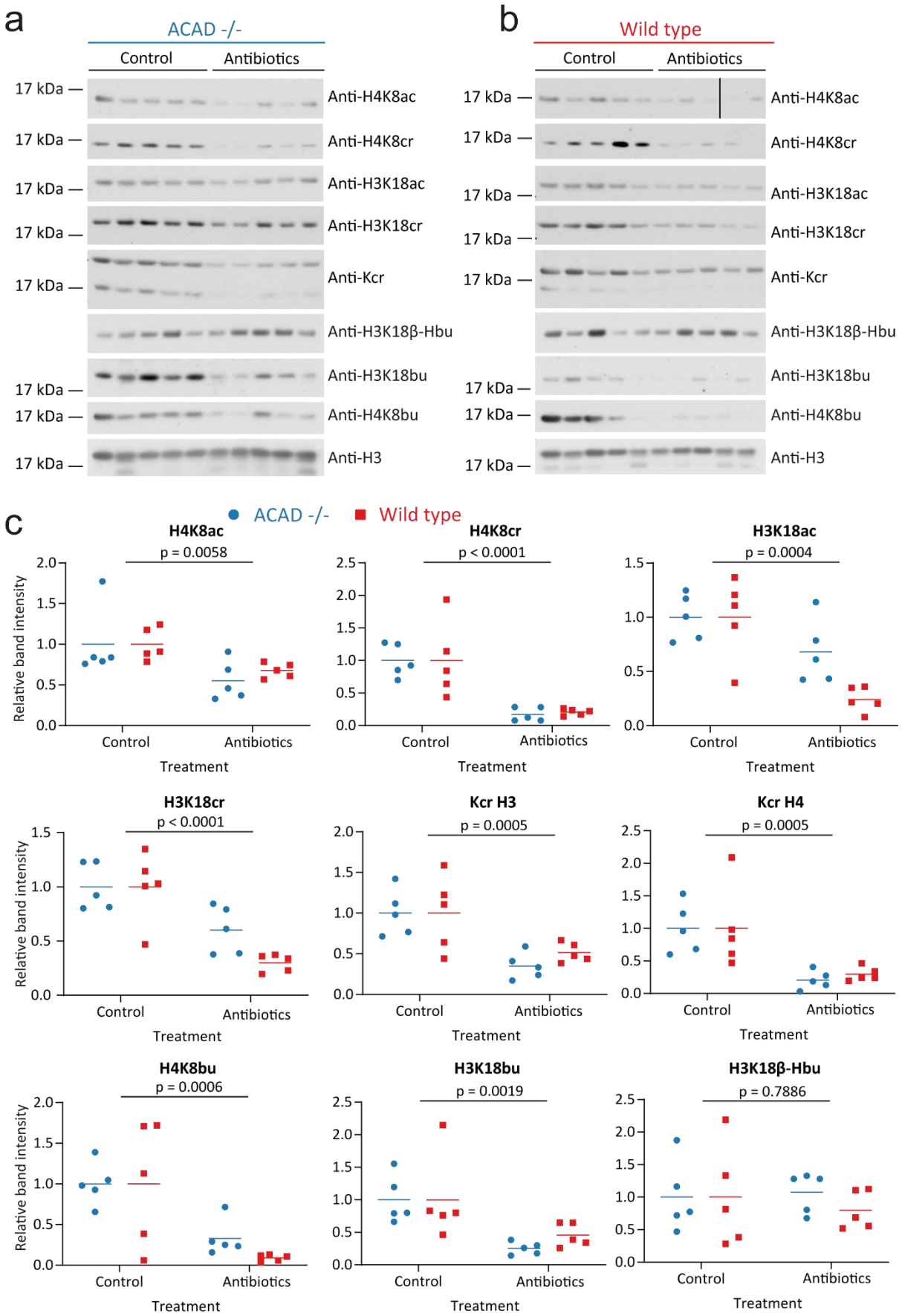

Figure 5.8. Antibiotics treatment reduces histone acylations in Balb/c mouse colon

Wild type mice or those with a deficiency in ACAD were treated with antibiotics or PBS (control) by gavage and extracts of colons investigated by western blot using the specified antibodies. Mouse colon extracts were probed with different antibodies for ACAD deficient (ACAD -/-) **(a)** or wild type mice **(b)**. The line on one of the blots indicates where a band was spliced out due to missloading of a sample which was reloaded in the lane to the right. **(c)** Quantifications of the western blots. Both genotypes are shown on the same graph with band quantifications relative to the anti-histone H3 quantification and the average of the control group. For ACAD deficient acetyl- and crotonyl-lysine blots, the third antibiotics H3 band was also used to quantify the fourth acyl band as the fourth H3 band had a transfer problem. Two-way ANOVA was performed using genotype and treatment factors. The p values of the effect of treatment are plotted on the graphs, with p values of > 0.05 as not significant, $n = 5$.

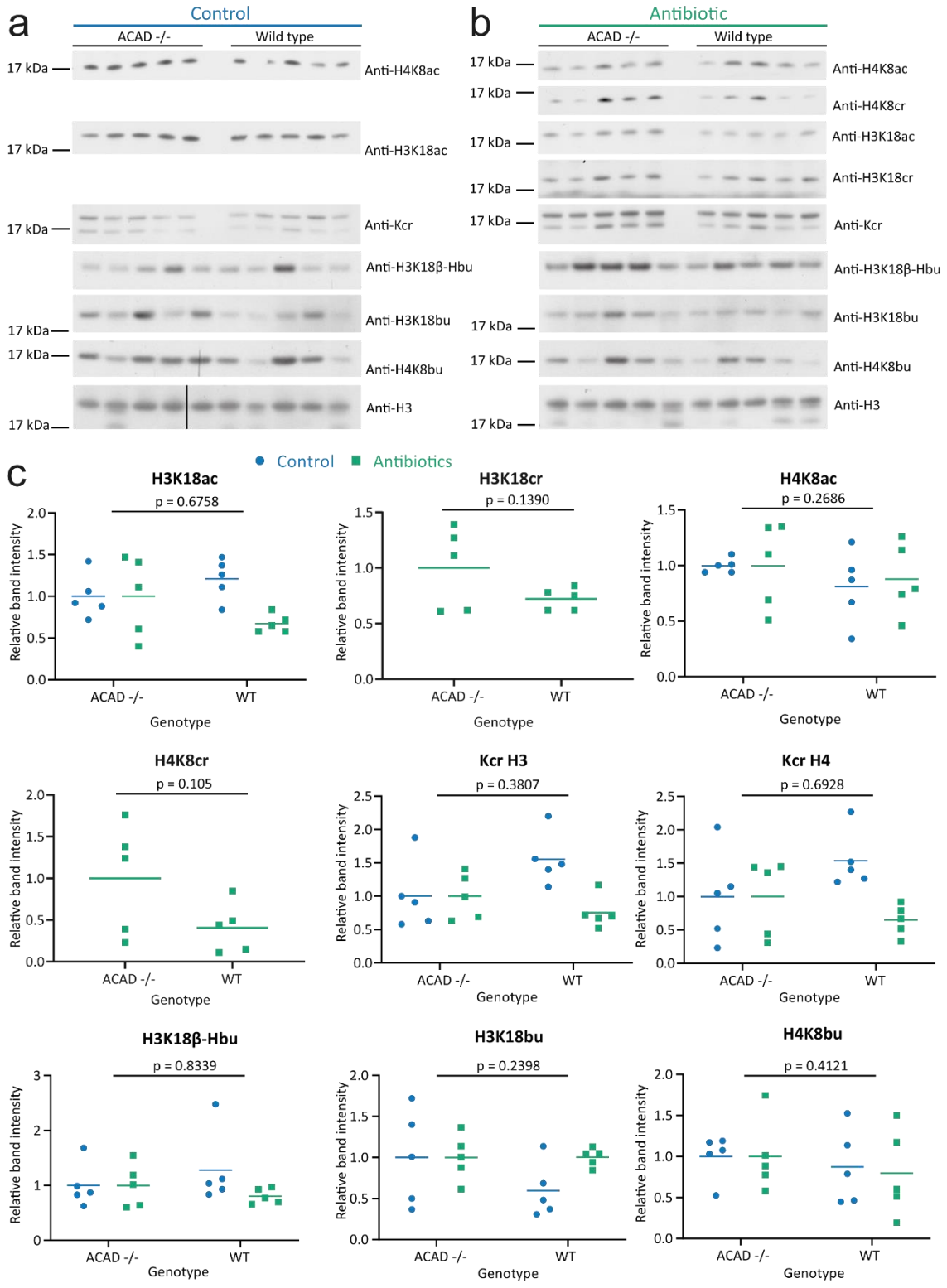

Figure 5.9. ACAD deciciency does not alter histone acylations in colon

Wild type mice or those with a deficiency in ACAD (ACAD -/-) were treated with antibiotics or PBS (control) by gavage and extracts of colons investigated by western blot using the specified antibodies. Mouse colon extracts probed with different antibodies for control mice **(a)** or antibiotics treated mice **(b)**. Gaps in part a are where the blot was problematic and had high background and are not shown. The line on one of the blots indicates

where a band was spliced out due to missloading of a sample which was reloaded in the lane to the right. These are the same samples as in Figure 5.8 but the order is switched to compare genotypes rather than treatment. **(c)** Quantifications of the western blots. Both treatments are shown on the same graph with band quantifications relative to the anti-histone H3 quantification and the average of the control group. Quantifications of H3 intensity only included the upper band, the lower band likely being due to a small amount of protein degradation. Two-way ANOVA was performed with genotype and treatment factors. The p values of the effect of genotype are plotted on the graphs, with a threshold p value of 0.05, n = 5.

5.2.4 The effect of antibiotics treatment and ACAD deficiency in mouse liver

Some SCFAs, in particular acetate and propionate, are released into the portal circulation where they are metabolised in the liver (den Besten *et al.*, 2013). To test if antibiotics treatment altered histone acetylation in the liver, we performed western blots on liver extracts from wild type or ACAD deficient mice treated with antibiotics (Figure 5.10). Histone acetylation was reduced in wild type mice, as detected with an anti-Kac antibody, in agreement with that seen in the colon. In addition, ACAD deficiency reduced histone acetylation in control or treated mice to a level similar to the antibiotics treated wild type. As ACAD catalyses an important step in beta-oxidation to produce acetyl-CoA, ACAD deficiency could mean that liver cells cannot effectively use fatty acids resulting in low acetyl-CoA levels and histone acetylation even with a healthy microbiota. If acetyl-CoA is already low in ACAD deficient mice, this could also mean that antibiotics does not reduce it any further. The difference in the effects of ACAD deficiency between colon and liver may be due to the role of the liver as an essential metabolic organ which performs a variety of biochemical transformations meaning that ACAD is more important for the functions of the liver. Further experiments are necessary to elucidate the effect of antibiotics treatment and ACAD deficiency on Kac in the liver. Interestingly, H3K18ac was reduced only in the ACAD deficient mice on antibiotics treatment. This suggests that other acetyl marks are responsive to ACAD activity, possibly including H4K8ac, but the blot has too high background to be sure. A technical repeat is needed to investigate how H4K8ac changes in the liver on antibiotics treatment. It would also be interesting to determine the effects on ACAD deficiency on histone crotonylation in the liver.

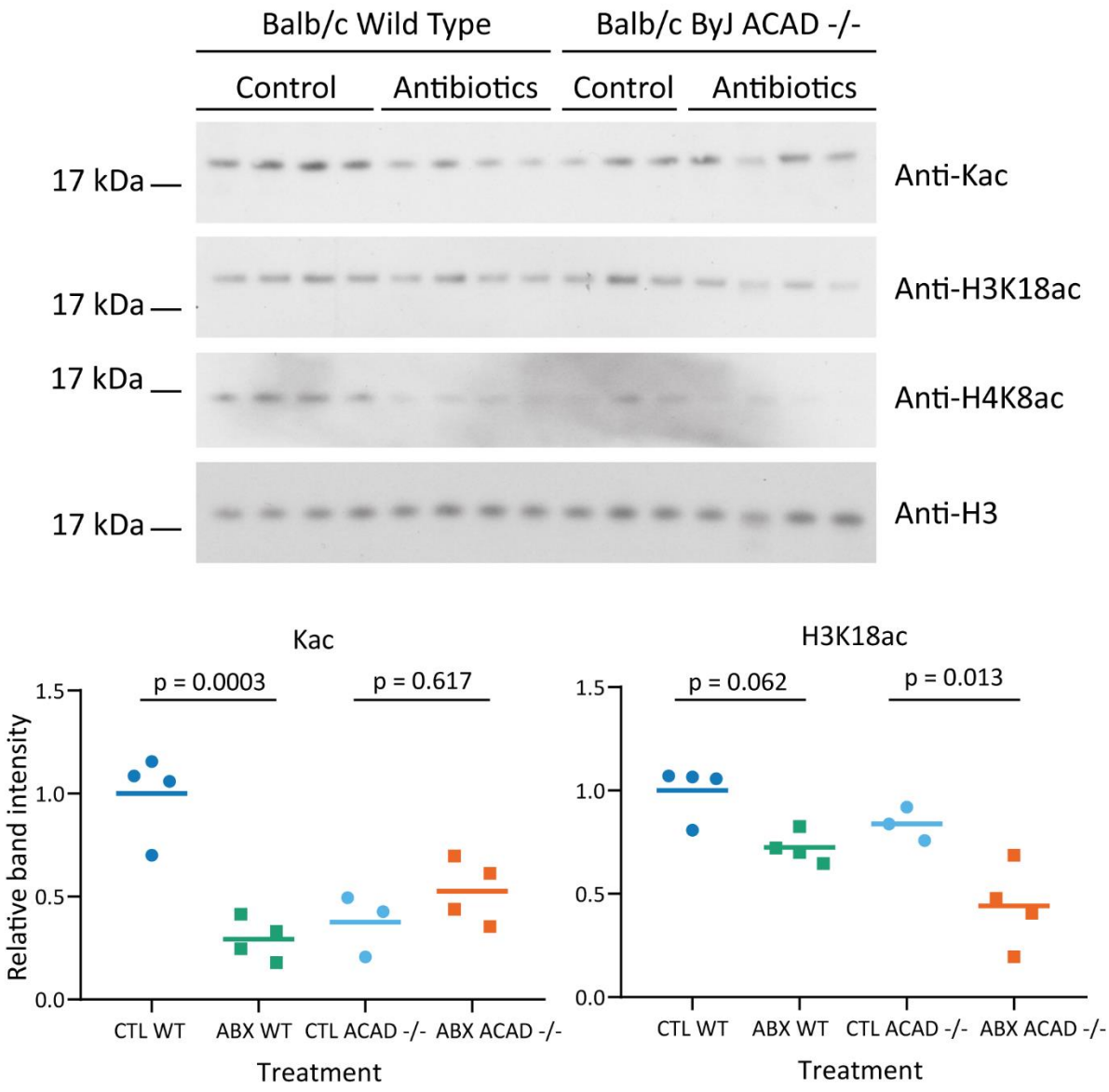

Figure 5.10. The effect of antibiotics treatment on histone acetylation in mouse liver

Wild type mice or those with a deficiency in ACAD were treated with antibiotics or PBS (control) by gavage and extracts of livers investigated by western blot using anti-Kac, anti-H3K18ac, anti-H4K8ac and anti-histone H3 antibodies. Quantifications are shown for each band with values relative to the H3 quantification and the average of the control wild type group. CTL is control, ABX is antibiotics. The anti-H4K8ac blot was not quantified due to high background. One-way ANOVA was performed and the pairwise comparisons of the difference between control and antibiotics are shown on the graph (correction with Holm-Sidak method), n = 4.

5.2.5 Characterisation of H4K8 acetylation and crotonylation in colon carcinoma cells

Histone crotonylation and acetylation are associated with active gene expression (Sabari *et al.*, 2015). We were therefore interested in finding out which genes had reduced in histone acylation on

antibiotics treatment and whether these changed in expression. H4K8cr was highly responsive to antibiotics treatment in previous experiments (Figure 5.3 and Figure 5.6), making it a good target for investigating how its genomic localisation changed. As H4K8cr ChIP had not been performed before and the available antibodies were not validated for ChIP, we first tested it in colon carcinoma cells. We did not know what the genomic distribution of H4K8cr would be but we supposed that it might be similar to H3K18cr. *KLF11* and *KLF13* had high H3K18cr, whilst *CYS1* had low H3K18cr in a previous ChIP-qPCR experiment on small intestinal crypts (Figure 4.3). QPCR analysis of H4K8cr suggested that crotonyl marks had been specifically pulled down as *KLF11* was 2 to 7-fold higher than the negative target *CYS1* (Figure 5.11a). There was some variability between technical repeats and no clear difference between crotonate treated and untreated cells. However, when the ChIP DNA library was sequenced, the enrichment was marginal to non-existent with no difference between the crotonate treated and untreated conditions (Figure 5.11b). This lack of enrichment over input was also seen in the scatter plot of read counts in the H4K8cr ChIP against input, showing that read density in the ChIP was very similar to input (Figure 5.11c). Additionally, a cumulative distribution plot did not show any clear differences between the crotonate treated H4K8cr ChIP, untreated H4K8cr ChIP and input (Figure 5.11d). As the ChIP had low recovery relative to input (0.07 – 0.44 % of input for *KLF11*), small differences between targets in qPCR could easily be interpreted as high fold-enrichment. Additionally, with only one positive target in the qPCR it is hard to know if the antibody could effectively pull down the crotonylated chromatin. Crotonylation is low in abundance relative to acetylation. In the colon H3K18cr is present on 2 % of H3 histones, compared to H3K18ac on 30 % of H3 histones (Fellows *et al.*, 2018). This mass spectrometry analysis, performed by members of the Tiziana Bonaldi group, found that H4 crotonylation was less abundant than H3K18cr. The abundance of H4K8cr across the genome could have been so low in HCT116 cells that many of the reads in ChIP-seq were distributed to background regions.

We also tested H4K8ac by ChIP-seq as this mark was also reduced on antibiotics treatment. In contrast to H4K8cr, H4K8ac ChIP-seq produced clear enrichment over input with mostly sharp peaks (Figure 5.12a). Investigating where H4K8ac peaks were relative to genes revealed an enrichment for the TSS (Figure 5.12b), in agreement with a study by Hayashi-Takanaka *et al.* (2015) that found H4K8ac was associated with TSS in embryonic stem cells. Filtering MACS peaks by their position showed that the majority of peaks are at the start of genes (63 %), with a lesser proportion in the gene body (23 %) and only a small proportion outside of genes (12 %) (Figure 5.12c). Wang *et al.* (2008) found that H4K8ac was present in transcribed regions of active genes, which could explain the presence of this mark in the gene body. Out of 58270 genes annotated in the human genome, 10632 contained a MACS peak for H4K8ac (18.2%). This was compared to 14897 H4K8ac MACS peaks in total. When only protein-

coding genes were included, 8264 out of 19836 protein-coding genes contained a H4K8ac MACS peak (41.6%). The abundance of H4K8ac was correlated with gene expression (Figure 5.12d). When read counts at TSS were grouped according to the expression of that gene as determined by RNA-seq, the level of H4K8ac at TSS increased with increasing gene expression. There was no correlation in the input. There were a few outliers, meaning that for some genes, high H4K8ac does not mean high gene expression. It could also be because in some cases the TSS of two genes are overlapping. A high level of H4K8ac at the TSS of one gene could result in high gene expression but an adjacent gene, which is lowly expressed, would still be counted as having high H4K8ac. H4K8ac MACS peaks were present at many housekeeping genes, including EIF3A, GAPDH and ACTB. To understand the function of genes associated with H4K8ac, we performed gene ontology analysis comparing genes containing H4K8ac MACS peaks to a standard reference *Homo sapiens* list (Figure 5.12e). Chromatin organisation and protein acetylation were enriched, suggesting that histone acetylation is involved in the regulation of other epigenetic marks and chromatin conformation. Interestingly, a group of dual specificity protein phosphatases (MAPK inactivation term) were enriched, along with the cell cycle term and terms involving RNA metabolism, indicating a correlation of H4K8ac with translation and cell signalling.

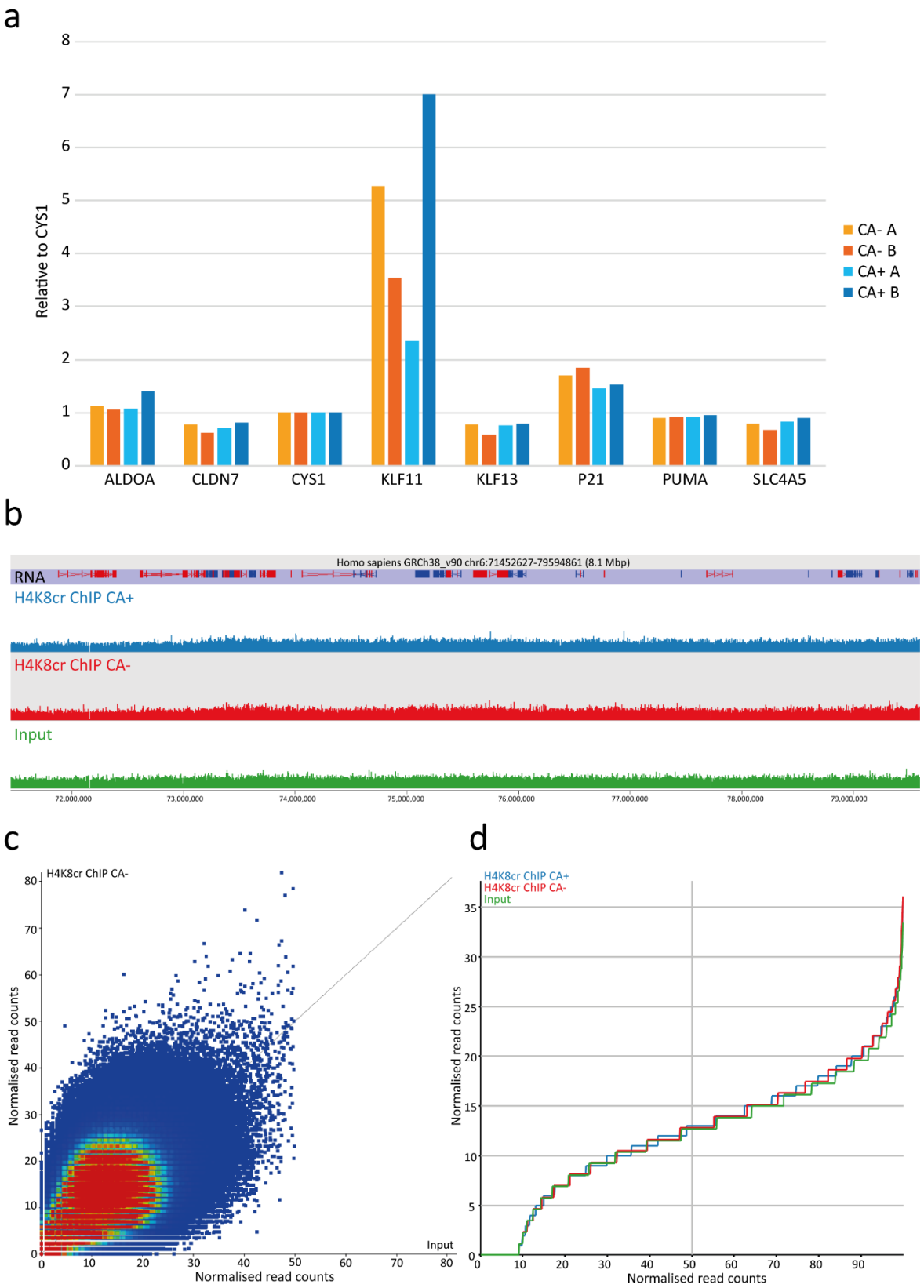

Figure 5.11. H4K8cr ChIP was not enriched relative to input

ChIP was performed on sonicated chromatin from HCT116 cells using anti-H4K8cr antibody. Two biological replicates were prepared for the ChIP plus an input sample for each condition. **(a)** Quantitative PCR on purified

DNA from the ChIP procedure using primers against the promoters of the specified genes. CYS1 and SLC4A5 are thought to be negative for crotonylation. CA- is untreated cells, CA+ indicates cells treated with 5 mM crotonate for 24 hours, A and B are technical replicates. **(b)** Browser view of a segment from chromosome 6 showing a representative profile of H4K8cr ChIP-seq. **(c)** Comparison of H4K8cr and input by scatter plot with running window probes quantitated by linear read count quantitation relative to the largest data store. **(d)** Cumulative distribution plot of ChIP samples and input with linear read count quantitation of running window probes.

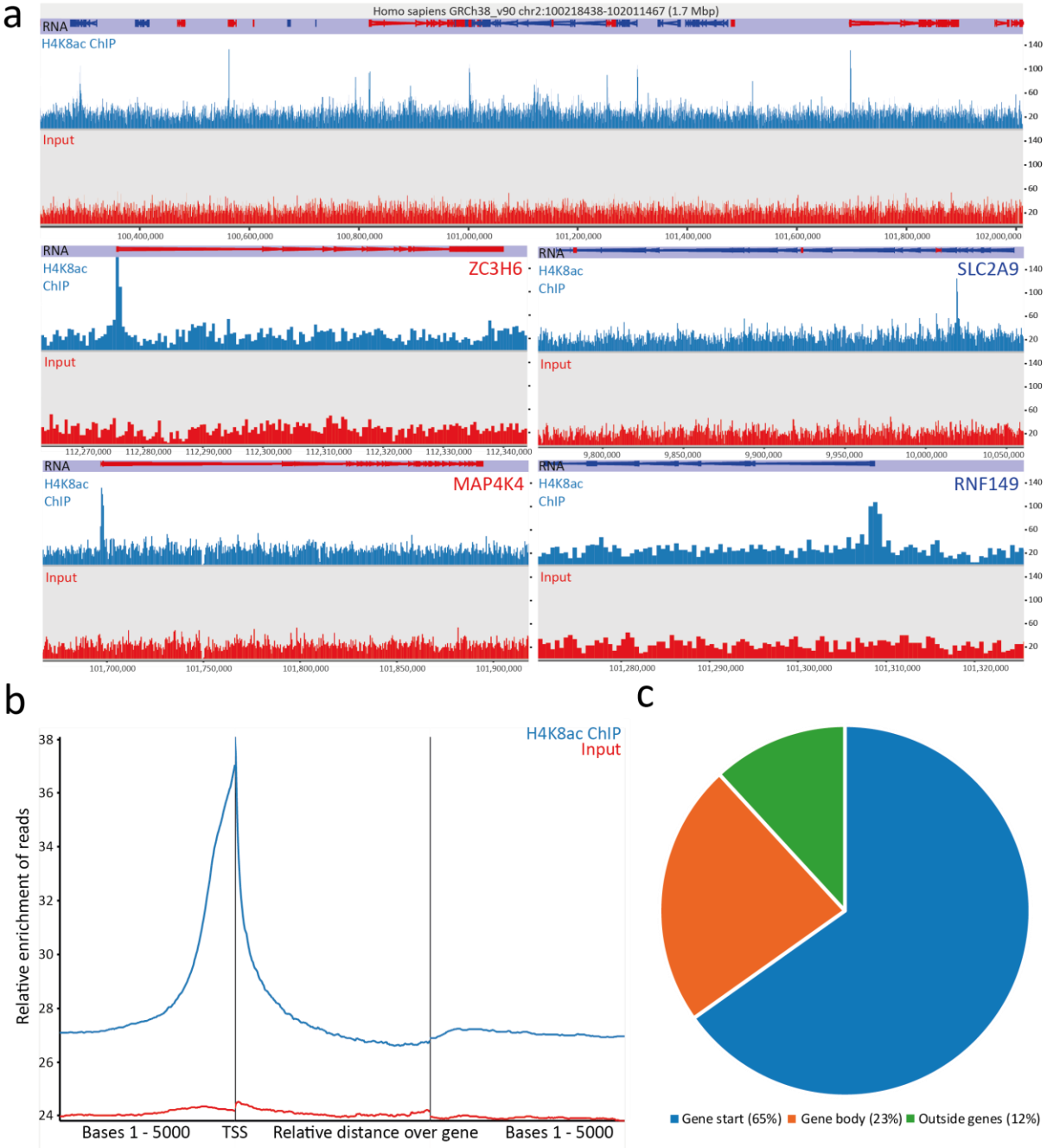

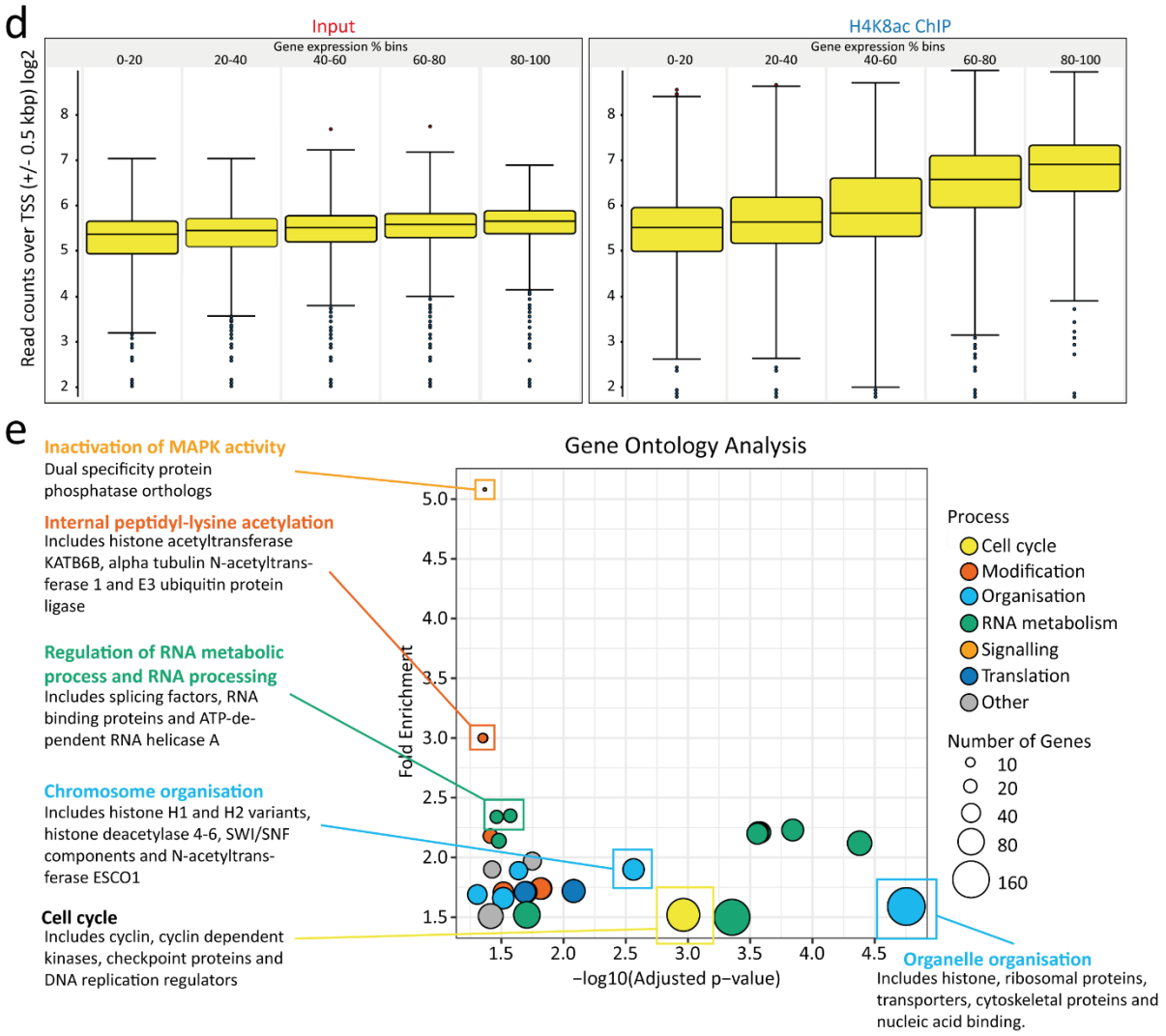

Figure 5.12. Characterisation of H4K8 acetylation in human carcinoma cells

ChIP was performed on sonicated chromatin from HCT116 cells using anti-H4K8ac. Two biological replicates were prepared for the ChIP plus an input sample. **(a)** Browser view of a segment from chromosome 2 showing a representative profile of H4K8ac peaks compared to input. **(b)** Quantitation trend plot of H4K8ac ChIP and input using linear read count quantitation of running window probes showing distribution relative to TSS. **(c)** Distribution of MACS peaks at the start of genes, in the gene body or outside genes as shown by a pie chart. MACS peaks were created using Seqmonk standard pipeline. **(d)** Number of H4K8ac reads at TSS relative to gene expression. Genes were put into percentile bins according to their enrichment by RNA-seq. The read counts of H4K8ac over TSS were quantified and box plot generated according to the expression of that gene for input and H4K8ac ChIP. **(e)** Gene ontology analysis using Panther statistical overrepresentation test of genes containing H4K8ac MACS peaks. The standard *Homo sapiens* reference list was used as background. Terms are grouped in to colours by function and interesting genes within terms highlighted in the description.

5.2.6 Comparison of H4K8ac in mouse colon and liver

We were interested to see the distribution of H4K8ac in mouse and how it differed between tissues. We chose colon and liver as these were most relevant to the microbiota and therefore this data would be useful generate qPCR primers for use in further experiments. In agreement with the H4K8ac analysis in colon carcinoma cells, H4K8ac in colon and liver are also associated with TSS (Figure 5.13b). The browser view of a segment of chromosome 6, shows that in some places H4K8ac is present in both liver and colon, whilst in other places it is only present in the liver (Figure 5.13a). Some of the differences in the H4K8ac signal between the tissues could be due to technical differences in the quality of the libraries as the liver H4K8ac ChIP is more enriched relative to input than the colon H4K8ac ChIP. However, this was adjusted for when MACS peaks were generated and enrichment normalised between samples. There were 68953 H4K8ac MACS peaks in colon and 92157 H4K8ac MACS peaks in liver, of which 14185 and 15013 were in protein coding genes respectively (64.6 and 68.4 % of total protein coding genes). MACS peaks were present at housekeeping genes such as *Eef2*, *Ppia*, *Actb* and *Eif3a* which have low tissue specificity. Looking at certain genes that are known to be tissue specific, liver specific genes such as *Itih4*, *Serpinc1* and *Fga* only have H4K8ac peaks in the liver samples whilst the colon specific genes *Vil1*, *Isx* and *Mep1a* only have H4K8ac peaks in the colon samples. To investigate the overlap of H4K8ac peaks in these two tissues at a genome wide level, we plotted read counts in MACS peaks in the colon against those in the liver. A large number of H4K8ac MACS peaks are present in both tissues (Figure 5.13c). Those MACS peaks with acetylation in only colon have the highest enrichment relative to liver and vice versa, as would be expected. To better visualise the overlap between liver and colon, we generated Venn diagrams counting every gene or promoter that contained a MACS peak in liver or colon (Figure 5.13d). There was a substantial overlap between liver and colon which increased when only peaks in promoters were counted. Interestingly, of the colon specific acetylated peaks, a greater proportion are at the promoter compared to the proportion of promoter associated peaks that are specific to the liver.

As in the colon carcinoma cells, the majority of H4K8ac in liver and colon was present at the start of the gene or in the gene body. However, a substantial proportion (15-25%) of MACS peaks were present outside genes. It is well known that many regions outside genes have an important regulatory function including in regions called enhancers. We were interested to understand what genomic feature was best associated with H4K8ac and if the regions containing H4K8ac outside genes were enhancers. Defining regions that are enhancers is problematic, as there is no consensus sequence. So far, we have described promoters as 500 bp upstream or downstream of the transcription start site but in fact, promoter regions can also be difficult to identify as they are not always at the start of the gene. As a

best estimate of enhancer and promoter regions we used a mouse candidate regulatory element track from ENCODE, a higher-level analysis, which assembled data from ChIP-seq on histone modifications and chromatin accessibility analysis such as ATAC-sequencing. Figure 5.13e shows the proportion of H4K8ac peaks that overlap regulatory elements in liver only, colon only or those peaks that are present in both tissues. For the tissue specific genes, the regulatory element track overlapped with around 78-81% of H4K8ac peaks. Most interestingly, the regulatory element track explained 99% of the H4K8ac peaks that were present in both tissues. In conclusion, the localisation of H4K8ac appears to be broad and is not restricted to a single tissue.

To investigate the function of genes that contain H4K8ac in a tissue specific manner, we performed gene ontology analysis. This included only peaks that were overlapping a gene, as it is difficult to identify which gene or group of genes that an enhancer element is regulating. We made gene ontology plots that compare the fold enrichment to statistical significance with the size of the points differing based on the number of genes in an ontology term (Figure 5.13f). We also coloured the terms by categories that were based on their functions. Many of the terms that come up in the gene ontology analysis of H4K8ac in only colon or only liver, imply regulation of tissue specific functions. In the colon, terms including homeostasis, sequestering of calcium ions and regulation of cellular component biogenesis are identified as particularly significant or enriched. The colon is a highly regenerative tissue meaning that generation of new biomolecules would be constantly required. In the liver, terms such as lipid translocation, metabolism, transport and localisation come up strongly in line with the liver's important role in lipid processing. Intriguingly, terms such as development and signalling also appear. For those genes with acetylation in both liver and colon, the function seems to be more associated with active gene expression including nucleic acid metabolism, translation initiation, elongation and termination. Fascinatingly, chromatin remodelling is highly enriched, matching what was seen previously in the colon carcinoma cells. This makes sense as histone acetylation is involved in switching the chromatin to a more open state. As the same background list was used for gene ontology analysis of the liver and colon specific H4K8ac and those present in both tissues, the significantly enriched terms may reflect the patterns of gene expression present in each tissue or of housekeeping genes present in both. As histone acetylation is associated with active genes, this still suggests that H4K8ac could have a role in regulating the gene expression patterns in these tissues.

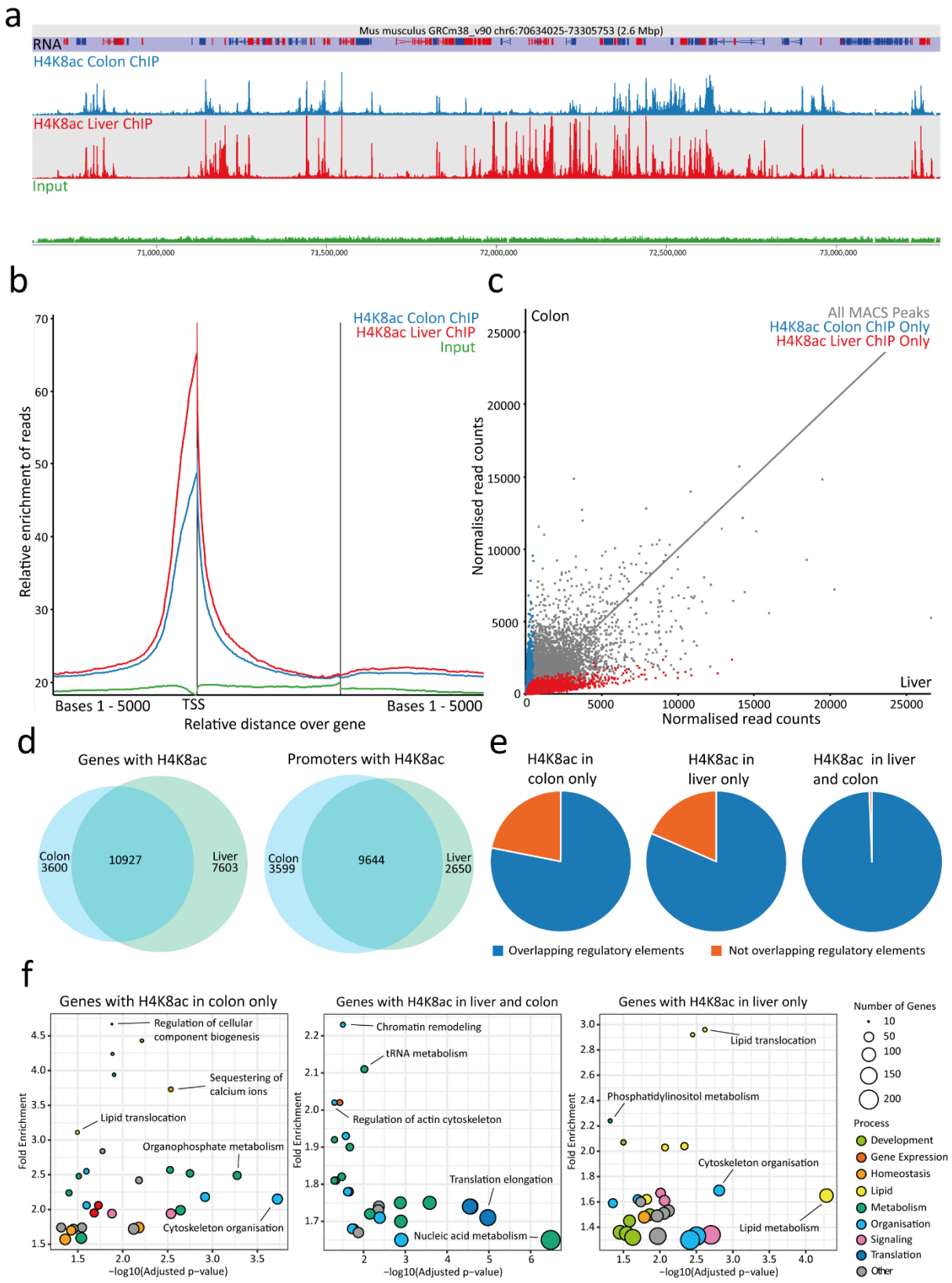

Figure 5.13. Comparison of H4K8 acetylation in liver and colon

ChIP was performed on sonicated chromatin from mouse colon or liver using anti-H4K8ac antibody. Three biological replicates for the ChIP and an input were generated for each tissue. **(a)** Browser view of a segment from chromosome 6 showing a representative profile of H4K8ac peaks compared to input. **(b)** Quantitation trend

plot of H4K8ac ChIP and input using linear read count quantitation of running window probes showing distribution relative to TSS. **(c)** Scatter plot of MACS peaks comparing colon and liver with peaks only in colon or only in liver highlighted in blue and red respectively. **(d)** Venn diagrams of genes or promoters containing H4K8ac MACS peaks showing the overlap between colon and liver **(e)** Comparison between H4K8ac peaks and a regulatory element track from ENCODE which compiles various markers of enhancers and promoters. Pie charts show the overlap for MACS peaks only in the colon, only in the liver or those only in both tissues. **(f)** Gene ontology analysis using Panther statistical overrepresentation test of genes containing H4K8ac MACS peaks in just colon, in both tissues or in just liver. The standard *Mus musculus* reference list was used as background. Terms are grouped in to colours by function and interesting terms are labelled on the graph.

5.2.7 Chromatin state analysis in the liver

As H4K8ac was strongly linked to regulatory elements in liver and colon, we wanted to find out how it was related to other histone marks and in particular those associated with different chromatin states. In the liver, we compared H3K27me3 which is associated with gene silencing, H3K4me3 which is associated with promoters, H3K27ac and H3K4me1 which are marks of enhancers and H3K36me3 which is a mark of transcription elongation to H4K8ac. It is important to note that there is some overlap between these categories, as H3K27ac and H3K4me1 can be found at promoters and H3K4me3 can be found at enhancers (Pekowska *et al.*, 2011). We used the ChromHMM tool, which groups the genome into states according to the presence of different chromatin markers, to identify the optimal number of chromatin states (Ernst and Kellis, 2012). Figure 5.14 shows heat maps of the emission (part a) and transition (part b) parameters of a six-state model. Each state has been assigned a label, such as promoters or enhancers, according to which histone modifications were present. Chromatin state 1 (promoters) typically contains regions with high H3K4me3, whilst chromatin state 3 (enhancers) typically contains high H3K27ac. Actively transcribed (state 4, high H3K36me3), repressed (state 6, high H3K27me3) and background (state 5) regions contained little H4K8ac. Instead H4K8ac strongly associates with both enhancer and promoter marks in agreement with the findings in Figure 5.13. Fascinatingly, state 2 contains mostly H4K8ac with a low level of H3K4me1 (Figure 5.14a). In Figure 5.14c, a representative browser view is shown of the profiles of the different histone modification ChIP-seq data used in the ChromHMM analysis along with with six states derived from this data. This reveals that chromatin state 2 contains H3K4me1 and H4K8ac and lower levels of H3K4me3 or H3K27ac. These are often close to promoter and enhancer regions. There are also some regions of chromatin state 2 are distinct from state 1 or 3 and could have their own regulatory function. However, further investigation will be necessary to determine the role of this predominantly H4K8ac/H3K4me1 state. Interestingly, Rhbdl3 gene at the left of the browser view appears to be in a poised state. It contains a high level of active-associated H3K4me3 at the start of the gene (state 1)

along with repressive-associated H3K27me3 (state 6 surrounding the TSS-associated state 1). Rhbdl3 contains very low levels of the transcription-associated H3K36me3 (state 5) over its gene body. This is in contrast to Zfp207 and Psmd11, which contain high H3K4me3 but low H3K27me3 at the gene start and high levels of the transcription-associated H3K36me3 over the gene body. This suggests that Rhbdl3 is poised for transcription, whilst Zfp207 and Psmd11 are being actively transcribed.

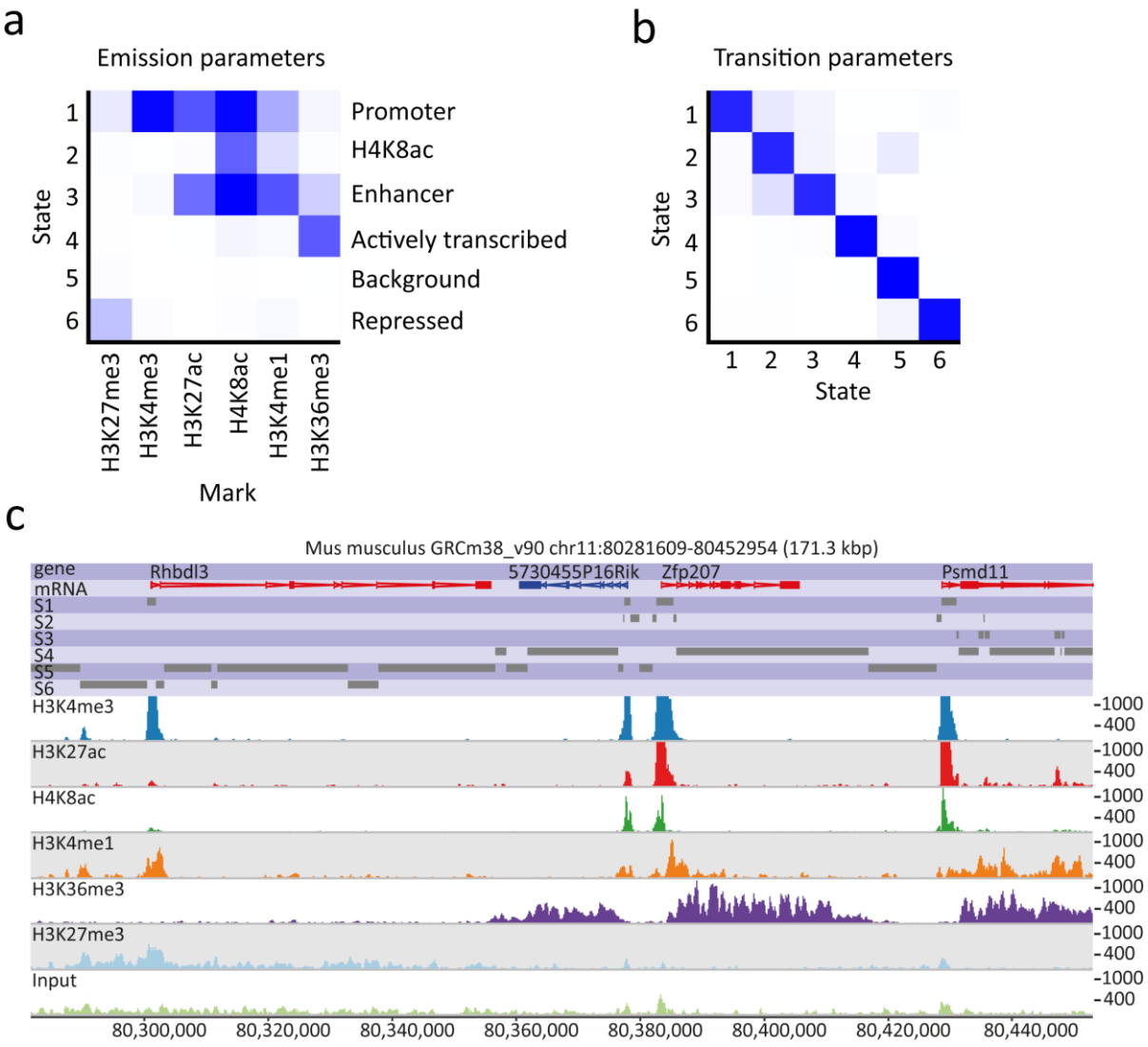

Figure 5.14. Chromatin state analysis using histone modifications in mouse liver

Chromatin state analysis performed using ChromHMM using H4K8ac ChIP-seq data from liver (shown in Figure 5.13) and publicly available ChIP-seq data from adult liver for the specified histone modifications from ENCODE. Two biological replicates are used for the ENCODE data and three biological replicates for H4K8ac. A six-state model was used with a 200 bp window size. **(a)** Heat map of emission parameters with chromatin state numbers on the left, histone modifications below and state descriptions shown to the right. **(b)** Heat map of transition parameters showing the similarity between the six states. **(c)** Browser view from SEQMONK showing a

representative distribution profile of H3K4me3, H3K27ac, H3K4me1, H3K36me3, H3K27me3 from ENCODE, H4K8ac and input data sets used in the ChromHMM program along with the chromatin state annotation tracks determined from the six-state model (S1-6).

5.2.8 Comparison of Kcr, H4K8ac and H3K18cr in untreated mouse colon

Histone acetylation and crotonylation occur at many of the same positions on the histone (Tan *et al.*, 2011) but relatively little is known about how their genomic distributions compare. Therefore, we compared the ChIP-seq profiles of H4K8ac, Kcr and H3K18cr in untreated mouse colon (Figure 5.15). H3K18cr ChIP-seq data was previously generated by Payal Jain and Claudia Stellato (Fellows *et al.*, 2018). A representative segment from chromosome 2, including close-ups of the distribution over four genes, shows that the position of the peaks in H4K8ac, Kcr and H3K18cr are strikingly similar (Figure 5.15a). We grouped the genome into percentile bins based on the level of gene expression in an RNA-seq data set from untreated mouse colon. The box plots in Figure 5.15e show the number of read counts over the TSS in each percentile bin for H4K8ac, H3K18cr or Kcr. All three modifications show increasing read counts at the TSS as gene expression increases, whilst input shows no change. We called MACS peaks of each ChIP-seq data set and investigated how these peaks overlapped, looking at peaks in genes. The H4K8ac, Kcr and H3K18cr peaks were highly overlapping (Figure 5.15b). Nearly all of the H3K18cr MACS peaks overlapped with H4K8ac and Kcr peaks (9649/10,086 or 96 %). 52 H3K18cr MACS peaks did not overlap with H4K8ac or Kcr MACS peaks. This was not because H4K8ac or Kcr were absent in these regions but just that the level did not reach the threshold to be called as a peak. Two examples of this are shown in Figure 5.15d, a peak is called only for H3K18cr but there is some enrichment for H4K8ac and Kcr as well. For H4K8ac, a lower proportion of peaks overlapped with H3K18cr and Kcr (9649/18,558 or 52 %). The lower proportional overlap of H4K8ac may be because there were more MACS peaks for H4K8ac than H3K18cr (18,588 and 10,086 respectively), possibly because the H4K8ac data set was more enriched relative to input than H3K18cr. To investigate what the function of genes containing all three modifications could be, we performed gene ontology analysis of the 9649 genes containing H4K8ac, Kcr and H3K18cr MACS peaks. In Figure 5.15c the significance of each gene ontology term is plotted against fold enrichment, with the size of point corresponding to the number of genes in that term and the colour to the functional category. Terms associated with a range of functions are significantly enriched relative to the *Mus musculus* background list. These include protein polyubiquitination, protein lipidation, autophagosome assembly, protein targeting, protein folding, cytoskeleton organisation and carbohydrate derivative biosynthetic process. Phosphatidylinositol metabolic process shows the greatest enrichment relative to the background list, whilst cellular localization is the most significant. This is in part related to the

number of genes in that term. Fewer genes reach higher enrichment more easily whilst a large number of genes in a term are more likely to be significant. In conclusion, H4K8ac, H3K18cr and Kcr are highly overlapping, correlated with higher levels of gene expression and diverse cellular functions.

The quantitation trend plot in Figure 5.15f, summarising read counts over TSS for the whole genome, shows that H4K8ac, H3K18cr and Kcr are highest enriched at the TSS. However, when exploring the ChIP-seq profiles of H4K8ac, Kcr and H3K18cr in SEQMONK, it seemed that whilst many peaks were at the start of genes, there were also peaks present in the gene body or outside genes, as the representative browser view in Figure 5.15a shows. Histone acylation MACS peaks were present at the gene start (+/- 500 bp of the TSS), gene body (the gene excluding the start region) and outside genes, as shown in the pie chart in Figure 5.15g. The proportions of MACS peaks in different regions did vary between the histone modifications. 34.5 % of H4K8ac MACS peaks were present at the gene start compared to 56.8 % for H3K18cr or 48.8 % for Kcr. H3K18cr also had the least peaks outside genes of 17.3 % compared to 19.7 % for Kcr or 27.2 % for H4K8ac. H3K18cr and Kcr were more similarly distributed between the three categories than H4K8ac. As some peaks were present outside genes, we thought that some of these might be related to enhancer elements. We compared each ChIP-seq MACS peak set to a mouse candidate regulatory element track from ENCODE. The majority of H4K8ac, Kcr and H3K18cr MACS peaks overlapped with regulatory elements (Figure 5.15h). If anything, H3K18cr and Kcr overlapped slightly more than H4K8ac, although they were very similar. The overlap of H4K8ac with regulatory elements is intermediate between what we previously observed for H4K8ac in colon only and H4K8ac in both liver and colon (Figure 5.13e).

Whilst this is interesting, it does not tell us about how these marks relate to other paradym marks such as those associated with promoters or repressive regions. Therefore, we compared these marks with H3K4me1, H3K4me3, H3K27ac and H3K27me3 using ChromHMM in the same way as for liver. No adult colon data could be found from ENCODE but some relevant data was available on GEO. Only one replicate was available for H3K27me3 and the transcription-associated H3K36me3 ChIP-seq has not been done in mouse colon, to our knowledge. The emission and transition parameter heat maps from the ChromHMM analysis in colon are shown in Figure 5.16a and b. A six-state model was chosen as it revealed three enhancer-like states (1-3) with slightly different abundances of H3K18cr, Kcr, H3K27ac, H4K8ac and H3K4me1 and a promoter-like state (state 4) containing all of these marks and also H3K4me3. States 1 and 2 mainly contained H4K8ac, H3K27ac and H4K4me1. State 5 was background and state 6 was repressed, as it was mainly H3K27me3. The heat map of transitions from the ChromHMM analysis shows that there was some similarity between state 1 (enhancer-like) and state 5 (background). The positions of each state were added as annotation tracks into SEQMONK to show how their distribution related to genes. A representative browser view is shown in Figure 5.16c.

Slc26a4 may be a poised gene as it contained state 4 (promoter), surrounded by state 6 (repressed) at the start of the gene. Whilst H3K4me3 was only present at promoters, the other active-associated marks were also distributed over the gene body and showed a highly similar profile. States 1-3 tended to be in the same regions and may be marking slight differences in the relative distribution of each modification. Possibly, a four- or five-state model could be adopted in further analysis. This ChromHMM study supports our previous findings that H4K8ac and Kcr are associated with active marks, as they were found in many of the same positions as the enhancer- and promoter- associated H3K27ac, H3K4me1 and H3K4me3.

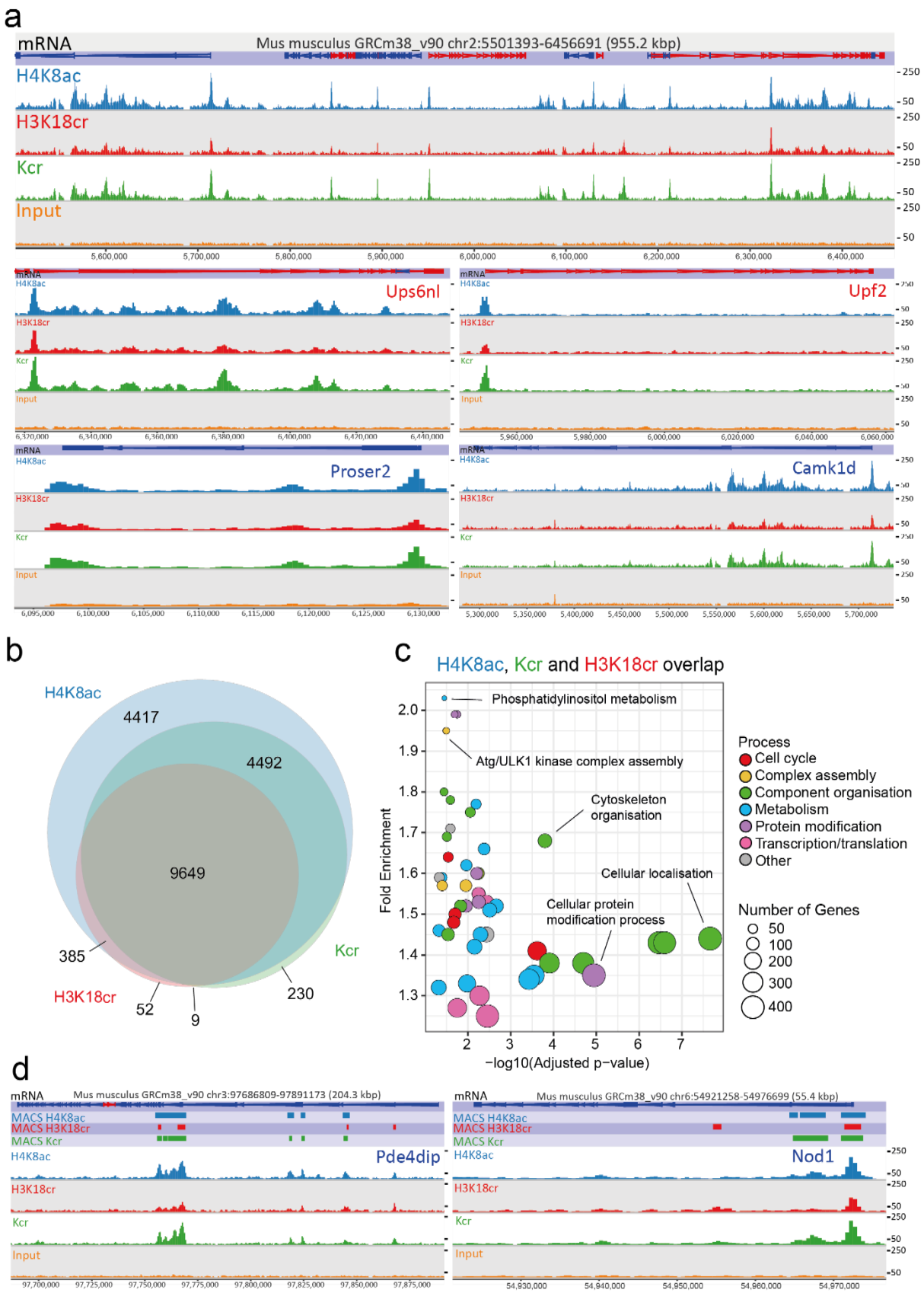
a
mRNA
Mus musculus GRCm38_v90 chr2:5501393-6456691 (955.2 kbp)
H4K8ac
H3K18cr
Kcr
Input
Ups6nl
Upf2
Proser2
Camk1d
b
H4K8ac
4417
4492
9649
385
H3K18cr
52
9
230
Kcr
c
H4K8ac, Kcr and H3K18cr overlap
Phosphatidylinositol metabolism
Atg/ULK1 kinase complex assembly
Cytoskeleton organisation
Cellular localisation
Cellular protein modification process
Fold Enrichment
−log10(Adjusted p−value)
Process
Cell cycle
Complex assembly
Component organisation
Metabolism
Protein modification
Transcription/translation
Other
Number of Genes
50
100
200
300
400
d
Mus musculus GRCm38_v90 chr3:97686809-97891173 (204.3 kbp)
Mus musculus GRCm38_v90 chr6:54921258-54976699 (55.4 kbp)
MACS H4K8ac
MACS H3K18cr
MACS Kcr
Pde4dip
Nod1

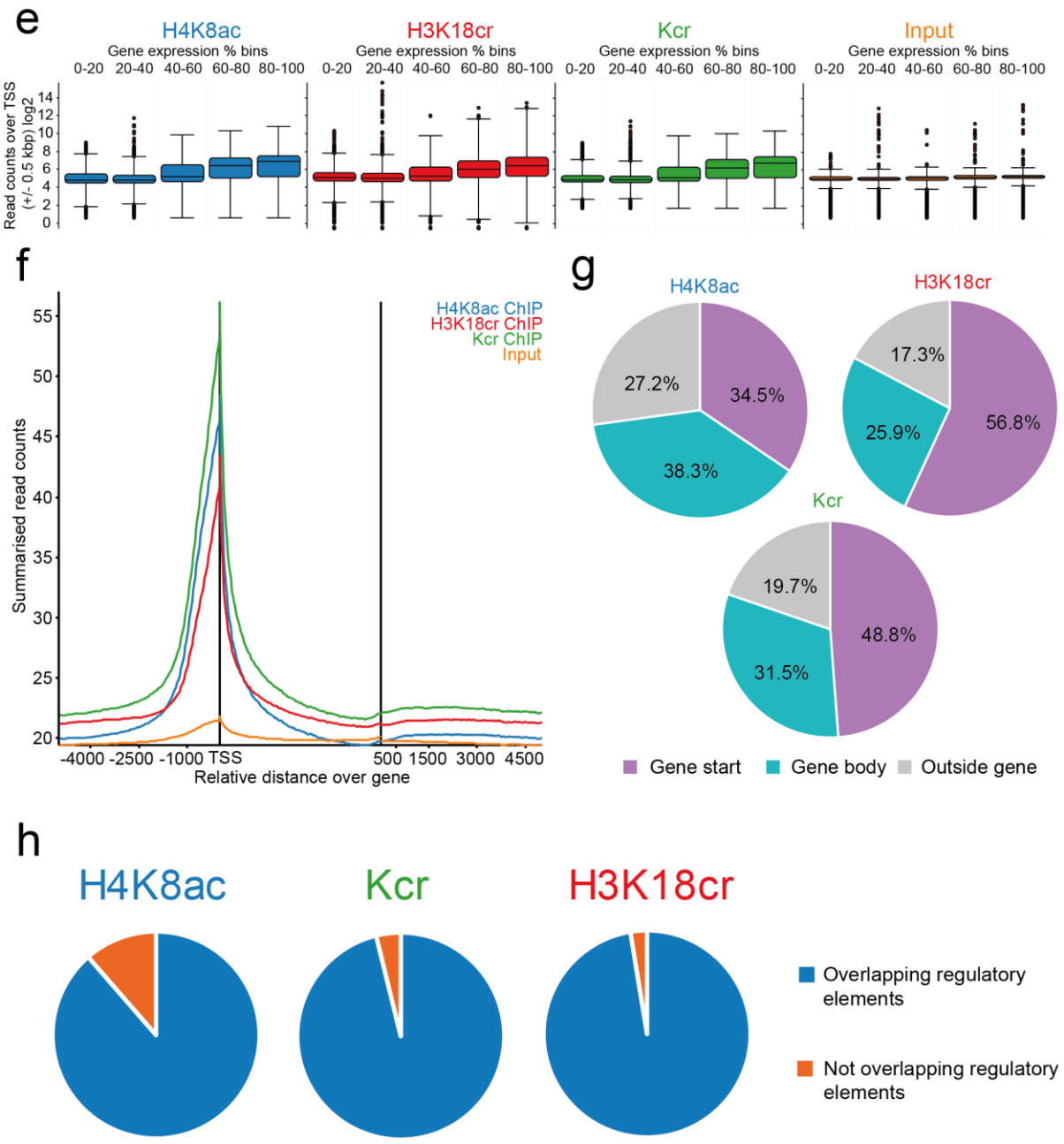

Figure 5.15. The association of H4K8ac, H3K18cr and Kcr with genomic features in mouse colon

Analysis was using anti-H4K8ac (blue), anti-Kcr (green) and anti-H3K18cr (red) antibodies in control (PBS or untreated) mouse colon epithelium extracts. Input is in yellow. H3K18cr ChIP-seq data was from Fellows *et al.* (2018) **(a)** Browser view of a segment from chromosome 2 showing a representative profile of ChIP peaks as well as close-ups of some genes around that region of chromosome 2. Linear read count quantitations of running window probes are shown with enrichment normalised. H3K18cr is a combination of two biological replicates, H4K8ac is a combination of three biological replicates, Kcr is a combination of four biological replicates and input is a combination of four biological replicates from H4K8ac, H3K18cr and Kcr data sets. **(b)** Overlap between H4K8ac, H3K18cr and Kcr data sets. MACS peaks were generated against each data set, combined in an annotated probe list and deduplicated. Gene lists were made based on their overlap in one or more data sets and a Venn diagram generated of numbers of genes. 385 genes have MACS peaks in H4K8ac and H3K18cr, 52

genes have MACS peaks only in H3K18cr, 9 genes have MACS peaks in H3K18cr and Kcr, and 230 genes have MACS peaks only in the Kcr data set. **(c)** Gene ontology analysis of genes containing H4K8ac, H3K18cr and Kcr MACS peaks using Panther statistical overrepresentation test against a standard Mus musculus reference list. Fold enrichment is plotted against significance. Terms are coloured based on functional categories, with size corresponding to the number of genes in the term in the input list. **(d)** Browser view of Pde4dip and Nod1 genes with positions of MACS peaks shown as annotation tracks, coloured according to the ChIP-seq data set. **(e)** Number of reads at TSS relative to gene expression. The read counts of H4K8ac, H3K18cr, Kcr or input over TSS were quantified and enrichment between ChIP-seq data sets normalised. Genes were put into percentile bins according to their normalized RNA-seq read counts from lowly expressed (0-20 %) to highly expressed (80-100 %) and box plots generated. **(f)** Quantitation trend plot of H4K8ac, H3K18cr, Kcr ChIP and input using linear read count quantitation of running window probes showing distribution relative to TSS. **(g)** The proportion of MACS peaks in the gene start (500 bp +/- TSS), gene body or outside genes in the H4K8ac, H3K18cr and Kcr data sets shown as pie charts. **(h)** Pie charts showing overlap of H4K8ac, Kcr or H3K18cr peaks and a mouse regulatory element track from ENCODE which compiles various markers of enhancers and promoters.

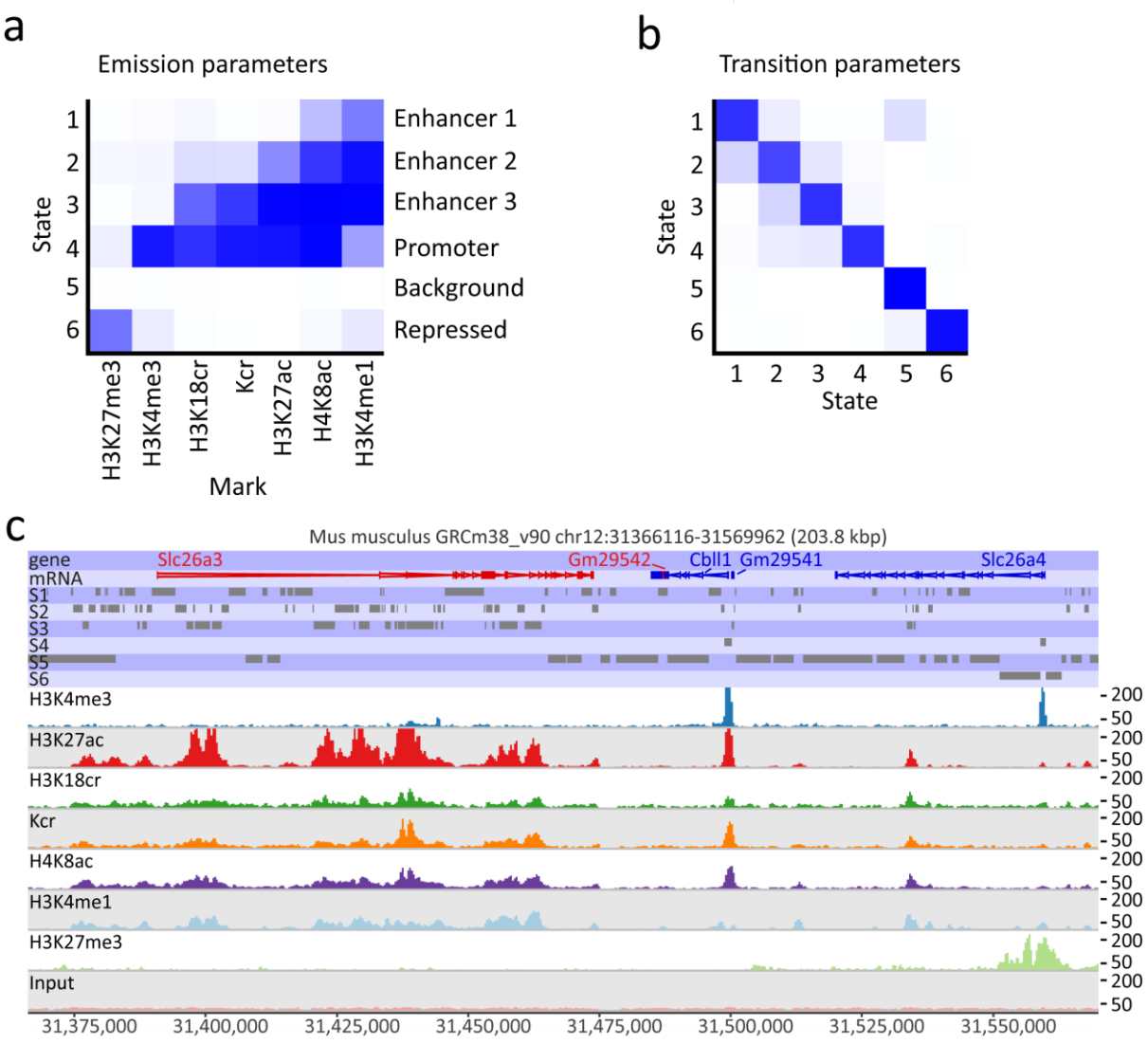

Figure 5.16. Chromatin state analysis in the mouse colon

Chromatin state analysis performed using ChromHMM on mouse colon ChIP-seq data. Data sets were H4K8ac and Kcr ChIP-seq data (3 and 4 replicates respectively) that I generated. H3K18cr ChIP-seq data were generated by Payal Jain and Claudia Stellato (2 replicates), H3K4me3 ChIP-seq data were generated by Jeremy Denizot (3 replicates) and are available at GEO under the accession GSE96035. H3K4me1 and H3K27ac data were generated by Qin *et al.* (2018), taking the low fibre diet, male samples (3 replicates for each) and are available at GEO under the accession GSE99670 (Qin *et al.*, 2018). H3K27me3 data were generated by Lo *et al.* (2017) (1 replicate) and are available at GEO under the accession GSE82181 (Lo *et al.*, 2017). A six-state model was used with a 200 bp window size. **(a)** Emission parameters with chromatin state numbers shown on the left, histone modifications below and state descriptions to the right. **(b)** Transition parameters showing the similarity between the six states. **(c)** Browser view from SEQMONK showing a representative distribution profile of H3K4me3, H3K27ac, H3K18cr, Kcr, H4K8ac, H3K4me1, H3K27me3 and input data sets used in the ChromHMM program along with the chromatin state annotation tracks determined from the six-state model (S1-6).

5.2.9 Antibiotics treatment induces differential expression of a large subset of genes

To understand how antibiotics treatment changes gut physiology, we conducted mRNA-seq on control and antibiotics treated mouse colon epithelium to identify how gene expression changes. Differential expression analysis was performed using DESeq2 and hits are highlighted on a scatter plot of control against antibiotics treated mouse colon (Figure 5.17a). Hierarchical clustering of the more than 800 dysregulated genes produced two clusters, as would be expected. Cluster 1 is of the 292 down regulated genes, labelled in green and cluster 2 is of the 551 up regulated genes, labelled in blue (Figure 5.17a and b). The cluster plot in Figure 5.17b shows that there is some variability between samples, particularly for the antibiotics treated replicates, but overall the up or down regulation is fairly consistent. Gene ontology analysis was performed for up and down regulated gene lists separately. Only one gene ontology term, cell adhesion, was identified in the downregulated group (Figure 5.17c, right panel). Some bacterial species, such as *Bifidobacterium infantis*, are thought to promote tighter junctions between IECs so that the barrier is maintained (Ewaschuk *et al.*, 2008). Therefore, when the microbiota is removed this pathway is downregulated. Ontology analysis of genes that were upregulated in gene expression on antibiotics treatment showed enrichment of many terms involved in respiration, oxidative phosphorylation, electron transport and ATP synthesis relative to the background list of expressed genes in the colon (Figure 5.17c, left panel). Occurance of gene ontology terms related to metabolism including lipid metabolism, TCA cycle and isoprenoid biosynthesis were also significantly enriched. This suggests increased energy production and metabolism in order to

compensate for the lack of microbial generation of energetic metabolites. The identification of terms such as immune system process, leukocyte activation and response to stimulus in this analysis may point towards changes in gut epithelium-environment interactions. Fascinatingly, circadian rhythms are also an enriched term, which could mean that the microbiota is involved in maintaining biological rhythms of gut functions, a link which has also been proposed in other studies (Paschos and FitzGerald, 2017).

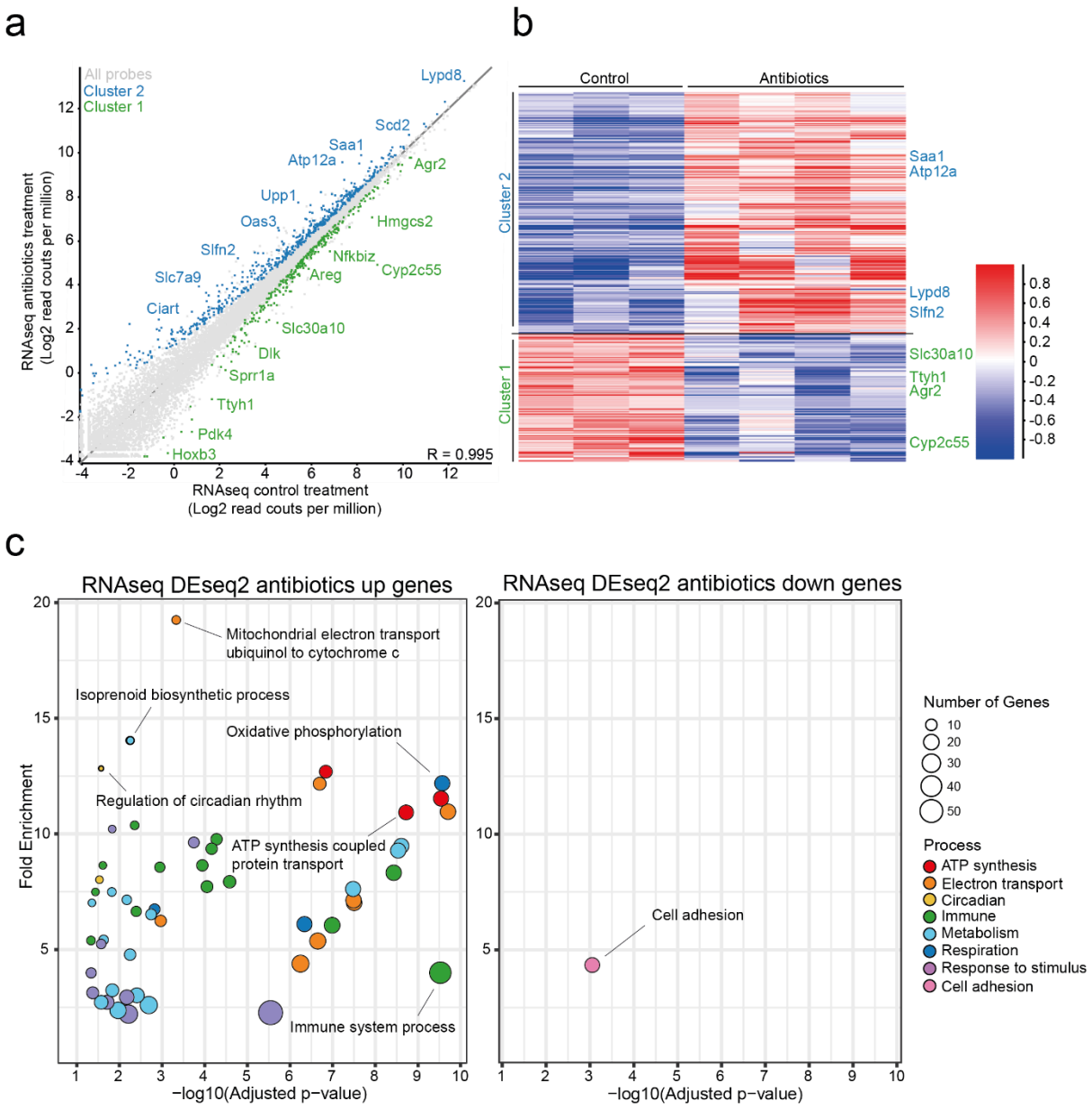

Figure 5.17. Antibiotics treatment produces substantial changes in gene expression in mouse colon

RNA-seq was performed on colons from antibiotics treated or control mice. **(a)** Scatter plot comparing RNA-seq of antibiotics treated colon to control colon after probes were generated using the SEQMONK RNA-seq pipeline and log2 transformed. Cluster 1 and 2 from the hierarchical clustering are highlighted in green and blue

respectively, with a few genes indicated. **(b)** Hierarchical clustering of differentially expressed genes as identified by DESeq2 with a threshold p value of 0.05. Gene labels on the right are approximate positions of that gene in the clustering. **(c)** Gene ontology analysis of antibiotics up regulated (left) or down regulated genes (right) using Panther statistical overrepresentation test against a reference list of all expressed genes in the RNA-seq data set (13607 genes, excluding unobserved probes). Fold enrichment is plotted against significance. Terms are coloured based on functional categories, with size corresponding to the number of genes in the gene ontology term in the DEseq2 up or down regulated list.

5.2.10 Changes to crotonylation correlate with a subset of gene expression changes on antibiotics treatment

As histone crotonylation showed striking reductions by western blot on antibiotics treatment (Figure 5.3 and Figure 5.6), we wanted to see how its genomic distribution changed and how this was related to differentially expressed genes. Initial tests of H4K8cr ChIP-seq in colon carcinoma cells had been unsuccessful (Figure 5.11) and whilst H3K18cr ChIP-seq was previously performed on mouse colon epithelial cells (Fellows *et al.*, 2018), further ChIP experiments with this antibody were unsuccessful (attempted by Mariana Portovedo). Therefore, we performed ChIP-seq experiments on antibiotics treated and control mice with anti-Kcr. We found hundreds of MACS peaks which significantly increased or decreased crotonylation between control and antibiotics treated mice (Figure 5.18a). In particular Schlafen 2 (*Slfn2*), which is associated with negative regulation of cell growth (Schwarz *et al.*, 1998), increased in crotonylation with the highest significance. Erythroid differentiation regulator 1 (*Erdr1*) was up-crotonylated 3.7-fold on antibiotics treatment. Expression of *Erdr1* has been demonstrated to be suppressed by the microbiota (Weis *et al.*, 2018). Gene ontology analysis of the genes with higher crotonylation in the antibiotics treated group revealed enrichment of terms related to regulation of biosynthetic processes (Figure 5.18e, left panel). Terms such as responses to acid chemical, hormone stimulus and retinoic acid were enriched terms in the down crotonylated gene group, along with enzyme linked receptor signalling and negative regulation of transcription (Figure 5.18e, right panel). This last term suggests that loss of crotonylation could be associated with reduced gene expression. *B4galnt2* was the most significantly down crotonylated gene. This encodes for Beta-1,4-N-acetyl-galactosaminyltransferase 2 which is an important part of the biosynthesis of Sd(a) antigen, a colon specific carbohydrate determinant (Montiel *et al.*, 2003).

Highlighting the genes that increased in expression (red) or decreased in expression (green) on the Kcr ChIP-seq volcano plot revealed that many genes which changed in Kcr level also changed in gene

expression (Figure 5.18a). This can also be seen if up crotonylated genes (yellow) and down crotonylated genes (purple), are highlighted on the RNA-seq volcano plot that shows significantly differentially expressed genes (Figure 5.18b). Very few significantly up crotonylated genes overlap with significantly down expressed genes and vice versa. We therefore plotted RNAseq fold change against Kcr ChIP-seq fold change, of only the significantly changing genes, to see if there was a correlation between the two. Figure 5.18c shows that there is a strong positive correlation (R^2=0.63), revealing that up crotonylated genes tend to also go up in expression. Some such as Slfn2 and Ttyh1, which encodes a chloride ion channel, change considerably in both gene expression and crotonylation. When the fold changes of all crotonylated genes that overlapped expressed genes were plotted, including ones that did not significantly change, there was only a weak positive correlation (R^2=0.05, Figure 5.19). The overlaps between differentially crotonylated and differentially expressed genes are visualised in venn diagrammatic form in Figure 5.18c. Up crotonylated and up regulated genes, and down crotonylated and down regulated genes, have highly significant overlaps relative to total expressed genes. 9.1% of the total up regulated genes and 4.5% of the total down regulated genes also changed in crotonylation. In contrast, the overlaps between up crotonylated and down regulated, or down crotonylated and up regulated were not significant. These results suggest that, in a subset of genes, changes to crotonylation could be linked to changes in gene expression.

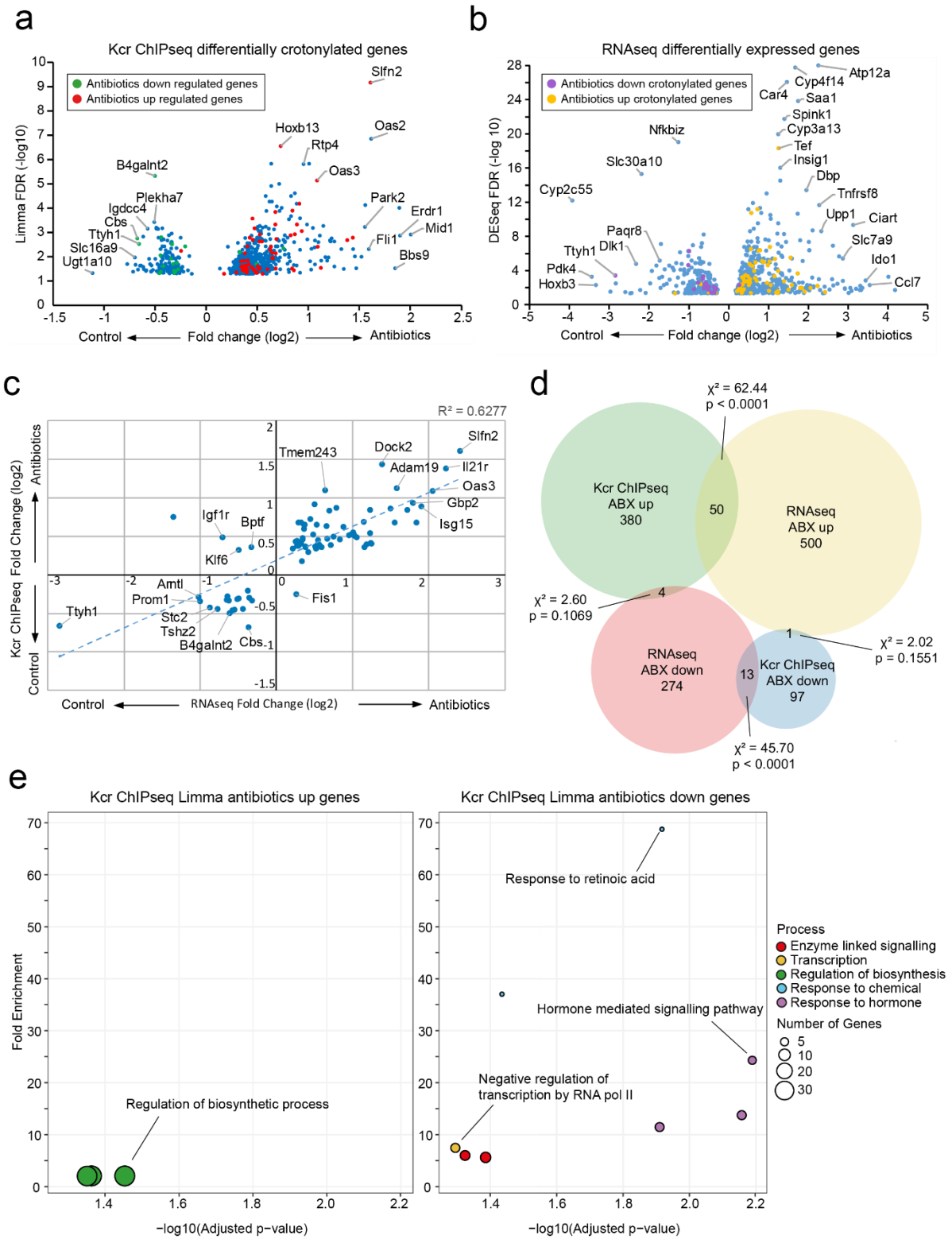

Figure 5.18. Changes to histone crotonylation correlate with changes to gene expression in a subset of genes on antibiotics treatment

RNA-seq and Kcr ChIP-seq was performed on colon extracts from control mice or mice treated with antibiotics. **(a)** Volcano plot of genes containing MACS peaks that changed in crotonylation, as identified using Limma statistical testing of the Kcr ChIP-seq data set, using a threshold p value of 0.05 and adjusting for multiple testing.

In cases where there was more than one MACS peak in a gene, only the MACS peak with the greatest fold change was included. Unannotated genes e.g. Gm20442 are not labelled. The most significant genes and those that changed the most on treatment are labelled. Genes that increase or decrease in gene expression, as identified by RNA-seq, are coloured red or green respectively. **(b)** Volcano plot of differentially expressed genes identified using DEseq2 analysis of the RNA-seq data set, using a threshold p value of 0.05 and adjusting for multiple testing. Particularly significant or changing genes are labelled, excluding unannotated genes. Genes that increase or decrease in histone crotonylation, as identified by Kcr ChIP-seq are coloured yellow or purple respectively. **(c)** XY plot showing the fold change of genes that change in both crotonylation and expression, with a trend line showing the relationship between the two. **(d)** Four-way Venn diagram showing the overlap between up-crotonylated, up-regulated, down-crotonylated and down-regulated genes on antibiotics treatment (ABX). The significance of overlap was tested using a 2x2 two-tailed Chi-square test with Yates correction and the total number of expressed genes of 13607, as determined from the RNA-seq data set excluding unobserved probes. **(e)** Gene ontology analysis of more crotonylated (left panel) or less crotonylated genes (right panel) on antibiotics treatment using Panther statistical overrepresentation test against a standard *Mus musculus* reference list. Fold enrichment is plotted against significance. Terms are coloured based on functional categories, with size corresponding to the number of genes in the gene ontology term in the DEseq2 up or down regulated list.

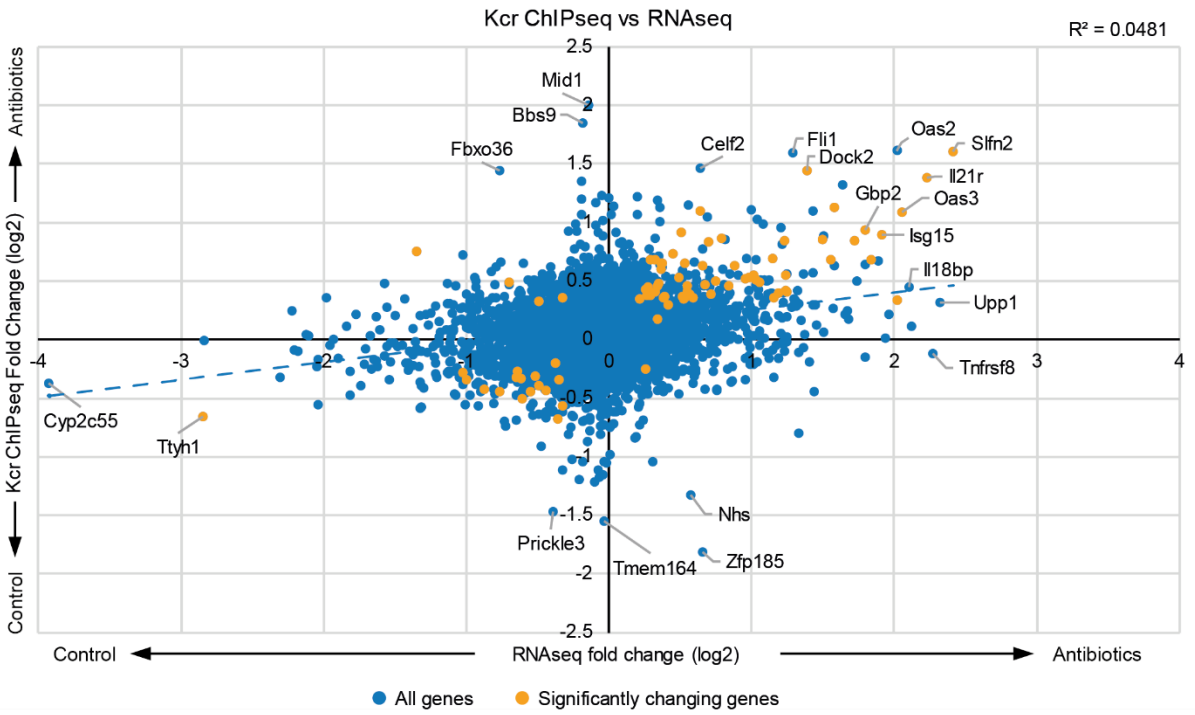

Figure 5.19. Comparison of changes in crotonylation over MACS peaks and changes in gene expression of associated genes between colon epithelial extracts from control and antibiotics treated mice

XY plot showing the fold change of MACS peaks in the Kcr ChIP-seq data set against fold change in the RNA-seq data set of control and antibiotics treated mouse colon. When there were more than one MACS Kcr peaks in a gene, the MACS peak with the greatest absolute fold change was used. Unobserved values were excluded from the RNA-seq list. The trend line was generated in excel and the R squared value is shown on the chart. Significantly differentially crotonylated and differentially expressed genes between untreated and control, as shown in Figure 5.18c, are highlighted on the graph.

5.2.11 Effect of antibiotic treatment on the genomic positions of H4K8ac in mouse colon

We had identified that H4K8ac is a broadly distributed modification across the genome and was associated with genes involved in a range of cellular functions (Figure 5.12 and Figure 5.13). As we had observed a correlation between crotonylation and gene expression, we wanted to see if this was true for H4K8ac which is also depleted globally on antibiotics treatment. H4K8ac ChIP-seq was performed on antibiotics treated and control mice, and was compared to the equivalent Kcr ChIP-seq data set (Figure 5.20). Over 900 hits were identified in the Kcr ChIP-seq using the LIMMA statistical test, although the majority of MACS peaks did not change (Figure 5.20a). In contrast, no LIMMA hits were identified in the H4K8ac ChIP-seq data set, despite a similar number of total MACS peaks (20608 in H4K8ac compared to 20950 in Kcr, Figure 5.20b). The Kcr MACS peaks that overlapped with antibiotics

up regulated genes (red) were closer to the antibiotics treated group on the y-axis, whilst the Kcr MACS peaks that overlapped with antibiotics down regulated genes (green) were more towards the control group on the x-axis (Figure 5.20c). In contrast, no such split of red and green was seen for the H4K8ac MACS peaks as up and down regulated genes were mixed in their distribution (Figure 5.20d). These differences are particularly intriguing considering the striking overlap between H4K8ac and Kcr seen in Figure 5.15. Many differentially expressed genes had higher Kcr or H4K8ac levels over TSS relative to input (Figure 5.20e and f), but the association of these genes with higher H4K8ac was less pronounced. Higher or lower expressed genes were equally associated with the level of Kcr or H4K8ac ChIP enrichment. Fold change in Kcr was plotted against fold change in H4K8ac between control and antibiotics for those MACS peaks that significantly changed in the Kcr data set (Figure 5.21). MACS peaks with higher read counts (in at least one of the replicates) are mainly those that change the least, whilst MACS peaks with fewer read counts have higher fold changes. One exception is Erdr1 which changes 3.7-fold in Kcr and has high read counts in the MACS peak. The fold changes in H4K8ac are similar to the changes in Kcr suggesting that changes to H4K8ac do occur on antibiotics treatment but high variability between samples has meant that these changes are not significant.

In ChIP-seq, changes in enrichment between treatments at particular region can be hard to identify as reads are distributed across the genome, meaning that enrichment of a sample at a locus is relative to the rest of the genome. Therefore, we tested candidate genes by H4K8ac ChIP-qPCR. We designed primers against the start region of genes that had changed most in gene expression, either up or down. For the downregulated genes we verified that H4K8ac was present in the ChIP-seq of the untreated colon and designed the primer region at that peak site. We also designed some primers against the promoter region of genes that were not identified in differential expression analysis. We performed ChIP-qPCR and gene targets are grouped into upregulated, downregulated or unchanged in gene expression on antibiotics treatment (Figure 5.22). Log scale is used as there was a scale related increase in variability between targets. Of the upregulated gene targets tested, two-way ANOVA statistical analysis found that overall the effect of treatment was not significant (Figure 5.22, upper panel). In the downregulated group, most gene targets were reduced in H4K8ac on ABX treatment and two-way ANOVA analysis found that there was overall a statistically significant decrease as a result of treatment (Figure 5.22, middle panel). In the group of gene targets which had not changed in gene expression, the difference in H4K8ac between treatments was not significant (Figure 5.22, lower panel). We plotted individual graphs of gene targets that changed most on antibiotics treatment, as seen from the volcano plots on the right of Figure 5.22, to better visualise the differences in H4K8ac between treatments (Figure 5.23). *Isg15*, which increased in expression, showed an upward trend.

Hmgcs2 showed a downward trend and this gene decreased in expression. However, none of these changes were significant, possibly due to high variability between samples.

Klf11 is a gene that showed enrichment in H4K8cr and H4K8ac ChIP-qPCR analysis in colon carcinoma cells (Figure 5.11 and Figure 5.12). Additionally, it was downregulated in gene expression on antibiotics treatment. Comparing H4K8ac at the start of *Klf11* gene between control and antibiotics treated mouse colons by ChIP-qPCR showed that this modification is slightly reduced on antibiotics treatment, although this difference was not statistically significant (Figure 5.22). We wondered whether this could be because the level of H4K8ac was much higher than the other targets. Antibiotics treatment might change the breadth of the peak without changing its height. We therefore tested different sites around the start of the *Klf11* gene by ChIP-qPCR. We then aligned the ChIP-qPCR result to the distribution of the H4K8ac ChIP-seq according to the position of the primer at the start of the *Klf11* gene (Figure 5.24). Whilst the level of H4K8ac in qPCR analysis correlated with the level of H4K8ac in sequencing analysis, the abundance of H4K8ac actually increased the difference between control and antibiotics treatment.

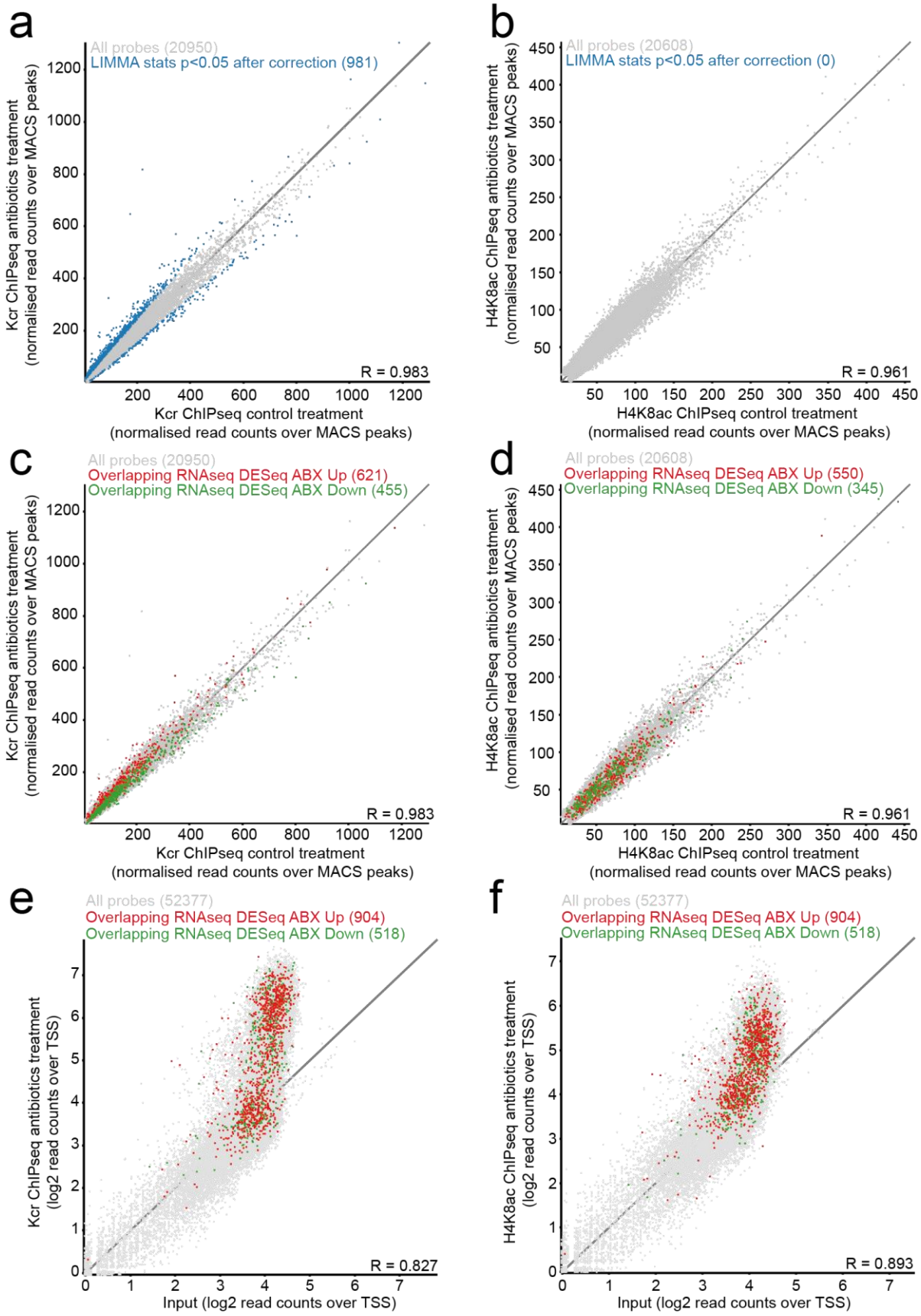

Figure 5.20 Antibiotic treatment leads to significant changes in Kcr but not H4K8ac in mouse colon epithelial cells

Scatter plot of MACS peaks (grey) in Kcr ChIP-seq **(a)** or H4K8ac ChIP-seq **(b)** in control against antibiotics treated mouse colon IECs. Peaks changing in Kcr or H4K8ac as determined by Limma statistical testing are highlighted in blue. No hits were identified for H4K8ac. Scatter plots of MACS peaks (grey) in antibiotics treated mice against control, for Kcr **(c)** or H4K8ac **(d)**. Peaks overlapping with up regulated (red) or down regulated (green) genes, as determined by DEseq2 on the RNA-seq data set in mouse colon, are highlighted. Scatter plots of probes generated over TSS (+/- 500 bp of gene start) and log2 transformed (grey) in combined Kcr ChIP-seq **(e)** or H4K8ac ChIP-seq **(f)** against input (two replicates). Peaks overlapping with up regulated (red) or down regulated (green) genes are highlighted.

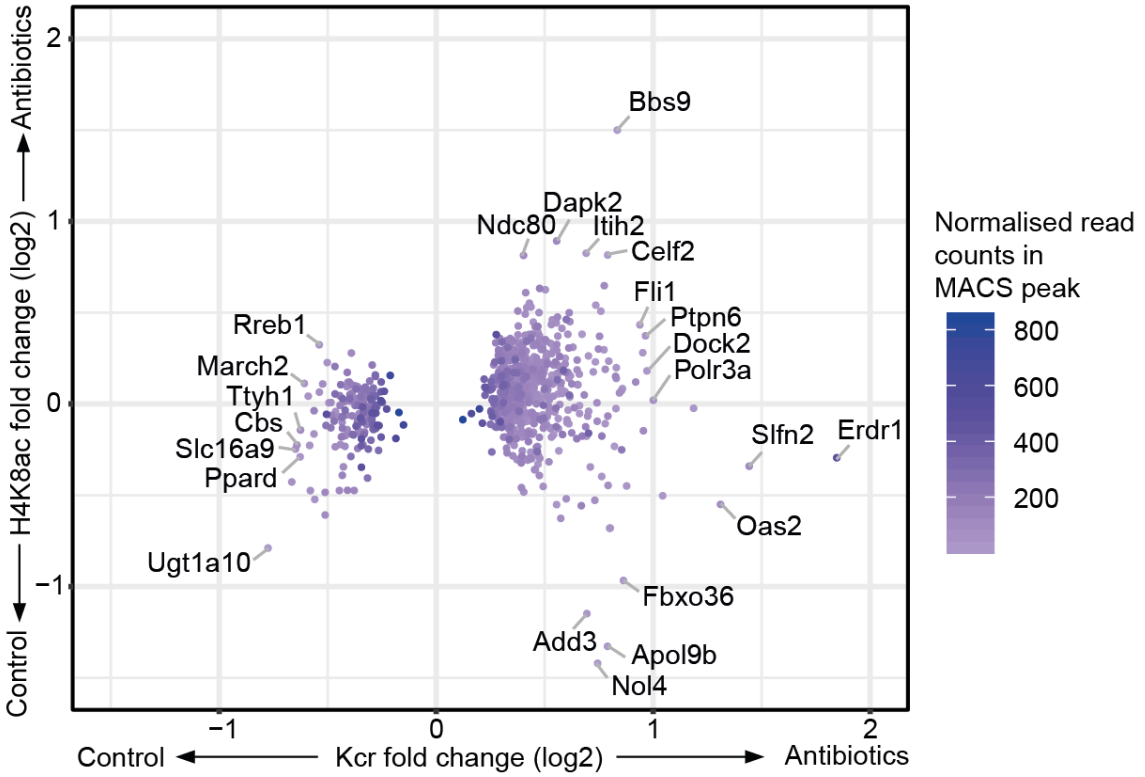

Figure 5.21. Comparison of fold changes on antibiotics treatment of Kcr and H4K8ac ChIP-seq

XY plot showing the log2 fold change of Kcr ChIP-seq against H4K8ac ChIP-seq, looking only at MACS peaks that were statistically different in the Kcr data set. Points are coloured in linear scale by read counts in the group (Kcr ABX, Kcr CTL, H4K8ac ABX or H4K8ac CTL) that contained the most read counts.

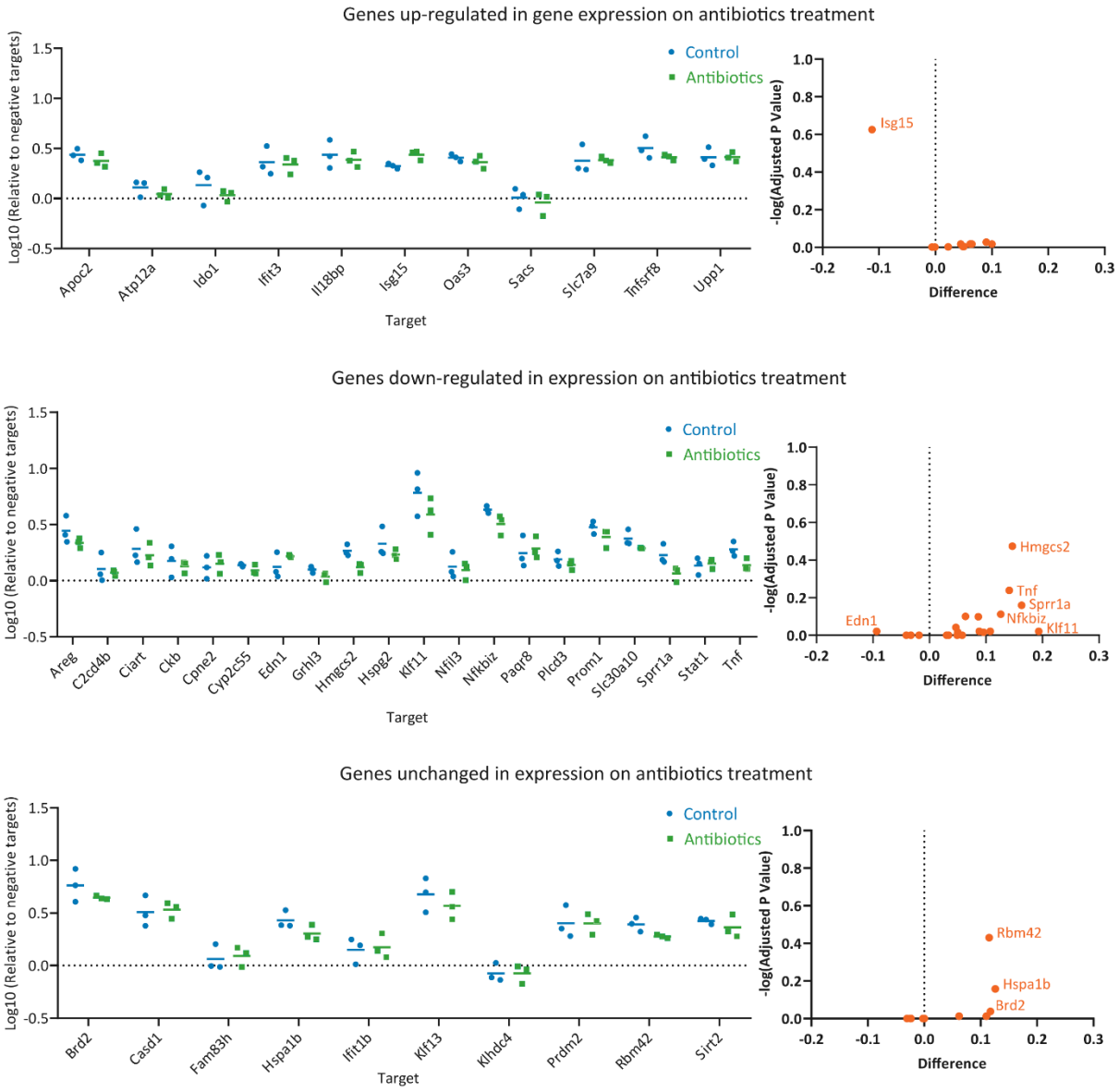

Figure 5.22. ChIP-qPCR of H4K8ac in antibiotics treated mouse colon

ChIP was performed on sonicated chromatin from colons from mice gavaged with antibiotics or PBS (control) using anti-H4K8ac. Quantitative PCR was performed using primers against the promoters of the specified genes and normalised to negative targets *Adam23*, *Cys1*, *March11* and *Slc4a5* to show relative enrichment in log10 scale. Two-way ANOVA was performed for each set of targets. The up-regulated and unchanged genes gave a significant difference between targets only ($p < 0.0001$), whilst the down-regulated genes gave a significant difference between treatments ($p = 0.0002$) and targets ($p < 0.0001$), with no interaction between the two. Pairwise comparisons of log transformed data of control against antibiotics were not significant and are shown as volcano plots to the left, with the difference between control and antibiotics against the significance of that difference as -log of the adjusted p value. Multiple testing correction used the Holm-Sidak method.

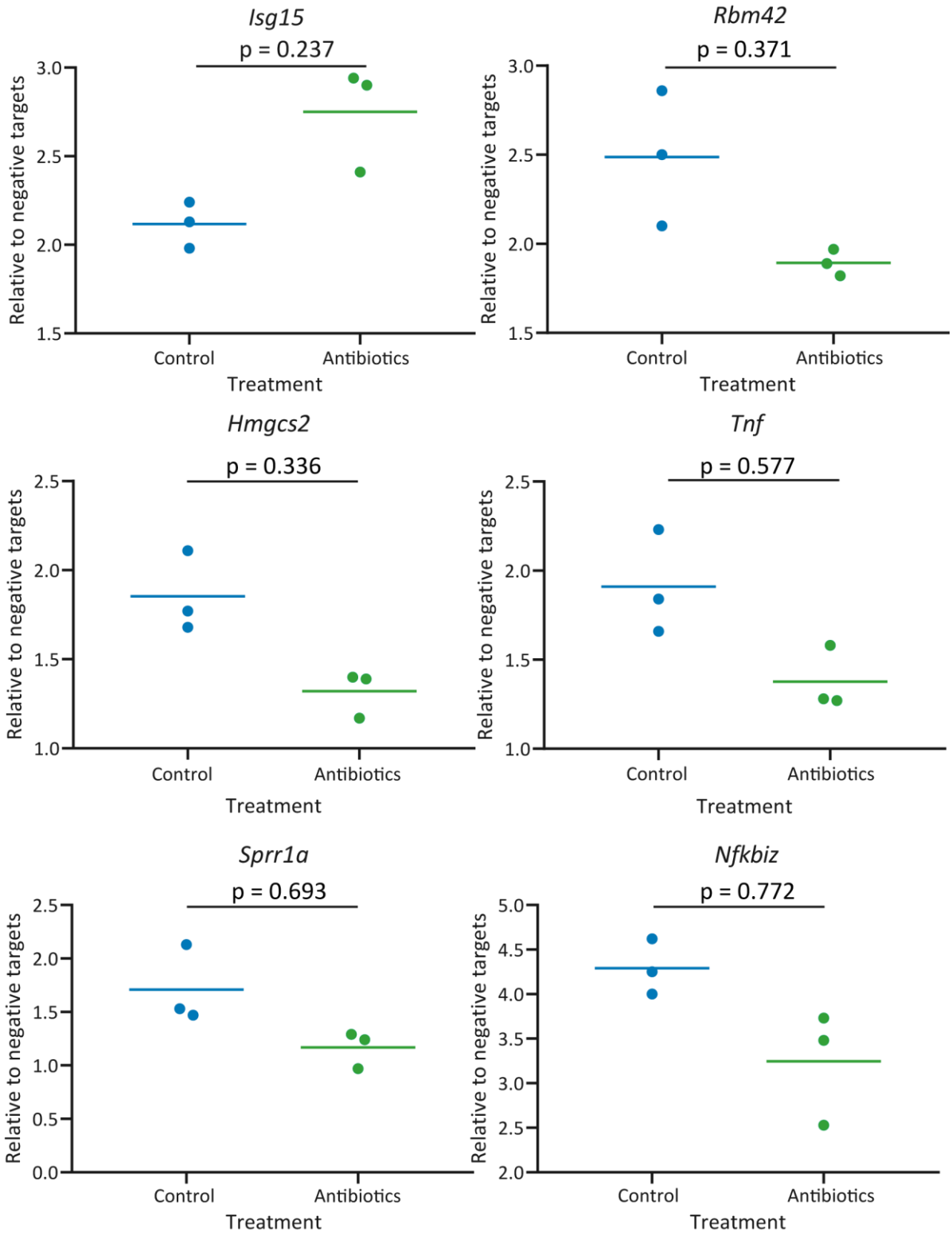

Figure 5.23. Interesting genes from ChIP-qPCR of H4K8ac in antibiotics treated mouse colon

The genes which were gave the lowest p-values by multiple comparison tests in Figure 5.22 are shown separately here with relative enrichment to negative targets plotted in linear scale. The p values of pairwise comparisons with multiple testing correction (using the Holm-Sidak method) on transformed data are indicated on the graphs.

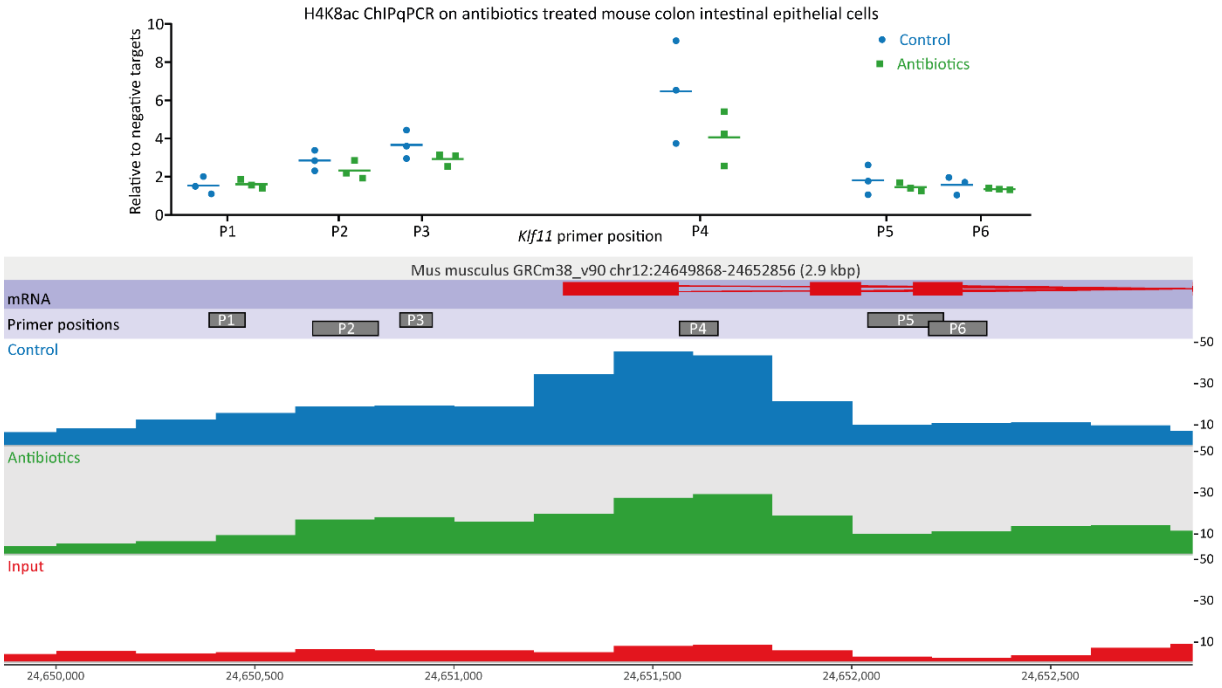

Figure 5.24. H4K8ac ChIP-qPCR compared to ChIP-seq at the *Klf11* gene

ChIP on sonicated chromatin from antibiotics treated or control colons using an anti-H4K8ac antibody was tested in qPCR using primers against different positions around the start of the *Klf11* gene. Position 4 is the same as the *Klf11* primer in Figure 5.22. Positions of these primers are annotated on the browser view of H4K8ac ChIP-seq that was performed on samples from the same ChIP experiment. The ChIP-seq data is the same as that shown in Figure 5.20.

5.3 Discussion

5.3.1 Antibiotics induced depletion of the gut microbiota reduces histone acetylation, crotonylation and butyrylation but not methylation

We found that antibiotics treatment reduced histone acetylation, crotonylation and butyrylation in the mouse colon. These changes to histone acylations were consistent between two different mouse strains, C57BL6 and Balb/c, indicating that this robust change is not dependent on a property of one particular mouse strain. We suggest that these changes in histone acylations are due to antibiotics induced depletion of gut microbial generated SCFAs, as serum and luminal SCFA concentrations were also reduced and some SCFAs could promote histone acylations in cell culture. We identified that histone acetylation abundance in IECs responds over a short period of time (3 days of antibiotic treatment) and that it can occur in mice that are adapted to the presence of the microbiota. As antibiotics are used to deplete the microbiota to treat certain diseases (Zarrinpar *et al.*, 2018), knowledge of how the gut cells respond can provide useful information about what the side-effects

of these treatments may be. However, we have not directly shown that microbial generated SCFAs are the cause of changes to histone acylations *in vivo*. The gut microbiota releases many different molecules that have potential to induce epigenetic changes in colonocytes (Krautkramer *et al.*, 2017). Depletion of the microbiota could also indirectly affect colonocyte histone modifications due to changes in immune activity or gut motility. Treating germ free mice with antibiotics would be a useful way to test if the antibiotics themselves can influence colonocytes in the whole organism, as experiments with organoids were inconclusive. Further experiments could introduce labelled SCFAs to mice in combination with mass spectrometry analysis to determine if these are the source of crotonyl- and acetyl-moeities on histones. Additionally, the abundance of other microbial metabolites could be compared between control and antibiotics-treated mice to identify potential acyl-modifiers.

Whilst many different histone acetyl- and crotonyl-marks were depleted, we saw no significant changes to paradym histone methylation marks such as H3K4me3 or H3K27me3. This is intriguing since broad depletion of the microbiota should reduce the concentration of many different microbial metabolites. The microbiota generates folate, which is essential for DNA methylation, and succinate, which inhibits demethylases (Crider *et al.*, 2012; Xiao *et al.*, 2012). As far as we are aware, no current evidence suggests that methylation can be influenced by acetate, propionate or butyrate. A different study tested the effect of increasing the microbiota, and thereby its metabolites, by colonising germ free mice with a microbiota from conventionally raised mice. They observed increases in histone acetylation in liver, colon and adipose tissue, along with increases in caecal acetate, propionate and butyrate concentrations, in colonised mice relative to germ-free mice (Krautkramer et al., 2016). This is in agreement with our study and suggests that histone acetylation is responsive to increases and decreases in the microbiota. Krautkramer *et al.* (2016) also found changes to methylation marks but these were not consistent across tissues as some modifications increased, whilst others decreased. Histone methylations are thought to be less dynamic and have slower turnover times than histone acylations (Barth and Imhof, 2010), therefore we suggest that methylation might be more involved in the development of an organism in symbiosis with the microbiota, whilst histone acylations may dynamically respond to short-term changes in the microbiota. Here, we have studied acute microbiota depletion over just three days. If antibiotic treatment was given over a longer period, it is possible that other modifications may change as a result of adaptation to this new environment.

5.3.2 The effect of antibiotics treatment on histone acetylation in the liver

In the liver, we observed a reduction in histone acetylation on antibiotics treatment in wild type mice with the anti-Kac antibody. 70% of acetate and 30% of propionate produced by the gut microbiota is taken up by the liver as an energy source (Krautkramer *et al.*, 2016). This in contrast to the colon where

70-90% of butyrate produced by the gut microbiota is consumed by colonocytes in preference to acetate or propionate (Cook and Sellin, 1998). Therefore, the reduction in histone acetylation in the liver on antibiotics treatment could be due to the reduction in serum propionate. However, this was a preliminary experiment and needs to be repeated to verify if acetylation does reduce, especially since H3K18ac did not change in wild type mice. The differences in the SCFA use by liver and colon provides an opportunity to investigate the how these SCFAs differentially affect histone acylations. In a further experiment, it would be informative to include measurement of propionate concentrations in the liver in control and antibiotics treated mice to see if it matched the propionate reduction in the gut lumen. An experiment to track labelled propionate in the liver would also help determine if propionate is involved in this change.

5.3.3 Characterisation of H4K8ac in liver and colon

H4K8ac was highly responsive to antibiotic induced microbial depletion in the colon and initial studies suggested that acetylation might also change in response to antibiotic treatment in the liver. Compared to some other histone acetylation marks, much less is known about H4K8ac and ChIP-seq analysis of H4K8ac had not been performed before in liver or colon. We therefore characterised H4K8ac in liver and colon and found that it has a broad distribution across the genome, enriched at TSS but also present in the gene body and outside genes. H4K8ac marks were associated with regulatory elements, particularly those that were present in both liver and colon, where 99% of H4K8ac peaks were at previously annotated regulatory elements. We found that H4K8ac was involved in a broad range of functions, including those involved in signalling, metabolism and transcription. Additionally, its function was not restricted to one tissue as it was associated with many functional gene ontology terms in both liver and colon. The terms identified were associated with many tissue specific functions, such as lipid metabolism in the liver and ion homeostasis and biogenesis in the colon. H4K8ac was also associated with gene transcription and translation related terms, particularly for the genes present in both tissues. As H4K8ac is associated with activation of gene expression and the background list used in the gene ontology analysis was not tissue specific, these terms identified might reflect which genes are expressed in different tissues.

When we compared H4K8ac to other well-characterised histone marks using chromatin state analysis, we found that this modification was associated with H3K4me3, H3K27ac and H3K4me1, marks of promoters and enhancers, in both colon and liver. This suggests that H4K8ac could also be involved in gene regulation, as H3K4me1, H3K27ac and H3K4me3 are associated with promoting gene expression. Interestingly, the presence of the gene silencing mark H3K27me3, along with H3K4me3, in some promoters suggests that some genes are marked by both activating and repressive modifications,

making them poised for gene expression. A recent study found that H4K8ac and H3K27ac were highly correlated, both associating with intergenic regions, introns and promoter TSS (Li *et al.*, 2019). We also found that H4K8ac is present at gene start, body and outside genes in both liver and colon. In agreement with our findings, Li *et al.* (2019) found that H4K8ac and H3K27ac are associated with H3K4me3, at regions known as super enhancers which are implicated in tumourigenesis. Interestingly, H4K8ac and H3K27ac were found at a similar percentage of enhancers in CD4+ T cells, at 12 and 17 % respectively (Wang *et al.*, 2008). As H3K27ac is a well described mark of active enhancers (Bonn *et al.*, 2012), H4K8ac could also have an important role in marking this genomic feature. In summary, our study adds further evidence that H4K8ac is a marker of regulatory regions, in particular enhancers and promoters.

5.3.4 Antibiotics treatment results in substantial changes in gene expression

Antibiotics treatment is a useful tool to study the effects of the microbiota as, unlike germ-free mice, the immune and homeostatic regulatory systems have developed normally. Whilst studies have been done on low dose antibiotics treatment to reduce microbiota diversity (Cho *et al.*, 2013; Cox *et al.*, 2014; Mahana *et al.*, 2016), less is known about the effects of higher dose antibiotic treatment to severely deplete the microbiota. Antibiotics are used routinely to deplete the microbiota to treat bacterial infections or prepare for microbial transplantation, therefore understanding how they impact colon function is essential. We identified hundred of genes that change in expression in mouse colon epithelial cells as a result of a short course of antibiotics treatment. Genes involved in mediating juctions between cells were reduced, which agrees with current evidence that the microbiota promote increased barrier function and prevent harmful bacteria from penetrating the underlying tissue (Pedicord *et al.*, 2016). Only one term was identified in the down-regulated gene group, despite it containing around a third of the total number of dysregulated genes. Other cellular pathways might be involved, but if low numbers of genes were dysregulated for each function it would not be identified by gene ontology analysis. In contrast, a large number of gene ontology terms were identified from the list of upregulated genes including oxidative phosphorylation, ATP synthesis, electron transport, respiration, lipid metabolism, TCA cycle and fatty acid metabolism. This suggests that colonocytes increase energy generation and endogenous metabolism to compensate for the lack of microbial derived butyrate. This is in agreement with recent study which also investigated the effects of antibiotics treatment on gene expression and investigated how this altered intestinal homeostasis (Zarrinpar *et al.*, 2018). They observed reductions in SCFAs in the gut lumen, changes to microbial metabolic pathways including involving lipid metabolism and differential regulation of mitochondrial and oxidative phosphorylation related genes in the caecum. In addition, they found that

glucose metabolism was upregulated, with changes to hormones such insulin and leptin, along with reduced expression of genes involved in fatty acid receptors, binding proteins and enzymes involved in beta-oxidation, including ACAD. Together our findings suggests that as a result of antibiotic induced depletion of the microbiota, host metabolism switches to accomodate the loss of microbial metabolites.

5.3.5 Histone crotonylation links to gene expression in a subset of genes on antibiotics treatment

In this study, we have found that changes to gene expression on antibiotics treatment are positively correlated to changes in crotonylation. Histone crotonylation is associated with active chromatin and has even been shown to activate the transcription of p53 to a greater extent than acetylation in a cell free assay (Sabari *et al.*, 2015). In addition, crotonylation preferentially binds different classes of reader proteins, the YEATS and DPF domains, rather than the acetylation binding bromodomains. Therefore, this suggests that modulation of crotonylation in the colon consitutes novel mechanism to regulate gene expression in response to the microbiota, an interaction that is critical for the normal functioning of the colon. Crotonylation was widely distributed across the genome with enrichment at TSS but with peaks also present in the gene body and outside genes. Despite its broad genomic localization, gene ontology terms linked to genes that changed in crotonylation on antibiotics treatment were specific, suggesting key functions for crotonylation in this context. However, the differentially regulated genes that changed significantly in crotonylation upon antibiotics-treatment were only a subset of the total number of differentially regulated genes. Furthermore, genes related to energy generation were differentially expressed but were not identified in the differentially crotonylated genes. Other epigenetic switches might mediate the changes in regulation for the remaining differentially expressed genes. Interestingly, there were also many genes which changed in crotonylation but which did not change in gene expression. The activity of a particular gene is thought to be dependent on the combinatorial action of multiple epigenetic switches. Some genes may gain crotonylation, but remain in a poised state due to the presence of repressive modifications. Conversely, some genes may be depleted in crotonylation but remain active due to the presence of transcription promoting marks. Changes to crotonylation may also decorate region not directly involved in gene regulation, e.g., origins of replication, as we have observed that this mark is not only present at TSS. Due to poor performance by anti-H4K8cr and anti-H3K18cr antibodies we used an anti-Kcr antibody, which also can recognise non-histone crotonylation. The ChIP experiment enriches for DNA associated proteins, but we cannot exclude that DNA-associated non-histone crotonylation may be detected in our analysis as well as histone crotonylation. However, western blotting using the anti-

Kcr antibody indicates that by far the most abundant crotonylated proteins migrate in a way that is consistent with them being histones H3 and H4.

5.3.6 Histone crotonylation co-localises with H4K8 acetylation in the colon

We found that MACS peaks of H4K8ac, H3K18cr and Kcr were highly overlapping, with a striking similarity in profiles across the genome. Their close overlap could be because p300/CBP and class I HDACs are responsible for both their addition and removal. These modifications were also present in the same enhancer-like states in the ChromHMM analysis in the colon where they all associated with H3K27ac and H3K4me1. H3K18cr and Kcr were more similar to each other than to H4K8ac as state 1 mainly contained H4K8ac and H3K4me1 but not the crotonyl marks. This high correlation between modifications may be because the same writers (p300) and the same erasers (class I HDACs) can act on all of these modifications. These enzymes could specifically target certain regions of the genome resulting in a similar distribution of these modifications. However, whilst only p300/CBP and MOF have been shown to have histone crotonyltransferase activity (Sabari *et al.*, 2015; X. Liu *et al.*, 2017), many HATs have been identified, which would mean that acetylation is present at more sites. In fact, we did observe that there were more H4K8ac peaks than H3K18cr or Kcr peaks, although this may be in part due to differences in enrichment. The pattern of distribution could reflect regions of more open chromatin. Furthermore, the presence of one type of acylation on a histone could promote the addition of other histone acylations on neighbouring nucleosomes. Mass spectrometry analysis of histone H3 crotonylation revealed that H3K18cr associated with H3K23ac, suggesting co-regulation of these modifications (Fellows *et al.*, 2018). As this analysis did not include H4 modifications, it remains to be seen whether H4K8ac is highly associated with H3K18cr in a nucleosome. H4K8ac, H3K18cr and Kcr were all associated with higher levels of transcription, enriched at TSS and strongly overlapped with candidate regulatory elements. This raises the question of whether histone crotonylation has a distinct function from histone acetylation in the gut. The genes containing all three modifications were associated with diverse functions including metabolism and protein modification. The presence of all three modifications, and potentially others, could have an additive function to maintain transcription of essential genes for housekeeping functions. As YEATS domains have a preference for histone crotonylation whilst bromodomains prefer histone acetylation (Flynn *et al.*, 2015b; Andrews *et al.*, 2016; Li, Benjamin R. Sabari, *et al.*, 2016; Zhang *et al.*, 2016; Zhao *et al.*, 2016), these hPTMs could interact with different complexes and induce separate cellular responses even if they are present at the same genomic sites. Additionally, there may be as yet unidentified crotonyl-interacting factors which do not interact with other histone acylations. We and others have demonstrated that the anti-Kcr antibody is specific to crotonylation and does not recognise acetylation (Tan *et al.*, 2011; Bao *et*

al., 2014; Sabari *et al.*, 2015). H4K8ac and H3K18cr have also been validated, although the poor performance of subsequent batches of anti-H3K18cr does mean that a new antibody will need to be developed for studies on this modification to be continued.

5.3.7 H4K8ac does not change over genomic elements on antibiotics treatment

Comparing H4K8ac ChIP-seq in control and antibiotics treated mouse colon found that there were no significant changes in the enrichment of MACS peaks between the two groups. Furthermore, comparison of H4K8ac ChIP-qPCR did not reveal any significant changes in the individual targets tested, despite some targets such as *Isg15* and *Hmgcs2* changing in the same direction as gene expression. This is surprising since H4K8ac did change when control and antibiotics groups were compared by western blot and hundreds of genes changed in crotonylation. However, there was a significant reduction in H4K8ac ChIPqPCR over all genes that reduced in expression. When we compared the fold changes of Kcr and H4K8ac, for genes that significantly changed in Kcr, the enrichment of H4K8ac was changing to a similar extent to Kcr. Possibly, the samples used in the H4K8ac ChIP-seq had higher variability making it more difficult to reach significance. Li *et al.* (2019) observed that H4K8ac changed between normal tissue and tumour tissue, particularly in intergenic regions and introns (Li *et al.*, 2019), so this modification can be responsive to changing conditions. As this H4K8ac ChIP-seq was the first comparison of acetylation between control and antibiotics treated mice, further analysis should be performed. Additionally, as Kcr detects all lysine crotonylation but H4K8ac is only specific to one mark, a better comparison could include H3K18ac. Ideally, H3K18cr would be compared to H3K18ac and H4K8cr with H4K8ac, but the current lack of ChIP-compatible crotonyl-specific antibodies makes this challenging.

5.3.8 Microbiota depletion differentially influences global and site-specific histone crotonylation

We identified that antibiotic treatment produced global reductions in histone crotonylation and acetylation by western blot. However, by ChIP-seq we identified significant increases and decreases in crotonylation on antibiotics-treatment at specific sites relative to the rest of the genome, whilst no significant changes were observed for acetylation. This suggests that there are distinct differences between local and global crotonylation and acetylation. Whilst the global levels of histone crotonylation are reduced on antibiotics treatment, certain regions such as promoters may be protected from removal by chromatin and transcriptional machinery. As ChIP-seq measures the relative distribution of proteins across the genome, these protected regions would give a stronger signal in the antibiotics treated group relative to other regions and would be higher than in the control group where background levels are maintained. Our hypothesis is that a large proportion of histone

crotonylation (and acetylation) are distributed over the genome in an unfocused manner, hence why we detect these modifications in intergenic regions, reflecting background noise or a link to replication (Fellows et al., 2018). Certain regulatory elements, such as promoters, are consistently enriched as a result of specific targeting of histone modifications to these sites, enabling us to detect 'peaks' of enrichment. We do not yet understand the relationship between the local, site specific actions of hPTMs and their global changes. One interesting possibility is that global reduction of a hPTM may focus binding proteins to the remaining hPTM sites, coupling to downstream factors and enabling an increase in transcription of certain genes despite less of the modification overall.

6

6 General discussion

6.1 Histone hydroxybutyrylation is influenced by different signals to that of acetylation or crotonylation

In chapter 4, we saw no changes to histone acetylation or crotonylation when mouse diet was restricted but we did not test histone hydroxybutyrylation. After this experiment was conducted, Xie *et al.* (2016) found that starvation or ketoacidosis increases histone hydroxybutyrylation and that changes to this modification are associated with those genes that change in gene expression (Xie *et al.*, 2016). In chapter 3, we found that histone crotonylation did not change when β-Hbu was added to HCT116 cells. Additionally, in chapter 5, hydroxybutyrylation did not change or increased when the microbiota was depleted with antibiotics whilst crotonylation and acetylation were strongly reduced. This implies that hydroxybutyrylation responds to different cues to that of acetylation or crotonylation. Hydroxybutyrate is derived from ketone bodies, a form of energy storage that is released upon starvation. Potentially, ketone bodies are the main source of hydroxybutyryl groups for histone transfer rather than metabolites released from the microbiota.

6.2 Histone crotonylation and acetylation are influenced by the microbiota

In this study we identified that the SCFAs crotonate, butyrate and propionate could promote histone crotonylation and acetylation in cell culture. We also showed that antibiotic induced depletion of the microbiota reduced SCFA concentrations, histone crotonylation and histone acetylation in mouse colon. Various different acetyl- and crotonyl-modifications were responsive to the microbiota including H4K8ac, H4K8cr and Kcr. Both H4K8ac and Kcr were associated with marks of regulatory elements such as H3K27ac and H3K4me3. But whilst the Kcr ChIP-seq revealed many genes which significantly changed in crotonylation on antibiotics treatment, there were no significant changes to H4K8ac in either ChIP-seq or ChIP-qPCR. However, we cannot rule out the possibility of acetylation not changing as a result of antibiotic treatment. In this study we compared H4K8ac to Kcr as ChIP experiments with H4K8cr and H3K18cr were unsuccessful. This was informative, but H4K8ac and Kcr

are not equivalent modifications. Future studies could test H3K18ac or other acetylation marks using higher sample numbers to allow for the variability we have seen so far.

We also found that a diet without fibre reduced some histone acetyl- and crotonyl- modifications along with colon luminal butyrate concentrations. Whilst we did not measure other microbial metabolites, the lack of changes to histone methylation suggests that it is not through metabolites such as folate or succinate. In support of this conclusion, a previous study found that colonization of germ-free mice promoted histone acetylation along with an increase in SCFA concentrations (Krautkramer *et al.*, 2016). Together, this evidence demonstates that the microbiota is an important regulator of histone crotonylation and acetylation, and implicates SCFAs in this interaction. However, although we have shown that butyrate and propionate can promote histone crotonylation and butyrate can promote histone acetylation in cell culture, we have not directly shown that it is the SCFAs that are modulating histone acylations *in vivo*. Antibiotic treatment and depletion of the microbiota is likely to cause widespread changes to gut physiology. Changes to cell proliferation, activity of immune cells, the loss of other signals such as MAMPs and switching to other sources of energy due to the lack of microbial metabolites have the potential to influence histone modifications. Indeed, we observed changes to the expression of genes involving metabolism, energy generation, immune processes and cell adhesion by RNA-seq in the colon of antibiotic treated mice suggesting that multiple changes are occurring in colonocyte processes. As the gut environment is complex, with interactions between diet, microbiota, epithelium and immune cells, detangling the different possibilities will be a complex task. We observed some changes to histone acylations on antibiotics treatment of colon organoids, although these were not dose-dependent, therefore antibiotics treatment of germ-free mice would be a useful further experiment to determine the affect of antibiotics itself without the influence of the microbiota. To study whether butyrate or other SCFAs are the cause of the changes to histone acylations that we have observed, mice could be transplanted with butyrate producing bacteria. We observed no differences in crotonate supplementation to the drinking water of conventional mice or butyrate gavage of germ-free mice. However, these SCFAs are likely to be diluted by the stomach and mostly absorbed by the small intestine rather than the colon. Use of slower release molecules such as tributyrin could be used to increase colon butyrate concentrations. Additionally, ^{13}C tracing experiments could be used to track specific molecules from the diet or SCFAs administered by gavage through to histone modifications in colonocytes. The timing of mouse collection is likely to be critical in these experiments as SCFA concentrations in the colon or serum will probably peak at a certain time after treatment.

6.3 By what mechanism do SCFAs change histone acetylation and crotonylation?

The mode by which microbiota derived SCFAs influence histone acetylation and crotonylation is important because it will inform us in what circumstances this occurs and what functions this may relate to. This is because butyrate was found to either promote proliferation or apoptosis depending on whether it acted as a HDAC inhibitor or metabolite (Donohoe *et al.*, 2012). We now know that it is possible for butyrate to promote crotonylation by HDAC inhibition as we and others have demonstrated that class I HDACs are histone decrotonylases (Madsen and Olsen, 2012; Wei, Liu, *et al.*, 2017; Fellows *et al.*, 2018; Kelly *et al.*, 2018). Our kinetic studies show that HDAC1 is an effective decrotonylase enzyme with only a three-fold lower rate than that of its HDAC activity. Furthermore, Wei *et al.* (2017) demonstrated that class I HDACs could act as decrotonylases in cell culture. The identification of class I HDACs as decrotonylases does not define the mode of action of SCFAs, but merely increases the number of possible routes for these microbial metabolites to influence histone crotonylation. Butyrate was shown to mediate the degradation of HDAC2 (Kramer *et al.*, 2003), therefore microbiota derived SCFAs could influence histone modifications by mediating HDAC abundance. In some experiments with antibiotic treated mice we saw a significant increase in HDAC2 abundance. We also saw some statistically significant reductions in HDAC abundance on high fibre diets, but the effects we saw were not consistent across experiments. HDAC3 expression was also shown to be induced in the presence of commensal bacteria and HDAC expression in IECs mediates regulation of intestinal homeostasis by the commensal bacteria (Alenghat and Artis, 2014). Therefore, whilst SCFAs might affect HDAC levels, other cues from the intestinal microbiota may balance HDAC expression to maintain homeostatic functioning of the gut.

SCFAs can also act as metabolites, providing acylated-CoAs for use by histone acyltransferases. We tested mice with a deficiency in ACAD, which converts butyryl-CoA to crotonyl-CoA, to determine how important the metabolism of butyrate by β-oxidation is for promoting crotonylation. ACAD deficient mice showed no difference in histone acylations to wild type mice, suggesting that this enzyme is not involved. Alternatively, histone acylations might have been upregulated by the action of ACSS2 which converts SCFAs to acyl-CoAs in the cytoplasm. Acetate, propionate and butyrate are provided by the microbiota and can be converted to their acyl-CoAs by ACSS2, but little is known about the presence of crotonate in the gut lumen. However, crotonate was identified in the faeces of Dachshunds at around three fold lower concentration than butyrate (Igarashi *et al.*, 2017) and many bacteria have the metabolic capability to use crotonate (Guccione *et al.*, 2010). Therefore, crotonate could be present in the mouse colon and provide crotonyl-CoA for the histone via ACSS2. Interestingly, we found in our mouse studies that the concentration of butyrate correlated better with histone acylations than that of propionate or acetate. Our cell culture work found that acetate did not

influence histone acetylation or crotonylation, but butyrate did. This implies that histone acylations are upregulated in the gut by inhibition of HDACs, as butyrate is a HDAC inhibitor but acetate isn't. However, further studies are required to determine the predominant mechanism of action of SCFAs, which is likely to vary depending on cell type. Testing the *in vivo* knock-down of enzymes such as HDAC1 and ACSS2, and heavy label tracing SCFAs in intestinal organoids will help us understand this complex interaction better.

6.4 Conclusion

Our study demonstrates a fascinating new link between the commensal gut microbiota and histone crotonylation. We have also shown that some of the changes to histone crotonylation on antibiotics treatment correlated with changes in gene expression. However, whether changes to histone crotonylation are the cause or a consequence of changes to gene expression remain unclear. This is a key issue in the field of histone modifications more generally, as these marks are often assumed to have a causative role in gene modulation without any direct evidence. In fact, loss of the strongly promoter-associated H3K4me3 had no effect on the levels of newly generated transcripts (Murray *et al.*, 2019). Instead, SCFAs might change metabolism, leading to changes in gene expression that in turn change histone crotonylation. However, the fields of histone crotonylation and microbiota-epigenetic interactions remain exciting new topics with many avenues for further investigation. As the microbiota has been linked to a range of disorders including, cancer, inflammatory bowel disease and obesity; whilst epigenetic switches are involved in gene regulation, this interrelationship is likely to be a vital part of our health and contribute to disease.

7

7 References

Van Den Abbeele, P., Belzer, C., Goossens, M., Kleerebezem, M., De Vos, W. M., Thas, O., De Weirdt, R., Kerckhof, F. M. and Van De Wiele, T. (2013) 'Butyrate-producing Clostridium cluster XIVa species specifically colonize mucins in an in vitro gut model', *ISME Journal*. Nature Publishing Group, 7(5), pp. 949–961. doi: 10.1038/ismej.2012.158.

Abu-Zhayia, E. R., Machour, F. E. and Ayoub, N. (2019) 'HDAC-dependent decrease in histone crotonylation during DNA damage', *Journal of Molecular Cell Biology*, 00, pp. 1–3. doi: 10.1093/jmcb/mjz019.

Agalioti, T., Chen, G. and Thanos, D. (2002) 'Deciphering the transcriptional histone acetylation code for a human gene', *Cell*, 111(3), pp. 381–392. doi: 10.1016/S0092-8674(02)01077-2.

Alam, M. T., Olin-Sandoval, V., Stincone, A., Keller, M. A., Zelezniak, A., Luisi, B. F. and Ralser, M. (2017) 'The self-inhibitory nature of metabolic networks and its alleviation through compartmentalization', *Nature Communications*. Nature Publishing Group, 8, pp. 1–13. doi: 10.1038/ncomms16018.

Alberts, B., Johnson, A., Lewis, J., Morgan, D., Raff, M., Roberts, K. and Walter, P. (2015) 'Chapter 4: DNA, chromosomes and genomes', in *Molecular Biology of the Cell*. 6th edn. New York: Garland Science, pp. 173–236.

Alenghat, T. and Artis, D. (2014) 'Epigenomic regulation of host–microbiota interactions', *Trends in Immunology*, 35(11), pp. 518–525. doi: 10.1016/j.it.2014.09.007.

Allis, C. D. and Jenuwein, T. (2016) 'The molecular hallmarks of epigenetic control', *Nature Reviews Genetics*. Nature Publishing Group, 17(8), pp. 487–500. doi: 10.1038/nrg.2016.59.

Anastasiou, D., Yu, Y., Israelsen, W. J., *et al.* (2012) 'Pyruvate kinase M2 activators promote tetramer formation and suppress tumorigenesis', *Nature Chemical Biology*, 8(10), pp. 839–847. doi: 10.1038/nchembio.1060.

Andersson, R., Gebhard, C., Miguel-Escalada, I., *et al.* (2014) 'An atlas of active enhancers across human cell types and tissues', *Nature*, 507(7493), pp. 455–461. doi: 10.1038/nature12787.

Andrews, F. H., Shinsky, S. A., Shanle, E. K., Bridgers, J. B., Gest, A., Tsun, I. K., Krajewski, K., Shi, X., Strahl, B. D. and Kutateladze, T. G. (2016) 'The Taf14 YEATS domain is a reader of histone crotonylation', *Nature chemical biology*, (April), pp. 1–4. doi: 10.1038/pj.2016.37.

Arib, G. and Akhtar, A. (2011) 'Multiple facets of nuclear periphery in gene expression control', *Current Opinion in Cell Biology*. Elsevier Ltd, 23(3), pp. 346–353. doi: 10.1016/j.ceb.2010.12.005.

Aune, D., Chan, D. S. M., Lau, R., Vieira, R., Greenwood, D. C., Kampman, E. and Norat, T. (2011) 'Dietary fibre, whole grains, and risk of colorectal cancer: systematic review and dose-response meta-analysis of prospective studies', *British medical journal*, 343, pp. 1–20. doi: 10.1136/bmj.d6617.

Backhed, F., Ding, H., Wang, T., Hooper, L. V., Koh, G. Y., Nagy, A., Semenkovich, C. F. and Gordon, J. I. (2004) 'The gut microbiota as an environmental factor that regulates fat storage', *Proceedings of the National Academy of Science*, 101(44), pp. 15718–15723. doi: 10.1073/pnas.0407076101.

Bader, J., Giinther, H., Schleicher, E., Simon, H., Pohl, S. and Mannheim, W. (1980) 'Utilization of (E)-2-butenoate (crotonate) by Clostridium kluyveri and some other Clostridium species', *Archives of Microbiology*, 125, pp. 159–165.

Banerjee, T. and Chakravarti, D. (2011) 'A Peek into the Complex Realm of Histone Phosphorylation', *Molecular and Cellular Biology*, 31(24), pp. 4858–4873. doi: 10.1128/mcb.05631-11.

Bao, X., Wang, Y., Li, Xin, Li, Xiao-meng, Liu, Z. and Yang, T. (2014) 'Identification of "erasers" for lysine crotonylated histone marks using a chemical proteomics approach', *eLIFE*, pp. 1–18. doi: 10.7554/eLife.02999.

Barnes, C. E., English, D. M. and Cowley, S. M. (2019) 'Acetylation & Co: an expanding repertoire of histone acylations regulates chromatin and transcription', *Essays In Biochemistry*, 63(1), pp. 97–107. doi: 10.1042/EBC20180061.

Barski, A., Cuddapah, S., Cui, K., Roh, T., Schones, D. E., Wang, Z., Wei, G., Iouri, C. and Zhao, K. (2007) 'Resource High-Resolution Profiling of Histone Methylations in the Human Genome', *Cell*, 129, pp. 823–837. doi: 10.1016/j.cell.2007.05.009.

Belcheva, A., Irrazabal, T., Robertson, S. J., *et al.* (2014) 'Gut Microbial Metabolism Drives Transformation of Msh2-Deficient Colon Epithelial Cells', *Cell*. Elsevier, 158(2), pp. 288–299. doi: 10.1016/j.cell.2014.04.051.

Bell, J. T. and Spector, T. D. (2011) 'A twin approach to unraveling epigenetics', *Trends in Genetics*. Elsevier Ltd, 27(3), pp. 116–125. doi: 10.1016/j.tig.2010.12.005.

Berndsen, C. E. and Denu, J. M. (2008) 'Catalysis and substrate selection by histone/protein lysine acetyltransferases', *Current Opinion in Structural Biology*, 18(6), pp. 682–689. doi: 10.1016/j.sbi.2008.11.004.

Besrat, A., Polan, C. E. and Henderson, L. M. (1969) 'Mammalian metabolism of glutaric acid.', *Journal of Biological Chemistry*, 244(6), pp. 1461–1467.

den Besten, G., van Eunen, K., Groen, A. K., Venema, K., Reijngoud, D.-J. and Bakker, B. M. (2013) 'The role of short-chain fatty acids in the interplay between diet, gut microbiota, and host energy metabolism.', *Journal of lipid research*, 54(9), pp. 2325–40. doi: 10.1194/jlr.R036012.

Bittencourt, D., Lee, B. H., Gao, L., Gerke, D. S. and Stallcup, M. R. (2014) 'Role of distinct surfaces of the G9a ankyrin repeat domain in histone and DNA methylation during embryonic stem cell self-renewal and differentiation', *Epigenetics and Chromatin*, 7(1), pp. 1–12. doi: 10.1186/1756-8935-7-27.

Black, J. C., Van Rechem, C. and Whetstine, J. (2012) 'Histone lysine methylation dynamics: establishment, regulation, and biological impact', *Molecular Cell*, 48(4), pp. 1–32. doi: 10.1038/jid.2014.371.

Blaser, M. J. and Kirschner, D. (2007) 'The equilibria that allow bacterial persistence in human hosts', *Nature*, 449(7164), pp. 843–849. doi: 10.1038/nature06198.

Blasi, T., Feller, C., Feigelman, J., Hasenauer, J., Imhof, A., Theis, F. J., Becker, P. B. and Marr, C. (2016) 'Combinatorial Histone Acetylation Patterns Are Generated by Motif-Specific Reactions', *Cell Systems*. Elsevier Inc., 2(1), pp. 49–58. doi: 10.1016/j.cels.2016.01.002.

Blouin, J. M., Penot, G., Collinet, M., Nacfer, M., Forest, C., Laurent-Puig, P., Coumoul, X., Barouki, R., Benelli, C. and Bortoli, S. (2011) 'Butyrate elicits a metabolic switch in human colon cancer cells by targeting the pyruvate dehydrogenase complex', *International Journal of Cancer*, 128(11), pp. 2591–2601. doi: 10.1002/ijc.25599.

Bojang, P. J. and Ramos, K. S. (2014) 'The promise and failures of epigenetic therapies for cancer treatment', *Cancer treatment reviews*, 40(1), pp. 1–41. doi: 10.1016/j.ctrv.2013.05.009.

Bonn, S., Zinzen, R. P., Girardot, C., Gustafson, E. H., Perez-Gonzalez, A., Delhomme, N., Ghavi-Helm, Y., Wilczyåski, B., Riddell, A. and Furlong, E. E. M. (2012) 'Tissue-specific analysis of chromatin state identifies temporal signatures of enhancer activity during embryonic development', *Nature Genetics*,

44(2), pp. 148–156. doi: 10.1038/ng.1064.

Borre, Y. E., O'Keeffe, G. W., Clarke, G., Stanton, C., Dinan, T. G. and Cryan, J. F. (2014) 'Microbiota and neurodevelopmental windows: implications for brain disorders', *Trends in molecular medicine*. Elsevier Ltd, 20(9), pp. 509–518. doi: 10.1016/j.molmed.2014.05.002.

Boukouris, A. E., Zervopoulos, S. D. and Michelakis, E. D. (2016) 'Metabolic Enzymes Moonlighting in the Nucleus: Metabolic Regulation of Gene Transcription', *Trends in Biochemical Sciences*. Elsevier Ltd, 41(8), pp. 712–730. doi: 10.1016/j.tibs.2016.05.013.

Bracken, A. P., Pasini, D., Capra, M., Prosperini, E., Colli, E. and Helin, K. (2003) 'EZH2 is downstream of the pRB-E2F pathway, essential for proliferation and amplified in cancer', *EMBO Journal*, 22(20), pp. 5323–5335. doi: 10.1093/emboj/cdg542.

Brestoff, J. R. and Artis, D. (2013) 'Commensal bacteria at the interface of host metabolism and the immune system', *Nature Immunology*, 14(7), pp. 676–684. doi: 10.1038/ni.2640.

Bulusu, V., Tumanov, S., Michalopoulou, E., *et al.* (2017) 'Acetate recapturing by nuclear acetyl-CoA synthetase 2 prevents loss of histone acetylation during oxygen and serum limitation', *Cell Reports*. ElsevierCompany., 18(3), pp. 647–658. doi: 10.1016/j.celrep.2016.12.055.

Cai, L., Sutter, B. M., Li, B. and Tu, B. P. (2011) 'Acetyl-CoA induces cell growth and proliferation by promoting the acetylation of histones at growth genes', *Molecular Cell*, 42(4), pp. 426–437. doi: 10.1016/j.molcel.2011.05.004.

Calo, E. and Wysocka, J. (2013) 'Modification of Enhancer Chromatin: What, How, and Why?', *Molecular Cell*. Elsevier Inc., 49(5), pp. 825–837. doi: 10.1016/j.molcel.2013.01.038.

Candido, E. P. M., Reeves, R. and Davie, J. R. (1978) 'Sodium butyrate inhibits histone deacetylation in cultured cells', *Cell*, 14(1), pp. 105–113. doi: http://dx.doi.org/10.1016/0092-8674(78)90305-7.

Caron, C., Pivot-Pajot, C., van Grunsven, L. A., Col, E., Lestrat, C., Rousseaux, S. and Khochbin, S. (2003) 'Cdyl: A new transcriptional co-repressor', *EMBO Reports*, 4(9), pp. 877–882. doi: 10.1038/sj.embor.embor917.

Casciello, F., Windloch, K., Gannon, F. and Lee, J. S. (2015) 'Functional role of G9a histone methyltransferase in cancer', *Frontiers in Immunology*, 6, pp. 3–9. doi: 10.3389/fimmu.2015.00487.

Casteleyn, C., Rekecki, A., Van Der Aa, A., Simoens, P. and Van Den Broeck, W. (2010) 'Surface area assessment of the murine intestinal tract as a prerequisite for oral dose translation from mouse to man', *Laboratory Animals*, 44(3), pp. 176–183. doi: 10.1258/la.2009.009112.

Cavalli, G. and Heard, E. (2019) 'Advances in epigenetics link genetics to the environment and disease', *Nature*. Springer US, 571(7766), pp. 489–499. doi: 10.1038/s41586-019-1411-0.

Chang, L., Loranger, S. S., Mizzen, C., Ernst, S. G., Allis, C. D. and Annunziato, A. T. (1997) 'Histones in transit: Cytosolic histone complexes and diacetylation of H4 during nucleosome assembly in human cells', *Biochemistry*, 36(3), pp. 469–480. doi: 10.1021/bi962069i.

Chen, Y., Sprung, R., Tang, Y., Ball, H., Sangras, B., Kim, S. C., Falck, J. R., Peng, J., Gu, W. and Zhao, Y. (2007) 'Lysine propionylation and butyrylation are novel post-translational modifications in histones', *Molecular & Cellular Proteomics*, 6(5), pp. 812–819. doi: 10.1074/mcp.M700021-MCP200.

Chin, H. G., Patnaik, D., Estève, P. O., Jacobsen, S. E. and Pradhan, S. (2006) 'Catalytic properties and kinetic mechanism of human recombinant Lys-9 histone H3 methyltransferase SUV39H1: Participation of the chromodomain in enzymatic catalysis', *Biochemistry*, 45(10), pp. 3272–3284. doi: 10.1021/bi051997r.

Cho, I., Yamanishi, S., Cox, L., *et al.* (2013) 'Antibiotics in early life alter the murine colonic microbiome and adiposity', *Nature*, 488(7413), pp. 621–626. doi: 10.1038/nature11400.

Chory, E. J., Calarco, J. P., Hathaway, N. A., Bell, O., Neel, D. S. and Crabtree, G. R. (2019) 'Nucleosome Turnover Regulates Histone Methylation Patterns over the Genome', *Molecular Cell*. Elsevier Inc., 73(1), pp. 61-72.e3. doi: 10.1016/j.molcel.2018.10.028.

Choudhary, C., Weinert, B. T., Nishida, Y., Verdin, E. and Mann, M. (2014) 'The growing landscape of lysine acetylation links metabolism and signalling', *Nature Publishing Group*, 15, pp. 536–550. doi: 10.1038/nrm3841.

Cieniewicz, A. M., Moreland, L., Ringel, A. E., Mackintosh, S. G., Raman, A., Gilbert, T. M., Wolberger, C., Tackett, A. J. and Taverna, S. D. (2014) 'The bromodomain of gcn5 regulates site specificity of lysine acetylation on histone H3', *Molecular and Cellular Proteomics*, 13(11), pp. 2896–2910. doi: 10.1074/mcp.M114.038174.

Clevers, H. and Batlle, E. (2013) 'SnapShot: The Intestinal Crypt', *Cell*. Elsevier, 152(5), pp. 1198-1198.e2. doi: 10.1016/j.cell.2013.02.030.

Clouaire, T., Webb, S., Skene, P., Illingworth, R., Kerr, A., Andrews, R., Lee, J. H., Skalnik, D. and Bird, A. (2012) 'Cfp1 integrates both CpG content and gene activity for accurate H3K4me3 deposition in embryonic stem cells', *Genes and Development*, 26(15), pp. 1714–1728. doi: 10.1101/gad.194209.112.

Cook, S. I. and Sellin, J. J. (1998) 'Short chain fatty acids in health and disease', *Aliment Pharmacol Ther*, 12, pp. 499–507. doi: 10.4324/9781315514659.

Corrêa-Oliveira, R., Fachi, J. L., Vieira, A., Sato, F. T. and Vinolo, M. A. R. (2016) 'Regulation of immune cell function by short-chain fatty acids', *Clinical and Translational Immunology*, 5(4), pp. 1–8. doi: 10.1038/cti.2016.17.

Cousens, L. S., Gallwitz, D. and Alberts, B. M. (1979) 'Different accessibilities in chromatin to histone acetylase', *Journal of Biological Chemistry*, 254(5), pp. 1716–1723.

Cox, L. M., Yamanishi, S., Sohn, J., *et al.* (2014) 'Altering the intestinal microbiota during a critical developmental window has lasting metabolic consequences', *Cell*, 158(4), pp. 705–721. doi: 10.1016/j.cell.2014.05.052.

Creyghton, M. P., Cheng, A. W., Welstead, G. G., *et al.* (2010) 'Histone H3K27ac separates active from poised enhancers and predicts developmental state', *Proceedings of the National Academy of Sciences*, 107(50), pp. 21931–21936. doi: 10.1073/pnas.1016071107.

Crider, K. S., Yang, T. P., Berry, R. J. and Bailey, L. B. (2012) 'Folate and DNA methylation: a review of molecular mechanisms and the evidence for folate's role', *Advances in Nutrition*, 3(1), pp. 21–38. doi: 10.3945/an.111.000992.

Dahan, S., Roth-Walter, F., Arnaboldi, P., Agarwal, S. and Mayer, L. (2007) 'Epithelia: lymphocyte interactions in the gut', *Immunological Reviews*, 215(1), pp. 243–253. doi: 10.1111/j.1600-065x.2006.00484.x.

Dai, L., Peng, C., Lu, Z., *et al.* (2014) 'Lysine 2-hydroxyisobutyrylation is a widely distributed active histone mark', *Nature Chemical Biology*. Nature Publishing Group, 10(5), pp. 365–370. doi: 10.1038/nchembio.1497.

Dang, W., Steffen, K. K., Perry, R., Dorsey, J. A., Johnson, F. B., Kaeberlein, M., Kennedy, B. K. and Berger, S. L. (2009) 'Histone H4 lysine-16 acetylation regulates cellular lifespan', *Nature*, 459(7248), pp. 802–807. doi: 10.1038/nature08085.

David, L. A., Maurice, C. F., Carmody, R. N., *et al.* (2014) 'Diet rapidly and reproducibly alters the human gut microbiome.', *Nature*. Nature Publishing Group, 505(7484), pp. 559–63. doi: 10.1038/nature12820.

Davies, P. G., Venkatesh, B., Morgan, T. J., Presneill, J. J., Kruger, P. S., Thomas, B. J., Roberts, M. S. and Mundy, J. (2011) 'Plasma acetate, gluconate and interleukin-6 profiles during and after cardiopulmonary bypass: A comparison of Plasma-Lyte 148 with a bicarbonate-balanced solution', *Critical Care*, 15(1), pp. 1–8. doi: 10.1186/cc9966.

Davis, L. M. G., Martínez, I., Walter, J., Goin, C. and Hutkins, R. W. (2011) 'Barcoded pyrosequencing

reveals that consumption of galactooligosaccharides results in a highly specific bifidogenic response in humans', *PLoS ONE*, 6(9), pp. 1–10. doi: 10.1371/journal.pone.0025200.

Deal, R. B., Henikoff, J. G. and Henikoff, S. (2010) 'Genome-Wide Kinetics of Nucleosome', *Science*, 328(5982), pp. 1161–1165. doi: 10.1126/science.1186777.

Dhingra, D., Michael, M., Rajput, H. and Patil, R. T. (2012) 'Dietary fibre in foods: A review', *Journal of Food Science and Technology*, 49(3), pp. 255–266. doi: 10.1007/s13197-011-0365-5.

Dion, M. F., Kaplan, T., Minkyu, K., Buratowski, S., Friedman, N. and Rando, O. J. (2007) 'Dynamics of replication independent histone turnover in budding yeast', *Science*, 315(5817), pp. 1405–1408. doi: 10.1126/science.1134053.

Donohoe, D. R., Collins, L. B., Wali, A., Bigler, R., Sun, W. and Bultman, S. J. (2012) 'The warburg effect dictates the mechanism of butyrate-mediated histone acetylation and cell proliferation', *Molecular Cell*. Elsevier Inc., 48(4), pp. 612–626. doi: 10.1016/j.molcel.2012.08.033.

Donohoe, D. R., Garge, N. N., Zhang, X., Sun, W., O'Connell, T. M., Bunger, M. K. and Bultman, S. J. (2011) 'The microbiome and butyrate regulate energy metabolism and autophagy in the mammalian colon', *Cell Metabolism*, 13(5), pp. 517–526. doi: 10.1016/j.cmet.2011.02.018.

Dorr, A., Kiermer, V., Pedal, A., Rackwitz, H. R., Henklein, P., Schubert, U., Zhou, M. M., Verdin, E. and Ott, M. (2002) 'Transcriptional synergy between Tat and PCAF is dependent on the binding of acetylated Tat to the PCAF bromodomain', *EMBO Journal*, 21(11), pp. 2715–2723. doi: 10.1093/emboj/21.11.2715.

Drazic, A., Myklebust, L. M., Ree, R. and Arnesen, T. (2016) 'The world of protein acetylation', *Biochimica et Biophysica Acta - Proteins and Proteomics*, 1864(10), pp. 1372–1401. doi: 10.1016/j.bbapap.2016.06.007.

Du, J., Zhou, Y., Su, X., *et al.* (2011) 'Sirt5 Is a NAD-Dependent Protein Lysine Demalonylase and Desuccinylase', *Science*, 334(6057), pp. 806–809. doi: 10.1126/science.1207861.

Duncan, S. H., Belenguer, A., Holtrop, G., Johnstone, A. M., Flint, H. J. and Lobley, G. E. (2007) 'Reduced dietary intake of carbohydrates by obese subjects results in decreased concentrations of butyrate and butyrate-producing bacteria in feces', *Applied and Environmental Microbiology*, 73(4), pp. 1073–1078. doi: 10.1128/AEM.02340-06.

Dunham, I., Kundaje, A., Aldred, S. F., *et al.* (2012) 'An integrated encyclopedia of DNA elements in the human genome', *Nature*, 489(7414), pp. 57–74. doi: 10.1038/nature11247.

Eberharter, A. and Becker, P. B. (2002) 'Histone acetylation: A switch between repressive and permissive chromatin. Second in review series on chromatin dynamics', *EMBO Reports*, 3(3), pp. 224–229. doi: 10.1093/embo-reports/kvf053.

Elamin, E. E., Masclee, A. A., Dekker, J., Pieters, H.-J. and Jonkers, D. M. (2013) 'Short-Chain Fatty Acids Activate AMP-Activated Protein Kinase and Ameliorate Ethanol-Induced Intestinal Barrier Dysfunction in Caco-2 Cell Monolayers', *The Journal of Nutrition*, 143(12), pp. 1872–1881. doi: 10.3945/jn.113.179549.

Ernst, J. and Kellis, M. (2012) 'ChromHMM: automating chromatin state discovery and characterization', *Nat Methods*, 9(3), pp. 215–216. doi: 10.1038/nmeth.1906.

Ernst, J., Kheradpour, P., Mikkelsen, T. S., *et al.* (2011) 'Mapping and analysis of chromatin state dynamics in nine human cell types', *Nature*. Nature Publishing Group, 473(7345), pp. 43–49. doi: 10.1038/nature09906.

Evertts, A. G., Zee, B. M., Dimaggio, P. A., Gonzales-Cope, M., Coller, H. A. and Garcia, B. A. (2013) 'Quantitative dynamics of the link between cellular metabolism and histone acetylation', *Journal of Biological Chemistry*, 288(17), pp. 12142–12151. doi: 10.1074/jbc.M112.428318.

Ewaschuk, J. B., Diaz, H., Meddings, L., Diederichs, B., Dmytrash, A., Backer, J., Langen, M. L. and Madsen, K. L. (2008) 'Secreted bioactive factors from Bifidobacterium infantis enhance epithelial cell barrier function', *American journal of physiology: Gastrointestinal and liver physiology*, 295(5), pp. 1025–1034. doi: 10.1152/ajpgi.90227.2008.

Fachi, J. L., Felipe, J. de S., Pral, L. P., *et al.* (2019) 'Butyrate Protects Mice from Clostridium difficile-Induced Colitis through an HIF-1-Dependent Mechanism', *Cell Reports*, 27(3), pp. 750-761.e7. doi: 10.1016/j.celrep.2019.03.054.

Faubert, B., Boily, G., Izreig, S., *et al.* (2013) 'AMPK is a negative regulator of the warburg effect and suppresses tumor growth in vivo', *Cell Metabolism*. Elsevier, 17(1), pp. 113–124. doi: 10.1016/j.cmet.2012.12.001.

Feldman, J. L., Baeza, J. and Denu, J. M. (2013) 'Activation of the protein deacetylase SIRT6 by long-chain fatty acids and widespread deacylation by Mammalian Sirtuins', *Journal of Biological Chemistry*, 288(43), pp. 31350–31356. doi: 10.1074/jbc.C113.511261.

Fellows, R., Denizot, J., Stellato, C., *et al.* (2018) 'Microbiota derived short chain fatty acids promote histone crotonylation in the colon through histone deacetylases', *Nature Communications*. Springer US, 9(105), pp. 1–15. doi: 10.1038/s41467-017-02651-5.

Fellows, R. and Varga-Weisz, P. (2018) 'In vitro enzymatic assays of histone decrotonylation on recombinant histones', *Bio-Protocol*, 8(14), pp. 1–20. doi: 10.21769/bioprotoc.2924.

Ferreira-Halder, C. V., Faria, A. V. de S. and Andrade, S. S. (2017) 'Action and function of Faecalibacterium prausnitzii in health and disease', *Best Practice and Research: Clinical Gastroenterology*, 31(6), pp. 643–648. doi: 10.1016/j.bpg.2017.09.011.

Filippakopoulos, P. and Knapp, S. (2012) 'The bromodomain interaction module', *FEBS Letters*, 586(17), pp. 2692–2704. doi: 10.1016/j.febslet.2012.04.045.

Filippakopoulos, P., Picaud, S., Mangos, M., *et al.* (2012) 'Histone Recognition and Large-Scale Structural Analysis of the Human Bromodomain Family', *Cell*, 149(1), pp. 214–231. doi: 10.1016/j.cell.2012.02.013.

De Filippo, C., Cavalieri, D., Di Paola, M., Ramazzotti, M., Poullet, J. B., Massart, S., Collini, S., Pieraccini, G. and Lionetti, P. (2010) 'Impact of diet in shaping gut microbiota revealed by a comparative study in children from Europe and rural Africa', *Proceedings of the National Academy of Sciences*, 107(33), pp. 14691–14696. doi: 10.1073/pnas.1005963107.

Fischer, E. H., Graes, D. J., Snyder Crittenden, E. R. and Krebs, E. G. (1959) 'Structure of the site phosphorylated in the phosphorylase b to a reaction.', *The Journal of biological chemistry*, 234(7), pp. 1698–1704.

Flint, H. J., Scott, K. P., Louis, P. and Duncan, S. H. (2012) 'The role of the gut microbiota in nutrition and health', *Nature Reviews Gastroenterology & Hepatology*. Nature Publishing Group, 9(10), pp. 577–589. doi: 10.1038/nrgastro.2012.156.

Flynn, E. M., Huang, O. W., Poy, F., Oppikofer, M., Bellon, S. F., Tang, Y. and Cochran, A. G. (2015) 'A subset of human bromodomains recognizes butyryllysine and crotonyllysine histone peptide modifications', *Structure*. Elsevier, 23(10), pp. 1801–1814. doi: 10.1016/j.str.2015.08.004.

Fnu, S., Williamson, E. A., De Haro, L. P., Brenneman, M., Wray, J., Shaheen, M., Radhakrishnan, K., Lee, S. H., Nickoloff, J. A. and Hromas, R. (2011) 'Methylation of histone H3 lysine 36 enhances DNA repair by nonhomologous end-joining.', *Proceedings of the National Academy of Sciences of the United States of America*, 108(2), pp. 540–545. doi: 10.1073/pnas.1013571108.

Ford, E. and Thanos, D. (2010) 'The transcriptional code of human IFN-β gene expression', *Biochimica et Biophysica Acta - Gene Regulatory Mechanisms*. Elsevier B.V., 1799(3–4), pp. 328–336. doi: 10.1016/j.bbagrm.2010.01.010.

Frenkel, E. P. and Kitchens, R. L. (1977) 'Purification and properties of acetyl coenzyme A synthetase

from Bakers yeast', *The Journal of biological chemistry*, 252(2), pp. 504–507.

Friis, R. M. N., Wu, B. P., Reinke, S. N., Hockman, D. J., Sykes, B. D. and Schultz, M. C. (2009) 'A glycolytic burst drives glucose induction of global histone acetylation by picNuA4 and SAGA', *Nucleic Acids Research*, 37(12), pp. 3969–3980. doi: 10.1093/nar/gkp270.

Gallo, R. L. and Hooper, L. V. (2012) 'Epithelial antimicrobial defence of the skin and intestine', *Nature Reviews Immunology*. Nature Publishing Group, 12(7), pp. 503–516. doi: 10.1038/nri3228.

Gansen, A., Tóth, K., Schwarz, N. and Langowski, J. (2015) 'Opposing roles of H3- and H4-acetylation in the regulation of nucleosome structure - A FRET study', *Nucleic Acids Research*, 43(3), pp. 1433–1443. doi: 10.1093/nar/gku1354.

Gao, X., Wang, H., Jenny, J. Y., Liu, X. and Liu, Z.-R. (2012) 'Pyruvate kinase M2 regulates gene transcription by acting as a protein kinase', *Molecular Cell*, 45(5), pp. 598–609. doi: 10.1158/0008-5472.CAN-10-4002.BONE.

Gaucher, J., Boussouar, F., Montellier, E., *et al.* (2012) 'Bromodomain-dependent stage-specific male genome programming by Brdt', *EMBO Journal*, 31(19), pp. 3809–3820. doi: 10.1038/emboj.2012.233.

Ghanta, S., Grossmann, R. E. and Brenner, C. (2013) 'Mitochondrial protein acetylation as a cell-intrinsic, evolutionary driver of fat storage: Chemical and metabolic logic of acetyl-lysine modifications', *Critical Reviews in Biochemistry and Molecular Biology*, 48(6), pp. 561–574. doi: 10.3109/10409238.2013.838204.

Gill, S. R., Pop, M., Deboy, R. T., Eckburg, P. B., Turnbaugh, P. J., Samuel, B. S., Gordon, J. I., Relman, D. A., Fraser-Liggett, C. M. and Nelson, K. E. (2006) 'Metagenomic Analysis of the Human Distal Gut Microbiome', *Science*, 312(5778), pp. 1355–1359. doi: 10.1126/science.1124234.

Goodrich, J. K., Di Rienzi, S. C., Poole, A. C., Koren, O., Walters, W. A., Caporaso, J. G., Knight, R. and Ley, R. E. (2014) 'Conducting a microbiome study.', *Cell*. Elsevier Inc., 158(2), pp. 250–262. doi: 10.1016/j.cell.2014.06.037.

Goudarzi, A., Zhang, D., Huang, H., *et al.* (2016) 'Dynamic Competing Histone H4 K5K8 Acetylation and Butyrylation Are Hallmarks of Highly Active Gene Article Dynamic Competing Histone H4 K5K8 Acetylation and Butyrylation Are Hallmarks of Highly Active Gene Promoters', *Molecular Cell*. The Authors, 62(2), pp. 169–180. doi: 10.1016/j.molcel.2016.03.014.

Guccione, E., Hitchcock, A., Hall, S. J., Mulholland, F., Shearer, N., van Vliet, A. H. M. and Kelly, D. J. (2010) 'Reduction of fumarate, mesaconate and crotonate by Mfr, a novel oxygen-regulated periplasmic reductase in Campylobacter jejuni', *Environmental Microbiology*, 12(3), pp. 576–591. doi:

10.1111/j.1462-2920.2009.02096.x.

Guillemot, F. Ç., Colombel, J. F., Neut, C., Verplanck, N., Lecomte, M., Romond, C., Paris, J. C. and Cortot, A. (1991) 'Treatment of diversion colitis by short-chain fatty acids - Prospective and double-blind study', *Diseases of the Colon & Rectum*, 34(10), pp. 861–864. doi: 10.1007/BF02049697.

Gupta, A. P., Zhu, L., Tripathi, J., Kucharski, M., Patra, A. and Bozdech, Z. (2017) 'Histone 4 lysine 8 acetylation regulates proliferation and host-pathogen interaction in Plasmodium falciparum', *Epigenetics and Chromatin*. BioMed Central, 10(1), pp. 1–17. doi: 10.1186/s13072-017-0147-z.

Haberland, M., Montgomery, R. L. and Olson, E. N. (2009) 'The many roles of histone deacetylases in development and physiology: Implications for disease and therapy', *Nature Reviews Genetics*, 10(1), pp. 32–42. doi: 10.1038/nrg2485.

Hafner, V., Dai, J., Gomes, A. P., Xiao, C. Y., Palmeira, C. M. and Sinclair, D. A. (2010) 'Regulation of the mPTP by SIRT3-mediated deacetylation of CypD at lysine 166 suppresses age-related cardiac hypertrophy', *Aging*, 2(12), pp. 914–923. doi: 10.18632/aging.100252.

Hague, A., Manning, A. M., Hart, D., Paraskeva, C. and Huschtscha, L. I. (1993) 'Sodium butyrate induces apoptosis in human colonic tumour cell lines in a p53-independent pathway: Implications for the possible role of dietary fibre in the prevention of large bowel cancer', *International Journal of Cancer*, 55(3), pp. 498–505. doi: 10.1002/ijc.2910550329.

Halley, F., Reinshagen, J., Ellinger, B., *et al.* (2011) 'A Bioluminogenic HDAC Activity Assay: Validation and Screening', *Journal of Biomolecular Screening*, 16(10), pp. 1227–1235. doi: 10.1177/1087057111416004.

Han, Z., Wu, H., Kim, S., *et al.* (2018) 'Revealing the protein propionylation activity of the histone acetyltransferase MOF (males absent on the first)', *Journal of Biological Chemistry*, 293(9), pp. 3410–3420. doi: 10.1074/jbc.RA117.000529.

Hanahan, D. and Weinberg, R. A. (2011) 'Hallmarks of cancer: The next generation', *Cell*. Elsevier Inc., 144(5), pp. 646–674. doi: 10.1016/j.cell.2011.02.013.

Hansson, G. C. (2012) 'Role of mucus layers in gut infection and inflammation', *Current Opinion in Microbiology*, 15(1), pp. 57–62. doi: 10.1016/j.mib.2011.11.002.

Hardie, D. G. (2011) 'AMP-activated protein kinase-an energy sensor that regulates all aspects of cell function', *Genes and Development*, 25(18), pp. 1895–1908. doi: 10.1101/gad.17420111.

Harig, J. M., Soergel, K. H., Komorowski, R. A. and Wood, C. M. (1989) 'Treatment of diversion colitis

with short chain fatty acid irrigation', *The New England Journal of Medicine*, 320(1), pp. 23–28.

Harley, C. B. and Reynolds, R. P. (1987) 'Analysis of E coli promoters', *Nucleic Acids Research*, 15(5), pp. 2343–2361.

Hassan, A. H., Neely, K. E. and Workman, J. L. (2001) 'Histone acetyltransferase complexes stabilize SWI/SNF binding to promoter nucleosomes', *Cell*, 104(6), pp. 817–827. doi: 10.1016/S0092-8674(01)00279-3.

Hawkins, R. D., Hon, G. C., Lee, L. K., *et al.* (2010) 'Distinct epigenomic landscapes of pluripotent and lineage-committed human cells', *Cell stem cell*, 6(5), pp. 479–491. doi: 10.3899/jrheum.121180.

Hayakawa, T. and Nakayama, J. (2011) 'Physiological Roles of Class I HDAC Complex and Histone Demethylase', *Journal of Biomedicine and Biotechnology*, 2011(129383), pp. 1–10. doi: 10.1155/2011/129383.

Hayashi-Takanaka, Y., Maehara, K., Harada, A., Umehara, T., Yokoyama, S., Obuse, C., Ohkawa, Y., Nozaki, N. and Kimura, H. (2015) 'Distribution of histone H4 modifications as revealed by a panel of specific monoclonal antibodies', *Chromosome Research*, 23(4), pp. 753–766. doi: 10.1007/s10577-015-9486-4.

He, G., Shankar, R. A., Chzhan, M., Samouilov, A., Kuppusamy, P. and Zweier, J. L. (1999) 'Noninvasive measurement of anatomic structure and intraluminal oxygenation in the gastrointestinal tract of living mice with spatial and spectral EPR imaging', *Proceedings of the National Academy of Sciences*, 96(8), pp. 4586–4591. doi: 10.1073/pnas.96.8.4586.

Vander Heiden, M. G., Cantley, L. C. and Thompson, C. B. (2009) 'Understanding The Warburg Effect: The Metabolic Requirements of Cell Proliferation', *Science*, 324(5930), pp. 1029–1033. doi: 10.1126/science.1160809.

Vander Heiden, M. G., Locasale, J. W., Swanson, K. D., *et al.* (2010) 'Evidence for an alternative glycolytic pathway in rapidly proliferating cells', *Science*, 329(5998), pp. 1492–1499. doi: 10.1126/science.1188015.

Heintzman, N. D., Stuart, R. K., Hon, G., *et al.* (2007) 'Distinct and predictive chromatin signatures of transcriptional promoters and enhancers in the human genome', *Nature Genetics*, 39(3), pp. 311–318. doi: 10.1038/ng1966.

Helander, H. F. and Fandriks, L. (2014) 'Surface area of the digestive tract - revisited', *Gastrointestinal anatomy*, 49(6), pp. 681–689. doi: 10.3109/00365521.2014.898326.

Henkes, L. M., Haus, P., Jäger, F., Ludwig, J. and Meyer-Almes, F. J. (2012) 'Synthesis and biochemical analysis of 2,2,3,3,4,4,5,5,6,6,7,7-dodecafluoro- N-hydroxy-octanediamides as inhibitors of human histone deacetylases', *Bioorganic and Medicinal Chemistry*. Elsevier Ltd, 20(2), pp. 985–995. doi: 10.1016/j.bmc.2011.11.041.

Hirschey, M. D., Shimazu, T., Jing, E., *et al.* (2011) 'SIRT3 deficiency and mitochondrial protein hyperacetylation accelerate the development of the metabolic syndrome', *Molecular Cell*, 44(2), pp. 177–190. doi: 10.1016/j.molcel.2011.07.019.

Hoffmann, K., Brosch, G., Loidl, P. and Jung, M. (1999) 'A non-isotopic assay for histone deacetylase activity.', *Nucleic acids research*, 27(9), pp. 2057–8. doi: 10.1093/nar/27.9.2057.

Howe, F. S., Fischl, H., Murray, S. C. and Mellor, J. (2017) 'Is H3K4me3 instructive for transcription activation?', *BioEssays*, 39(1), pp. 1–12. doi: 10.1002/bies.201600095.

Huang, H., Luo, Z., Qi, S., *et al.* (2018) 'Landscape of the regulatory elements for lysine 2-hydroxyisobutyrylation pathway', *Cell Research*. Nature Publishing Group, 28(1), pp. 111–125. doi: 10.1038/cr.2017.149.

Huang, H., Tang, S., Ji, M., *et al.* (2018) 'EP300-Mediated Lysine 2-Hydroxyisobutyrylation Regulates Glycolysis', *Molecular Cell*. Elsevier Inc., 70(4), pp. 663-678.e6. doi: 10.1016/j.molcel.2018.04.011.

Huang, H., Wang, D. L. and Zhao, Y. (2018) 'Quantitative Crotonylome Analysis Expands the Roles of p300 in the Regulation of Lysine Crotonylation Pathway', *Proteomics*, 18(15), pp. 1–8. doi: 10.1002/pmic.201700230.

Huang, H., Zhang, D., Wang, Y., Perez-Neut, M., Han, Z., Zheng, Y. G., Hao, Q. and Zhao, Y. (2018) 'Lysine benzoylation is a histone mark regulated by SIRT2', *Nature Communications*. Springer US, 9(1). doi: 10.1038/s41467-018-05567-w.

Hyun, K., Jeon, J., Park, K. and Kim, J. (2017) 'Writing, erasing and reading histone lysine methylations', *Experimental and Molecular Medicine*. Nature Publishing Group, 49(4). doi: 10.1038/emm.2017.11.

Igarashi, H., Ohno, K., Matsuki, N., Aki, F.-I., Kanemoto, H., Fukushima, K., Uchida, K. and Tsuijimoto, H. (2017) 'Analysis of fecal short chain fatty acid concentration in miniature dachshunds with inflammatory colorectal polyps', *Journal of Veterinary Medical Science*, 79(10), pp. 1727–1734. doi: 10.1292/jvms.17-0165.

Ishiguro, T., Tanabe, K., Kobayashi, Y., Mizumoto, S., Kanai, M. and Kawashima, S. A. (2018) 'Malonylation of histone H2A at lysine 119 inhibits Bub1-dependent H2A phosphorylation and chromosomal localization of shugoshin proteins', *Scientific Reports*, 8(1), pp. 1–10. doi:

10.1038/s41598-018-26114-z.

Issaeva, I., Zonis, Y., Rozovskaia, T., Orlovsky, K., Croce, C. M., Nakamura, T., Mazo, A., Eisenbach, L. and Canaani, E. (2007) 'Knockdown of ALR (MLL2) Reveals ALR Target Genes and Leads to Alterations in Cell Adhesion and Growth', *Molecular and Cellular Biology*, 27(5), pp. 1889–1903. doi: 10.1128/mcb.01506-06.

Jamai, A., Imoberdorf, R. M. and Strubin, M. (2007) 'Continuous Histone H2B and Transcription-Dependent Histone H3 Exchange in Yeast Cells outside of Replication', *Molecular Cell*, 25(3), pp. 345–355. doi: 10.1016/j.molcel.2007.01.019.

Jasencakova, Z., Scharf, A. N. D., Ask, K., Corpet, A., Imhof, A., Almouzni, G. and Groth, A. (2010) 'Replication Stress Interferes with Histone Recycling and Predeposition Marking of New Histones', *Molecular Cell*, 37(5), pp. 736–743. doi: 10.1016/j.molcel.2010.01.033.

Jiang, G., Nguyen, D., Archin, N. M., *et al.* (2018) 'HIV latency is reversed by ACSS2-driven histone crotonylation', *Journal of Clinical Investigation*, 128(3), pp. 1190–1198. doi: 10.1172/jci98071.

Jiang, H., Khan, S., Wang, Y., *et al.* (2013) 'SIRT6 regulates TNF-α secretion through hydrolysis of long-chain fatty acyl lysine', *Nature*. Nature Publishing Group, 496(7443), pp. 110–113. doi: 10.1038/nature12038.

Jin, Q., Yu, L. R., Wang, L., Zhang, Z., Kasper, L. H., Lee, J. E., Wang, C., Brindle, P. K., Dent, S. Y. R. and Ge, K. (2011) 'Distinct roles of GCN5/PCAF-mediated H3K9ac and CBP/p300-mediated H3K18/27ac in nuclear receptor transactivation', *EMBO Journal*. Nature Publishing Group, 30(2), pp. 249–262. doi: 10.1038/emboj.2010.318.

Jurica, M. S., Mesecar, A., Health, P. J., Shi, W., Nowak, T. and Stoddard, B. L. (1997) 'The allosteric regulation of pyruvate kinase by fructose-1,6-bisphosphate', *Structure*, 6(1), pp. 195–210. doi: 10.1371/journal.pone.0189138.

Kabani, M., Michot, K., Boschiero, C. and Werner, M. (2005) 'Anc1 interacts with the catalytic subunits of the general transcription factors TFIID and TFIIF, the chromatin remodeling complexes RSC and INO80, and the histone acetyltransferase complex NuA3', *Biochemical and Biophysical Research Communications*, 332(2), pp. 398–403. doi: 10.1016/j.bbrc.2005.04.158.

Kabat, A. M., Srinivasan, N. and Maloy, K. J. (2014) 'Modulation of immune development and function by intestinal microbiota', *Trends in Immunology*. Elsevier Ltd, 35(11), pp. 507–517. doi: 10.1016/j.it.2014.07.010.

Kaczmarska, Z., Ortega, E., Goudarzi, A., Huang, H., Kim, S., Márquez, J. A., Zhao, Y., Khochbin, S. and

Panne, D. (2017) 'Structure of p300 in complex with acyl-CoA variants', *Nature Chemical Biology*. Nature Publishing Group, 13(1), pp. 21–29. doi: 10.1038/nchembio.2217.

Kaiko, G. E., Ryu, S. H., Koues, O. I., Collins, P. L., Solnica-Krezel, L., Pearce, E. J., Pearce, E. L., Oltz, E. M. and Stappenbeck, T. S. (2016) 'The Colonic Crypt Protects Stem Cells from Microbiota-Derived Metabolites', *Cell*. Elsevier Inc., 165, pp. 1708–1720. doi: 10.1016/j.cell.2016.05.018.

Karhausen, J., Furuta, G. T., Tomaszewski, J. E., Johnson, R. S., Colgan, S. P. and Haase, V. H. (2004) 'Epithelial hypoxia-inducible factor-1 is protective in murine experimental colitis', *Journal of Clinical Investigation*, 114(8), pp. 1098–1106. doi: 10.1172/JCI200421086.

Kassam, Z., Lee, C. H., Yuan, Y. and Hunt, R. H. (2013) 'Fecal microbiota transplantation for Clostridium difficile infection: systematic review and meta-analysis', *American journal of gastroenterology*, 108(4), pp. 500–508. doi: 10.1038/ajg.2013.59.

Kebede, A. F., Nieborak, A., Shahidian, L. Z., *et al.* (2017) 'Histone propionylation is a mark of active chromatin', *Nature Structural and Molecular Biology*, 24(12), pp. 1048–1056. doi: 10.1038/nsmb.3490.

Kelly, C. J., Zheng, L., Campbell, E. L., *et al.* (2016) 'Crosstalk between microbiota derived short chain fatty acids and intestinal epithelial HIF augments tissue barrier function', *Cell Host and Microbe*, 17(5), pp. 662–671. doi: 10.1016/j.chom.2015.03.005.

Kelly, R. D. W., Chandru, A., Watson, P. J., *et al.* (2018) 'Histone deacetylase (HDAC) 1 and 2 complexes regulate both histone acetylation and crotonylation in vivo', *Scientific Reports*, 8(1), pp. 1–10. doi: 10.1038/s41598-018-32927-9.

Khersonsky, O. and Tawfik, D. S. (2010) 'Enzyme Promiscuity: A Mechanistic and Evolutionary Perspective', *Annual Review of Biochemistry*, 79(1), pp. 471–505. doi: 10.1146/annurev-biochem-030409-143718.

Kim, T. and Buratowski, S. (2009) 'Dimethylation of H3K4 by Set1 recruits the Set3 histone', *Cell*, 137(2), pp. 259–272. doi: 10.1016/j.cell.2009.02.045.

Kimura, A., Umehara, T. and Horikoshi, M. (2002) 'Chromosomal gradient of histone acetylation established by Sas2p and Sir2p functions as a shield against gene silencing', *Nature Genetics*, 32(3), pp. 370–377. doi: 10.1038/ng993.

Kleer, C. G., Cao, Q., Varambally, S., *et al.* (2003) 'EZH2 is a marker of aggressive breast cancer and promotes neoplastic transformation of breast epithelial cells', *Proceedings of the National Academy of Sciences of the United States of America*, 100(20), pp. 11606–11611. doi:

10.1073/pnas.1933744100.

Koh, A., De Vadder, F., Kovatcheva-Datchary, P. and Bäckhed, F. (2016) 'From dietary fiber to host physiology: Short-chain fatty acids as key bacterial metabolites', *Cell*, 165(6), pp. 1332–1345. doi: 10.1016/j.cell.2016.05.041.

Korem, T., Zeevi, D., Zmora, N., *et al.* (2017) 'Bread Affects Clinical Parameters and Induces Gut Microbiome-Associated Personal Glycemic Responses.', *Cell metabolism*. Elsevier Inc., 25(6), pp. 1243-1253.e5. doi: 10.1016/j.cmet.2017.05.002.

Kramer, O. H., Zhu, P., Ostendorff, H. P., *et al.* (2003) 'The histone deacetylase inhibitor valproic acid selectively induces proteasomal degradation of HDAC2', *EMBO Journal*, 22(13), pp. 3411–3420. doi: 10.1093/emboj/cdg315.

Krasnov, A. N., Mazina, M. Y., Nikolenko, J. V. and Vorobyeva, N. E. (2016) 'On the way of revealing coactivator complexes cross-talk during transcriptional activation', *Cell and Bioscience*. BioMed Central, 6(1), pp. 1–14. doi: 10.1186/s13578-016-0081-y.

Krautkramer, K. A., Kreznar, J. H., Romano, K. A., Vivas, E. I., Barrett-Wilt, G. A., Rabaglia, M. E., Keller, M. P., Attie, A. D., Rey, F. E. and Denu, J. M. (2016) 'Diet-microbiota interactions mediate global epigenetic programming in multiple host tissues', *Molecular Cell*. Elsevier, 64(5), pp. 982–992. doi: 10.1016/j.molcel.2016.10.025.

Krautkramer, K. A., Rey, F. E. and Denu, J. M. (2017) 'Chemical signaling between gut microbiota and host chromatin: What is your gut really saying?', *Journal of Biological Chemistry*, 292(21), pp. 8582–8593. doi: 10.1074/jbc.R116.761577.

Krishnan, V., Chow, M. Z. Y., Wang, Z., Zhang, L., Liu, B., Liu, X. and Zhou, Z. (2011) 'Histone H4 lysine 16 hypoacetylation is associated with defective DNA repair and premature senescence in Zmpste24-deficient mice', *Proceedings of the National Academy of Sciences of the United States of America*, 108(30), pp. 12325–12330. doi: 10.1073/pnas.1102789108.

Kundu, P., Blacher, E., Elinav, E. and Pettersson, S. (2017) 'Our Gut Microbiome: The Evolving Inner Self.', *Cell*. Elsevier Inc., 171(7), pp. 1481–1493. doi: 10.1016/j.cell.2017.11.024.

Kuo, M., Brownell, J. E., Sobel, R. E., Ranalli, T. A., Cook, R. G., Edmondson, D. G., Roth, S. Y. and Allis, C. D. (1996) 'Transcription-linked acetylation by Gcn5p of histones H3 and H4 at specific lysines', *Nature*, 383, pp. 269–272.

Laffel, L. (1999) 'Ketone bodies: a review of physiology, pathophysiology and application of monitoring to diabetes.', *Diabetes/metabolism research and reviews*, 15(6), pp. 412–426. doi: 10.1002/(SICI)1520-

7560(199911/12)15:6<412::AID-DMRR72>3.0.CO;2-8.

Lange, M., Kaynak, B., Forster, U. B., *et al.* (2008) 'Regulation of muscle development by DPF3, a novel histone acetylation and methylation reader of the BAF chromatin remodeling complex', *Genes and Development*, 22(17), pp. 2370–2384. doi: 10.1101/gad.471408.

Langer, M. R., Fry, C. J., Peterson, C. L. and Denu, J. M. (2002) 'Modulating acetyl-CoA binding in the GCN5 family of histone acetyltransferases', *Journal of Biological Chemistry*, 277(30), pp. 27337–27344. doi: 10.1074/jbc.M203251200.

Längst, G. and Manelyte, L. (2015) 'Chromatin remodelers: From function to dysfunction', *Genes*, 6(2), pp. 299–324. doi: 10.3390/genes6020299.

Lee, J. V., Haas, N. B., Venneti, S., *et al.* (2014) 'Akt-Dependent Metabolic Reprogramming Regulates Tumor Cell Histone Acetylation', *Cell Metabolism*. Elsevier Inc., 20(2), pp. 306–319. doi: 10.1016/j.cmet.2014.06.004.

Leemhuis, H., Nightingale, K. P. and Hollfelder, F. (2008) 'Directed evolution of a histone acetyltransferase - Enhancing thermostability, whilst maintaining catalytic activity and substrate specificity', *FEBS Journal*, 275(22), pp. 5635–5647. doi: 10.1111/j.1742-4658.2008.06689.x.

Leemhuis, H., Packman, L. C., Nightingale, K. P. and Hollfelder, F. (2008) 'The Human Histone Acetyltransferase P/CAF is a Promiscuous Histone Propionyltransferase', *ChemBioChem*, 9(4), pp. 499–503. doi: 10.1002/cbic.200700556.

Lenich, A. C. and Goodman, S. I. (1986) 'The purification and characterization of glutaryl-coenzyme A dehydrogenase from porcine and human liver', *Journal of Biological Chemistry*, 261(9), pp. 4090–4096.

Levrat, M.-A., Remesy, C. and Demigne, C. (1991) 'High propionic acid fermentations and mineral accumulation in the cecum of rats adapted to different levels of inulin', *The Journal of Nutrition*, 121(11), pp. 1730–1737.

Ley, R. E., Lozupone, C. A., Hamady, M., Knight, R. and Gordon, J. I. (2008) 'Worlds within worlds: evolution of the vertebrate gut microbiota', *Nature Reviews Microbiology*, 6(10), pp. 776–788. doi: 10.1038/nrmicro1978.

Ley, R. E., Peterson, D. A. and Gordon, J. I. (2006) 'Ecological and evolutionary forces shaping microbial diversity in the human intestine', *Cell*, 124(4), pp. 837–848. doi: 10.1016/j.cell.2006.02.017.

Li, L., Shi, Lan, Yang, S., *et al.* (2016) 'SIRT7 is a histone desuccinylase that functionally links to chromatin compaction and genome stability', *Nature Communications*. Nature Publishing Group, 7,

pp. 1–17. doi: 10.1038/ncomms12235.

Li, Q. L., Wang, D. Y., Ju, L. G., Yao, J., Gao, C., Lei, P. J., Li, L. Y., Zhao, X. L. and Wu, M. (2019) 'The hyper-activation of transcriptional enhancers in breast cancer', *Clinical Epigenetics*. Clinical Epigenetics, 11(1), pp. 1–17. doi: 10.1186/s13148-019-0645-x.

Li, X., Corsa, C. A. S., Pan, P. W., Wu, L., Ferguson, D., Yu, X., Min, J. and Dou, Y. (2010) 'MOF and H4 K16 Acetylation Play Important Roles in DNA Damage Repair by Modulating Recruitment of DNA Damage Repair Protein Mdc1', *Molecular and Cellular Biology*, 30(22), pp. 5335–5347. doi: 10.1128/mcb.00350-10.

Li, Y., Sabari, B. R., Panchenko, T., *et al.* (2016) 'Molecular Coupling of Histone Crotonylation and Active Transcription by AF9 YEATS Domain', *Molecular Cell*. Elsevier Inc., 62(2), pp. 181–193. doi: 10.1016/j.molcel.2016.03.028.

Li, Y., Wen, H., Xi, Y., *et al.* (2014) 'AF9 YEATS Domain Links Histone Acetylation to DOT1L-Mediated H3K79 Methylation', *Cell*, 159(3), pp. 558–571. doi: 10.1002/cyto.a.20594.

Li, Y., Xu, S., Mihaylova, M. M., *et al.* (2011) 'AMPK Phosphorylates and Inhibits SREBP Activity to Attenuate Hepatic Steatosis and Atherosclerosis in Diet-Induced Insulin-Resistant Mice', *Cell Metabolism*, 13(4), pp. 376–388. doi: 10.1016/j.cmet.2011.03.009.

Liu, S., Yu, H., Liu, Y., *et al.* (2017) 'Chromodomain Protein CDYL Acts as a Crotonyl-CoA Hydratase to Regulate Histone Crotonylation and Spermatogenesis', *Molecular Cell*. Elsevier Inc., 67(5), pp. 853–866. doi: 10.1016/j.molcel.2017.07.011.

Liu, X., Cooper, D. E., Cluntun, A. A., Warmoes, M. O., Zhao, S., Reid, M. A., Liu, J., Wellen, K. E., Kirsch, D. G. and Locasale, J. W. (2018) 'De novo acetate production is coupled to central carbon metabolism in mammals', *bioRxiv*, pp. 1–27. doi: 10.1017/CBO9781107415324.004.

Liu, X., Wei, W., Liu, Y., *et al.* (2017) 'MOF as an evolutionarily conserved histone crotonyltransferase and transcriptional activation by histone acetyltransferase-deficient and crotonyltransferase-competent CBP/p300', *Cell Discovery*. Nature Publishing Group, 3(17016). doi: 10.1038/celldisc.2017.16.

Liu, Y., Li, M., Fan, M., *et al.* (2018) 'Chromodomain Y-like Protein–Mediated Histone Crotonylation Regulates Stress-Induced Depressive Behaviors', *Biological Psychiatry*. Elsevier Inc, (11), pp. 1–15. doi: 10.1016/j.biopsych.2018.11.025.

Lo, Y.-H., Chung, E., Li, Z., *et al.* (2017) 'Transcriptional Regulation by ATOH1 and its Target SPDEF in the Intestine', *Cellular and Molecular Gastroenterology and Hepatology*, 3(1), pp. 51–71. doi:

10.1016/j.jcmgh.2016.10.001.

Locasale, J. W. and Cantley, L. C. (2011) 'Metabolic flux and the regulation of mammalian cell growth', *Cell Metabolism*, 14(4), pp. 443–451. doi: 10.1016/j.cmet.2011.07.014.

Louis, P. and Flint, H. J. (2009) 'Diversity, metabolism and microbial ecology of butyrate-producing bacteria from the human large intestine', *FEMS Microbiology Letters*, 294(1), pp. 1–8. doi: 10.1111/j.1574-6968.2009.01514.x.

Love, M. I., Huber, W. and Anders, S. (2014) 'Moderated estimation of fold change and dispersion for RNA-seq data with DESeq2', *Genome Biology*, 15(12), pp. 1–21. doi: 10.1186/s13059-014-0550-8.

Loyola, A., Bonaldi, T., Roche, D., Imhof, A. and Almouzni, G. (2006) 'PTMs on H3 Variants before Chromatin Assembly Potentiate Their Final Epigenetic State', *Molecular Cell*, 24(2), pp. 309–316. doi: 10.1016/j.molcel.2006.08.019.

Lu, Y., Xu, Q., Liu, Y., Yu, Y., Cheng, Z.-Y., Zhao, Y. and Zhou, D.-X. (2018) 'Dynamics and functional interplay of histone lysine butyrylation, crotonylation, and acetylation in rice under starvation and submergence', *Genome Biology*. Genome Biology, 19(1), pp. 1–14. doi: 10.1186/s13059-018-1533-y.

Luciano, L., Hass, R., Busche, R., Engelhardt, W. V. and Reale, E. (1996) 'Withdrawal of butyrate from the colonic mucosa triggers "mass apoptosis" primarily in the G0/G1 phase of the cell cycle', *Cell and Tissue Research*, 286(1), pp. 81–92. doi: 10.1007/s004410050677.

Lynch, S. V. and Pedersen, O. (2016) 'The human intestinal microbiome in health and disease', *New England Journal of Medicine*, 375(24), pp. 2369–2379. doi: 10.1056/nejmra1600266.

Macia, L., Tan, J., Vieira, A. T., *et al.* (2015) 'Metabolite-sensing receptors GPR43 and GPR109A facilitate dietary fibre-induced gut homeostasis through regulation of the inflammasome', *Nature Communications*. Nature Publishing Group, 6, pp. 1–15. doi: 10.1038/ncomms7734.

Madsen, A. S. and Olsen, C. A. (2012) 'Profiling of substrates for zinc-dependent lysine deacylase enzymes: HDAC3 exhibits decrotonylase activity in vitro', *Angewandte Chemie - International Edition*, 51(36), pp. 9083–9087. doi: 10.1002/anie.201203754.

Mahana, D., Trent, C. M., Kurtz, Z. D., Bokulich, N. A., Battaglia, T., Chung, J., Müller, C. L., Li, H., Bonneau, R. A. and Blaser, M. J. (2016) 'Antibiotic perturbation of the murine gut microbiome enhances the adiposity, insulin resistance, and liver disease associated with high-fat diet', *Genome Medicine*. Genome Medicine, 8(1), pp. 1–20. doi: 10.1186/s13073-016-0297-9.

Martin, C. and Zhang, Y. (2005) 'The diverse functions of histone lysine methylation', *Nature Reviews*

Molecular Cell Biology, 6(11), pp. 838–849. doi: 10.1038/nrm1761.

McCabe, M. T., Mohammad, H. P., Barbash, O. and Kruger, R. G. (2017) 'Targeting Histone Methylation in Cancer', *Cancer Journal (United States)*, 23(5), pp. 292–301. doi: 10.1097/PPO.0000000000000283.

McDonnel, E., Crown, S. B., Fox, S. b, Kitir, B., Ilkayeva, O. R., Olsen, C. A., Grimsrud, P. A. and Hirschey, M. D. (2016) 'Lipids repogram metabolism to become a major carbon source for histone acetylation', *Cell reports*, 17(6), pp. 1463–1472. doi: 10.1016/j.celrep.2016.10.012.

McIntyre, A., Gibson, P. R. and Young, G. P. (1993) 'Butyrate production from dietary fibre and protection against large bowel cancer in a rat model', *Gut*, 34(3), pp. 386–391. doi: 10.1136/gut.34.3.386.

McLoughlin, K., Schluter, J., Rakoff-Nahoum, S., Smith, A. L. and Foster, K. R. (2016) 'Host Selection of Microbiota via Differential Adhesion', *Cell Host and Microbe*. Elsevier Inc., 19(4), pp. 550–559. doi: 10.1016/j.chom.2016.02.021.

Meier, K. and Brehm, A. (2014) 'Chromatin regulation: How complex does it get?', *Epigenetics*, 9(11), pp. 1485–1495. doi: 10.4161/15592294.2014.971580.

Mellor, J. (2016) 'The molecular basis of metabolic cycles and their relationship to circadian rhythms', *Nature Structural and Molecular Biology*. Nature Publishing Group, 23(12), pp. 1035–1044. doi: 10.1038/nsmb.3311.

Mentch, S. J., Mehrmohamadi, M., Huang, L., *et al.* (2015) 'Histone Methylation Dynamics and Gene Regulation Occur through the Sensing of One-Carbon Metabolism', *Cell Metabolism*, 22(5), pp. 861–873. doi: 10.1016/j.cmet.2015.08.024.

Metallo, C. M. and Vander Heiden, M. G. (2013) 'Understanding metabolic regulation and its influence on cell physiology', *Molecular Cell*, 49(3), pp. 388–398. doi: 10.1016/j.molcel.2013.01.018.

Mi, H., Muruganujan, A., Ebert, D., Huang, X. and Thomas, P. D. (2019) 'PANTHER version 14: More genomes, a new PANTHER GO-slim and improvements in enrichment analysis tools', *Nucleic Acids Research*. Oxford University Press, 47(D1), pp. D419–D426. doi: 10.1093/nar/gky1038.

Mikkelsen, T. S., Ku, M., Jaffe, D. B., *et al.* (2007) 'Genome-wide maps of chromatin state in pluripotent and lineage-committed cells', *Nature*, 448(7153), pp. 553–560. doi: 10.1038/nature06008.

Miller, K. M., Tjeertes, J. V., Coates, J., Legube, G., Polo, S. E., Britton, S. and Jackson, S. P. (2010) 'Human HDAC1 and HDAC2 function in the DNA-damage response to promote DNA nonhomologous end-joining', *Nature Structural and Molecular Biology*. Nature Publishing Group, 17(9), pp. 1144–1151.

doi: 10.1038/nsmb.1899.

Montellier, E., Rousseaux, S., Zhao, Y. and Khochbin, S. (2012) 'Histone crotonylation specifically marks the haploid male germ cell gene expression program: Post-meiotic male-specific gene expression', *BioEssays*, 34(3), pp. 187–193. doi: 10.1002/bies.201100141.

Montgomery, D. C., Sorum, A. W. and Meier, J. L. (2014) 'Chemoproteomic profiling of lysine acetyltransferases highlights an expanded landscape of catalytic acetylation', *Journal of the American Chemical Society*, 136(24), pp. 8669–8676. doi: 10.1021/ja502372j.

Montiel, M.-D., Krzewinski-Recchi, M.-A., Delannoy, P. and Harduin-Lepers, A. (2003) 'Molecular cloning, gene organization and expression of the human UDP-GalNAc:Neu5Acalpha2-3Galbeta-R beta1,4-N-acetylgalactosaminyltransferase responsible for the biosynthesis of the blood group Sda/Cad antigen: evidence for an unusual extended cytoplasmic', *Biochemical Journal*, 373(2), pp. 369–379. doi: 10.1042/bj20021892.

Moore, L. C., Horowitz, S. B. and Paine, P. L. (1975) 'Nuclear envelope permeability', *Nature*, 254(5496), pp. 109–14. Available at: http://www.ncbi.nlm.nih.gov/entrez/query.fcgi?cmd=Retrieve&db=PubMed&dopt=Citation&list_uids=1117994.

Morinière, J., Rousseaux, S., Steuerwald, U., *et al.* (2009) 'Cooperative binding of two acetylation marks on a histone tail by a single bromodomain', *Nature*, 461(7264), pp. 664–668. doi: 10.1038/nature08397.

Mujtaba, S., He, Y., Zeng, L., Farooq, A., Carlson, J. E., Ott, M., Verdin, E. and Zhou, M. M. (2002) 'Structural basis of lysine-acetylated HIV-1 Tat recognition by PCAF bromodomain', *Molecular Cell*. Cell Press, 9(3), pp. 575–586. doi: 10.1016/S1097-2765(02)00483-5.

Murray, S. C., Lorenz, P., Howe, F. S., *et al.* (2019) 'H3K4me3 is neither instructive for, nor informed by, transcription', *bioRxiv*, p. 709014. doi: 10.1101/709014.

Musselman, C. A., Khorasanizadeh, S. and Kutateladze, T. G. (2014) 'Towards understanding methyllysine readout', *Biochimica et Biophysica Acta*, 1839(8), pp. 686–693. doi: 10.1016/j.physbeh.2017.03.040.

Musso, G., Gambino, R. and Cassader, M. (2011) 'Interactions Between Gut Microbiota and Host Metabolism Predisposing to Obesity and Diabetes', *Annual Review of Medicine*, 62(1), pp. 361–380. doi: 10.1146/annurev-med-012510-175505.

Napolitano, L. M. and Edmiston, C. E. (2017) 'Clostridium difficile disease: Diagnosis, pathogenesis,

and treatment update', *Surgery (United States)*. Elsevier Inc., 162(2), pp. 325–348. doi: 10.1016/j.surg.2017.01.018.

Neto, F. T. L., Bach, P. V., Najari, B. B., Li, P. S. and Goldstein, M. (2016) 'Spermatogenesis in humans and its affecting factors', *Seminars in Cell and Developmental Biology*. Elsevier Ltd, 59, pp. 10–26. doi: 10.1016/j.semcdb.2016.04.009.

Nicholson, J. K., Holmes, E., Kinross, J., Burcelin, R., Gibson, G., Jia, W. and Pettersson, S. (2012) 'Host-gut Metabolic Interactions', *Science*, 336(June), pp. 1262–1268. doi: 10.1126/science.1223813.

Nishitsuji, K., Xiao, J., Nagatomo, R., Umemoto, H., Morimoto, Y., Akatsu, H., Inoue, K. and Tsuneyama, K. (2017) 'Analysis of the gut microbiome and plasma short-chain fatty acid profiles in a spontaneous mouse model of metabolic syndrome', *Scientific Reports*. Springer US, 7(1), pp. 1–10. doi: 10.1038/s41598-017-16189-5.

Nord, A. S., Blow, M. J., Attanasio, C., *et al.* (2013) 'Rapid and pervasive changes in genome-wide enhancer usage during mammalian development', *Cell*. Elsevier, 155(7), pp. 1521–1531. doi: 10.1016/j.cell.2013.11.033.

van Nuland, R., Schram, A. W., van Schaik, F. M. A., Jansen, P. W. T. C., Vermeulen, M. and Marc Timmers, H. T. (2013) 'Multivalent engagement of TFIID to nucleosomes.', *PloS one*, 8(9). doi: 10.1371/journal.pone.0073495.

Oakhill, J. S., Steel, R., Chen, Z., Scott, J. W., Ling, N., Tam, S. and Kemp, B. E. (2011) 'AMPK Is a Direct Adenylate', *Science*, 1433(June), pp. 2008–2011. doi: 10.1126/science.1200094.

Oden, K. L. and Clarke, S. (1983) 'S-Adenosyl-L-methionine Synthetase from Human Erythrocytes: Role in the Regulation of Cellular S-Adenosylmethionine Levels', *Biochemistry*, 22(12), pp. 2978–2986. doi: 10.1021/bi00281a030.

Ogiwara, H., Ui, A., Otsuka, A., Satoh, H., Yokomi, I., Nakajima, S., Yasui, A., Yokota, J. and Kohno, T. (2011) 'Histone acetylation by CBP and p300 at double-strand break sites facilitates SWI/SNF chromatin remodeling and the recruitment of non-homologous end joining factors', *Oncogene*, 30(18), pp. 2135–2146. doi: 10.1038/onc.2010.592.

Pace, N. R. (2001) 'The universal nature of biochemistry', *PNAS*, 98(3), pp. 805–808.

Parira, T., Figueroa, G., Laverde, A., Casteleiro, G., Gomez Hernandez, M. E., Fernandez-Lima, F. and Agudelo, M. (2017) 'Novel detection of post-translational modifications in human monocyte-derived dendritic cells after chronic alcohol exposure: Role of inflammation regulator H4K12ac', *Scientific Reports*. Springer US, 7(1), pp. 1–14. doi: 10.1038/s41598-017-11172-6.

Park, J., Chen, Y., Tishkoff, D. X., *et al.* (2013) 'SIRT5-Mediated Lysine Desuccinylation Impacts Diverse Metabolic Pathways', *Molecular Cell*. Elsevier Inc., 50(6), pp. 919–930. doi: 10.1016/j.molcel.2013.06.001.

Paschos, G. K. and FitzGerald, G. A. (2017) 'Circadian clocks and metabolism: implications for microbiome and aging', *Trends in Genetics*. Elsevier Ltd, 33(10), pp. 760–769. doi: 10.1016/j.tig.2017.07.010.

Pedicord, V. A., Lockhart, A. A. K., Rangan, K. J., Craig, J. W., Loschko, J., Rogoz, A., Hang, H. C. and Mucida, D. (2016) 'Exploiting a host-commensal interaction to promote intestinal barrier function and enteric pathogen tolerance', *Science Immunology*, 1(3). doi: 10.1126/sciimmunol.aai7732.

Pekowska, A., Benoukraf, T., Zacarias-Cabeza, J., Belhocine, M., Koch, F., Holota, H., Imbert, J., Andrau, J. C., Ferrier, P. and Spicuglia, S. (2011) 'H3K4 tri-methylation provides an epigenetic signature of active enhancers', *EMBO Journal*, 30(20), pp. 4198–4210. doi: 10.1038/emboj.2011.295.

Peng, C., Lu, Z., Xie, Z., *et al.* (2011) 'The First Identification of Lysine Malonylation Substrates and Its Regulatory Enzyme', *Molecular & Cellular Proteomics*, 10(12), p. M111.012658. doi: 10.1074/mcp.m111.012658.

Pennacchio, L. A., Bickmore, W., Dean, A., Nobrega, M. A. and Bejerano, G. (2015) 'Enhancers: five essential questions', *Nature Reviews Genetics*, 14(4), pp. 288–295. doi: 10.1038/nrg3458.

Pfister, S. X., Ahrabi, S., Zalmas, L. P., *et al.* (2006) 'SETD2-Dependent Histone H3K36 Trimethylation Is Required for Homologous Recombination Repair and Genome Stability', *Cell Reports*, 7(6), pp. 2006–2018. doi: 10.1016/j.celrep.2014.05.026.

Phillips, D. M. P. (1963) 'The presence of acetyl groups in histones', *Biochemical journal*, 87, pp. 258–263. doi: 10.1016/0304-4165(65)90032-2.

Pietrocola, F., Galluzzi, L., Bravo-San Pedro, J. M., Madeo, F. and Kroemer, G. (2015) 'Acetyl coenzyme A: A central metabolite and second messenger', *Cell Metabolism*, 21(6), pp. 805–821. doi: 10.1016/j.cmet.2015.05.014.

Pomare, E. W., Branch, W. J. and Cummings, J. H. (1985) 'Carbohydrate fermentation in the human colon and its relation to acetate concentrations in venous blood', *Journal of Clinical Investigation*, 75(5), pp. 1448–1454. doi: 10.1172/JCI111847.

Pougovkina, O., te Brinke, H., Wanders, R. J. A., Houten, S. M. and de Boer, V. C. J. (2014) 'Aberrant protein acylation is a common observation in inborn errors of acyl-CoA metabolism', *Journal of Inherited Metabolic Disease*, 37(5), pp. 709–714. doi: 10.1007/s10545-014-9684-9.

Powell, D. W., Pinchuk, I. V., Saada, J. I., Chen, X. and Mifflin, R. C. (2011) 'Mesenchymal Cells of the Intestinal Lamina Propria', *Annual Review of Physiology*, 73(1), pp. 213–237. doi: 10.1146/annurev.physiol.70.113006.100646.

Probst, A. V., Dunleavy, E. and Almouzni, G. (2009) 'Epigenetic inheritance during the cell cycle', *Nature Reviews Molecular Cell Biology*, 10(3), pp. 192–206. doi: 10.1038/nrm2640.

Qin, Y., Roberts, J. D., Grimm, S. A., Lih, F. B., Deterding, L. J., Li, R., Chrysovergis, K. and Wade, P. A. (2018) 'An obesity-associated gut microbiome reprograms the intestinal epigenome and leads to altered colonic gene expression', *Genome Biology*. Genome Biology, 19(1), pp. 1–14. doi: 10.1186/s13059-018-1389-1.

Rada-Iglesias, A., Bajpai, R., Swigut, T., Brugmann, S. A., Flynn, R. A. and Wysocka, J. (2011) 'A unique chromatin signature uncovers early developmental enhancers in humans', *Nature*. Nature Publishing Group, 470(7333), pp. 279–285. doi: 10.1038/nature09692.

Radman-Livaja, M., Liu, C. L., Friedman, N., Schreiber, S. L. and Rando, O. J. (2010) 'Replication and active demethylation represent partially overlapping mechanisms for erasure of H3K4me3 in budding yeast', *PLoS Genetics*, 6(2). doi: 10.1371/journal.pgen.1000837.

Radman-Livaja, M., Verzijlbergen, K. F., Weiner, A., van Welsem, T., Friedman, N., Rando, O. J. and van Leeuwen, F. (2011) 'Patterns and mechanisms of Ancestral Histone protein inheritance in Budding yeast', *PLoS Biology*, 9(6). doi: 10.1371/journal.pbio.1001075.

Rajilic-Stojanovic, M., Heilig, H. G. H. J., Tims, S., Zoetendal, E. G. and Vos, W. M. De (2013) 'Long-term monitoring of the human intestinal microbiota composition', *Environmental Microbiology*, 15(4), pp. 1146–1159. doi: 10.1111/1462-2920.12023.

Ramirez-Farias, C., Slezak, K., Fuller, Z., Duncan, A., Holtrop, G. and Louis, P. (2009) 'Effect of inulin on the human gut microbiota: Stimulation of Bifidobacterium adolescentis and Faecalibacterium prausnitzii', *British Journal of Nutrition*, 101(4), pp. 541–550. doi: 10.1017/S0007114508019880.

Rao, R. C. and Dou, Y. (2015) 'Hijacked in cancer: the MML/KMT2 family of methyltransferases', *Nature Reviews Caner*, 15(6), pp. 334–346. doi: 10.1016/j.physbeh.2017.03.040.

Raqib, R., Sack, D. A., Agerberth, B., Andersson, J., Ara, G., Nasirul Islam, K. M., Gudmundsson, G. H., Lindh, M., Bergman, P. and Sarker, P. (2006) 'Improved outcome in shigellosis associated with butyrate induction of an endogenous peptide antibiotic', *Proceedings of the National Academy of Sciences*, 103(24), pp. 9178–9183. doi: 10.1073/pnas.0602888103.

Raqib, R., Sarker, P., Mily, A., Alam, N. H., Arifuzzaman, A. S. M., Rekha, R. S., Andersson, J.,

Gudmundsson, G. H., Cravioto, A. and Agerberth, B. (2012) 'Efficacy of sodium butyrate adjunct therapy in shigellosis: a randomized, double-blind, placebo-controlled clinical trial', *BMC Infectious Diseases*. BMC Infectious Diseases, 12(1), p. 1. doi: 10.1186/1471-2334-12-111.

Reeves, P. G., Nielsen, F. H. and Fahey, G. C. (1993) 'AIN-93 Purified Diets for Laboratory Rodents: Final Report of the American Institute of Nutrition Ad Hoc Writing Committee on the Reformulation of the AIN-76A Rodent Diet', *The Journal of Nutrition*, 123(11), pp. 1939–1951. doi: 10.1093/jn/123.11.1939.

Reid, M. A., Dai, Z. and Locasale, J. W. (2017) 'The impact of cellular metabolism of chromatin dynamics and epigenetics', *Nature Cell Biology*, 19(11), pp. 1298–1306. doi: 10.1038/ncb3629.

Rémésy, C., Demigné, C. and Chartier, F. (1980) 'Origin and utilization of volatile fatty acids in the rat.', *Reproduction, nutrition, development*, 20(4 B), pp. 1339–1349. doi: 10.1051/rnd:19800725.

Ribeiro, W., Vinolo, M., Calixto, L. and Ferreira, C. (2018) 'Use of Gas Chromatography to Quantify Short Chain Fatty Acids in the Serum, Colonic Luminal Content and Feces of Mice', *Bio-Protocol*, 8(22), pp. 1–11. doi: 10.21769/bioprotoc.3089.

Richards, R., Dowling, J., Vreman, H., Feldman, C. and Weiner, M. (1976) 'Acetate levels in human plasma', *Proceedings of the Clinical Dialysis and Transplant Forum*, 6, pp. 73–79.

Ringel, A. E. and Wolberger, C. (2016) 'Structural basis for acyl-group discrimination by human Gcn5L2', *Acta Crystallographica Section D Structural Biology*. International Union of Crystallography, 72(7), pp. 841–848. doi: 10.1107/s2059798316007907.

Rivière, A., Selak, M., Lantin, D., Leroy, F. and De Vuyst, L. (2016) 'Bifidobacteria and Butyrate-Producing Colon Bacteria: Importance and Strategies for Their Stimulation in the Human Gut', *Frontiers in Microbiology*, 7(979), pp. 1–21. doi: 10.3389/fmicb.2016.00979.

Roda, G., Sartini, A., Zambon, E., Calafiore, A., Marocchi, M., Caponi, A., Belluzzi, A. and Roda, E. (2010) 'Intestinal epithelial cells in inflammatory bowel diseases', *World Journal of Gastroenterology*, 16(34), pp. 4264–4271. doi: 10.3748/wjg.v16.i34.4264.

Ruiz-Andres, O., Sanchez-Niño, M. D., Cannata-Ortiz, P., Ruiz-Ortega, M., Egido, J., Ortiz, A. and Sanz, A. B. (2016) 'Histone lysine crotonylation during acute kidney injury in mice', *Disease Models & Mechanisms*, 9(6), pp. 633–645. doi: 10.1242/dmm.024455.

Sabari, B. R., Tang, Z., Huang, H., *et al.* (2015) 'Intracellular Crotonyl-CoA Stimulates Transcription through p300-Catalyzed Histone Crotonylation', *Molecular Cell*. Elsevier Inc., 58(2), pp. 203–215. doi: 10.1016/j.molcel.2015.02.029.

Sabari, B. R., Zhang, D., Allis, C. D. and Zhao, Y. (2017) 'Metabolic regulation of gene expression through histone acylations', *Nature Reviews Molecular Cell Biology*. Nature Publishing Group, 18(2), pp. 90–101. doi: 10.1038/nrm.2016.140.

Saltiel, A. R. and Kahn, C. R. (2001) 'Insulin signalling and the regulation of glucose and lipid metabolism', *Nature*, 414(6865), pp. 799–806. doi: 10.1038/414799a.

Sánchez-Gaya, V., Casaní-Galdón, S., Ugidos, M., Kuang, Z., Mellor, J., Conesa, A. and Tarazona, S. (2018) 'Elucidating the Role of Chromatin State and Transcription Factors on the Regulation of the Yeast Metabolic Cycle: A Multi-Omic Integrative Approach', *Frontiers in Genetics*, 9(578), pp. 1–14. doi: 10.3389/fgene.2018.00578.

Sánchez-Molina, S., Estarás, C., Oliva, J. L., Akizu, N., Asensio-Juan, E., Rojas, J. M. and Martínez-Balbás, M. A. (2014) 'Regulation of CBP and Tip60 coordinates histone acetylation at local and global levels during Ras-induced transformation', *Carcinogenesis*, 35(10), pp. 2194–2202. doi: 10.1093/carcin/bgu111.

Sanna, S., van Zuydam, N. R., Mahajan, A., *et al.* (2019) 'Causal relationships among the gut microbiome, short-chain fatty acids and metabolic diseases', *Nature Genetics*. Springer US, 51(4), pp. 600–605. doi: 10.1038/s41588-019-0350-x.

Santos-Rosa, H., Schneider, R., Bannister, A. J., Sherriff, J., Bernstein, B. E., Emre, N. C. T., Schreiber, S. L., Mellor, J. and Kouzarides, T. (2002) 'Active genes are tri-methylated at K4 of histone H3', *Nature*, 419(6905), pp. 407–411. doi: 10.1038/nature01080.

Schultz, B. E., Misialek, S., Wu, J., Tang, J., Conn, M. T., Tahilramani, R. and Wong, L. (2004) 'Kinetics and comparative reactivity of human class I and class IIb histone deacetylases.', *Biochemistry*, 43(34), pp. 11083–91. doi: 10.1021/bi0494471.

Schulz, H. (1991) 'Beta oxidation of fatty acids', *Biochimica et Biophysica Acta*, 1081, pp. 109–120.

Schulze, J. M., Wang, A. Y. and Kobor, M. S. (2009) 'YEATS domain proteins: a diverse family with many links to chromatin modification and transcription', *Biochemistry and Cell Biology*, 87(1), pp. 65–75. doi: 10.1139/O08-111.

Schwarz, D. A., Katayama, C. D. and Hedrick, S. M. (1998) 'Schlafen, a new family of growth regulatory genes that affect thymocyte development', *Immunity*, 9(5), pp. 657–668. doi: 10.1016/S1074-7613(00)80663-9.

Sender, R., Fuchs, S. and Milo, R. (2016) 'Revised Estimates for the Number of Human and Bacteria Cells in the Body.', *PLoS biology*, 14(8), p. e1002533. doi: 10.1371/journal.pbio.1002533.

Shahbazian, M. D. and Grunstein, M. (2007) 'Functions of Site-Specific Histone Acetylation and Deacetylation', *Annual Review of Biochemistry*, 76(1), pp. 75–100. doi: 10.1146/annurev.biochem.76.052705.162114.

Sharifi-Zarchi, A., Gerovska, D., Adachi, K., *et al.* (2017) 'DNA methylation regulates discrimination of enhancers from promoters through a H3K4me1-H3K4me3 seesaw mechanism', *BMC Genomics*. BMC Genomics, 18(1), pp. 1–21. doi: 10.1186/s12864-017-4353-7.

Sharma, G. G., So, S., Gupta, A., *et al.* (2010) 'MOF and Histone H4 Acetylation at Lysine 16 Are Critical for DNA Damage Response and Double-Strand Break Repair', *Molecular and Cellular Biology*, 30(14), pp. 3582–3595. doi: 10.1128/mcb.01476-09.

Shilatifard, A. (2012) 'The COMPASS Family of Histone H3K4 Methylases: Mechanisms of Regulation in Development and Disease Pathogenesis', *Annual Review of Biochemistry*, 81(1), pp. 65–95. doi: 10.1146/annurev-biochem-051710-134100.

Shreiner, A. B., Kao, J. Y. and Young, V. B. (2015) 'The gut microbiome in health and in disease', *Current Opinion Gastroenterology*, 31(1), pp. 69–75. doi: 10.1097/MOG.0000000000000139.

Simithy, J., Sidoli, S., Yuan, Z. F., *et al.* (2017) 'Characterization of histone acylations links chromatin modifications with metabolism', *Nature Communications*. Springer US, 8(1). doi: 10.1038/s41467-017-01384-9.

Sin, H. S., Barski, A., Zhang, F., Kartashov, A. V., Nussenzweig, A., Chen, J., Andreassen, P. R. and Namekawa, S. H. (2012) 'RNF8 regulates active epigenetic modifications and escape gene activation from inactive sex chromosomes in post-meiotic spermatids', *Genes and Development*, 26, pp. 2737–2748. doi: 10.1101/gad.202713.112.

Singh, N., Gurav, A., Sivaprakasam, S., *et al.* (2014) 'Activation of Gpr109a, receptor for niacin and the commensal metabolite butyrate, suppresses colonic inflammation and carcinogenesis', *Immunity*. Elsevier Inc., 40(1), pp. 128–139. doi: 10.1016/j.immuni.2013.12.007.

Smestad, J., Erber, L., Chen, Y. and Maher, L. J. (2018) 'Chromatin Succinylation Correlates with Active Gene Expression and Is Perturbed by Defective TCA Cycle Metabolism', *iScience*. Elsevier Inc., 2, pp. 63–75. doi: 10.1016/j.isci.2018.03.012.

Smith, E. and Morowitz, H. J. (2004) 'Universality in intermediary metabolism', *PNAS*, 101(36), pp. 13168–13173. doi: 10.1109/DRC.2005.1553143.

Smyth, G. K. (2004) 'Linear models and empirical bayes methods for assessing differential expression in microarray experiments.', *Statistical applications in genetics and molecular biology*, 3(3). doi:

10.2202/1544-6115.1027.

Sobel, R. E., Cook, R. G., Perry, C. A., Annunziato, A. T. and Allis, C. D. (1995) 'Conservation of deposition-related acetylation sites in newly synthesized histones H3 and H4', *Proceedings of the National Academy of Sciences of the United States of America*, 92(4), pp. 1237–1241. doi: 10.1073/pnas.92.4.1237.

Someya, S., Yu, W., Hallows, W. C., Xu, J., Vann, J. M., Leeuwenburgh, C., Tanokura, M., Denu, J. M. and Prolla, T. A. (2010) 'Sirt3 mediates reduction of oxidative damage and prevention of age-related hearing loss under caloric restriction', *Cell*, 143(5), pp. 802–812. doi: 110.1016/j.cell.2010.10.002.

Sommer, F. and Bäckhed, F. (2013) 'The gut microbiota-masters of host development and physiology', *Nature Reviews Microbiology*. Nature Publishing Group, 11(4), pp. 227–238. doi: 10.1038/nrmicro2974.

Stappenbeck, T. S., Wong, M. H., Saam, J. R., Mysorekar, I. U. and Gordon, J. I. (1998) 'Notes from some crypt watchers: Regulation of renewal in the mouse intestinal epithelium', *Current Opinion in Cell Biology*, 10(6), pp. 702–709. doi: 10.1016/S0955-0674(98)80110-5.

Sunkara, L. T., Jiang, W. and Zhang, G. (2012) 'Modulation of Antimicrobial Host Defense Peptide Gene Expression by Free Fatty Acids', *PLoS ONE*, 7(11). doi: 10.1371/journal.pone.0049558.

Sutendra, G., Kinnaird, A., Dromparis, P., Paulin, R., Stenson, T. H., Haromy, A., Hashimoto, K., Zhang, N., Flaim, E. and Michelakis, E. D. (2014) 'A nuclear pyruvate dehydrogenase complex is important for the generation of Acetyl-CoA and histone acetylation', *Cell*. Elsevier Inc., 158(1), pp. 84–97. doi: 10.1016/j.cell.2014.04.046.

Takahashi, H., McCaffery, J. M., Irizarry, R. A. and Boeke, J. D. (2006) 'Nucleocytosolic acetyl-coenzyme A synthetase is required for histone acetylation and global transcription', *Molecular Cell*, 23(2), pp. 207–217. doi: 10.1016/j.molcel.2006.05.040.

Takahashi, J. S. (2015) 'Molecular architecture of the circadian clock in mammals', *Diabetes obesity and metabolism*, 17 Suppl 1(0 1), pp. 6–11. doi: 10.1111/dom.12514.

Tan, M., Luo, H., Lee, S., *et al.* (2011) 'Identification of 67 histone marks and histone lysine crotonylation as a new type of histone modification', *Cell*, 146(6), pp. 1016–1028. doi: 10.1016/j.cell.2011.08.008.

Tan, M., Peng, C., Anderson, K. A., *et al.* (2014) 'Lysine glutarylation is a protein posttranslational modification regulated by SIRT5', *Cell Metabolism*, 19(4), pp. 605–617. doi: 10.1016/j.cmet.2014.03.014.

Tang, L., Nogales, E. and Ciferri, C. (2010) 'Structure of SWI/SNF Chromatin Remodeling Complexes and the Mechanistic Implications in Transcription', *Progress in biophysics and molecular biology*, 102(2–3), pp. 122–128. doi: 10.1016/j.pbiomolbio.2010.05.001.

Tang, Y., Zhao, W., Chen, Y., Zhao, Y. and Gu, W. (2008) 'Acetylation Is Indispensable for p53 Activation', *Cell*, 133(4), pp. 612–626. doi: 10.1016/j.cell.2008.03.025.

Tanner, K. G., Trievel, R. C., Kuo, M., Howard, R. M., Berger, S. L., Allis, C. D., Marmorstein, R. and Denu, J. M. (1999) 'Catalytic Mechanism and Function of Invariant Glutamic Acid 173 from the Histone acetyltransferase GCN5 transcriptional coactivator', *Biochemistry*, 274(26), pp. 18157–18160. doi: 10.1074/jbc.274.26.18157.

Tap, J., Mondot, S., Levenez, F., *et al.* (2009) 'Towards the human intestinal microbiota phylogenetic core', *Environmental Microbiology*, 11(10), pp. 2574–2584. doi: 10.1111/j.1462-2920.2009.01982.x.

Thompson, D. G. (2010) *15.1 Structure and function of the gut*, *Oxford Textbook of medicine*. doi: 10.1258/jrsm.98.7.333.

Tollinger, C. D., Vreman, H. J. and Weiner, M. W. (1979) 'Measurement of acetate in human blood by gas chromatography: Effects of sample preparation, feeding, and various diseases', *Clinical Chemistry*, 25(10), pp. 1787–1790.

Topping, D. L. and Clifton, P. M. (2001) 'Short-Chain Fatty Acids and Human Colonic Function: Roles of Resistant Starch and Nonstarch Polysaccharides', *Physiological Reviews*, 81(3), pp. 1031–1064. doi: 10.1152/physrev.2001.81.3.1031.

Tumanov, S., Bulusu, V., Gottlieb, E. and Kamphorst, J. J. (2016) 'A rapid method for quantifying free and bound acetate based on alkylation and GC-MS analysis', *Cancer and Metabolism*. Cancer & Metabolism, 4(1), pp. 1–12. doi: 10.1186/s40170-016-0157-5.

Turnbaugh, P. J. and Gordon, J. I. (2009) 'The core gut microbiome , energy balance and obesity', *Journal of Physiology*, 587(17), pp. 4153–4158. doi: 10.1113/jphysiol.2009.174136.

Varambally, S., Dhanasekaran, S. M., Zhou, M., *et al.* (2002) 'The polycomb group protein EZH2 is involved in progression of prostate cancer', *Nature*, 419(6907), pp. 624–629. doi: 10.1038/nature01075.

Vastenhouw, N. L. and Schier, A. F. (2012) 'Bivalent histone modifications in early embryogenesis', *Current Opinion in Cell Biology*, 24(3), pp. 374–386. doi: 10.1016/j.ceb.2012.03.009.

Velichutina, I., Shaknovich, R., Geng, H., Johnson, N. A., Gascoyne, R. D., Melnick, A. M. and Elemento,

O. (2010) ‘EZH2-mediated epigenetic silencing in germinal center B cells contributes to proliferation and lymphomagenesis’, *Blood*, 116(24), pp. 5247–5255. doi: 10.1182/blood-2010-04-280149.

Ventura, M., Mateo, F., Serratosa, J., Salaet, I., Carujo, S., Bachs, O. and Pujol, M. J. (2010) ‘Nuclear translocation of glyceraldehyde-3-phosphate dehydrogenase is regulated by acetylation’, *International Journal of Biochemistry and Cell Biology*. Elsevier Ltd, 42(10), pp. 1672–1680. doi: 10.1016/j.biocel.2010.06.014.

Verdin, E. and Ott, M. (2015) ‘50 years of protein acetylation: From gene regulation to epigenetics, metabolism and beyond’, *Nature Reviews Molecular Cell Biology*. Nature Publishing Group, 16(4), pp. 258–264. doi: 10.1038/nrm3931.

Vermeulen, M., Eberl, H. C., Matarese, F., *et al.* (2010) ‘Quantitative Interaction Proteomics and Genome-wide Profiling of Epigenetic Histone Marks and Their Readers’, *Cell*. Elsevier Inc., 142(6), pp. 967–980. doi: 10.1016/j.cell.2010.08.020.

Visel, A., Blow, M. J., Li, Z., *et al.* (2009) ‘ChIP-seq accurately predicts tissue-specific activity of enhancers’, *Nature*, 457(7231), pp. 854–858. doi: 10.1038/nature07730.

Vital, M., Howe, C. and Tiedje, M. (2014) ‘Revealing the Bacterial Butyrate Synthesis Pathways by Analyzing (Meta) genomic Data’, *mBio*, 5(2), pp. 1–11. doi: 10.1128/mBio.00889-14.

Vlaicu, S. I., Tegla, C. A., Cudrici, C. D., *et al.* (2010) ‘Epigenetic modifications induced by RGC-32 in colon cancer’, *Experimental and Molecular Pathology*, 88(1), pp. 67–76. doi: 10.1038/jid.2014.371.

Voet, D. and Voet, J. G. (2011) *Biochemistry*. 4th edn. John Wiley & Sons.

Voss, A. K. and Thomas, T. (2009) ‘MYST family histone acetyltransferases take center stage in stem cells and development’, *BioEssays*, 31(10), pp. 1050–1061. doi: 10.1002/bies.200900051.

Wagner, E. J. and Carpenter, P. B. (2012) ‘Understanding the language of Lys36 methylation at histone H3’, *Nature Reviews Molecular Cell Biology*. Nature Publishing Group, 13(2), pp. 115–126. doi: 10.1038/nrm3274.

Wagner, G. R. and Hirschey, M. D. (2014) ‘Nonenzymatic Protein Acylation as a Carbon Stress Regulated by Sirtuin Deacylases’, *Molecular Cell*. Elsevier Inc., 54(1), pp. 5–16. doi: 10.1016/j.molcel.2014.03.027.

Wagner, G. R. and Payne, R. M. (2013) ‘Widespread and enzyme-independent Nε-acetylation and Nε-succinylation of proteins in the chemical conditions of the mitochondrial matrix’, *Journal of Biological Chemistry*, 288(40), pp. 29036–29045. doi: 10.1074/jbc.M113.486753.

Walker, A. W., Duncan, S. H., Louis, P. and Flint, H. J. (2014) 'Phylogeny, culturing, and metagenomics of the human gut microbiota', *Trends in Microbiology*. Elsevier Ltd, 22(5), pp. 267–274. doi: 10.1016/j.tim.2014.03.001.

Walker, A. W., Duncan, S. H., McWilliam Leitch, C. E., Child, M. W. and Flint, H. J. (2005) 'pH and peptide supply can radically alter bacterial populations and short chain fatty acid ratios within microbial communities from the human colon', *Applied and environmental microbiology*, 71(7), pp. 3692–3700. doi: 10.1128/AEM.71.7.3692.

Walker, A. W., Ince, J., Duncan, S. H., *et al.* (2011) 'Dominant and diet-responsive groups of bacteria within the human colonic microbiota', *ISME Journal*. Nature Publishing Group, 5(2), pp. 220–230. doi: 10.1038/ismej.2010.118.

Wan, J., Liu, H. and Ming, L. (2019) 'Lysine crotonylation is involved in hepatocellular carcinoma progression', *Biomedicine and Pharmacotherapy*. Elsevier, 111(November 2018), pp. 976–982. doi: 10.1016/j.biopha.2018.12.148.

Wang, X., Zhu, W., Chang, P., Wu, H., Liu, H. and Chen, J. (2018) 'Merge and separation of NuA4 and SWR1 complexes control cell fate plasticity in Candida albicans', *Cell Discovery*. Springer US, 4(1). doi: 10.1038/s41421-018-0043-0.

Wang, Y., Guo, Y. R., Liu, K., *et al.* (2017) 'KAT2A coupled with the α-KGDH complex acts as a histone H3 succinyltransferase', *Nature*. Nature Publishing Group, 552(7684), pp. 273–277. doi: 10.1038/nature25003.

Wang, Y., Jin, J., Chung, M. W. H., Feng, L., Sun, H. and Hao, Q. (2018) 'Identification of the YEATS domain of GAS41 as a pH-dependent reader of histone succinylation', *Proceedings of the National Academy of Sciences*, 115(10), p. 201717664. doi: 10.1073/pnas.1717664115.

Wang, Z., Zang, C., Rosenfeld, J. A., *et al.* (2008) 'Combinatorial patterns of histone acetylations and methylations in the human genome', *Nature Genetics*, 40(7), pp. 897–903. doi: 10.1038/ng.154.

Wang, Z., Zhao, Y., Xu, N., *et al.* (2019) 'NEAT1 regulates neuroglial cell mediating Aβ clearance via the epigenetic regulation of endocytosis-related genes expression', *Cellular and Molecular Life Sciences*. Springer International Publishing, (0123456789). doi: 10.1007/s00018-019-03074-9.

Warburg, O. (1956) 'On the origin of cancer cells', *Science*, 123(3191), pp. 309–314.

Ward, P. S. and Thompson, C. B. (2012) 'Metabolic Reprogramming: A Cancer Hallmark Even Warburg Did Not Anticipate', *Cancer Cell*. Elsevier Inc., 21(3), pp. 297–308. doi: 10.1016/j.ccr.2012.02.014.

Weaver, G. A., Krause, J. A., Miller, T. L. and Wolin, M. J. (1988) 'Short chain fatty acid distributions of enema samples from a sigmoidoscopy population: An association of high acetate and low butyrate ratios with adenomatous polyps and colon cancer', *Gut*, 29(11), pp. 1539–1543. doi: 10.1136/gut.29.11.1539.

Wegener, D., Wirsching, F., Riester, D. and Schwienhorst, A. (2003) 'A fluorogenic histone deacetylase assay well suited for high-throughput activity screening.', *Chemistry & biology*, 10(1), pp. 61–8.

Wei, W., Liu, X., Chen, J., *et al.* (2017) 'Class I histone deacetylases are major histone decrotonylases: evidence for critical and broad function of histone crotonylation in transcription', *Cell Research*, 27(7), pp. 898–915. doi: 10.1038/cr.2017.68.

Wei, W., Mao, A., Tang, B., *et al.* (2017) 'Large-Scale Identification of Protein Crotonylation Reveals Its Role in Multiple Cellular Functions', *Journal of Proteome Research*, 16(4), pp. 1743–1752. doi: 10.1021/acs.jproteome.7b00012.

Weinert, B. T., Iesmantavicius, V., Moustafa, T., Scholtz, C., Wagner, S. A., Magnes, C., Zechner, R. and Choudhary, C. (2014) 'Acetylation dynamics and stoichiometry in Saccharomyces cerevisiae', *Molecular Systems Biology*, 10(716), pp. 1–13. doi: 10.1002/msb.134766.

Weis, A. M., Soto, R. and Round, J. L. (2018) 'Commensal regulation of T cell survival through Erdr1', *Gut microbes*. Taylor & Francis, 9(5), pp. 458–464. doi: 10.1080/19490976.2018.1441662.

Wellen, K. E., Hatzivassiliou, G., Sachdeva, U. M., Bui, T. V, Cross, J. R. and Thompson, C. B. (2009) 'ATP-citrate lyase links cellular metabolism to histone acetylation', *Science*, 324(5930), pp. 1076–1080. doi: 10.1126/science.1164097.

Wolever, T. M. and Chiasson, J. L. (2000) 'Acarbose raises serum butyrate in human subjects with impaired glucose tolerance.', *The British journal of nutrition*. BBSRC, 84(1), pp. 57–61. Available at: http://www.ncbi.nlm.nih.gov/pubmed/10961161.

Wu, J. I. (2012) 'Diverse functions of ATP-dependent chromatin remodeling complexes in development and cancer', *Acta biochimica et biophysica Sinica*, 44, pp. 54–69. doi: 10.1093/abbs/gmr099.

Wu, Q., Li, W., Wang, C., Fan, P., Cao, L., Wu, Z. and Wang, F. (2017) 'Ultradeep lysine crotonylome reveals the crotonylation enhancement on both histones and nonhistone proteins by SAHA treatment', *Journal of Proteome Research*, 16(10), pp. 3664–3671. doi: 10.1021/acs.jproteome.7b00380.

Xiao, M., Yang, H., Xu, W., *et al.* (2012) 'Inhibition of α-KG-dependent histone and DNA demethylases by fumarate and succinate that are accumulated in mutations of FH and SDH tumor suppressors',

Genes and Development, 26(12), pp. 1326–1338. doi: 10.1101/gad.191056.112.

Xie, Z., Zhang, D., Chung, D., *et al.* (2016) 'Metabolic Regulation of Gene Expression by Histone Lysine β-Hydroxybutyrylation', *Molecular Cell*. Elsevier Inc., 62(2), pp. 194–206. doi: 10.1016/j.molcel.2016.03.036.

Xiong, X., Panchenko, T., Yang, S., *et al.* (2016) 'Selective recognition of histone crotonylation by double PHD fingers of MOZ and DPF2', *Nature chemical biology*, 12(12), pp. 1111–1118. doi: 10.1038/nchembio.2218.

Xu, W., Wan, J., Zhan, J., Li, X., He, H., Shi, Z. and Zhang, H. (2017) 'Global profiling of crotonylation on non-histone proteins', *Cell Research*, 27(7), pp. 946–949. doi: 10.1038/cr.2017.60.

Yan, W. and McCarrey, J. R. (2009) 'Sex chromosome inactivation in the male', *Epigenetics*, 4(7), pp. 452–456. doi: 10.4161/epi.4.7.9923.

Yang, W., Xia, Y., Hawke, D., Li, X., Liang, J., Xing, D., Aldape, K., Hunter, T., Yung, W. K. A. and Lu, Z. (2012) 'PKM2 Phosphorylates histone H3 and promotes gene transcription and tumorigenesis', *Cell*, 150(4), pp. 685–696. doi: 10.1056/NEJMcibr1012075.

Yang, X. (2015) 'MOZ and MORF acetyltransferases: Molecular interaction, animal development and human disease', *Biochimica et Biophysica Acta - Molecular Cell Research*. Elsevier B.V., 1853(8), pp. 1818–1826. doi: 10.1016/j.bbamcr.2015.04.014.

Yi, C. H., Pan, H., Seebacher, J., *et al.* (2011) 'Metabolic regulation of protein N-alpha-acetylation by Bcl-xL promotes cell survival', *Cell*. Elsevier Inc., 146(4), pp. 607–620. doi: 10.1016/j.cell.2011.06.050.

Yoon, S. and Eom, G. H. (2016) 'HDAC and HDAC Inhibitor: From Cancer to Cardiovascular Diseases', *Chonnam Medical Journal*, 52(1), p. 1. doi: 10.4068/cmj.2016.52.1.1.

You, S.-H. H., Lim, H.-W., Sun, Z., Broache, M., Won, K.-J. and Lazar, M. A. (2013) 'Nuclear receptor co-repressors are required for the histone-deacetylase activity of HDAC3 in vivo', *Nature Structural and Molecular Biology*. Nature Publishing Group, 20(2), pp. 182–187. doi: 10.1038/nsmb.2476.

Zarrinpar, A., Chaix, A., Xu, Z. Z., Chang, M. W., Marotz, C. A., Saghatelian, A., Knight, R. and Panda, S. (2018) 'Antibiotic-induced microbiome depletion alters metabolic homeostasis by affecting gut signaling and colonic metabolism', *Nature Communications*. Springer US, 9(1). doi: 10.1038/s41467-018-05336-9.

Zentner, G. E., Tesar, P. J. and Scacheri, P. C. (2011) 'Epigenetic signatures distinguish multiple classes of enhancers with distinct cellular functions', *Genome Research*, 21(8), pp. 1273–1283. doi:

10.1101/gr.122382.111.

Zhang, K., Chen, Y., Zhang, Z. and Zhao, Y. (2009) 'Identification and Verification of Lysine Propionylation and Butyrylation in Yeast Core Histones Using PTMap Software Identification and Verification of Lysine Propionylation and Butyrylation in Yeast Core Histones Using PTMap Software', *Journal of Proteome Research*, pp. 900–906. doi: 10.1021/pr8005155.

Zhang, Q., Zeng, L., Zhao, C., Ju, Y., Konuma, T. and Zhou, M.-M. (2016) 'Structural Insights into Histone Crotonyl-Lysine Recognition by the AF9 YEATS Domain', *Structure*. Elsevier Ltd, 24(9), pp. 1606–1612. doi: 10.1016/j.str.2016.05.023.

Zhang, X., Cao, R., Niu, J., Yang, S., Ma, H., Zhao, S. and Li, H. (2019) 'Molecular basis for hierarchical histone de-B-hydroxybutyrylation by Sirt3', *Cell Discovery*, 5(35), pp. 1–15. doi: 10.1038/s41421-019-0103-0.

Zhang, Y., Liu, T., Meyer, C. A., *et al.* (2008) 'Model-based analysis of ChIP-Seq (MACS)', *Genome Biology*, 9(9). doi: 10.1186/gb-2008-9-9-r137.

Zhang, Y., Yang, X., Gui, B., Xie, G., Zhang, D., Shang, Y. and Liang, J. (2011) 'Corepressor protein CDYL functions as a molecular bridge between polycomb repressor complex 2 and repressive chromatin mark trimethylated histone lysine 27', *Journal of Biological Chemistry*, 286(49), pp. 42414–42425. doi: 10.1074/jbc.M111.271064.

Zhang, Z., Tan, M., Xie, Z., Dai, L., Chen, Y. and Zhao, Y. (2011) 'Identification of lysine succinylation as a new post-translational modification', *Nature Chemical Biology*. Nature Publishing Group, 7(1), pp. 58–63. doi: 10.1038/nchembio.495.

Zhao, D., Guan, H., Zhao, S., Mi, W., Wen, H., Li, Y., Zhao, Y., Allis, C. D., Shi, X. and Li, H. (2016) 'YEATS2 is a selective histone crotonylation reader', *Cell Research*, 26(5), pp. 629–632. doi: 10.1038/cr.2016.49.

Zhao, D., Li, Y., Xiong, X., Chen, Z. and Li, H. (2017) 'YEATS Domain—A Histone Acylation Reader in Health and Disease', *Journal of Molecular Biology*. Elsevier Ltd, 429(13), pp. 1994–2002. doi: 10.1016/j.jmb.2017.03.010.

Zhao, S., Zhang, X. and Li, H. (2018) 'Beyond histone acetylation—writing and erasing histone acylations', *Current Opinion in Structural Biology*. Elsevier Ltd, 53, pp. 169–177. doi: 10.1016/j.sbi.2018.10.001.

Zheng, Y., Thomas, P. M. and Kelleher, N. L. (2013) 'Measurement of acetylation turnover at distinct lysines in human histones identifies long-lived acetylation sites', *Nature communications*. Nature

Publishing Group, 4(2203), pp. 1–19. doi: 10.1038/ncomms3203.

Zheng, Y., Tipton, J. D., Thomas, P. M., Kelleher, N. L. and Sweet, S. M. (2014) 'Site-specific human histone H3 methylation stability: fast K4me3 turnover', *Proteomics*, 14(19), pp. 2190–2199. doi: 10.1038/jid.2014.371.

Zhu, J., Adli, M., Zou, J. Y., *et al.* (2013) 'Genome-wide chromatin state transitions associated with developmental and environmental cues', *Cell*. Elsevier Inc., 152(3), pp. 642–654. doi: 10.1016/j.cell.2012.12.033.

8

8 Appendix

8.1 Bio-protocol paper: In vitro Enzymatic Assays of Histone Decrotonylation on Recombinant Histones

Rachel Fellows[1] and Patrick Varga-Weisz[1, 2, *]

[1]Babraham Institute, Cambridge, UK; [2]School of Biological Sciences, University of Essex, Colchester, UK

*For correspondence: Patrick.varga-weisz@essex.ac.uk

[Abstract] Class I histone deacetylases (HDACs) are efficient histone decrotonylases, broadening the enzymatic spectrum of these important (epi-)genome regulators and drug targets. Here, we describe an *in vitro* approach to assaying class I HDACs with different acyl-histone substrates, including crotonylated histones and expand this to examine the effect of inhibitors and estimate kinetic constants.

Keywords: Crotonylation, Acetylation, Butyrylation, Histone deacetylase, Enzyme, Kinetic, Chromatin

[Background] Posttranslational modifications of histones are an important facet of genome regulation, including gene expression (for example see Pengelly *et al*., 2013; reviewed in Castillo *et al.,* 2017). Histone modifications alter chromatin structure and/or regulate the binding of proteins, such as nucleosome remodeling factors (reviewed in Bannister and Kouzarides, 2011). Most histone modifications are reversible and can be removed enzymatically. For example, histone acetylation is removed by histone deacetylases (HDACs), of which there exist several classes. In recent years new histone lysine acylations, including succinylation, propionylation, butyrylation, hydroxybutyrylation and crotonylation have emerged as new alternative acylations to the canonical histone acetylation and the functional relevance of many of these newly discovered histone modifications have been demonstrated (reviewed in Sabari *et al.,* 2017). In particular, histone crotonylation is associated with active gene expression and is thought to be influenced by the metabolic state of the cell (Sabari *et al,.* 2015; Fellows *et al.,* 2018). Class I histone deacetylases have recently been shown to also efficiently

decrotonylate histones (Wei *et al,.* 2017; Fellows *et al*., 2018).

Histone deacetylation assays are often performed using fluorescent acetyl substrates, such as BOC-lys(acetyl)-AMC, because this allows high-throughput *in vitro* approaches, suitable for drug discovery (Wegener *et al*., 2003a: 2003b and 2003c). However, we found that the analogous fluorescent crotonyl substrate BOC-lys(crotonyl)-AMC was inhibitory to histone deacetylases (Fellows *et al.,* 2018). In this protocol, we describe a method for analysis of the activity of histone deacetylases with *in vitro* crotonylated histone H3, and we investigate the effect of an inhibitor and estimate kinetic parameters using an *in vitro* approach. This method does not require the use of radioisotopes. It also does not rely on fluorescent peptide mimics, and thus, the kinetic constants determined may be more representative of those found *in vivo*. The approach depends on the recognition of histone acylations, such as crotonylation, by specific antibodies. It is a versatile approach, which could be applied to study a variety of other histone modifications, enzymes, and inhibitors.

Materials and Reagents

1. 8-strip 0.2 ml non-flex flat cap PCR tubes with individual lids (STARLAB INTERNATIONAL, catalog number: I1402-3700)
2. 250 ml and 1 L cylinders (Corning, catalog number: 3022P-250, 3022P-1L)
3. Pre-cut extra thick blot paper, 7 x 8.4 cm (Bio-Rad Laboratories, catalog number: 1703966)
4. Amersham Protran 0.45 µm nitrocellulose membrane, 300 mm x 4 m (GE Healthcare, catalog number: 10600002)
5. 5, 10 and 25 ml Costar® Stripette® serological pipettes (Corning, catalog numbers: 4487, 4488, 4489)
6. 50 ml Falcon® tubes, polypropylene (Corning, catalog number: 352070)
7. Eppendorf® tubes 5.0 ml, Eppendorf Quality™ (Eppendorf, catalog number: 0030119401)
8. X-ray film 18 x 24 cm double sided (Scientific Laboratory Supplies, catalog number: MOL7016)
9. Transparent acetate sheet, *e.g.*, colour copier transparency film (Interaction-Connect, Q-CONNECT®, catalog number: KF00533)
10. Milli-Q® water
11. Recombinant human histone H3.1 protein, 1 mg/ml (New England Biolabs, catalog number: M2503S)
    Note: Prepare aliquots (e.g., 10 µl aliquots) and store at -80 °C.
12. Recombinant catalytic domain of human p300 protein (Enzo Life Sciences, catalog number: BML-SE451-0100), 100 µg, 15.18 µM (exact concentration may vary by batch, check the tube)
    Note: Prepare aliquots (e.g., 10 µl aliquots) and store at -80 °C.
13. Crotonyl-coenzyme A trilithium salt ~90% pure as per HPLC (Sigma-Aldrich, catalog number: 28007)
    Note: For acetylation we used: Acetyl-coenzyme A (Sigma-Aldrich, catalog number: ACOA-RO ROCHE).
    Prepare 5 mM stock solution in water, aliquot and store at -80 °C.
    Manufacturer: Roche Diagnostics, catalog number: 10101893001.

14. Trizma®-hydrochloride, ≥ 99.0% (Sigma-Aldrich, catalog number: T3253)
15. Potassium chloride, 99.5-101.0% AnalaR NORMAPUR® (VWR, catalog number: 26764.298)
16. UltraPure™ 0.5 M EDTA, pH 8.0 (Thermo Fisher Scientific, catalog number: 15575020)
17. Tween 20 (Sigma-Aldrich, catalog number: P1379)
18. Glycerol, ≥ 99% (Sigma-Aldrich, catalog number: G5516)
19. Dithiothreitol (DTT) (Thermo Fisher Scientific, catalog number: R0861)
20. Magnesium chloride hexahydrate, ≥ 99.0% (Sigma-Aldrich, catalog number: M2670)
21. Zinc sulfate heptahydrate (Sigma-Aldrich, catalog number: Z0251)
22. Recombinant human HDAC1 protein (Active Motif, catalog number: 31908) 50 µg, 0.1 mg/ml, 1.78 µM (exact concentration may vary by batch, check tube)
    Note: Prepare aliquots (e.g., 10 µl aliquots) and store at -80 °C.
23. 2x Laemmli sample buffer (Bio-Rad Laboratories, catalog number: 1610737)
    Note: Add 2-mercaptoethanol to 5% v/v as described by supplier.
24. 2-mercaptoethanol, ≥ 99.0% (Sigma-Aldrich, catalog number: M6250)
25. Sodium Butyrate, 98% (Sigma-Aldrich, catalog number: 303410)
    Note: Prepare a 1 M solution in water, adjust to pH 7 and aliquot.
26. Precast RunBlue 4-12% Bis-Tris (Expedeon, catalog number: NBT41227)
27. 20x RunBlue MES run buffer (Expedeon, catalog number: NXB70500)
28. PageRuler™ Prestained protein ladder, 10 to 180 kDa (Thermo Fisher Scientific, catalog number: 26616)
29. 10x Tris/glycine/SDS electrophoresis buffer (Bio-Rad Laboratories, catalog number: 1610732EDU)
30. UltraPure™ Tris buffer (Thermo Fisher Scientific, catalog number: 15504020)
31. Glycine, ≥ 99.7% AnalaR NORMAPUR® (VWR, catalog number: 101196X)
32. Methanol, ≥ 99.8% AnalaR NORMAPUR® (VWR, catalog number: 20847.307)
33. Sodium chloride, 99.5-100.5% AnalaR NORMAPUR® (VWR, catalog number: 27810.295)
34. Bovine serum albumin, heat shock fraction pH 7 ≥ 98% (Sigma-Aldrich, catalog number: A9647)
35. Anti-crotonyl-histone H3 lys18 (H3K18cr) rabbit polyclonal antibody (PTM Biolabs, catalog number: PTM-517)
36. Anti-rabbit IgG HRP linked whole antibody (GE Healthcare, catalog number: NA934-1ML)
37. Enhanced chemiluminescence (ECL) Western blotting reagents (GE Healthcare, catalog number: RPN2106)
38. Synthetic crotonylated H3K18cr peptide 95% pure, lyophilized (TGGKAPR-Lys(Crotonyl)-QLATKAA-EDA-Biotin, BioGenes, Peptide 60556.1) (EDA is a spacer amino acid sequence)
39. Histone acylation buffer (see Recipe 1)
40. HDAC assay buffer (see Recipe 2)
41. MES Run buffer (see Recipe 3)
42. Tris glycine SDS (TGS) buffer (see Recipe 4)
43. Transfer buffer (see Recipe 5)

44. Tris-buffered saline, pH 7.5 (TBS) (see Recipe 6)
45. TBS with tween 20 (TBS-T) (see Recipe 7)
46. TBS-T with 3% (w/v) bovine serum albumin (TBS-T BSA) (see Recipe 8)

Equipment

1. Pipettes (Gilson, catalog numbers: F123602, F123601, F123600, F144801, model: P1000, P200, P20, P2)
2. Pipette controller PIPETBOY acu2 (VWR, INTEGRA Biosciences, catalog number: 612-2964)
3. Fume hood (*e.g.*, Protector Xstream Laboratory Hood, Labconco)
4. Milli-Q Water Purification System (Merck, catalog number: ZRXQ003WW)
5. GE Healthcare Amersham™ Hypercasette™ Autoradiography Cassette (GE Healthcare, catalog number: RPN11643)
6. Vortex-genie 2 (Scientific Industries, model: Vortex-Genie 2, catalog number: SI-0236)
7. Microcentrifuge (STARLAB INTERNATIONAL, model: Mini Fuge, catalog number: N2631-0007)
8. Two T100™ Thermal Cyclers (Bio-Rad Laboratories, catalog number: 1861096)
9. Amersham electrophoresis power supply EPS 301 (GE Healthcare, catalog number: 18113001)
10. XCell SureLock™ Mini-Cell Electrophoresis System (Thermo Fisher Scientific, catalog number: EI0001)
11. Transblot® SD semi-dry electrophoretic transfer cell (Bio-Rad Laboratories, catalog number: 1703940)
12. MI-5 x-ray film processor (Jet x-ray)
13. Epson expression 1680 scanner (Seiko Epson, model: Epson Expression 1680)

    Note: Equivalent models of equipment specified here may also be used.

Software

1. ImageJ version 1.50 b
2. Windows Excel 2016
3. Adobe Illustrator CC 2015.3
4. Graphpad Prism version 7.0
5. Epson Scan Software in professional mode

   Note: Other versions of this software or similar software may be used but the instructions specified in the data analysis section may then differ.

Procedure

We found that decrotonylation by HDACs did not occur on synthetic, modified histone tail peptides, necessitating the use of the full-length recombinant histone. In our assay, we first

crotonylate histones *in vitro* using recombinant histone H3.1 and the catalytic domain of p300 ('p300'). We then follow decrotonylation by class I HDACs using specific antibodies, here against histone H3 crotonylated at lysine 18 (H3K18cr). H3K18cr is the dominant histone crotonylation mediated by p300 (Sabari *et al.,* 2015) and appears to be the most abundant histone crotonylation in histones isolated from intestinal cells (Fellows *et al.,* 2018). Importantly, highly specific antibodies have been generated that recognize H3K18cr (Sabari *et al*., 2015). We describe an assay for decrotonylation to address three questions: can HDAC1 remove the crotonyl group and how much of it is required, how effective is the HDAC inhibitor butyrate at preventing decrotonylation by HDAC1 and what are the kinetic parameters of HDAC1 regarding the decrotonylation of histone H3? The same steps can be performed for other acylations, such as acetylation, butyrylation or propionylation using the relevant acyl-CoA and antibody. This protocol can also be used to test other HDAC enzymes, using the relevant recombinant protein, and other HDAC inhibitors such as Trichostatin A (TSA) and Vorinostat (suberoyl anilide hydroxamic acid, SAHA).

Part I: *In vitro* decrotonylation assay

A. *In vitro* crotonylation of recombinant histone H3.1 using the catalytic domain of p300

1. Defrost all reagents on ice.
2. Dilute the 5 mM crotonyl-CoA stock solution 1:50 in histone acylation buffer.
3. Prepare the reaction mix in a 0.2 ml PCR tube as described in Table 1.

Table 1. Histone H3 crotonylation reaction set-up

Component	Volume (µl)	Concentration in reaction (µM)
Diluted Crotonyl-CoA	40	87.00
Histone H3.1	4	5.65
p300 Catalytic domain ('p300')	2	0.66

4. Mix well by pipetting or brief vortexing.
5. Incubate for 2 h at 30 °C in a thermocycler.
6. Transfer to a thermocycler at 65 °C and incubate for 5 min to stop the reaction.
   Note: Histone tails are unstructured. Therefore heat inactivation is unlikely to affect the modification.
7. Place the tube on ice.

B. HDAC1 mediated histone decrotonylation assay

1. Decrotonylation assay with different concentrations of HDAC1

We verify the activity of the HDAC1 enzyme towards the substrate and demonstrate the minimum amount required to observe the decrotonylation reaction.

a. Dilute the reaction from Part I Procedure A 1:3 in HDAC assay buffer, *i.e.*, 46 µl of reaction mix and 92 µl of HDAC assay buffer.

b. Cut 3 tubes away from an 8-tube strip leaving a 5-tube strip.

c. Label these PCR tubes as 1-5.

d. On ice, add diluted reaction mix, HDAC assay buffer and HDAC1 as described below and shown in Table 2.

Note: This sets up a two-fold serial dilution of HDAC1 in tubes 1-4 whilst keeping the other reagents constant. Tube 5 is the negative control without any HDAC1. As soon as HDAC1 has been added to tube 1, perform all steps as quickly as possible as the reaction will start from this point. Whilst it is impossible to capture the first few seconds of the reaction, as it takes a few seconds to set it up, it is important to be quick so that the initial phase of the reaction is recorded.

i. To tube 1, add 28 µl of diluted reaction mix.

ii. To tubes 2-5, add 14 µl of diluted reaction mix.

iii. Add 1 µl HDAC assay buffer to tubes 2-5 to allow for the HDAC1 volume.

iv. Add 2 µl of HDAC1 to tube 1 and mix well (0.1 mg/ml, 1.78 µM stock. 0.12 µM final concentration).

v. Remove 15 µl from tube 1, add to tube 2 and mix well.

vi. Remove 15 µl from tube 2, add to tube 3 and mix well.

vii. Repeat with tubes 3 and 4 but not tube 5.

Table 2. Reaction set-up with a serial dilution of HDAC1

Tube Number	1	2	3	4	5
Diluted reaction mix (µl)	28	14	14	14	14
HDAC Assay Buffer (µl)	-	1	1	1	1
HDAC1 (µl) Final HDAC1 concentration (ng/µl)	2 6.66	- 3.33	- 1.67	- 0.83	- 0
Serial Dilution	→	→	→	→	No serial dilution

e. Vortex all tubes briefly by holding both sides of the strip.

f. Spin tubes briefly to bring all of the liquid to the bottom of the tube.

g. Incubate in a thermocycler at 30 °C for 2 h.

h. As soon as the time is up, remove from the thermocycler.

   i. If the sample is to be run on a gel, add 15 µl (an equal volume) of 2x Laemmli with 5% (v/v) 2-mercaptoethanol and incubate at 95 °C for 1 min to stop the reaction.

   ii. If the sample is to be dot-blotted, just incubate at 95 °C for 1 min to stop the reaction.

i. At this point the tubes can be frozen at -20 °C for at least a few days or continued with further analysis as explained in Part II.

2. Exploring the effect of an HDAC inhibitor on histone decrotonylation

   Here, butyrate is introduced in serial dilution which allows testing of the ability of the compound to inhibit the decrotonylation. This can be used to estimate the concentration of inhibitor required to halve the amount of created product (IC50).

   a. Dilute the reaction mix from Part I A 1:3 in HDAC assay buffer *i.e.*, 46 µl of reaction mix and 92 µl of HDAC assay buffer.

   b. Label an 8-strip of PCR tubes as 1-8.

   c. On ice, add diluted reaction mix, HDAC assay buffer, butyrate and HDAC1 as described below and shown in Table 3.

      Note: A double reaction is prepared in tube 1 and single reactions in tubes 2-6, allowing a two-fold serial dilution of butyrate to be performed in tubes 1-6 whilst keeping the other reagents constant. Tube 7 and 8 are negative controls, tube 7 is without butyrate and tube 8 is without butyrate and HDAC1. As soon as HDAC1 has been added to tube 1, perform all steps as quickly as possible as the reaction will start from this point.

      i. To tube 1, add 28 µl of diluted reaction mix.

      ii. To tubes 2-8, add 14 µl of diluted reaction mix.

      iii. Add 1 µl HDAC assay buffer to tubes 2-7 to allow for the volume of butyrate added to tube 1.

      iv. Add 2 µl HDAC assay buffer to tube 8 to allow for the volume of butyrate and HDAC1.

      v. Add 2 µl of 160 mM butyrate to tube 1 to give a final concentration of 10 mM once all reagents have been added.

      vi. Add 2 µl of HDAC1 to tube 1 and mix well (0.1 mg/ml, 1.78 µM stock. 0.11 µM final concentration).

      vii. Add 1 µl of HDAC1 to tubes 2-7.

      viii. Remove 16 µl from tube 1, add to tube 2 and mix well.

      ix. Remove 16 µl from tube 2, add to tube 3 and mix well.

      x. Repeat with tubes 3, 4, 5 and 6 but not tubes 7 or 8.

Table 3. Reaction set-up with a serial dilution of butyrate and constant HDAC1

Tube Number	1	2	3	4	5	6	7	8
Diluted reaction mix (µl)	28	14	14	14	14	14	14	14
HDAC Assay Buffer (µl)	-	1	1	1	1	1	1	2
160 mM butyrate (µl) Final Butyrate Concentration (mM)	2 10	- 5	- 2.5	- 1.25	- 0.625	- 0.313	- -	- -
HDAC1 (µl)	2	1	1	1	1	1	1	-
Serial Dilution	→	→	→	→	→	→	No serial dilution	No serial dilution

d. Vortex all tubes by holding both sides of the strip.

e. Incubate at 30 °C for 2 h.

f. As soon as the time is up, remove from the thermocycler.

   i. If the sample is to be run on a gel, add 16 µl (an equal volume) of 2x Laemmli with 5% (v/v) 2-mercaptoethanol and incubate at 95 °C for 1 min.

   ii. If the sample is to be dot-blotted, just incubate at 95 °C for 1 min.

g. At this point the tubes can be frozen at -20 °C for at least a few days or continued with further analysis as explained in Part II.

3. Determination of kinetic parameters of histone decrotonylation

Determination of kinetic parameters such as the maximum initial rate allows assessment of whether the enzyme follows Michaelis-Menten kinetics and is a useful way to find out important kinetic parameters such as K_{cat}, V_{max} and K_m. It allows comparison of an enzyme's activity with different substrates or comparison of the activity of different enzymes with the same substrate. This requires the change in substrate or product concentration to be plotted over time so that the initial rate can be determined (see Figure 1 for illustration). The concentration of the enzyme must be optimized so that the initial rate is within a measurable timeframe. Initial rates are then plotted against the substrate concentration at the start of the reaction, to determine the maximum rate (V_{max}) and substrate concentration at half V_{max} (K_m) as shown in Figure 1. As the reactions performed here are analyzed by antibody-based approaches, they cannot be measured in real time. Therefore, it is necessary to set up

a reaction for each time point. Here, six identical reactions are set up and stopped at 0, 0.5, 1, 2, 4 and 10 min. The shortest time point that is practical with the method we present is 30 sec. To reliably determine kinetic parameters, it is also necessary to perform the reaction three times for each substrate concentration, and five different substrate concentrations are recommended. This means that 90 reactions are required (5 substrate concentrations x 6 time points x 3 replicates). These have been grouped into three replicate sets named A, B, and C. In our hands, and as described below, the initial reaction occurs in the first minute. Reducing the amount of enzyme may allow longer reaction times and thus more time points during the initial phase. However, this must be balanced against keeping the change in substrate concentration for all reactions distinguishable from background noise.

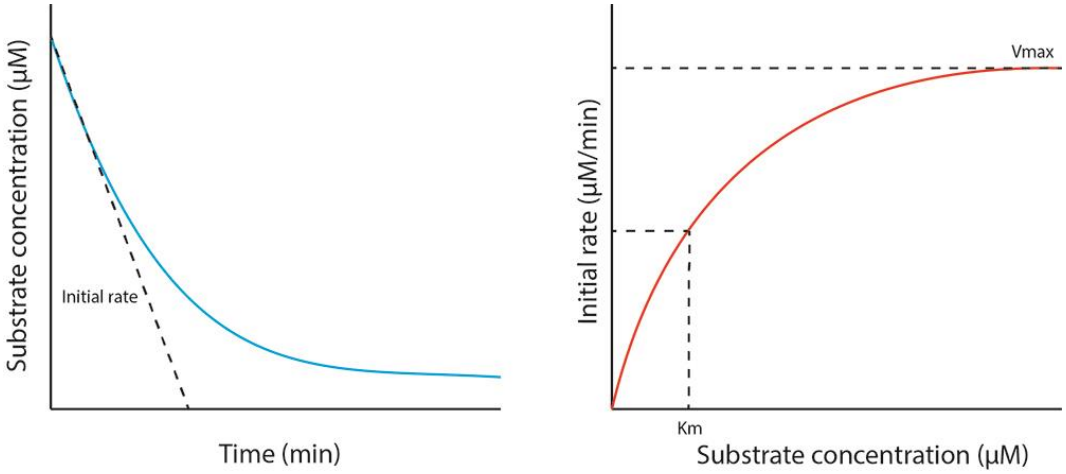

Figure 1. Enzyme kinetic graphs. The left graph shows the output of the assay, which gives the change in substrate concentration over time. The initial rate is determined from this by finding the gradient of the first part of the reaction which is linear. In the right graph, the initial rates of all the substrate concentrations tested are plotted to give the Michaelis-Menten curve which is hyperbolic. This allows determination of the kinetic parameters V_{max} and K_m.

a. Crotonylate H3.1 as described in Part I Procedure A.
   i. To prepare enough crotonylated H3 for 90 assays, use more of each component to give a total volume of 230 µl as described in Table 4.

Table 4. Histone H3 crotonylation reaction set-up with a larger volume

Component	Volume (µl)	Concentration in reaction (µM)
Diluted Crotonyl-CoA	200	87.00
Histone H3.1	20	5.65

p300 Catalytic domain ('p300')	10	0.66

ii. Incubate in a thermocycler at 30 °C for 2 h.

iii. Transfer the tube to another thermocycler at 65 °C and incubate for 5 min to stop the reaction.

iv. Place tube on ice.

b. On ice, dilute the reaction mix in HDAC assay buffer to give 1:4, 1:6, 1:8, 1:10 and 1:12 dilutions of the crotonylated histone H3.

Note: Table 5 describes how to do this serially whilst using the minimal quantity of starting reaction mix. However, this can be done in a different way if required. At least 260 µl is needed for each dilution of the crotonylated histone H3 for the following steps.

Table 5. Preparation of different dilutions of the crotonyl-H3 reaction mix

Dilution	1		1:4		1:6		1:8		1:10		1:12
Reaction mix (µl)	230	→ 210	→ 210	→ 550	→ 550	→ 540	→ 540	→ 440	→ 440	→ 250	→ 250
HDAC assay buffer (µl)			630		275		180		110		50

c. Prepare three 5-strip tubes numbered 0 min and labeled 1:4, 1:6, 1:8, 1:10 and 1:12 (first row of Figures 2A, 2B, or 2C in blue).

d. Prepare 15 more 5-strip tubes numbered 0.5, 1, 2, 4 or 10 (minutes) and labeled 1:4, 1:6, 1:8, 1:10 and 1:12 (the following five rows in Figure 2 in red).

e. On ice, add 14 µl of the 1:4, 1:6, 1:8, 1:10 or 1:12 diluted reaction mix to each one. The tubes are kept on ice until HDAC1 is added.

f. To one strip of reactions labeled 0 min (in Figure 2 in blue), add 1 µl HDAC assay buffer.

g. Vortex briefly by holding both sides of the strip.

Note: The tubes may be spun down or liquid carefully tapped to the bottom if there are bubbles or liquid on the sides or lid of the tube.

h. Incubate immediately in a thermocycler at 30 °C for 1 min.

Note: If HDAC1 is added to a reaction it would not be zero time, but would run for a few seconds until the reaction could be stopped. However, a negative control is needed to provide a baseline level. To make sure that no change in substrate concentration is seen without enzyme, we incubated a reaction without HDAC1 for 2 h and saw no reduction in crotonylated H3. Therefore, 1 min was chosen as this is easy to perform.

i. Transfer to a thermocycler at 95 °C for 1 min.

j. Repeat Steps B3f to B3i with the two other strips of tubes labelled 0 min.

k. Dilute the HDAC1 stock solution 1:4 in HDAC assay buffer, *i.e.*, 20 µl HDAC1 and 60 µl HDAC assay buffer.

l. To each tube in one strip of reactions labeled 0.5 min (in Figure 2 in red), add 1 µl of diluted HDAC1 (for 0.03 µM final concentration).

m. Vortex briefly by holding both sides of the strip and briefly spin or tap liquid down if required.

n. Incubate immediately in a thermocycler set to 30 °C for 30 sec.

Note: It will take about 20-30 sec to add the HDAC and vortex. If time points shorter than 30 sec are needed, reduce the amount of enzyme rather than doing shorter reaction times as these will be inaccurate.

o. Transfer the strip to a thermocycler at 95 °C for 1 min to stop the reaction.

p. Repeat Steps B3l-B3o with the other 0.5 min strips and then with the 1, 2, 4 and 10 min strips in stages, varying the incubation at 30 °C accordingly.

Note: It is necessary to start the reactions in stages so that the time points can be exact.

q. Organize the tubes so that you have replicate sets of reactions labeled A, B and C. The tubes can be frozen at this point or the experiment continued as described in Part II Procedure B.

A		Diluted Reaction Mix (µl)				
		1:4	1:6	1:8	1:10	1:12
Time (min)	0	14	14	14	14	14
	0.5	14	14	14	14	14
	1	14	14	14	14	14
	2	14	14	14	14	14
	4	14	14	14	14	14
	10	14	14	14	14	14

B		Diluted Reaction Mix (µl)				
		1:4	1:6	1:8	1:10	1:12
Time (min)	0	14	14	14	14	14
	0.5	14	14	14	14	14
	1	14	14	14	14	14
	2	14	14	14	14	14
	4	14	14	14	14	14
	10	14	14	14	14	14

C		Diluted Reaction Mix (µl)				
		1:4	1:6	1:8	1:10	1:12
Time (min)	0	14	14	14	14	14
	0.5	14	14	14	14	14
	1	14	14	14	14	14
	2	14	14	14	14	14
	4	14	14	14	14	14
	10	14	14	14	14	14

Figure 2. Setup of reactions

The setup of all 90 reactions is shown, organized into replicate number, time and dilution of reaction mix.

Part II: Revealing the decrotonylation result using antibody-based approaches

A. Western blot

Western blot is suited to assays with a low number of individual reactions and provides clear bands of defined molecular weight, showing how the reaction progressed.

1. Open a pre-cast SDS-PAGE gel and rinse the wells with Milli-Q water to rinse away the preserving solutions and bubbles in the wells.
2. Assemble the gel in the electrophoresis tank with 200 ml of 1x MES buffer in the inner chamber and fill the outer chamber half full with 1x MES buffer.

   Note: Make sure that the inner tank is not leaking. Use a buffer dam if there is only one gel in the tank. MES buffer should be fresh each time in the inner chamber but can be used up to three times in the outer chamber. Placing the tank on ice may improve the quality of the run.
3. Load 5 µl of pre-stained protein marker in the first well of the pre-cast SDS-PAGE gel.
4. Load 8 µl of each sample in the subsequent wells.
5. Run at 100-150 V, 250 mA for 1-1.5 h until the blue dye front reaches the bottom of the gel and/or the different sized bands of the marker have separated.
6. Rinse gel in 1x TGS buffer briefly and cut off the wells from the top of the gel.
7. Soak blotting paper in transfer buffer and place onto the semi-dry transfer machine.
8. Soak a piece of nitrocellulose membrane that is the same size as the blotting paper in transfer buffer and layer on top of the blotting paper taking care not to introduce bubbles in between the layers.
9. Layer the gel on top of the stack, positioning the marker so that it is parallel to the vertical side of the membrane and so that the blue line, showing how far the samples have reached, is above the membrane.

   Note: Again take care not to introduce bubbles in between the layers.
10. Trim the gel so that it is the same size as the membrane.

    Note: When many gels are run, it is useful to cut a corner or corners of the membrane to distinguish them. Pen is not advised as it will run.
11. Place another piece of blotting paper soaked in transfer buffer on top.
12. Roll a round tube, such as a 10 ml pipette, firmly from one side to the other on top of the stack to remove any remaining bubbles.
13. Transfer proteins onto the membrane for 45 min at 15 V, 270 mA.

    Note: One hour is recommended when two or three stacks are in the transfer machine.
14. Place the membrane in a 50 ml Falcon tube and rinse membrane in TBS-T for a few seconds.
15. Block by adding 15 ml TBS-T BSA and incubate with gentle agitation at room temperature for 1 h.
16. In a 5 ml Eppendorf tube, prepare a 5 ml solution of anti-H3K18 crotonyl antibody at 1:2,000 to 1:5,000 dilution (depending on lot number of antibody) in TBS-T BSA.
17. Pour the used TBS-T BSA solution into another tube, which should be stored at 4 °C for later use and add the solution of primary antibody to the membrane containing tube.
18. Incubate overnight at 4 °C with gentle agitation (rocking or rolling).
19. Wash three times briefly (5-10 sec) with 10 ml TBS-T.

20. Wash twice for 15 min with 15 ml TBS-T and gentle agitation.
21. Wash once for 15 min with 15 ml TBS-T BSA.
    Note: The TBS-T BSA from the previous day can be re-used.
22. In a 5 ml Eppendorf tube, prepare a 5 ml solution of anti-rabbit antibody coupled with horseradish peroxidase (HRP) at 1:10,000 dilution in TBS-T BSA.
23. Discard the TBS-T BSA and incubate in anti-rabbit antibody for 1 h at room temperature.
24. Wash three times briefly (5-10 sec) with 10 ml TBS-T and then wash three times for 15 min with 15 ml TBS-T.
25. Remove the membrane from the falcon tube and place on a clean, flat surface *e.g.*, on a large weigh boat.
26. Pipette 1 ml of ECL chemiluminescent substrate (1:1 ratio of A and B), making sure that all of the membrane is covered and leave for 1 min.
27. Dab off excess ECL by touching the edge of the membrane against a paper towel and place ~~in~~ on a sheet of transparent acetate (or some other transparent sheet) in a developing cassette.
28. Layer another acetate sheet on top, taking care not to introduce bubbles.
29. Seal edges with tape, close the lid and avoid exposing membrane to light.
30. In a dark room, place x-ray film on membrane for 15 sec to 5 min depending on the signal.
31. Pass the exposed film into the automatic developer and wait for it to come out at the other side.

Notes:

a. *There may be lot-to-lot variation between antibodies, therefore it is good practice to validate the specificity of the anti-H3K18cr antibody (or whatever anti-acyl antibody used), e.g., using peptide dot blots.*
b. *While we have not tested other image capturing systems as alternatives for the ECL/X-ray film setup, it is likely that such systems that can capture chemiluminescence are not only practical, but potentially even better suited than the use of x-ray films.*

B. Dot blot

Dot blot is more appropriate than Western blot when multiple reactions (more than 15) need to be analyzed. It allows all the reactions to be put on a single membrane, so that their spot intensities can be directly compared. Reactions must be spotted in quadruplicate to allow for variation in pipetting or spreading of the solution on the membrane. This protocol is described as required for Part I Procedure B3.

1. Cut one a piece of nitrocellulose membrane for each of the A, B and C sets of reactions.
   Note: Cut a slightly larger piece that you think you need and trim it later. A typical size for a 10 x 12 spot grid once trimmed is 5.5 x 7.5 cm.
2. Pipette 2 µl of the reactions using a P2 micropipette in quadruplicate in grid format as shown in Figure 3.
   Note: Hold the pipette steady and dispense liquid at an even rate to reduce variability in spots. Use a pencil to mark the grid as you go so that you can put the spots in a line. The consistency and speed of

spotting may be improved by using a vacuum-based dot blot apparatus such as Bio-dot® from Bio-Rad. However, we have not tested such a device.

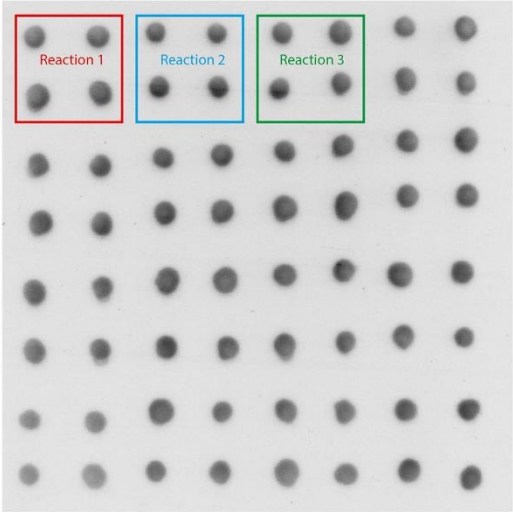

Figure 3. Layout of reaction spots on a nitrocellulose membrane for dot blot assay. Placing the spots in this ordered way makes quantification easier later on.

3. Allow spots to dry fully. This takes 5-10 min.
4. Rinse briefly in transfer buffer and then with TBS-T.
5. Continue with the Western blot protocol (Part II Procedure A) from Step A15, blocking the membrane.
   Note: It can be useful to use a larger volume of antibody as the pieces of membrane are bigger for this dot blot. Ten to fifteen milliliters is recommended for both primary and secondary antibody. The membrane pieces may be too large for a falcon tube, so a suitably sized tray could be used instead.

Data analysis

A. Quantify each spot or band

1. Scan films to a computer using an Epson scanner and its software. Select the following parameters: positive film, 8-bit grayscale and 400 dpi. Scan it and save it as a TIFF file, including the date, experiment and exposure time in the file name.
2. Choose an appropriate exposure time for each substrate concentration where the spots are not too faint or overexposed.
   Note: If the spot is too faint it will be hard to distinguish over background. If the spot is over-exposed (at saturation), it reaches the maximum intensity possible in that area and differences

between spots will not be observed. Different exposure times can be chosen for each substrate concentration so that the most suitable exposure is chosen for each.

3. In a suitable program such as Adobe Illustrator or Photoshop, add a square of black and a square of white. Save it as a TIFF file.

   Note: When ImageJ gives the quantitative peaks for an image selection it shows the highest peak at the top of the window regardless of whether this peak is high in other selections. This makes comparison difficult between spots when they cannot be selected together (for example when there are too many spots). To avoid this problem, an area of black is included which gives the maximum possible value, and an area of white is included which gives the minimum possible value. This means that all values are relative to this and different selections can be compared.

4. Open the image in ImageJ.
5. Select an area of spots using the rectangle tool including the area of white and black.
6. On the analyze tab, under the gels section, choose 'select first lane' (shortcut: Ctrl+1) as shown in Figure 4.

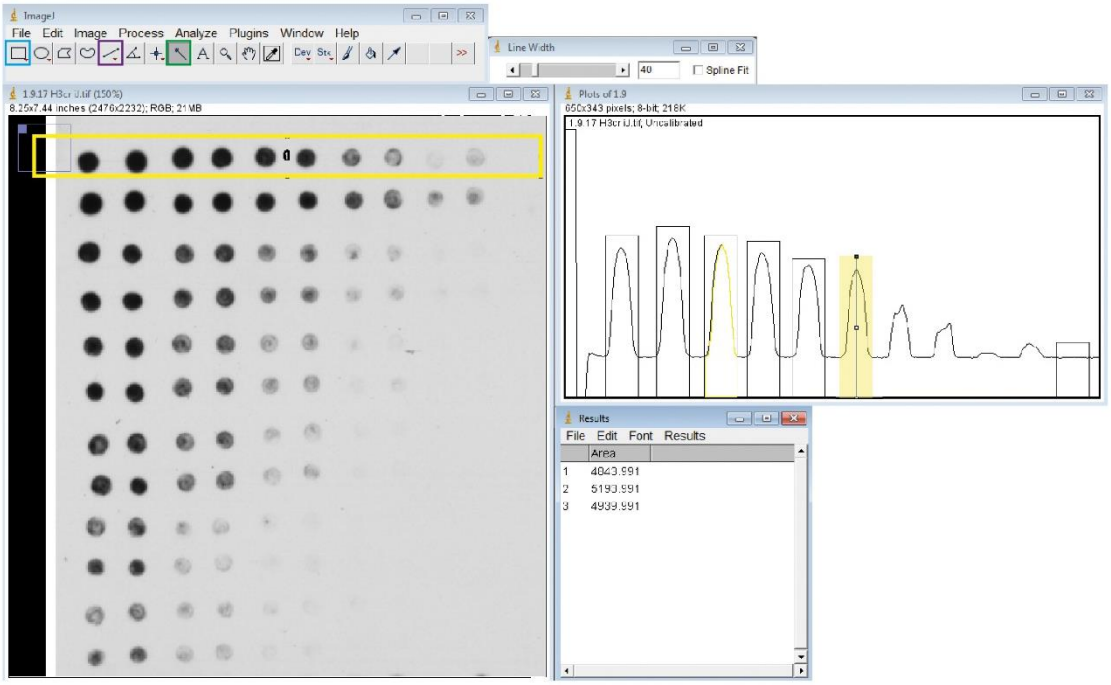

Figure 4. Determination of spot intensity using ImageJ software. Once the image is opened in ImageJ, a horizontal line of bands can be selected using the rectangle tool (blue box). Once this selection is plotted, the individual peaks corresponding to different spots can be selected using the line tool (purple box). The wand tool (green box) is then used to show the values of

selected peaks in the results tab. In the image above, the first two peaks have been selected, the third has been highlighted with the wand tool, and the sixth peak is being selected with the line tool (these are combined screenshots to show many operations at once).

7. In the same section, choose 'plot lanes' (shortcut: Ctrl+3).
8. Double-click the line tool and type a suitable value in the window to set it to the appropriate width, then select peaks corresponding to a spot or band.
   Note: The value only changes when you type the number, not when you press enter. Try out a few widths to find one that fits the peak well and then use this for all of the selected peaks. A value of 50 to 60 (no units given) usually fits the peaks from a spot and 70 to 100 for a band. Control/command-Z can be used to remove a selection if it is in the wrong place.
9. With the same width setting, select an area without a peak which corresponds to the background.
10. Using the wand tool, click on each peak area in turn and the values will come up in a results window.
11. Select these, copy and paste the values into Excel.
12. Attribute a reaction name to each value according to its position on the membrane.
13. Repeat Steps 5 to 12 for the other rows.
    Note: Keep track of the order that you analyze spots and remember that there are four replicates for each reaction which are split into two rows.

B. Calculate the initial reaction rate for each substrate concentration in Excel

This is only applicable to Part I B3 where multiple time points and substrate concentrations were measured.

1. Subtract values for each spot by the background value.
2. Calculate the average of the values for the four spots for each reaction.
3. Calculate the value of each time point relative to the zero time point.
   Note: For each dilution of substrate, divide each time point by the zero time point so that zero time is 1 and other values are relative to this.
4. Convert dilutions of substrate to µM of crotonyl-H3. This assumes that the 5.65 µM of H3.1 was fully crotonylated at lysine 18 in the first reaction, which has been tested in Figure 5.
   Notes:
   a. *Multiply each relative value by the concentration of modified histone in the reaction mix, as shown in Table 6, to convert spot intensity to substrate concentration.*
   b. *We assume this because we also spotted 0.45 to 45 µM of a synthetic crotonylated H3K18cr peptide (a short section of amino acids around the K18 position) and found that the preparation of 5.65 µM crotonylated H3 had an intensity in between 4.5 and 9 µM of crotonyl-peptide as shown*

in Figure 5. The peptide was diluted in HDAC assay buffer.

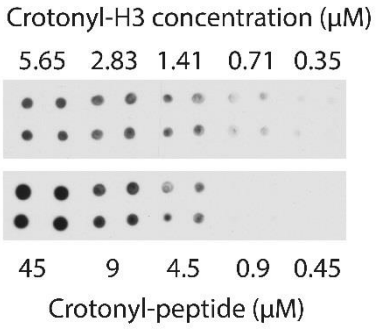

Figure 5. Comparison of ECL intensity of crotonylated histone H3 and the H3K18cr crotonyl-peptide by dot blotting. The H3K18cr peptide sequence was TGGKAPR-Lys(Crotonyl)-QLATKAA-EDA-Btn, EDA is a spacer and Btn indicates C-terminal biotinylation. The intensity of spots for 5.65 μM crotonyl-H3 corresponds to an intensity of crotonyl-peptide between 4.5 and 9 μM.

Table 6. Converting dilutions of crotonyl-H3 reaction mix to concentration

		Concentration (μM)
Dilution of crotonyl-H3 reaction mix	Undiluted	5.65
	1:4	1.41
	1:6	0.94
	1:8	0.71
	1:10	0.57
	1:12	0.47

5. Plot substrate concentration against time for each crotonylated histone concentration as shown in Figure 6.

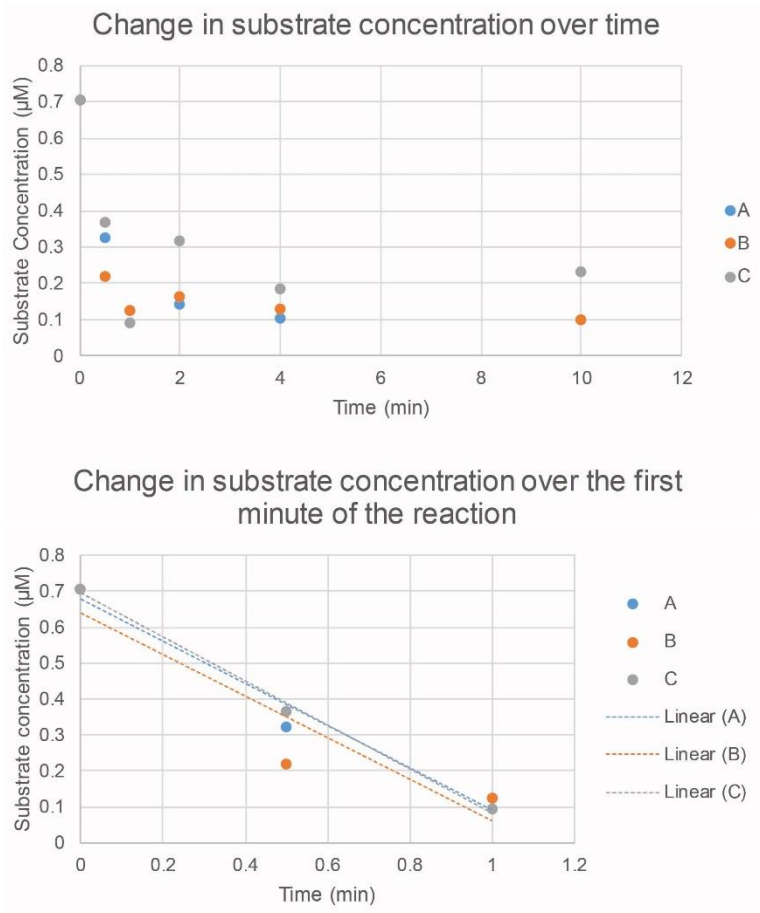

Figure 6. Determination of initial rate by plotting substrate concentration against time. Plotting the substrate concentration for each time point and replicate allows us to see how the reaction has progressed. In the first graph (upper panel), the reaction is fastest during the first minute, so only these time points are plotted in the second graph (lower panel) which now shows a linear relationship and allows the initial rate (the gradient of the line) to be determined. Three replicates: A, B and C.

6. Determine duration for the initial rate of the reaction before it starts to slow and fit a linear regression line for just these points.

   Note: In the set of reactions shown in Figure 6, the initial rate occurs in the first thirty seconds to first minute of the reaction. Choose whichever matches the data points closest.

7. Take the gradient of the line for each of A, B and C replicates, this gives the rate.
8. Repeat for the other substrate concentrations.
9. Create a table of substrate concentration against rate and transfer to GraphPad Prism.

C. Calculate kinetic constants using GraphPad Prism version 7

1. Plot the initial rate of reaction against substrate concentration.
2. In the analysis section, choose non-linear regression.
3. Select enzyme kinetics-substrate versus velocity, choose Michaelis-Menten and click 'OK'.
4. This will give you V_{max}, the maximum initial rate for that enzyme concentration when all active sites are occupied. It will also give you K_m, the substrate concentration required to give half of the maximum rate.
5. Select the enzyme kinetics-substrate versus velocity section again but this time choose K_{cat}. In the constrain tab by the parameter name 'Et', constrain 'constant equal to' and input the concentration of enzyme used into the value box, in our case this is 0.03, corresponding to the 0.03 µM of HDAC1 used.

   Note: An example of such an analysis is shown in Figure 7b of Fellows et al. (2018), depicting an analysis of the comparative kinetics of HDAC1 decrotonylation and deacetylation.

Recipes

1. Histone acylation buffer

   50 mM Tris-HCl pH 8

   50 mM KCl

   0.1 mM EDTA

   0.01% Tween 20

   10% Glycerol

   1 mM DTT

   Aliquot and store at -20 °C until use

2. HDAC Assay buffer

25 mM Tris-HCl pH 7.5

50 mM KCl

1 mM $MgCl_2$

1 µM $ZnSO_4$

Aliquot and store at -20 °C until use

3. 1x MES buffer
   50 ml 20x RunBlue MES buffer
   950 ml distilled or Milli-Q water
4. 1x TGS buffer
   100 ml 10x Tris/glycine/SDS electrophoresis buffer (Bio-Rad)
   900 ml distilled or Milli-Q water
5. Transfer Buffer (recipe for 1 L buffer)
   5.8 g Tris

   2.9 g Glycine

   200 ml Methanol

   800 ml distilled or Milli-Q water

6. Tris-buffered saline (TBS)
   302.5 g Tris

   438.0 g NaCl

   1 L distilled or Milli-Q water

7. TBS with tween 20 (TBS-T)
   2.5 ml of 20% Tween 20 in 1 L of TBS
8. TBS-T with 3% (w/v) bovine serum albumin (TBS-T BSA)
   Dissolve 6 g of BSA in 200 ml TBS-T and store at 4 °C

Acknowledgments

This work was supported by an MRC DTP studentship to RF, BBSRC and MRC funding to PVW. We thank Tabitha Rücker and Karolina Doubkova for critical reading of the manuscript. The authors declare no conflicts of interest. This is an elaborated method based on the work published by Fellows *et al.* (2018).

References

1. Bannister, A. J. and Kouzarides, T. (2011). Regulation of chromatin by histone modifications. *Cell Res* 21(3): 381-395.
2. Castillo, J., Lopez-Rodas, G. and Franco, L. (2017). Histone post-translational modifications and nucleosome organisation in transcriptional regulation: some open questions. *Adv Exp Med Biol* 966: 65-92.
3. Fellows, R., Denizot, J., Stellato, C., Cuomo, A., Jain, P., Stoyanova, E., Balazsi, S., Hajnady, Z., Liebert, A., Kazakevych, J., Blackburn, H., Correa, R. O., Fachi, J. L., Sato, F. T., Ribeiro, W. R., Ferreira, C. M., Peree, H., Spagnuolo, M., Mattiuz, R., Matolcsi, C., Guedes, J., Clark, J., Veldhoen, M., Bonaldi, T., Vinolo, M. A. R. and Varga-Weisz, P. (2018). Microbiota derived short chain fatty acids promote histone crotonylation in the colon through histone deacetylases. *Nat Commun* 9(1): 105.
4. Pengelly, A. R., Copur, O., Jackle, H., Herzig, A. and Muller, J. (2013). A histone mutant reproduces the phenotype caused by loss of histone-modifying factor Polycomb. *Science* 339(6120): 698-699.
5. Sabari, B. R., Tang, Z., Huang, H., Yong-Gonzalez, V., Molina, H., Kong, H. E., Dai, L., Shimada, M., Cross, J. R., Zhao, Y., Roeder, R. G. and Allis, C. D. (2015). Intracellular crotonyl-CoA stimulates transcription through p300-catalyzed histone crotonylation. *Mol Cell* 58(2): 203-215.
6. Sabari, B. R., Zhang, D., Allis, C. D. and Zhao, Y. (2017). Metabolic regulation of gene expression through histone acylations. *Nat Rev Mol Cell Biol* 18(2): 90-101.
7. Wegener, D., Hildmann, C., Riester, D. and Schwienhorst, A. (2003a). Improved fluorogenic histone deacetylase assay for high-throughput-screening applications. *Anal Biochem* 321(2): 202-208.
8. Wegener, D., Hildmann, C. and Schwienhorst, A. (2003b). Recent progress in the development of assays suited for histone deacetylase inhibitor screening. *Mol Genet Metab* 80(1-2): 138-147.
9. Wegener, D., Wirsching, F., Riester, D. and Schwienhorst, A. (2003c). A fluorogenic histone deacetylase assay well suited for high-throughput activity screening. *Chem Biol* 10(1): 61-68.
10. Wei, W., Liu, X., Chen, J., Gao, S., Lu, L., Zhang, H., Ding, G., Wang, Z., Chen, Z., Shi, T., Li, J., Yu, J. and Wong, J. (2017). Class I histone deacetylases are major histone decrotonylases: evidence for critical and broad function of histone crotonylation in transcription. *Cell Res* 27(7): 898-915.